LUND UNIVERSITY

Dynamic Power System Load -Estimation of Parameters from Operational Data

Romero, Ines

2005

Link to publication

Citation for published version (APA):
Romero, I. (2005). *Dynamic Power System Load -Estimation of Parameters from Operational Data*. [Doctoral Thesis (monograph), Industrial Electrical Engineering and Automation]. Department of Industrial Electrical Engineering and Automation, Lund Institute of Technology.

Total number of authors:
1

General rights
Unless other specific re-use rights are stated the following general rights apply:
Copyright and moral rights for the publications made accessible in the public portal are retained by the authors and/or other copyright owners and it is a condition of accessing publications that users recognise and abide by the legal requirements associated with these rights.
• Users may download and print one copy of any publication from the public portal for the purpose of private study or research.
• You may not further distribute the material or use it for any profit-making activity or commercial gain
• You may freely distribute the URL identifying the publication in the public portal

Read more about Creative commons licenses: https://creativecommons.org/licenses/

Take down policy
If you believe that this document breaches copyright please contact us providing details, and we will remove access to the work immediately and investigate your claim.

LUND UNIVERSITY

PO Box 117
221 00 Lund
+46 46-222 00 00

Download date: 12. Oct. 2024

Dynamic Power System Load

Estimation of Parameters from Operational Data

Inés Romero Navarro

LUND UNIVERSITY

Doctoral Dissertation in Industrial Electrical Engineering

Department of Industrial Electrical Engineering
and Automation

Department of
Industrial Electrical Engineering and Automation
Lund University
P.O. Box 118
SE-221 00 LUND
SWEDEN

http://www.iea.lth.se

ISBN 91-88934-37-3
CODEN: LUTEDX/(TEIE-1045)/1-275/(2005)

© Inés Romero Navarro, 2005
Printed in Sweden by Media-Tryck
Lund University
Lund, 2005

Abstract

The significance of load modeling for voltage stability studies has been emphasized by several disturbances, which have taken place in the past years. They have shown that the loads in combination with other dynamics are among the main contributors of prolonged low voltage conditions, voltage instability and collapse in the power system. As a result of these disturbances new investigations have come up to better understand the nature of the load. However, power system loads keep being very difficult to model; the load generally aggregates a large number of individual components of different nature, different load dynamics are excited depending on the time frame of actuation and the type of disturbance affecting the system, and the load is highly dependent on external factors such as weather conditions.

This thesis investigates the load-voltage characteristic during two different time scales, long-term over several minutes, and short-term covering ms to several seconds, for different sized disturbances, and its impact on the calculation of transfer limits and security margins in voltage stability studies. The accurate determination of transfer limits will be an increasingly important task to maintain the operational security and economic dispatch of the power system. The location of the stability limits and the determination of transfer limits depend on the load-voltage characteristic since load relief due to the load-voltage dependency results in larger transfer limits. Moreover, the importance of using dynamic load models instead of static ones in stability studies is highlighted in this thesis.

Due to the large amount of electrical heating loads in Sweden and its effect on voltage stability, a dynamic load model with exponential recovery, previously proposed by Hill and Karlsson, [Karlsson and Hill, 1994], has been the starting point for the investigations. Field measurements from continuous normal operation at the 20 kV-level from a substation in Sweden

have provided a large amount of data covering all seasons during the time period July 2001-June 2002, and have resulted in extensive, unique and interesting recordings of active and reactive load characteristic and its dependency with small voltage variations. The data have revealed the variation of the load parameters and their dependency with weather and season of the year. The work has also contributed to a better approach for the normalization of traditional reactive load models.

Furthermore the load-voltage characteristic during large disturbances has been investigated based on field measurements of phase-to-phase faults in a non-effectively earthed 50 kV system in Sweden. Three-phase currents and voltages have been used to estimate the active and reactive power. The recordings exhibited voltage dips up to 30% in the positive sequence voltage. The severity of the disturbances accentuates the nonlinear behavior of the load; the active and reactive power rapidly increase after fault clearing to levels even above the pre-disturbance value due to the re-acceleration of motors. The full recovery of the voltage is delayed due to the re-connection of tripped load. Moreover, it is shown that traditional load models do not accurately reflect the load behavior during these disturbances, for voltage dips around 12 % or larger due to the nonlinearities. An alternative load model, which represents the nonlinearities, has been tested. The superior behavior is demonstrated with the field measurements.

Finally, some guidelines for industry to better account for the load in future stability studies have been included as a corollary of this thesis.

Keywords

Load modeling, large disturbances, normal operation, voltage stability, dynamic load models, modeling and identification, normalization in reactive load models.

Preface

The work presented in this thesis has been carried out at the Department of Industrial Electrical Engineering and Automation at Lund University in Sweden for most of its time, but also some contributions have been the result of research in Vancouver (Canada), at the researching and consulting company Powertech Labs and at the Department of Electrical Engineering at University of British Colombia in Vancouver (Canada). This thesis is the outcome of a research project on load modeling, which was started in January 2000, and has been funded by Elforsk through the Elektra program during this time. Previous results have been published in a Licentiate thesis 'Dynamic load models for power systems. Estimation of time-varying parameters during normal operation', (2002), and in several conference papers, journals, and internal reports.

The topic of the thesis is focused on the investigation of the load characteristic in several time-scales, and the analysis of its effect in stability studies. This investigation has provided deep insight into the nature of load dynamics and their dependency with voltage, and has made it possible to carry out an adequacy study of traditional models for load representation, and to compare with alternative more accurate ones. The work is a valuable contribution for academia, but it is also significantly relevant to the industry due to its practical approach, and field measurement based results. The author's aim was to provide a global idea of the load-modeling problem in stability studies from a practical point of view, and to mark out the directions for industry to improve load representation for stability analysis.

The thesis consists of four parts, which are summarized in the abstract and outlined in the introduction.

Acknowledgements

During the last couple of years I have realized how strongly the decision to pursue my PhD studies in Sweden has affected me professionally and personally. My life in Sweden and among Swedish people has surprised and enriched me in ways you cannot imagine. I am therefore truly grateful to all you that have encouraged and supported this journey. Dr. Mats Larsson and Prof. Gustaf Olsson were my first professional contacts in Lund and with the department of IEA. Prof. Gustaf Olsson, one of my supervisors, has always been a source of encouragement and optimism.

I have no words to express my gratitude to Prof. Sture Lindahl. He was a member of my steering group when I met him, but in the last years, he has voluntarily acted as one of my main supervisors. His support and encouragement, valuable ideas and many excellent comments have been crucial for accomplishing this work. Dr. Olof Samuelsson has co-supervised my work along these years. I am truly thankful for his guidance and support, for his critics and for many interesting discussions. There is a lot I have learnt from him. I am very thankful for his unlimited help with the measurements at Tomelilla, and the proof reading of my work.

Many other people have contributed to the success of this project. I would like to start with my project steering group; Bo Eliasson, Lars Gertman, Daniel Karlsson, György Sárosi, Kenneth Walve, Lars Åke, and Jan Ronne-Hansen. Dr. Daniel Karlsson deserves special thanks. His PhD thesis has been the base of my research; he has constantly shown interest and confidence on my work. Thanks for your trust! Many thanks go to Chalmers University of Technology, and especially Gunilla Le Dous for their interest in this project and the data they have shared with me. I also wish to thank Stefan Solyom from the department of automatic control for many interesting discussions on identification and power systems.

My stay as a guest researcher at both Powertech Labs and the University of British Colombia in Canada has been an unforgettable experience. I owe my gratitude to everyone involved in this exchange. I particularly appreciate the collaboration with Prof. Prabha Kundur and Hamid Hamadani. It has been a privilege to be part of your team, and I am grateful for this opportunity. At the University of British Colombia, Prof. Martí and Luis Linares introduced me to the exciting world of Microtran, and from the very first time, they made me feel at home. Thank you for taking such good care of me!

The availability of field measurements has been crucial to accomplish this work. I would like to express my sincere gratitude to Ulf Thorén, Sydkraft Elnät Syd AB, and Lars Prabin, Elektro-Sandberg, for their help during the measurements at Tomelilla, and to Zoran Gajic, ABB Västerås, for providing me with field measurements from Öland. This project has been financially supported by ELFORSK as ELEKTRA project number 3355 'Lastmodellering i realtid'. This support is gratefully acknowledged.

I would like to thank everyone at IEA for providing a friendly and interesting atmosphere at the department. I have really enjoyed crayfish, beers, coffee breaks and parties. I especially would like to thank Getachew Darge for his unlimited help at the lab; to Anita, for being such a sweet secretary; to Gunnar for his constant work with the computers. I also wish to thank to all my friends in Sweden and abroad. Thanks to your lunches, visits, parties and emails, I have survived the winters away from home. Believe me, you are very important to me!

Thanks to my family, both the Spanish and the Swedish one, for their support and unconditional love. Thank you so much for your phone calls and emails. I am in debt to you! Finally, it is your turn Mikael! I have been lucky to find you; thanks for all your love, support and endless faith in me. Thanks for sharing my dreams and life projects. We are a great team, and I am really happy we have already shared so many adventures.

Lund, January 24, 2005

Inés Romero Navarro

Abbreviations

A	*transient active load parameter (linearized form)*
A_q	*transient reactive load parameter (linearized form)*
a_1-a_6	*polynomial load model parameters*
α	*active load-voltage dependence*
α_s	*steady state active load-voltage dependence*
α_t	*transient active load-voltage dependence*
B	*susceptance*
B	*steady state active load parameter (linearized form)*
B_q	*steady state reactive load parameter (linearized form)*
β	*reactive load-voltage dependence*
β_s	*steady state reactive load-voltage dependence*
β_t	*transient reactive load-voltage dependence*
λ	*eigenvalue*
χ_s	*steady state reactive load-voltage dependence (normalized)*
χ_t	*transient reactive load-voltage dependence (normalized)*
θ_g	*angle at the generator bus*
θ_l	*angle at the load bus*
f	*frequency*
f_o	*rated frequency*
G	*conductance*
I_1, I_2, I_0	*(1) positive-, (2) negative- and (0) zero-sequence currents*
J	*Jacobian matrix*
J_R	*reduced Jacobian matrix*
k_p	*active load-voltage sensitivity*
k_q	*reactive load-voltage sensitivity*
L	*window length*
n_p	*active power exponential dependence*
n_q	*reactive power exponential dependence*
p	*parameter vector*
P_d	*active power dissipated by losses*

P_{drop}	*% percent of disconnected active load*
P_{dyn}	*% percent of dynamic active load*
P_{max}	*maximum active power transfer capability*
$P_{measured}$	*measured active power*
P_l	*total active power load*
P_o	*active power at the pre-disturbance conditions*
P_r	*active power recovery*
P_s	*static active characteristic*
$P_{simulated}$	*simulated active power*
P_t	*transient active characteristic*
Q_d	*reactive power dissipated by losses*
Q_{drop}	*% percent of reactive load disconnected*
Q_{dyn}	*% percent of dynamic reactive load*
Q_{max}	*maximum reactive power transfer capability*
$Q_{measured}$	*measured reactive power*
Q_l	*total reactive power load*
Q_o	*reactive power at the pre-disturbance conditions*
Q_r	*reactive power recovery*
Q_s	*static reactive characteristic*
$Q_{simulated}$	*simulated reactive power*
Q_t	*transient reactive characteristic*
Q_{losses}	*reactive power losses*
R_r	*rotor resistance*
R_s	*stator resistance*
s	*Laplace operator*
s	*slip*
t	*time*
t_o	*time for the change in voltage*
T_e	*electrical torque*
T_m	*mechanical torque*
T_p	*active load recovery time constant [s]*
T_q	*reactive load recovery time constant [s]*
T_1	*active load time constant (linearized form)*
V	*measured voltage*
V_g	*voltage at the generator bus*
V_{max}	*maximum voltage (maximum loadability)*
V_l	*voltage at the load bus*
V_o	*supply voltage at the pre-disturbance conditions*
V_1, V_2, V_0	*(1) positive-, (2) negative- and (0) zero-sequence voltages*
w	*rotor speed*

w_o	*nominal angular frequency*
x	*state*
X_{eq}	*equivalent reactance*
X_m	*magnetizing reactance*
X_r	*rotor reactance*
X_s	*stator reactance*
Y	*admittance matrix*
Z_1, Z_2, Z_0	*(1) positive-, (2)negative- and (0) zero-sequence impedance*
RST/ABC	*three-phase system* $L_1L_2L_3$

Contents

1 Introduction 1
1.1 New challenges 2
1.2 Motivation 3
1.3 Objectives 5
1.4 Contributions 5
1.5 Outline of the Thesis 7
1.6 Publications 8

PART I

2 Load Modeling 13
2.1 Introduction 14
2.2 Load Characterization 17
2.3 Standard Load Models 20
2.4 Exponential Dynamic Load Model 23
3 Voltage and Load Stability 27
3.1 The Swedish Power System 28
3.2 Voltage and Load Stability 29
3.3 Transfer Limits 32
3.4 Conclusions 43
4 Limits for Voltage Dependent Loads 45
4.1 Determination of Voltage Stability Limits 46
4.2 Simulations and Results 52
4.3 Voltage Security Assessment 56
4.4 Conclusions 66

PART II

5 Field Measurements 71
5.1 Field Measurements 71
5.2 Test No.1 72
5.3 Test No.2 75

5.4 Analysis of Normal Operation Data.....81
6 Determination of Parameters in Dynamic Load Models.....93
6.1 Introduction.....93
6.2 Linearization.....93
6.3 Optimization.....96
6.4 Robustness of the Model.....97
6.5 Effect of Spontaneous Load Variations.....101
7 Automatic Determination of Parameters.....105
7.1 Conditions for Parameter Estimation.....106
7.2 Excitation.....106
7.3 Detection of Voltage Variations.....107
7.4 Data Sequence Length.....108
7.5 Normalization of Dynamic Reactive Load Models.....116
8 Analysis of Experimental Results.....125
8.1 Analysis of Variability of the Parameters.....126
8.2 Active and Reactive Load Correlation.....139
8.3 Conclusions.....141

PART III

9 Field Measurements.....145
9.1 The System Description.....145
9.2 Load Area Description.....146
9.3 Field Measurements.....149
9.4 Measurement Equipment.....150
9.5 Wind Power Presence.....150
10 Determination of Load Estimates.....153
10.1 Determination of Symmetrical Components.....153
10.2 Load Estimates.....156
10.3 Estimates of the Active and Reactive Power.....157
10.4 Load Representation.....158
10.5 Load Estimates from Field Measurements.....159
10.6 Conclusions.....163
11 Dynamic Load Models.....165
11.1 Load Response during Large Voltage Variations.....165
11.2 Induction Motors.....169
11.3 Traditional Dynamic Load Model.....172
11.4 Identification of Nonlinear Systems.....173
11.5 Load Model Validation.....176
11.6 Load-voltage characteristic.....182

11.7 Conclusions 185
12 Alternative Dynamic Load Models 187
12.1 Introduction 187
12.2 Dynamic Load Model for Short-Term Stability 188
12.3 Validation of the Model 189
12.4 Network Effects and Reactive Compensation 193
12.5 Analysis of the Results 197
12.6 Conclusions 207

PART IV

13 Load Modeling Recommendations 211
13.1 Loads and Critical Scenarios 211
13.2 Load Modeling Guidelines for Stability Studies 217
13.3 Load Model Overview 220
13.4 Load Modeling Procedure 222
13.5 Conclusions 223
14 Conclusions and Further Work 225
14.1 Summary of the Main Results 225
14.2 Future Research 232

REFERENCES 233

Appendix I Load Models and Jacobian Matrix 245
Appendix II Equivalent Distribution System 249
Appendix III Symmetrical Components 251
Appendix IV Network Effects 257

Chapter 1

Introduction

The global electric power demand is rapidly increasing, and big efforts and investments must be dedicated to research into new technology trends to satisfy these changes. The increasing disparity between demand of energy and supply leads to a number of concerns in relation to the present and future availability of energy sources in the world, the environmental costs that will be associated to this growth, and how third world countries will handle the increasing energy needs of their growing populations [Bearden, 2000]. Our power industry depends more and more on the industry growth rate and the use of the existing capacity in the most effective way. Therefore current challenges in power engineering include optimizing the use of the available resources and keeping high reliability for operating conditions that will include narrow stability and security margins.

The Washington Times April 14, 2004, *"A forecast released Wednesday predicts world energy demand will grow more than 50 percent by 2025 with increased use of nearly every type of fuel. The U.S. Energy Information Administration said robust economic growth worldwide, and particularly in China, India and Eastern Europe, will result in a 54-percent overall increase in demand with growth rates of 33 percent in the industrialized world and a whopping 91 percent in the developing world. Nuclear, coal and renewable energy, which includes hydroelectric, are expected to see growth, but not like the doubling of electricity demand and 67 percent boom in natural gas demand. Oil consumption is projected to climb from 77 million barrels per day to around 121 million bpd by 2025, although the*

price by that time won't change much. The EIA pegged the price of a barrel of crude 20 years from now at around $272.

Chapter 1 is structured as follows: Section 1.1 gives an overview of the current trends within the electricity industry, emphasizing the importance of optimizing the use of available resources, the integration of new technologies and the application of real-time monitoring and control. Sections 1.2, 1.3 and 1.4, describe the origin, motivation, objectives and contributions of the project. Sections 1.5 and 1.6 present an outline of the thesis and the main publications of the author.

1.1 New challenges

Changes in the power generation and transmission systems, optimizing the available resources while making environmental consideration, and ensuring high reliability in the system operation, are necessary in order to match the increasing demand in the load areas. The available production margins will almost surely shrink in comparison with the traditional power systems. Some of the changes can be characterized as follows:

- The system planning must ensure controllable generation for regulating both frequency (by controlling the output of the active power) and voltage (by controlling the output of reactive power), and must control the costs and ability to operate as spinning reserves when needed. An optimization and coordination of the available resources, as well as the construction of new generation plants will thus be necessary.
- The transmission system expansion must be adequate to place new generating units and to support load demand variations. This will involve the optimization in the use of the existing transmission system but also its expansion.
- The integration of distributed generation and storage of energy will make it possible to support the reliability of the system in emergency situations.

- The use of advanced technologies will transform the static grid to an intelligent network, with available real-time control and monitoring of the system.
- The general de-regulation will also add new economical and organizational problems. The operational margins will almost surely be decreasing. At the same time the electricity from several producers has to be satisfactorily distributed in the available network, which will require a significant control and operation effort.

Distributed Generation of power (DG), especially those facilities based on emerging technologies (solar panels, wind power, fuel cells, micro gas turbines, etc.) or hybrid systems will play a key role in the future, supporting the available capacity to meet peak power demands. DG provides, among other many potential advantages, an improved user power quality and reliability (voltage support, source of reactive power), low-cost energy in co-generation applications (combined uses of heat and power), elimination of transmission and distribution line losses, and a cost-effective source of peak demand power.

The use of advanced technologies will transform the system to an intelligent system where a real-time feedback of information will be required in order to be competitive and successful in the new deregulated market. In a near future, the power system control centers will become information technology centers, where the continuous monitoring and control of different signals and components will result in powerful diagnosis of the system [IEEEStability, 2002], and therefore in high reliability.

Moreover, environmental issues in relation to the emissions and the location of new generation areas will limit the construction of new plants and the expansion of the transmission network.

1.2 Motivation

The transfer limits or the maximum power flows that are allowed across certain sections of the power system, depend on the operating conditions of the power system, and therefore on a large number of factors, such as

network topology, loading and generating conditions, which lead to different flow patterns. In order to simplify these calculations, a number of approximations are used, which introduce high or low uncertainty in the obtained transfer limits, according to the used assumptions [Taylor, 1994]. An optimistic approach may lead the system to unacceptable values under severe conditions and therefore compromise the security of the system. A pessimistic approach will avoid risks in the delivery by introducing larger security margins, but on the other hand it will lead to a poor utilization of the resources. As mentioned in the previous section the continuous changes in the electricity industry are forcing changes in the transmission system. To avoid an unnecessary expansion it would be optimal to use the existing lines and transformers to their full capacity. The accurate determination of the transfer limits will play an important role in maintaining the secure and economic operation of the power system.

The work presented here is motivated by the need of finding more accurate dynamic load models. The result will provide a better understanding of the load dynamics and its representation, making it possible to decrease uncertainty margins, and therefore optimizing both, the economy and reliability of the system operation. The background is described in the following. Accurate power system models are necessary in order to reduce power system operational uncertainty. Accurate models of different complexity for generators, lines and transformers are available today, whereas load models are usually simplified. Different studies, [Taylor, 1994] and [IEEELoad, 1993], have shown the importance of the load representation in voltage stability analysis. Static load models are not accurate enough for capturing the dynamics of the network. Therefore dynamic load models are needed even if voltage collapse, in many cases, is a slow phenomenon. This situation is particularly critical in Sweden, [Johansson and Sjögren, 1995], [Arnborg, 1997], where the limiting factor is often voltage stability and where load dynamics due to the large percent of electric heating and tap changer operations, are the main issues.

Furthermore, additional efforts must be devoted to the analysis of the load-voltage characteristic also during large disturbances, to be able to determine the risk of instability. There is limited information available on the voltage dependence of loads during severe voltage reductions [Ihara, *et al.*, 1981], [Sabir and Lee, 1982] and [Concordia and Ihara, 1982]. Large voltage changes occur for example at short-circuits and earth-faults, and are in some

cases the starting point for a scenario ending with instability. The majority of current load models are valid for small voltage variations around an operating point. Research and studies have indicated that the transient load characteristic might be represented by impedance for small voltage variations. The load may then recover towards constant power, or another load characteristic, after a while. There are very few examples of models that have been verified for large voltage variations.

1.3 Objectives

The primary objective of this work is to investigate the load-voltage characteristic and the dynamics involved in the load response for two different time scales, long-term (in the order of several minutes) and short-term (in the order of ms to several seconds), in order to improve the load representation in stability studies, and therefore the calculation of transfer limits and security margins.

A number of secondary objectives can be enunciated, which have been investigated to understand and achieve the primary objective: 1) Literature research of available models for load representation in voltage stability studies. 2) Investigation of load voltage stability, and the impact of the load characteristic in determining stability limits and security margins. 3) Signal processing for different type of measurements, including the design and implementation of software to carry out the measurements, and software for detection of excitation in the recordings. 4) Identification procedure to estimate parameters, and mathematical modeling based on a physical approach.

1.4 Contributions

The main contributions of the work are included in Part IV of this thesis, and can be summarized as:

1. Analysis of the impact of the load-voltage characteristic in the planning and operation of power systems. This includes the investigation of the impact of the load characteristic in the

determination of transfer limits and stability limits. A voltage security assessment on the Nordic 32 test system has been carried out.

2. Analysis of the load characteristic during small voltage variations based on field measurements. Identification of parameters and model validation.

3. Continuous acquisition of data from normal operation. An automatic procedure for acquisition of continuous data has been implemented. Also, a method to detect voltage variations and to determine the load parameters has been proposed. The method has been validated with continuous data from normal operation. The identification window for the parameters has been investigated.

4. Analysis of the seasonal load characteristic based on continuous data from normal operation. The data has resulted in interesting recordings that have provided valuable information related to load dynamics, and has helped to analyze typical daily operations at a substation. The yearly, weekly and daily load model parameters have been investigated.

5. Unexpected deviations in the reactive load parameters have led to a new representation of the reactive load. The reactive power level, which was previously used as normalization factor is inappropriate. A better approach for the normalization of reactive load models has been proposed.

6. A method to determine the phase load estimates P and Q during large voltage variations from measurements of phase-voltages and currents has been proposed

7. Adequacy analysis of traditional models to represent the load during large voltage variations. An investigation of the load characteristic during these conditions has been carried out. Traditional models for representing the load are compromised for large voltage variations. An alternative model has been positively validated with field measurements. The model parameters have been investigated.

8. Digital fault recorders (DFR) data is shown to be of great advantage for the investigation of the load characteristic during voltage dips.

9. The reactive power response at the load bus during symmetrical and asymmetrical faults, when a large amount of induction motors is present in the area, is explained. This is a result of the fault current contribution of the induction motors.

10. Guidelines for load modeling (in industry) are given. They provide an overall idea of load modeling for stability studies from a practical point of view, and mark out the directions for industry to improve the load representation in stability studies.

1.5 Outline of the Thesis

The thesis is organized in four parts:

Part 1. Voltage and Load Stability

It includes a general introduction to voltage stability and load modeling. An investigation of the effect of the load characteristic in the determination of transfer limits is also included.

Part II. Load-voltage Characteristic during Normal Operation

This second part provides an analysis of the load-voltage characteristic during normal operation. Unique and valuable results on the seasonal variations of the load characteristic during normal operation are included.

Part III. Load-voltage Characteristic during Large Voltage Variations

The third part is focused on the investigation of the load-voltage characteristic during large voltage variations. The active and reactive load characteristics are studied, as well as the critical dynamics that affect their response. The adequacy of traditional models for the load representation is investigated, and an alternative load model is introduced.

Part IV. Conclusions

The last part includes a discussion section, and also gathers the main conclusions of the work and potential ideas for further work. A contribution for industry is included in this last part, where important recommendations for load modeling are compiled.

1.6 Publications

The project has resulted in several contributions that have been published along the time. Paper 4 describes a part of the material included in Part I of this thesis. Publications 2-3 and 5-6 summarize the contents of Part II. Papers 7-8 cover some chapters from Part III. The analysis, implementation, and the writing of these papers are attributed to the author of this thesis, with support from Samuelsson and/or Lindahl.

1. I. Romero Navarro, M. Larsson, G. Olsson, 'Object-Oriented Modeling and Simulating of Power Systems using MODELICA', *IEEE Winter Meeting, Singapore, January 2000.*

2. I. Romero Navarro, and O. Samuelsson, 'Analysis Window for Determination of Parameters in Dynamic Load Models', *Reglermötet, (National Swedish Symposium on Control 2002), Linköping, May 2002.*

3. I. Romero Navarro, 'Dynamic Load Models for Power Systems. Estimation of Time-varying Parameters during Normal Operation', *Licentiate Thesis ISBN 91-88934-26-8, Department of Industrial Electrical Engineering and Automation (IEA), Lund University, Sweden 2002.*

4. I. Romero Navarro, O. Samuelsson, 'Influence of the Load Characteristic in Voltage Stability Analysis', *IASTED International Conferences, power and energy systems PES 2003, California, February 2003.*

5. I. Romero Navarro, O. Samuelsson and S. Lindahl, 'Influence of Normalization in Dynamic Reactive Load Models', *IEEE Transactions on Power Systems, Vol 18, issue 2, pp 972-973, 2003.*

6. I. Romero Navarro, O. Samuelsson and S. Lindahl, 'Automatic Determination of Parameters in Dynamic Load Models from Normal

Operation Data', *Panel session on load modeling at IEEE Power Engineering Society General Meeting, Vol. 3, pp. 1378-1381, Toronto, July 2003.*

7. I. Romero Navarro, O. Samuelsson and S. Lindahl, 'Off-line Analysis of the Load Response during Large Voltage Variations', *IEEE Latin America T&D 2004, Sao Paulo, November 2004.*

8. I. Romero Navarro, O. Samuelsson and S. Lindahl, 'Estimation of the load characteristic from operational data', *IEEE Transactions on Power Systems (Manuscript).*

Technical Reports

- I. Romero Navarro, 'Cold Load Pick Up using MODELICA', *Technical Report CODEN:LUTEDX/(TEIE-7148), IEA, Lund University, Sweden, 2000.*
- I. Romero Navarro, 'Analysis and Identification of Load Responses in the Österlen Test System using MODELICA-MATLAB', *Technical Report CODEN: LUTEDX/(TEIE-7149), IEA, Lund University, Sweden, 2001.*
- I. Romero Navarro, 'Recording of Voltage, Active and Reactive Power at Tomelilla. TOMELILLA I', *Technical Report CODEN: LUTEDX/(TEIE-7150), IEA, Lund University, Sweden, 2002.*
- I. Romero Navarro, 'Recording of Voltage, Active and Reactive Power at Tomelilla. TOMELILLA II', *Technical Report CODEN: LUTEDX/(TEIE-7151), IEA, Lund University, Sweden, 2002.*
- I. Romero Navarro, 'Automatic Determination of Parameters in Dynamic Load Models', *Technical Report CODEN: LUTEDX/(TEIE-7203), IEA, Lund University, Sweden, 2002.*
- I. Romero Navarro, 'Estimation of Load Time-Varying Parameters During Normal Operation', *Technical Report TEIS-1034, IEA, Lund University, Sweden, 2003.*

- I. Romero Navarro, 'A Voltage Security Assessment of the Nordic 32 Test System using VSAT', *Technical Report CODEN: LUTEDX/(TEIE-7204), IEA, Lund University, Sweden, 2003.*
- I. Romero Navarro, 'Influence of the Load Characteristic in Determining the Stability Limit of an Ideal 4Bus-case', *Technical Report CODEN: LUTEDX/(TEIE-7205), IEA, Lund University, Sweden, 2003.*
- I. Romero Navarro, 'Study of Induction Motors in Voltage Stability Studies using MicroTran', *Technical Report CODEN: LUTEDX/(TEIE-7206), IEA, Lund University, Sweden, 2003.*
- I. Romero Navarro, 'Power Market Economics. De-regulation: Socio-economical and Technical Issues', Technical Report *CODEN: LUTEDX/(TEIE-7207),* IEA, Lund University, Sweden, 2004.

Part I

Load and Voltage Stability

Summary: *Power system loads are still considered as one of the most uncertain and difficult components to model; the large diversity of load components, their variable composition and nature, and their dependency with external factors make it complicated to define a load model valid for all time scales and all type of components. The fact that loads are generally voltage dependent is a critical aspect for the planning and operation of the power system. The load characteristic may result in a very optimistic or pessimistic design if it is not chosen appropriately, leading the system to voltage collapse or on the other hand to very over-sized security margins. Moreover, some types of loads such as electric heating are especially critical for voltage stability because of their recovery characteristic.*

Part I of this thesis investigates the effect of voltage dependent loads in the determination of transfer limits and stability limits. PV curves show that a system reaches its stability limit at the nose of the curves when the load is defined as constant power, but this point is located further below the nose for voltage dependent loads. The investigation has been carried out firstly on a four bus ideal case and secondly on a security assessment of the Nordic 32 test system.

.

Chapter 2

Load Modeling

The interest in load modeling has been continuously increasing in the last years, and power system load has become a new research area in power systems stability. Several studies, [IEEEStability 1990], [Taylor 1994], have shown the critical effect of load representation in voltage stability studies, and therefore the need of finding more accurate load models than the traditionally used ones.

Voltage collapse is a phenomenon that in most cases takes several minutes; most of the load modeling work done in the past has been focused on induction machines, critical in the range of some seconds after a disturbance. Other static nonlinear models have been used for analyzing the long-term power system behavior; the load response is then described as a function of voltage [Karlsson and Hill, 1994]. Finding a dynamic model that is able to cover the short and the long-term has been a goal in the last years. Now it is not only important to study the effect of induction motors, but also how tap-changers, spontaneous load variations as well as other components are affecting the stability of the power system [Johansson and Sjögren, 1995]. The idea of using static load models in stability analysis is changing in favor of dynamic load models.

Even though power system load has gained more attention in the last years, it is still considered as one of the most uncertain and difficult components to model due to the large number of diverse load components, to its high distribution, variable composition with time of day and week, weather and through time, and also because of lack of precise information on the composition of the load. Different utilities are available for load forecasting

purposes [Willis, *et al*., 1995], but also new techniques for the determination of the load characteristics from measured composition data have been developed [Dovan, *et al.*, 1987]. The result of these new techniques will lead to a better understanding of the load dynamics and therefore to an improved load representation, making it possible to decrease uncertainty margins, resulting in a positive impact on both economy and reliability of the system operation. Moreover the combination of an accurate load model and a real-time monitoring application will bring up new competitive possibilities for the electricity industry.

2.1 Introduction

Different modeling approaches and types of data for load modeling purposes, are described in this section.

2.1.1 Physical vs. black box models

A model based on fundamental engineering knowledge about the physical phenomena that affect the system is called *physical model*. A basic model based on elementary laws will provide accurate results when simulating, but in case of a high complexity system, the high difficulty in obtaining all the physical laws affecting the system and the specific parameters will make it necessary to develop the model based on empirical laws. When a model is based on the empirical relations between input and output signals, it is called a *black box or empirical model*. Black-box models are thus applied when there is not enough knowledge to create a physical model, or the functioning of the system is very complex, but there is available data to establish a mathematical relation between the input and output measurements of the system.

Physical models, which will be described further in Part II and Part III, have been chosen for the realization of this work.

2.1.2 Data for Load Modeling

Two basic approaches are used to obtain data on composite load characteristics, the measurement-based approach, and the component-based

approach. The *measurement-based approach* involves direct measurements at representative substations and feeders to determine the voltage and frequency sensitivity of the active P and reactive Q load. The data is obtained from measurements in-situ, and includes voltage and frequency variations, and the corresponding variations in active and reactive load, either to intentional disturbances, test measurements, or to natural events, normal operation data. By fitting the measured data to a model, the parameters of that load model are identified. Such an approach is sometimes called gray-box modeling, since a structure of the model is assumed. The techniques used for the determination are related to the complexity of the chosen model and the characteristics of the field measurements. The main advantage of using a measurement-based approach is the high availability of actual data from the system under study, and the possibility to track seasonal variations but also deviations from normal operation. On the other hand, this approach implies economical investment in appropriate equipment for carrying out the measurements and monitoring the most important loads in the system.

The component-based approach involves developing a composite load model [Taylor, 1994] from information on its constituent parts, i.e., mix of classes at the substation, composition of each of those classes, and main characteristics of each single load component. The *load class mix data* describes which is the percentage of each of several load classes such as industrial, residential and commercial, to the load consumption at a specific bus of the system. The *load composition data* describes the percentage of each load component, such as electric heating, air conditioner, induction motors to the active consumption of a particular load class, and the *load characteristic data* is related to the physical characteristics of each one of the load components. The main advantages of this method are that it does not require field measurements, it is easier to adapt to different systems and conditions, and to put into use. On the other hand, since the load class mix data varies from bus to bus and is dependent on weather and time, it is necessary to often determine and update the load class mix data for each bus of the system.

In order to get a better description of the load characteristic, it would be optimal to combine both methods. In this thesis the measurement-based approach has been used.

2.1.3 Type of Measurements

The use of *continuous field measurements* provides real-time information of the status of the system. The collection of data involves a continuous monitoring process to store and to present the information in a suitable form, and data post-processing. When the process is limited to data collection and monitoring, the operators must take the control decisions related to irregularities in the system. Other more advanced solutions integrate the on-line information from the acquisition with an automatic control system, and the observations made by the operators. A disadvantage of carrying out these measurements is the implementation and maintenance cost of the equipment.

Off-line data processing provides information from the system corresponding to a period of time previous to the data analysis and processing, which makes it possible to analyze different characteristics of the system, at different places and times, and basically it constitutes rich databases for research purposes. The main disadvantage of these measurements is that the analysis, detection of irregularities in the system and control actions, do not take place in the system, and therefore it is not possible to observe how the system would react to them. Moreover since power system load models show variations in model structure and model parameters due to different system and environment conditions, the quantity of data that needs to be collected off-line is large.

Both measurement techniques can be the result of either *field test measurements* or measurements from *normal operation*. The use of normal operating data is advantageous from a technical and economical point of view. The alternative of running a test involves alterations in the normal operation of the system and inconvenience for the customers. The need for manpower further results in very expensive tests. From a technical point of view, normal operation data will not only describe a specific phenomenon, but also the effect of all the dynamics that are acting on the system.

Off-line processing of data both from field test and normal operation data have been used in obtaining the results of this thesis.

2.2 Load Characterization

This section introduces different load types that are present in an aggregated load. Typical types of load are described and various compositions are mentioned.

2.2.1 Load Types

According to the description presented in the previous section, the load composition of a particular area is characterized by the load class data, the composition of each one of the classes, and the characteristics of each single load component. The load class data is often grouped in industrial, residential, commercial and agricultural load data. An *industrial load* is mainly related to industrial processes, and most of the load corresponds to motors, up to 95%. Heavy industries may include electric heating processes such as melting. A *residential load* includes most of the devices related to housing habits, but also a large percent of electric heating and air conditioner units during winter and summer respectively. A *commercial load* corresponds to air conditioner units and a large percent of discharge lighting, and an *agricultural load* to induction motors for driving pumps.

In general the different load components that constitute the different load classes can be classified into loads with 'fast dynamics' such as induction motors, loads with 'slow' characteristics such as electric heating, loads with high sensitivity to voltage excursions such as motors and some types of lighting (they may trip or extinguish for some voltage levels), and loads whose response to voltage faults do not present significant discontinuities. A brief description of some load components [Taylor, 1994], [Agneholm, 1999], [Kundur, 1994], [IEEELoad, 1993] such as induction motors, street lighting, electric heating and on load tap changers (LTCs), follows in this section.

Induction Motors

A large amount of power consumption goes to induction motors in residential, commercial and industrial areas. A common use of motors in

residential and commercial areas is for the compressors of air conditioning and refrigeration. These loads require nearly constant torque at all speeds, and are the most demanding from a stability point of view. On the other hand, pumps, fans and compressors account for more than half of the industrial motor use. Typically motors consume 60 to 70 % of the total power system energy and their dynamics are important for voltage stability and long-term stability studies.

Lighting

Mercury vapor, sodium vapor and fluorescent lamps constitute the main kind of lighting used in industry and street lighting, and correspond to a large percent of the load composition in commercial areas. They are very sensitive to voltage variations, since they extinguish at about 80% voltage. *Mercury devices* are based on the operation of an electric discharge, i.e. when a mercury lamp is switched on it is characterized by a weak blue illumination, that will change into lighter white as long as the pressure and temperature increase. This process takes between 2 and 5 minutes to stabilize, and during that time the consumption corresponds to 40 to 50 % of the stationary value. After a lamp has been switched off, it needs some time, glowing time, to cool down before the discharge can be re-ignited and then restarted.

Sodium lamps work in the same way as mercury lamps. Since they work at higher pressure and temperature, the quality of the illumination is better, and the glowing time is shorter. *Fluorescent lamps* are the most common type of light used in offices, supermarkets, and in general in commercial areas because of their low production cost, and high efficiency to produce light. Just some seconds after the lamp is turned on, the power consumption reaches more than 90 % of its steady state value.

Thermal Loads

A large percent of loads in residential, (water heaters, ovens, electric heating), and in industrial areas, (soldering and molding machines, boilers), behave similar to a constant resistance in the short-term. Right after a voltage drop the possible variations from power in the input of the device hardly affect the temperature and therefore the resistance characteristic. After some seconds, and since the heat production has decreased, the ‘on

cycle' of the thermostats in thermal loads will be prolonged in order to recover the temperature. Under low voltage conditions the temperature will then increase slower than under normal conditions during the 'on cycle' of the thermostat. On the other hand, those thermostats that are in the 'off cycle' will not respond to the voltage drop until they enter in the 'on' period, and therefore the temperature will drop to the same rate during the 'off cycle'.

When the voltage is low the thermostats are mainly working on the 'on cycle' all the time, and therefore the load consumption is similar to the one under normal conditions. This type of load behaves as a constant power load in the long-term. In case of extreme weather conditions, as on a cold winter day, the full restoration of the temperature may be impossible since the thermostats are already working 100 % in the 'on cycle'.

Load Tap Changers

Load tap changer transformers do not correspond to a load component, but seen from the transmission system they may be considered as part of the load. After a disturbance, they restore the secondary side voltages to their pre-disturbance values, but they also affect the status of the voltage sensitive loads. The restoration of the voltage, and consequently the increase of these loads may lead the system to voltage instability and collapse. The restoration process takes several minutes.

2.2.2 Load Composition

The composition of the load is strongly dependent on the time of day, month and season, but also on weather. In cold countries the winters are characterized by high load consumption mainly related to electric heating, while during the summer the consumption is low and hardly affected by the small percent of air conditioner units. In warmer countries the situation is the opposite, and it is during the summer when the load consumption reaches the highest values due to connection of air conditioning loads. Both air conditioning and electric heating loads vary seasonally.

Weekday consumption is mainly dominated by industrial and commercial loads. The industrial processes may also correspond to evening hours and weekend days. The commercial load consumption varies mainly when comparing weekdays and weekend, and the larger demand corresponds to the working hours.

2.3 Standard Load Models

A model is a set of equations that describes the relationship between the input and output of a system. In the case of load modeling this mathematical representation is related to the measured voltage and/or frequency at a bus, and the power consumed by the load, active and reactive. Due to the high diversity and distribution of power system loads, several alternatives have been proposed trough out the time for their representation, depending on their main purpose. The main classification is in static and dynamic models. A *static load model* is not dependent on time, and therefore it describes the relation of the active and reactive power at any time with the voltage and/or frequency at the same instant of time. On the other hand, a *dynamic load model* expresses this relation at any instant of time, as a function of the voltage and/or frequency time history, including normally the present moment.

The static load models have been used for a long time for both purposes, to represent static load components, such as resistive and lighting loads, but also to approximate dynamic components.

2.3.1 Static Load Models

Common static load models for active and reactive power are expressed in a polynomial or an exponential form, and can include, if it is necessary, a frequency dependence term, [IEEELoad, 1993], [IEEELoad, 1995]. A brief description of some of these models follows:

ZIP model or polynomial model

The static characteristics of the load can be classified into constant power, constant current and constant impedance load, depending on the power relation to the voltage. For a constant impedance load, the power

dependence on voltage is quadratic, for a constant current it is linear, and for a constant power, the power is independent of changes in voltage. The *ZIP model*, equations (2.1) and (2.2), is a *polynomial model* that represents the sum of these three categories:

$$P = P_o\left[a_1\left(\frac{V}{V_o}\right)^2 + a_2\left(\frac{V}{V_o}\right) + a_3\right] \tag{2.1}$$

$$Q = Q_o\left[a_4\left(\frac{V}{V_o}\right)^2 + a_5\left(\frac{V}{V_o}\right) + a_6\right] \tag{2.2}$$

V_o, P_o and Q_o are the pre-disturbance conditions of the system, and the coefficients a_1 to a_6 are the parameters of the model.

Exponential Load Model

Equations (2.3) and (2.4) express the power dependence, as a function with a non-integer exponent.

$$P = P_o\left(\frac{V}{V_o}\right)^{np} \tag{2.3}$$

$$Q = Q_o\left(\frac{V}{V_o}\right)^{nq} \tag{2.4}$$

The parameters of this model are n_p, n_q, and the values of the active and reactive power, P_o and Q_o, at the initial conditions. Common values for the exponents of the model [Taylor, 1994], [Le Dous, 1999], for different load components are included in Table 2.1.

For the special case, where n_p or n_q are equal to 0, 1 and 2, the load model will represent a constant power, constant current or constant impedance load respectively.

Load Component	n_p	n_q
Air Conditioner	0.50	2.50
Resistance Space Heater	2.00	0.00
Fluorescent Lighting	1.00	3.00
Pumps, fans other motors	0.08	1.60
Large industrial motors	0.05	0.50
Small industrial motors	0.10	0.60

Table 2.1: Common values for the exponents n_p and n_q, for different load components.

Frequency Load Model

The exponential load model can also include frequency dependency, by multiplying the equations by the factor of the form (2.5):

$$[1 + A(f - f_o)] \tag{2.5}$$

f_o and f are the rated frequency and the frequency of the bus voltage, and the parameter A represents the frequency sensitivity of the model.

Induction Load Model

A simplified induction motor model can be obtained from the scheme in Figure 2.1.

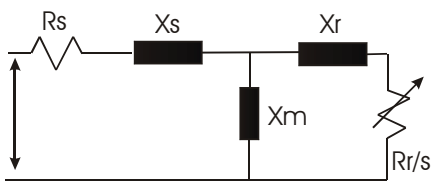

Figure 2.1: Equivalent scheme of a steady state induction motor**.**

R_s, R_r, X_s and X_r are the stator and rotor resistances and reactances respectively. X_m is the magnetizing reactance, and s is the slip of the motor. The stator flux dynamics are normally neglected in stability analysis, and the rotor flux in long-term analysis. Figure 2.2 shows the transient state equivalent circuit, where the induction motor is modeled by a transient emf E' behind a transient impedance X' [Taylor, 1994].

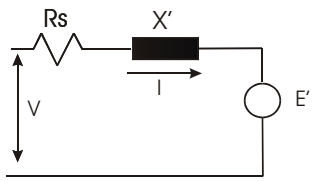

Figure 2.2: Equivalent scheme of a transient-state induction motor.

2.3.2 Dynamic Load Models

When the traditional static load models are not sufficient to represent the behavior of the load, the alternative dynamic load models are necessary. The parameters of these load models can be determined either by using a measurement-based approach, by carrying out field measurements and observing the load response as a result of alterations in the system, or by using a component-based approach; first by identifying individual load characteristics and then by aggregating them in one single load. The literature for dynamic load models is quite large depending on the results from different field measurements and their purposes [Lin, *et al.*, 1993], [Ju *et al.*, 1996], [Lian *et al.*, 1998], [Karlsson, 1992]. The main interest of this thesis is related to exponential dynamic load models, and more specifically to [Karlsson and Hill, 1994].

2.4 Exponential Dynamic Load Model

Due to the large amount of electrical heating loads in Sweden and its critical effect on voltage stability [Karlsson and Hill, 1994] have proposed a load model with exponential recovery. The model is presented below, as a set of non-linear equations, where real (active) and reactive power have a non-linear dependency on voltage.

$$T_p \frac{dP_r}{dt} + P_r = P_o \left(\frac{V}{V_o} \right)^{\alpha_s} - P_o \left(\frac{V}{V_o} \right)^{\alpha_t} \tag{2.6}$$

$$P_l = P_r + P_o\left(\frac{V}{V_o}\right)^{\alpha_t} \tag{2.7}$$

The V_o and P_o are the voltage and power consumption before a voltage change. P_r is the active power recovery, P_l is the total active power response, T_p is the active load recovery time constant, α_t is the transient active load-voltage dependence, and α_s is the steady state active load-voltage dependence. Similar equations are also valid for reactive power. Figure 2.3 shows the meaning of equation (2.6) and (2.7), when an ideal voltage step is applied.

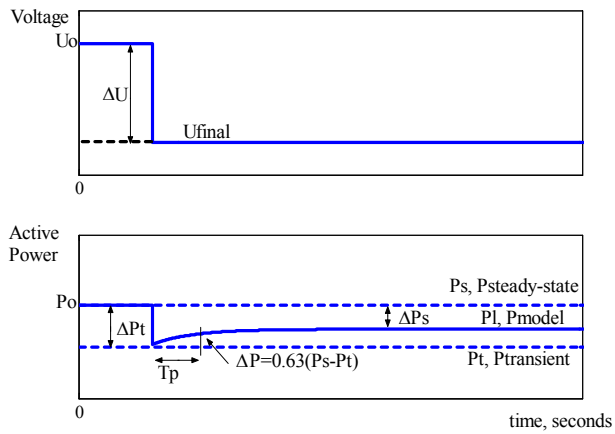

Figure 2.3: Load response under a voltage step, from the *Uo*-level.

The load behavior is thus characterized by a time constant, and a transient and steady state load-voltage dependence parameters. T_p represents the time that the power recovery needs to reach 63% of its final value, α_s or the steady state load-voltage dependence quantifies how much load has been restored after the recovery; a value equal to 0 means a fully restored load, while a different value indicates partly restored load. Furthermore, the parameter α_s, steady state voltage dependency, may present negative values. The stationary level reached by the load after the recovery is then higher than the expected one, resulting in an overshooting in the load. α_t or the transient load-voltage dependence, describes how the load behaves at the disturbance moment. If α_t is equal to 0, the load behaves as constant power,

if it is equal to 1 the load behaves as constant current, and if it is equal to 2 as constant impedance.

Chapter 3

Voltage and Load Stability

The on-going changes in the electricity industry are resulting in new features of the power systems, which are characterized by complex interconnections, and the utilization of a large variety of controllers for optimizing the system operation and the use of the available sources. The degree of complexity of the system, the nature of its dynamics, and the effect of external factors interacting simultaneously require special attention, in order to provide proper planning and design.

A power system must provide high supply reliability at minimum cost and ensure minimum impact on the environment. In order to avoid inconvenience to the customers and severe technical problems which will lead to expensive costs, the system must be able to meet the frequent variations in active and reactive load. High level of system security, availability of 'spinning' reserve of active and reactive power, high quality in the design of the system components and availability of different paths for the delivery of the energy are some of the factors that can help to ensure this reliability [Machowski, *et al*., 1997].

Voltage stability and the impact of the load representation in stability studies, is described throughout this chapter. Section 3.1 introduces the Swedish power system as an integrated part of the Nordel system. A general classification of power system stability is introduced in section 3.2. Definitions of voltage stability and instability are also included. Throughout section 3.3 the transfer capacity of the system and the transfer limiting factors are studied. PV curves are introduced for the determination of the maximum transfer power of the system. The influence of the load

characteristic on voltage stability is described and the use of dynamic models for the representation of the load is motivated.

3.1 The Swedish Power System

The Swedish power system is integrated into a more complex system, denominated Nordel [Nordel, 2001], that comprises the interconnected power systems of Norway, Sweden, Finland and parts of Denmark (see Figure 3.1). Denmark is divided in two separate grid areas. Jutland/Funen is connected to the Continental grid, and Zealand to the Nordic grid. Both areas joined the open Nordic market in 2000. The Nordel organization was created in 1963 and it constitutes a union for electricity cooperation in the Scandinavian countries. Several AC connections exchange energy between Sweden, Norway, Finland and Zealand (East part of Denmark), while the West part of Denmark and the Polish and German networks are connected to the system through HVDC links. Even though there are common regulations between these countries, every individual system is characterized by structural differences.

The main purpose of the system is to guarantee the power system operation with high reliability and at low cost. Moreover, the system controls and regulates the available transfer capacity, power balance in each country, and the possibility of exchange included in that balance.

The Swedish power system is characterized by a concentration of consumption in the southern part of the country, while the generation area is in the North. Even though the use of renewable energies such as wind power has gained interest in the recent years, still most of the generation is hydro and nuclear power. The transmission system is extended across the country from North to South, connecting the generation and load areas though a meshed system with voltage levels of 400 kV, 220 kV and 130 kV, to deliver the electricity to the consumption areas. The distribution system topography is typically radial with voltage values of 50 kV and 20 kV. A factor limiting the N-S transfers is voltage stability.

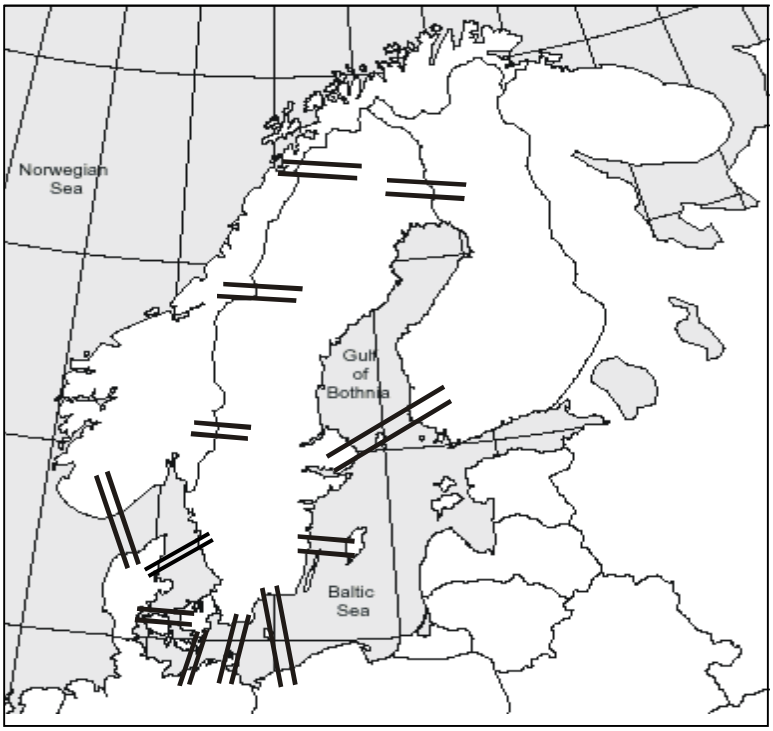

Figure 3.1: Outline of the Nordel Power System.

3.2 Voltage and Load Stability

Power system stability can be defined according to [IEEEStability, 2004]: *'The ability of an electric power system, for a given initial operating condition, to regain a state of operating equilibrium after being subjected to a physical disturbance, with most system variables bounded so that practically the entire system remains intact'*. Figure 3.2 shows its classification into angle, voltage and frequency stability [IEEEStability, 2004].

The capability of the system to keep synchronism in interconnected machines is defined as *'rotor angle stability'*. Small disturbances, *'small-*

disturbance (or small-signal) rotor angle stability', result in undamped electromechanical oscillations due to insufficient damping torque, while larger disturbances, *'large-disturbance rotor angle stability or transient stability'*, may lead to lack of synchronizing torque. The time frame for angle stability is denominated short-term time scale and it is approximately in the order of a few seconds.

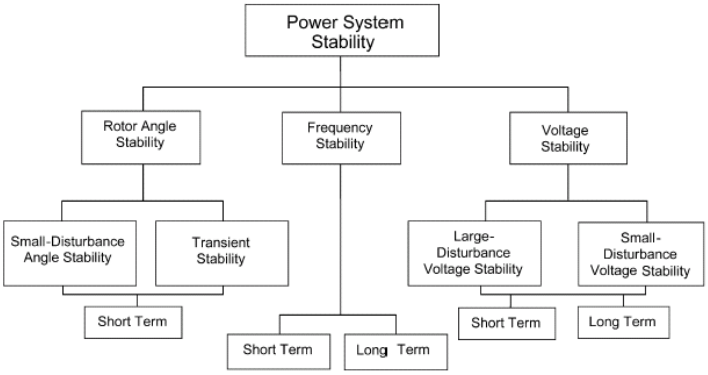

Figure 3.2: Classification of power system stability.

'*Frequency stability*' problems are the result of power imbalance between generators and loads after a large disturbance, and can result in system islanding. Frequency stability refers to the ability of maintaining steady frequency following a severe disturbance. Frequency-stability can be classified into *'short and long-term stability'*.

'Voltage stability' is defined as the ability of a power system to maintain steady acceptable voltage at all buses in the system at normal operating conditions, and after being subjected to a disturbance. It is thus a characteristic of the power system to remain in equilibrium under normal conditions, and to react, restoring the status of the system to acceptable conditions after a disturbance, i.e. the voltage after a disturbance is restored to a value close to the pre-disturbance situation. When the voltage in the system is uncontrollable and continuously decreases due to failures in the design, external factors, variations in load or inappropriate voltage control devices, the system becomes unstable and enters in the stage of voltage instability.

According to CIGRE definitions [CIGRE, 1993], '*voltage instability is the absence of voltage stability, and results in progressive voltage collapse (or increase)*'. The main reason to lead a power system to an unstable situation and therefore to instability, is the incapacity of satisfying the reactive load demand under heavily stressed conditions, to keep voltage at acceptable levels. Voltage collapse follows voltage instability, and it is often the result of the action of voltage control devices, load tap changers, the voltage dependence characteristic of the load, the generator reactive power limits or the combination of several of them. Voltage collapse leads the system to low-voltage values in a large part of the power system, and therefore to partial or total collapse.

According to IEEE definitions [IEEEStability, 2004], *'voltage collapse is the process by which the sequence of events accompanying voltage instability leads to a blackout or abnormal low voltages in a significant part of the power system'*.

Voltage stability is often denominated load stability; the load characteristic and its dynamics indicate the dependency between the load and the voltage. A voltage drop will initially result in decay in load, but after few seconds, a load restoration process will start. The restoration can lead to heavily loaded conditions, and to voltage instability and voltage collapse if under those conditions, appropriate control decisions are not taken, and/or the system is not able to meet the reactive load demand.

Voltage stability can be classified into *'large- and small-disturbance voltage stability'*. The *'large-disturbance voltage stability'* occurs in a time frame of about a few seconds up to tens of minutes, and refers to the ability of the system to maintain steady voltages following large disturbances such as system faults and loss of generation, which depends on the system and load characteristic, and the interaction of controls and protections. On the other hand, the *'small-disturbance voltage stability'* refers to the ability of maintaining steady voltages during small disturbances such as incremental changes in system load, and depends on the load characteristic, and the controls at a given instant.

Voltage stability can be also classified into *'short-term and long-term voltage stability'* since it covers a time frame that varies from a few seconds

up to tens of minutes. The *'short-term voltage stability'* describes the dynamics of components such as induction motors, electronically controlled loads, static Var compensators, and excitation of synchronous generators. When the dynamics of the system corresponds to slower equipments such as tap-changing transformers, thermostatically controlled loads and generator current limiters, the stability is denominated '*long-term voltage stability'*.

3.3 Transfer Limits

In this section voltage stability and particularly the limits for voltage collapse are discussed. PV curves are defined. It is also shown that the load representation will have a significant influence on the voltage stability computations.

3.3.1 Introduction

The Swedish power system is integrated into a more complex interconnected system denominated Nordel. A system of these characteristics is often subjected to risk from many disturbances that may lead it to heavily loaded conditions, and consequently closer to its transfer capacity limits. It is a challenge to increase the transfer capacity, which is very much related to congestion management and power transfer limits, while maintaining high system security.

As an example, Figure 3.3 shows a problem concerning stability limits. Three criteria are usually considered in the calculation; the thermal capacity limits, the voltage stability limits, and the angle stability limits. The secure operation area is defined by these limits. However, transfer limits are generally difficult to determine with sufficient accuracy and reliability, due to the high uncertainty related to internal and external factors, and therefore conservative criteria are often used for their determination, which results in smaller secure operation areas.

Figure 3.3 shows both transfer limits but also margins. Note that by defining security margins, the secure operation area is reduced.

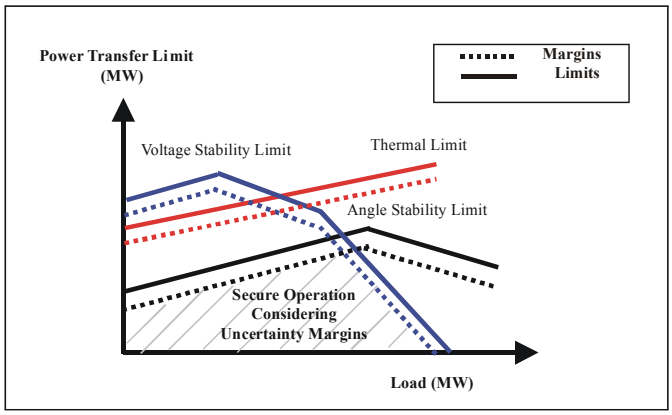

Figure 3.3: Power Transfer Limits operation with uncertainty margins [Uhlen, *et al.*, 2002].

3.3.2 Static aspect of voltage stability

The determination of the maximum amount of power that a system can supply to a load will make it possible to define the voltage stability margins of the system, and how they can be affected by for example connection and disconnection of loads, or as a result of dynamic events. The PV or nose curve, [Taylor, 1994], corresponds to the graphical representation of the power-voltage function at the load bus, (see Figure 3.4).

The PV curves are characterized by a parabolic shape, which describes how a specific power can be transmitted at two different voltage levels, high and low voltage. The desired working points are those at high voltage, in order to minimize power transmission losses due to high currents at low voltages. The vertex of the parabola determines the maximum power that can be transmitted by the system and it is often called the point of maximum loadability or point of collapse.

The simplified system in Figure 3.5 has been used to determine the analytical expression for the load-voltage function, and its PV implementation (Figure 3.4).

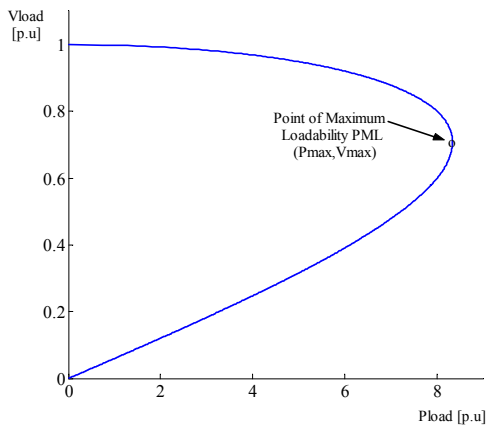

Figure 3.4: Nose curve. Representation of the power-voltage function for the system in Figure 3.5.

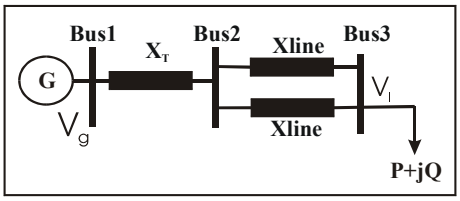

Figure 3.5: Three bus simplified transmission system.

The generator is assumed to have a constant voltage, V_g, equal to 1 p.u. The equivalent reactance for the transformer, X_T, is equal to 0.01 p.u, and through bus 2 it is connected to two parallel lines, both with a transmission reactance of 0.1 p.u, and zero line resistance. Through bus 3 the two lines are connected to the load, which is defined by a pure active load, nominal reactive load equal to zero and constant power factor, $cos\phi$, equal to 1. Equations (3.1) and (3.2) define the active and reactive power that can be transmitted to Bus 3:

$$P_l = \frac{V_g \cdot V_l}{Xeq} \cdot \sin(\theta_g - \theta_l) \tag{3.1}$$

$$Q_l = \frac{V_g \cdot V_l}{X_{eq}} \cdot \cos(\theta_g - \theta_l) - \frac{V_l^2}{X_{eq}} \tag{3.2}$$

V_g, θ_g, V_l and θ_l are the voltages and angles at the generator and load buses respectively. X_{eq} is the equivalent reactance of the system. By combining both equations, equation (3.3) is obtained. Taking into account the relation defined by equation (3.4), the power-voltage function is given by equation (3.5).

$$P_l^2 + \left(Q_l + \frac{V_l^2}{X_{eq}}\right)^2 = \left(\frac{V_g \cdot V_l}{X_{eq}}\right)^2 \tag{3.3}$$

$$\tan\phi = \frac{Q_l}{P_l} \tag{3.4}$$

where the subscript l refers to the load

$$P_l = \frac{V_l^2}{X_{eq} \cdot \left[1 + (\tan\phi)^2\right]} \cdot \left[-\tan\phi + \sqrt{-1 + \frac{\left[1 + (\tan\phi)^2\right] \cdot V_g^2}{V_l^2}} \right] \tag{3.5}$$

The vertex of the parabola, *point of maximum loadability*, is often named point of collapse, but this denomination is no longer true if the load is represented with a characteristic other than constant power. A study on the location of the voltage stability limit for voltage dependent load is included further in Chapter 4. The operating point corresponding to the maximum loadability is calculated by determining the maximum of the function defined in equation (3.5), i.e. the derivative of P_l with respect to V_l equals to zero. This point is thus given by equations (3.6) and (3.7):

$$V_{\max} = \frac{V_g}{\cos\phi} \cdot \sqrt{\frac{1 - \sin\phi}{2}} \tag{3.6}$$

$$P_{\max} = \frac{V_g^2}{2 \cdot X_{eq} \cdot \cos\phi}(1 - \sin\phi) \tag{3.7}$$

When the point of collapse is reached, the system becomes unstable, and the voltage starts decreasing quickly since the reactive support of the system under these heavily loaded conditions is not enough. Figure 3.6 shows the PV representation for different values of *tan* ϕ. By local reactive compensation it is possible to increase the transfer capacity of the system, but at the same time the system operates closer to the security margins, since the point of collapse is placed closer to acceptable voltages.

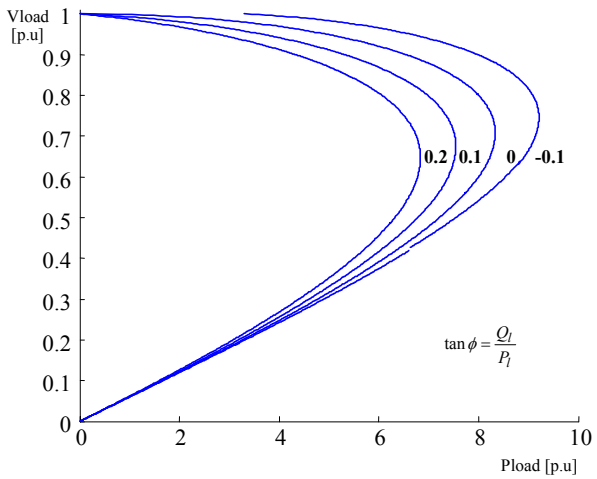

Figure 3.6: PV curves for different load compensation cases. $tan\phi$ equal to 0.2, 0.1, 0 and –0.1.

3.3.3 Influence of the load characteristic on voltage stability

The effect of the load representation on voltage stability is studied in this section. The main objective is to prove that under the same conditions in the system, the load representation will affect the location of the operating point in the PV curves, leading the system closer to or further away from the collapse point. An optimistic design may lead the system to voltage collapse under severe conditions, while a conservative design will ensure the delivery of energy due to larger security margins. The importance of using dynamic load models instead of static ones in stability studies is also discussed throughout the section.

Static and dynamic characteristic of the load

In order to analyze the effect of power loads on voltage stability, it is necessary to study both the static and the dynamic characteristic of the load. Equation (3.8) describes the voltage sensitivity, given by the parameter α, for general static models in exponential form:

$$P_s = P_o \left(\frac{V}{V_o} \right)^{\alpha} \tag{3.8}$$

Constant impedance, constant current and constant power characteristics are obtained by using the typical values of α equal 2, 1 and 0. To describe the dynamic characteristic of the load, a non-linear dynamic load model with exponential recovery has been chosen [Karlsson and Hill, 1994]. The model, which has been described in the previous chapter by equations (2.6) and (2.7), is characterized by three parameters; α_s is the steady state active load-voltage dependence, α_t is the transient active load-voltage dependence and T_p is the active load recovery time.

Figure 2.3 has shown the response of the load when a disturbance is affecting the system. In this case an ideal voltage step has been applied. The response of the load can be divided into a transient characteristic, $P_t(V)$, right after the disturbance, and a steady state characteristic, $P_s(V)$, after the recovery, [Hill, 1993] and [Karlsson, 1992]. Expressions for both characteristics, steady state and transient, are given by equations (3.9) and (3.10) respectively. This model is further studied in Part II.

$$P_s(V) = P_o \left(\frac{V}{V_o} \right)^{\alpha_s} \tag{3.9}$$

$$P_t(V) = P_o \left(\frac{V}{V_o} \right)^{\alpha_t} \tag{3.10}$$

Dynamic aspects of voltage stability

The stability of the system described in Figure 3.5 is studied now, when a disconnection of one of the parallel lines has occurred. Figure 3.7 shows a simplified scheme of the transmission system under these new conditions.

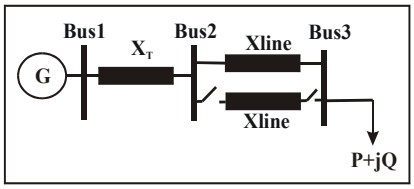

Figure 3.7: Line disconnection on a simplified three-bus transmission system.

Figure 3.8 shows a PV representation of the pre-disturbance, curve (1), and post-disturbance situation, curve (2). The disconnection of one of the lines reduces the maximum amount of power that can be transmitted by the system. The total reactive consumption in the transmission system is higher and the voltage in the load bus has decreased.

The static load characteristic for different values of α, voltage sensitivity, is also shown. Since equations (3.8) and (3.9) have the same form, the exponent that describes the power-voltage dependency will be referred to as the parameter α. For a typical case where the load power is not affected by the voltage, constant power, the parameter is equal to 0. Those values, which are higher than 0, express load-voltage dependency. As exemplified in the figure, the larger this parameter is, the further the new operating point is from the PV nose. For a static representation, this parameter expresses the load-voltage dependency. For a dynamic representation, the exponent is associated with the long-term characteristic of the load. Those values larger than zero correspond to partial restoration of the load to its pre-disturbance value.

The negative values of the parameter are associated with the long-term dynamic restoration of the load, and the effect of discrete tap changers [Karlsson, 1992], i.e. by action of tap changers the voltage in one of the sides of the controlled transformer is regulated to an acceptable value. Since the load representation is voltage sensitive, the load is increasing at the same time as the voltage. If the regulation of the voltage is discrete, there is a possibility of overshooting in the voltage and therefore in the load, which

means that the steady state value for the load will be higher than the pre-disturbance one. The larger the negative value is, the larger is the overshoot in power, indicating that the system is closer to the voltage stability limits. Figure 3.8 shows a situation when α_s is equal to –0.5. This is unstable since the curves do not intersect.

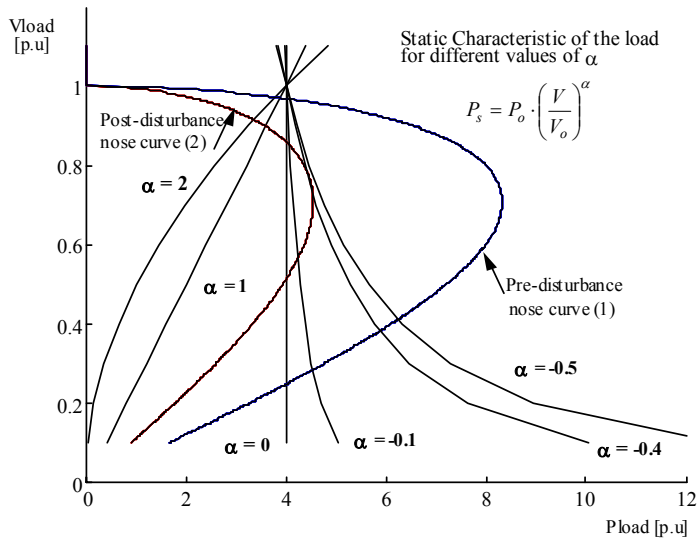

Figure 3.8: Influence of the static load characteristic on PV curves when the disconnection of a parallel line has occurred. The load characteristic is shown for α equal to 2, 1, 0, -0.1, -0.4 and -0.5.

Figure 3.8 has shown how the load representation affects voltage stability and the location of the new operating points, further or not to the collapse point, after a disturbance. From a planning and operating point of view the difference between these new operating points is important. The traditional way of representing power loads in voltage stability studies is by using static models, and in many cases, assuming a constant power characteristic because of the use of tap changers for voltage regulation, [IEEEStability, 2002]. The fact that loads are generally voltage dependent is a critical aspect of voltage stability studies. Figure 3.9 shows a case where the voltage sensitivity of the load helps the stability of the system, by providing

some system relief. This figure corresponds to the case described in Figure 3.7, when one parallel line is disconnected.

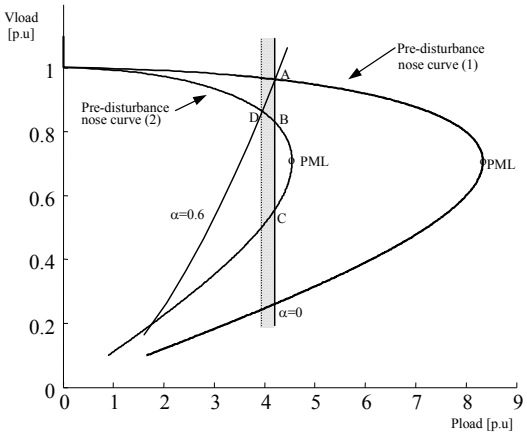

Figure 3.9: Influence of the static load characteristic on PV curves, voltage dependent, $\alpha=0.6$, and voltage independent, $\alpha=0$, when the disconnection of a parallel line has occurred. A shaded area marks the exceeded security margins. PML = point of maximum loadability.

By using a constant power representation in power flow calculations, the voltage solution will correspond to the points A and B, before and after the disturbance. However, since most power loads are voltage dependent the load-voltage sensitivity, for example for a value of α equal to 0.6, is also shown. The solution is now point D. The difference between these two points D and B is important. The actual situation at D corresponds to less loaded conditions and higher voltage than was predicted by the power flow. In this case, by assuming a constant power characteristic, the impact of the load in the system is over-emphasized and the theoretical transfer capacity is reduced despite increasing security margins, which at the end leads to a poor utilization of the system.

Electric heating, which shows a thermostatic effect, is a special load to take into account. When a disturbance is affecting the system and the voltage is reduced, the drop in power consumption of the individual loads activates the thermostats in order to keep the loads connected longer, i.e. on an aggregated base this means that more electric heating is connected at the same time yielding a higher load. The global effect in load is to increase the

nominal load to a level close or equal to the pre-disturbance one, at the post-disturbance voltage. In the case of electric heating loads, this situation is more critical during the winter than the summer, especially in cold countries. The behavior of these loads is well described by equations (2.6) and (2.7). The effect of the thermostat characteristic is important to consider in long-term simulations, and in those areas where most of the load is of this type and a significant number of on-load tap changers. The dynamic representation of this type of load is characterized then, by a transient part, and a long-term part. The change in the characteristic, and the recovery time from the transient state to the steady state is critical in voltage stability [IEEEStability, 2002].

Figure 3.10 shows an ideal voltage step in an area where most of the load is electric heating, and both load responses, A) a dynamic model with partial recovery to constant current, and B) a static model with a constant current characteristic.

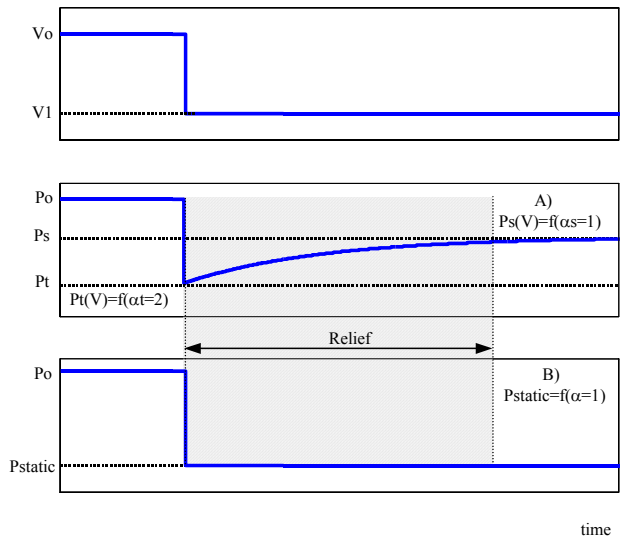

Figure 3.10: Load response under a voltage drop in an area where most of the load corresponds to electric heating. A) Dynamic representation of the load, B) Constant current representation.

A constant current characteristic is a typical representation for the load in wintertime. By using a static model it has been assumed that the load behaves as a constant current. In reality, the drop in voltage will reduce the power load. The reduction will activate the thermostats for longer time and this will result in the increase of the aggregated load consumption to a value close or equal to the pre-disturbance conditions. The resulting operating point is more critical than the one predicted by the static model, since the load demand is higher, and this may bring the system to a severe situation. However, during the recovery time *T*, there is a relief in load, and by taking an effective and quick action the stability of the system may be maintained

Figure 3.11 shows again the situation described in Figure 3.7. The load is mainly electric heating.

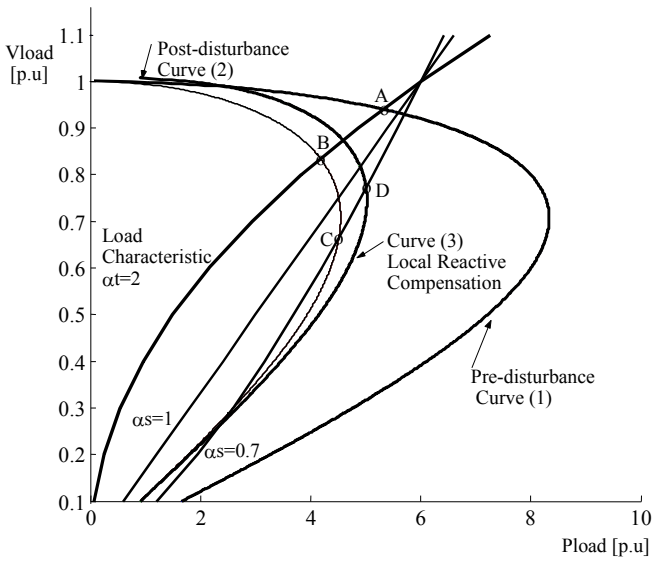

Figure 3.11: Influence of the thermostatic characteristic of electric heating loads on voltage stability. Curves (1), (2) are the pre- and post-disturbance curves respectively, and curve (3) corresponds to the system transfer capacity when local reactive support is used.

The pre-contingency system was operating at the intersection of the load characteristic curve and the pre-disturbance PV curve, point A, with a voltage of 0.92 p.u and a power transfer of 5.3 p.u. After the disturbance,

the system has moved to the point B, with voltage equal to 0.85 and power transfer equal to 4.2 p.u. At this point the voltage has dropped. Also the load demand has decreased, since the load-voltage sensitivity has resulted in a relief in load. However, the thermostatic characteristic of the electric heating will tend to increase the actual load to the pre-disturbance nominal value. The load characteristic will start changing towards a constant power characteristic, (α moving towards zero). The intersection of the new curves with the post-disturbance PV curve will lead the system to very low voltage operating points and eventually to a voltage collapse, point C. During the transition it is possible to take some corrective actions in order to move the operating point to a stable situation in the upper part of the new curve, point D. Some of these actions are local reactive compensation of the load, (Figure 3.11), load shedding, or the start of small-scale gas turbines.

3.4 Conclusions

The effect of the load representation on voltage stability has been studied. Under the same conditions in the system, the load representation affects the location of the operating point in the PV curves, leading the system closer to or further away from the collapse point. Since the load behavior is critical for the stability of the system, more accurate load models are necessary. The traditional static models are not enough to represent the load dynamics and therefore dynamic load models have been introduced.

Moreover, some types of load such as electric heating are especially critical for stability because of their thermostatic characteristic. After a disturbance in the system, (voltage and power drop), and due to the effect of the thermostats, the aggregated load tends to increase the load to a level close or equal to the pre-disturbance one, at the low voltage. This situation may result in severe conditions for the system operation. However, during the recovery time it may be possible to take some corrective actions such as local reactive compensation, load shedding, or the start of small-scale gas turbines, which may lead the system to stable operating points instead.

Chapter 4

Limits for Voltage Dependent Loads

The load representation is critical for the determination of transfer limits. PV curves have shown that a system reaches its stability limit at the nose of the curves when load is defined as constant power, but this point is located further below the nose for voltage dependent loads. Therefore an interesting task is to investigate the maximum power that can be transferred from the system to the load for different load characteristics, and if those operating conditions coincide or not with the stability limit of the system. For voltage dependent loads, the stability limit and the maximum power transfer capability that a system can transfer do not coincide. In a PV curve representation, the stability limit moves below the nose, to the lower part of the curve, and its location depends on the load composition. The bifurcation theory is a useful technique for understanding the voltage collapse phenomenon [Cutsem and Vournas, 1998], [Begovic and Phadke, 1990], [Kwatny, *et al*., 1986], [Dobson and Chiang, 1989], [Cañizares, *et al.*, 1992], [Ajjarapu and Lee, 1992], [Gao, *et al.*, 1992].

This chapter introduces some definitions related to stability and bifurcation for ordinary differential (ODE) and differential algebraic (DAE) equations. The bifurcation theory is then applied to an ideal power system to determine its stability limits for different load compositions. Numerical and graphical results are presented. Furthermore a security assessment on the Nordic32 test system is included.

4.1 Determination of Voltage Stability Limits

4.1.1. Mathematical Background: Equilibrium and Stability

Given an ordinary differential equation ODE of the form (4.1), the equilibrium points of the system are given by the solutions of the algebraic equations (4.2), for different values of the parameter vector *p*. *X* and *p* are a state and a parameter vector respectively.

$$\dot{x} = f(x, p) \tag{4.1}$$

$$f(x^*, p) = 0 \tag{4.2}$$

A local stability study of the solutions from equation (4.2), classifies them as stable, asymptotically stable or unstable [Rudin, 1976], [Seydel, 1988]. A solution x^* is stable if all solutions with an initial condition close to x* remain near to x^* for all time. The solution is asymptotically stable when all trajectories with initial conditions close to x^* approach x^* when the time tends to infinity. The solution is unstable for all the other cases. The region of attraction or domain of x*, describes the space *S* such that all trajectories with initial conditions inside *S* will approach an asymptotically equilibrium x^*. This theory can be applied to both linear and nonlinear systems. Given the linear system in (4.3), where there is only one equilibrium point $x^*= 0$, the stability of this solution is studied by calculating the eigenvalues of the matrix A. An equilibrium point is asymptotically stable if all eigenvalues have negative real parts, whereas it is unstable if there is at least one eigenvalue with a positive real part.

$$\dot{x} = Ax \tag{4.3}$$

For nonlinear systems, the number of equilibrium points is not constant, and it may happen that there is one, more than one or no equilibrium at all. Moreover, the fact that there is an equilibrium point does not assure the stability of the entire system. A common solution for determining stability in a nonlinear system is to study the stability of the linearized system around an equilibrium point x^*. By defining increments and differences

(4.4), and applying Taylor expansion of the function f around x^*, the linearized system in equation (4.5) is obtained:

$$\Delta x = x - x^* \tag{4.4}$$

$$\Delta \dot{x} = A \cdot \Delta x \tag{4.5}$$

The matrix A is called the Jacobian of the function f with respect to x evaluated at x^*. By evaluating this matrix it is possible to evaluate the stability of the equilibrium point x^*. Consider a general power system described by a set of n-differential and m-algebraic equations DAE, as the one given by (4.6) and (4.7):

$$\dot{x} = f(x, y, p) \tag{4.6}$$

$$0 = g(x, y, p) \tag{4.7}$$

X is the vector of n-state variables, y is the vector of m-algebraic equations, and p are the k-parameter variables. DAE systems are analyzed using *the implicit function theorem* [Rudin, 1976], which ensures that there is a locally unique, smooth function F, (4.8), that can represent the DAE system, if the Jacobian of the function g_y is nonsingular.

$$\dot{x} = F(x, p) \tag{4.8}$$

$$g_y = (x, y, p) \tag{4.9}$$

For a fixed value of the parameter vector p, the equilibrium points of the system in (4.6) and (4.7) are given by the solutions of (4.10) and (4.11):

$$f(x, y, p) = 0 \tag{4.10}$$

$$g(x, y, p) = 0 \tag{4.11}$$

The stability is then determined by evaluating the unreduced Jacobian matrix of the DAE system in equation (4.13), [Cutsem and Vournas, 1998], [Ajjarapu and Lee, 1992], [Gao, et al., 1992].

$$\begin{bmatrix} \Delta \dot{x} \\ 0 \end{bmatrix} = J \cdot \begin{bmatrix} \Delta x \\ \Delta y \end{bmatrix} \tag{4.12}$$

$$J = \begin{bmatrix} f_x & f_y \\ g_x & g_y \end{bmatrix} \tag{4.13}$$

If the sub matrix g_y is non-singular, the reduced Jacobian matrix can be calculated by eliminating the term Δy. The stability of an equilibrium point of a DAE system for a given value of the parameter vector p depends on the eigenvalues of the Jacobian matrix J.

$$J_R = f_x - f_y \cdot g_y^{-1} \cdot g_x \tag{4.14}$$

4.1.2. Bifurcation Theory in Power Systems

The bifurcation theory is a useful technique to understand voltage collapse. It approaches the behavior of nonlinear systems when abrupt changes in the system response appear following from smooth parameter variation. Depending on the different values of the parameter vector p in equations (4.6) and (4.7), the DAE system may experience changes and bifurcations as defined for the ordinary differential equations. This chapter will only refer to the saddle-node bifurcation (SNB) because of its application in PV curves. A SNB, saddle-node bifurcation, is a point where two branches of equilibrium meet. At the meeting point or bifurcation, the equilibrium becomes a saddle node, and the Jacobian of the function f with respect to x evaluated at that point becomes singular.

In a PV curve representation, the maximum power that a system can transfer to the load coincides with the operating point at the nose of the curve. For constant power load, this point is also coincident with the stability limit of the system, and it is a saddle node. The necessary condition for a saddle-node bifurcation of a DAE system to happen, or for a power system to reach its voltage stability limit, is thus that the unreduced

Jacobian J is singular at the bifurcation point [Cutsem and Vournas, 1998], [Gao, *et al.*, 1992]**.** In traditional voltage stability analysis, the Jacobian matrix of a power system is built without taking the load characteristic into consideration, which increases the complexity of determining voltage stability limits for a load other than constant power. If models for voltage dependent loads are not included in the Jacobian matrix, the information obtained from modal analysis is not enough to determine the location of the stability limit, i.e. the matrix evaluation at operating points located below the PV nose, on the lower part of the curve, will result in negative eigenvalues. In that case, the stability limit will be calculated at the point where the powerflow solution diverges. This approach is not always solid, since it becomes very uncertain to determine whether the divergence of a powerflow on the lower part of the PV curve is due to numerical problems, or because the stability limit has been reached. A better approach is to include the load characteristic into the Jacobian matrix of the system. The study of singularity of the Jacobian matrix will then provide an accurate location of the stability limit for different load compositions.

Case Study

The simplified 4-bus system in Figure 4.1 has been used to study the system voltage stability limits, for different load characteristics at the load bus 3.

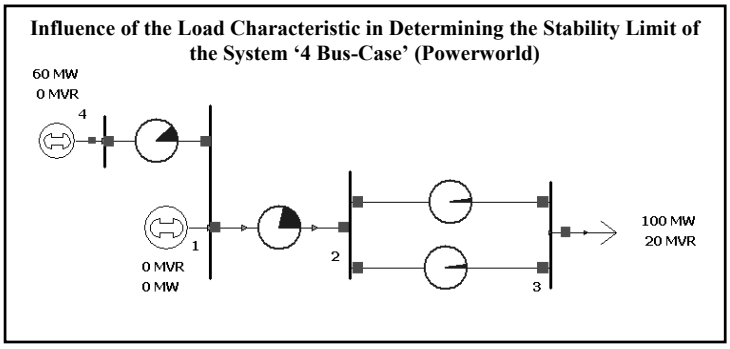

Figure 4.1: Four Bus-case

The system is constituted by four buses: an infinite bus, bus 1, is connected through a transmission line to bus 2, two parallel lines are feeding the load at bus 3, and a PV generator is connected at bus 4. The Jacobian matrix of the system is easily built by using equations (4.15), (4.16) and (4.17), where P and Q are the active and reactive system power vectors, V is the system voltage vector, Y is the system admittance matrix, P_{bus} and Q_{bus} are the total active and reactive power at each bus, P_{lbus} and Q_{lbus} are the active and reactive load at each bus, and P_{gbus} and Q_{gbus} are the active and reactive generation at each bus.

$$[P + jQ] = [V] \cdot [Y]^T \cdot [V]^* \tag{4.15}$$

$$\lfloor P_{bus} + P_{lbus} - P_{gbus} \rfloor = 0 \tag{4.16}$$

$$\lfloor Q_{bus} + Q_{lbus} - Q_{gbus} \rfloor = 0 \tag{4.17}$$

The evaluation of the above equations at each one of the buses results in the following equations:

Bus 4: $[P_4 + \cancel{Pl_4} - Pg_4] = 0$

Bus 2: $[P_2 + \cancel{Pl_2} - \cancel{Pg_2}] = 0$

Bus 1: $[P_1 + \cancel{Pl_1} - Pg_1] = 0$

Bus 3: $[P_3 + Pl_3 - \cancel{Pg_3}] = 0$

The full steady state Jacobian matrix is given by equation (4.18). It investigates the relationship between the incremental change in bus voltage magnitude and the incremental change in bus reactive power injection. The terms $J_{P\theta}$, J_{PV}, $J_{Q\theta}$ and J_{QV} are given by equations (4.19), (4.20), (4.21) and (4.22) respectively, where n is the total number of buses and i represents each one of the buses:

$$J = \begin{bmatrix} J_{P\theta} & J_{PV} \\ J_{Q\theta} & J_{QV} \end{bmatrix} \tag{4.18}$$

$$J_{P\theta} = \left[\frac{\partial P_i}{\partial \theta_n}\right] \quad (4.19) \qquad J_{PV} = \left[\frac{\partial P_i}{\partial V_n}\right] \quad (4.20)$$

$$J_{Q\theta} = \left[\frac{\partial Q_i}{\partial \theta_n}\right] \quad (4.21) \qquad J_{QV} = \left[\frac{\partial Q_i}{\partial V_n}\right] \quad (4.22)$$

The reduced steady state system Jacobian matrix is obtained by making $\Delta P = 0$ in equation (4.23). The resulting expression is given by equation (4.24):

$$\begin{bmatrix} \Delta P \\ \Delta Q \end{bmatrix} = J \cdot \begin{bmatrix} \Delta \theta \\ \Delta V \end{bmatrix} \tag{4.23}$$

$$J_R = J_{QV} - J_{Q\theta} \cdot J_{P\theta}^{-1} \cdot J_{PV} \tag{4.24}$$

The reduced Jacobian matrix of the system represents the linearized relationship between the incremental changes in bus voltage magnitude and bus reactive power injection [Kundur, *et al.*, 1993]**.** Equations (4.25) and (4.26) are general expressions for an active and reactive exponential voltage dependent load representation, ZIP model [IEEEStability, 2002], [Taylor, 1994]**.** The active load composition is given by the parameters *a*, *b,* and *c,* constant power, current, and impedance percent composition respectively. The same is applicable for the parameters *d, e* and *f* for reactive power. P_o, Q_o and V are the active and reactive power levels and the voltage at the load bus respectively. Expressions (4.25) and (4.26) can be directly included in equation (4.16) and (4.17) instead of the variables P_{lbus} and Q_{lbus}. The Jacobian matrix described in (4.18) will then include the load characteristic (Appendix I).

$$P_{lbus} = a \cdot P_o + b \cdot P_o \cdot V + c \cdot P_o \cdot V^2 \tag{4.25}$$

$$Q_{lbus} = d \cdot Q_o + e \cdot Q_o \cdot V + f \cdot Q_o \cdot V^2 \tag{4.26}$$

4.2 Simulations and Results

To carry out the simulations *Voltage Stability software from Powertech Labs* has been used [VSAT, 2000]. The software is useful for determining stability limits and security margins. Modal analysis can be requested, including or not load models in the Jacobian matrix. The stability limits for the 4 bus-case described in Figure 4.1 have been studied for different load compositions, when load models are included in the Jacobian matrix. The program basically builds up PV curves by a continuous increase in load. At each operating point the Jacobian matrix is calculated, and the eigenvalues of the reduced Jacobian matrix are evaluated. At the stability limit the powerflow solution does not converge. If modal analysis is requested, it will be computed at the last stable point before instability is reached. The evaluation of the reduced Jacobian matrix at this point will result in at least one small eigenvalue in the neighborhood of zero**.** Continuation Power Flow method [Seydel, 1988] has been used for determining the lower part of the PV curves when numerical limitations have been found.

The main observations from the simulations are summarized as follows.

- For the general case of a **pure constant PQ load**, the stability limit of the system coincides with the maximum power that can be delivered from the system to the load. This point corresponds to the nose of the PV curve representation. Below this point the actual power delivered decreases with an increase in load demand. Modal analysis at this point results in at least one eigenvalue in the proximity of zero.

- For **pure impedance/current load**, the voltage instability cannot occur. The maximum power delivered to the load at a given power factor is independent of the load type. The system is stable for all the points in the lower part of the PV curves. Modal analysis results in positive eigenvalues for all the solved points of the curve.

- For those cases with a **mixed load composition**, the stability limit has been found to be below the nose of the PV curve, where the load characteristic becomes tangent to the system PV curve, i.e. saddle-node bifurcation. Below this point the system is unstable,

and at least one of the eigenvalues of the reduced Jacobian matrix is negative.

Table 4.1, Table 4.2, and Table 4.3, show the results from modal analysis computation for the case study in Figure 4.1. Three different load compositions have been used: 25% constant PQ and 75% constant current; 25% Constant PQ, 25% constant current and 50% constant impedance; and 25% constant PQ and 75% constant impedance. The tables include voltages and angles at each one of the buses, the corresponding operating point for each modal analysis calculation, the value of the active and reactive power at the load bus for those operating points, and the smallest eigenvalue evaluated at the requested points.

No.	**λi**	**V1 p.u**	**V2 p.u**	**V3 p.u**	**V4 p.u**
2	0.7967	1.000	0.83598	0.56441	1.000
5	0.1160	1.000	0.80952	0.48391	1.000
6	-0.075	1.000	0.80203	0.45972	1.000
θ1	**θ2**	**θ3**	**θ4**	**Pl MW**	**Ql MVar**
0.00	-7.85	-45.09	7.75	228.4	45.7
0.00	-7.56	-50.36	7.88	212.9	42.6
0.00	-7.40	-51.90	7.91	206.7	41.3

Table 4.1: Modal Analysis for the four-bus system where the load is defined as 25% Constant PQ and 75% constant current. λ_i, most positive eigenvalue.

No.	**λi**	**V1 p.u**	**V2 p.u**	**V3 p.u**	**V4 p.u**
5	2.066	1.0000	0.8605	0.6339	1.0000
12	0.099	1.0000	0.7968	0.4427	1.0000
13	-0.124	1.0000	0.7903	0.4205	1.0000
θ1	**θ2**	**θ3**	**θ4**	**Pl MW**	**Ql MVar**
0.00	-7.82	-40.26	5.56	234.1	46.8
0.00	-7.28	-52.96	4.64	201.9	40.4
0.00	-7.09	-54.34	4.45	195.2	39.0

Table 4.2: Modal Analysis for the four-bus system where the load is defined as 25% constant current, 50% constant impedance and 25% Constant PQ. λ_i, most positive eigenvalue.

No.	λi	V1 p.u	V2 p.u	V3 p.u	V4 p.u
7	1.0523	1.0000	0.83862	0.57209	1.0000
10	0.4337	1.0000	0.81160	0.49049	1.0000
13	0.0555	1.0000	0.79039	0.42054	1.0000
14	-0.192	1.0000	0.78441	0.39951	1.0000
θ1	**θ2**	**θ3**	**θ4**	**Pl MW**	**Ql MVar**
0.00	-7.86	-44.57	5.43	229.4	45.9
0.00	-7.59	-49.94	5.01	214.5	42.9
0.00	-7.09	-54.34	4.45	195.2	39.0
0.00	-6.90	-55.36	4.26	188.4	37.7

Table 4.3: Modal Analysis for the four-bus system where the load is defined as 25% Constant PQ and 75% constant impedance. λ_i, most positive eigenvalue.

The stability limit for the cases presented in Table 4.1, Table 4.2, and Table 4.3, occurs at the operating points 5, 12 and 13, with load bus voltages equal to 0.48391, 0.4427 and 0.42054 p.u, respectively. The results show that the smallest eigenvalues obtained from the reduced Jacobian matrix at these points, are in the neighborhood of zero.

Figure 4.2 represents the intersection of the load characteristic with the system PV curve, at each one of the stability limits (tangent solution) for the three mentioned compositions. It is observed that the stability limit is reached below the nose of the PV curve for voltage dependent loads. Figure 4.3 shows a QV curve representation, [Taylor, 1994], [Kundur, 1994], for cases 1 and 2, 25% constant PQ and 75% constant current, and 25% constant PQ, 25% constant current and 50% constant impedance. In each one of the cases it has been obtained that at the stability limit one eigenvalue becomes zero. Moreover, these limits correspond to the bottom of a QV curve representation.

Both QV curves in Figure 4.3 reach their minimum at the corresponding stability limit, i.e. the margin to instability is equal to zero, which verifies that these points certainly coincide with the stability limits, and below the minimum, the system is unstable. Any injection of reactive power in the system will result in lower and lower voltage and therefore in instability. For the general case of a constant power load, the QV curve minimum coincides with the operating point obtained at the nose in a PV curve representation.

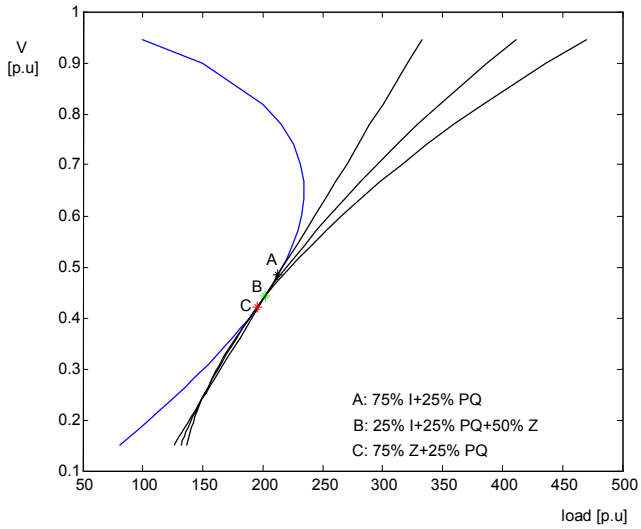

Figure 4.2: Stability limit for the 4 bus-case and mixed load composition: A) 75% constant current and 25% constant PQ, B) 25% constant current, 25% constant PQ and 50% constant impedance, and C) 75% constant impedance and 25% constant PQ.

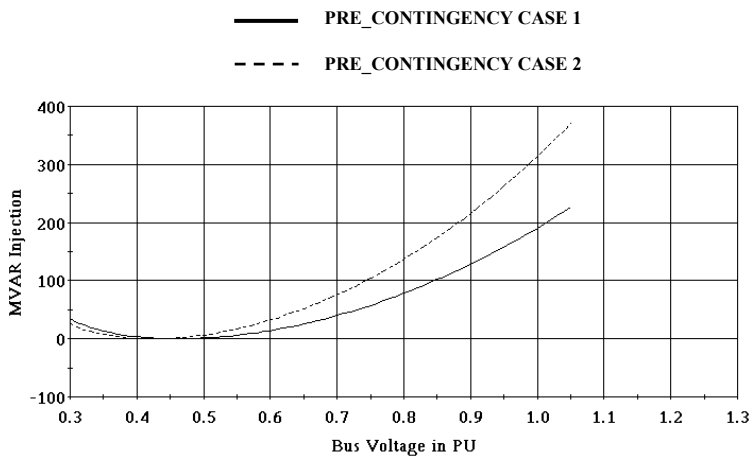

Figure 4.3: QV curves for cases 1 and 2, evaluated at the stability limit

4.3 Voltage Security Assessment

It has been already shown that the load-voltage characteristic has a critical impact in the determination of transfer limits and stability limits. The objective of this section is to carry out a voltage security assessment on the Nordic 32 test system [CIGRE, 1995] for an ideal scenario, to show the effect of the load composition in the determination of transfer limits. Carrying out such a study shows that this information is valuable to improve the planning and operation of the power system. An exponential load-voltage dependent model has been used for the load representation.

A security assessment on a power system determines its security level. According to the obtained level of security after a disturbance, if the system is found to be insecure, it will be necessary to take preventive actions in order to make the system secure again. It consists mainly of a *pre-processing* of information, which mainly includes static state estimation and event screening and ranking, a *security assessment* to determine the level of security in the system, a *post-processing* to estimate the dynamic status of the system (stable or unstable), the determination of stability margins and the sensitivity of the transfer limits to those margins, and finally a *control process* to implement the appropriate actions to ensure security in the system again.

A software package tool for the assessment of power system voltage security developed by Powertech Labs, Vancouver, Canada, has been used for the simulations, VSAT [VSAT, 2000]. The package includes a number of advanced techniques such as the *Fast Time Simulation Module*, which is used to compute the time domain trajectory of the system after a disturbance, and the *Modal Analysis Module*, which is best for identifying the location of the voltage stability limit of the system. The package offers an efficient and powerful tool for an accurate analysis of large complex power systems. It has been designed for both off-line and on-line applications. However, it is mostly used in off-line applications for planning and operational planning studies.

4.3.1. NORDIC 32 Test System

The Nordic 32 test system consists of 32 nodes and 23 synchronous generators on the voltage levels 400, 200 and 130 kV. The system is divided into four major parts: north, central, southwest and external. The north part represents the northern part of Sweden, which is characterized by a large hydro generation and some load. The central part corresponds to the central and southern parts of Sweden, mainly composed of heavy load and large thermal generation. The southwest and external regions correspond to the Danish island Zealand, consisted of thermal generation and load, and to Finland, with high load and generation. The test system main utility is the analysis of transient and voltage stability, as well as the study of long term dynamics. The load is represented by exponential models, which include the load-voltage and frequency dependencies. The test also includes tap changer and current limiter models. Figure 4.4 shows a simplified layout of the system. The network is rather long and the transfer at peak load is basically from the North to the Central part. The transfer from the North to the South has limited voltage support, which increases the risk of voltage collapse in the intermediate region (buses 4021, 4031, etc). Some of the information from the powerflow file follows:

- **Regions and Areas:** The four major parts of the system are divided into 8 different areas; areas 1, 2 and 3 belong to the North region, areas 4, 5 and 8 to the Central one, area 6 to the Southwest, and the area 7 to the External. (See third digit of bus number).
- **Generators and Loads:** The loads are classified into thermal, hydro and synchronous compressor loads.
- **Flows and Tie-lines:** Table 4.4 and Table 4.5 include the active and reactive flows between the main regions, from area to area and from line to line. From these tables it is easy to observe which lines are the more stressed in the system.

Further data on the connection lines between the different regions and areas, and on the distribution of the loads and generators in the system, are included in [Romero, 2003].

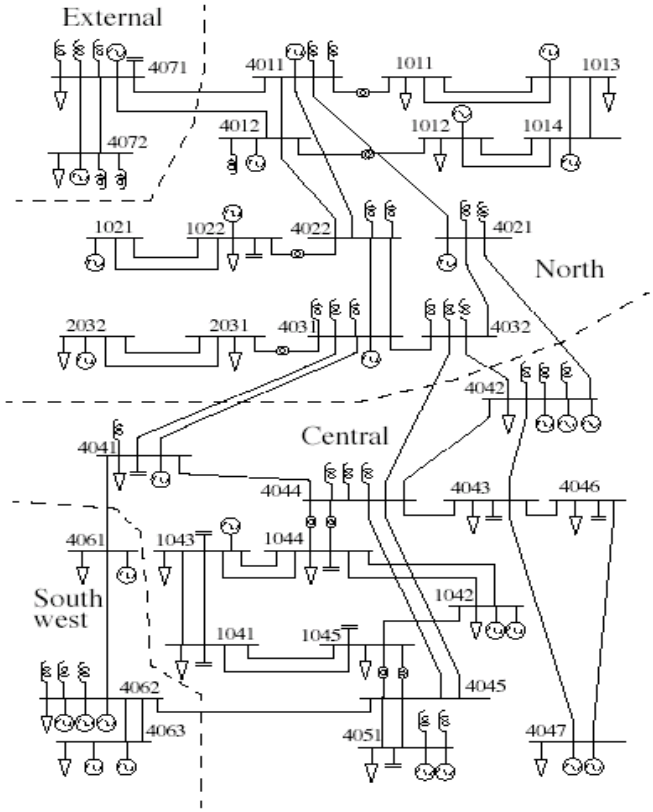

Figure 4.4: Layout of the CIGRE Nordic 32 Test System.

FLOW FROM SOUTH-WEST TO CENTRAL REGION			
FROM AREA	**TO AREA**	**P**	**Q**
5	6	326.07	32.43
8	6	1244.01	488.50
FLOW FROM NORTH TO CENTRAL REGION			
FROM AREA	**TO AREA**	**P**	**Q**
8	3	2627.20	-389.40
8	2	633.09	-122.32
FLOW FROM NORTH TO EXTERNAL REGION			
FROM AREA	**TO AREA**	**P**	**Q**
7	1	0.13	-146.92

Table 4.4: Powerflow between the 4 major parts of the Nordic 32 Test System

TIE LINE FLOWS FROM NORTH TO EXTERNAL REGION					
FROM AREA	**BUS**	**TO AREA**	**BUS**	**P**	**Q**
1	4012	7	4071	35.96	-79.78
1	4011	7	4071	-35.83	-67.14
TIE LINE FLOWS FROM NORTH TO CENTRAL REGION					
FROM AREA	**BUS**	**TO AREA**	**BUS**	**P**	**Q**
8	4042	2	4032	-633.09	122.32
8	4044	3	4032	-713.22	30.25
8	4042	3	4032	-575.76	143.43
8	4041	3	4032	-669.11	107.86
TIE LINE FLOWS FROM SOUTH-WEST TO CENTRAL REGION					
FROM AREA	**BUS**	**TO AREA**	**BUS**	**P**	**Q**
8	63	6	4063	-590	-256.22
8	62	6	4062	-300	-80.03
8	61	6	4061	-500	-112.31
8	4041	6	4061	145.99	-39.95

Table 4.5: Tie line flows between the 4 major parts of the Nordic 32 Test System

4.3.2. Nordel Grid Planning Rules

During the last 20 years the 220-420 kV Nordic main grid has expanded and the density of its network has increased. The new changes have resulted in new difficulties to maintain a high reliability in the system. A review of the planning rules established in 1972 has been necessary to give better consideration to lines that are out of operation and to take into consideration more stressed operating conditions. The rules are mainly related to the planning and design of the system rather than to the demands on security supply [Nordel, 1992]. The power system must be planned, built and operated so that sufficient transmission capacity will be available for utilizing the generation capacity and meeting the needs of the customers at the lowest cost.

In order to maintain a minimum level of reliability for the interconnected Nordic power system, it is necessary to establish and fulfill minimum requirements on reliability for the necessary transmission capacity in the system. The accepted criteria are based on a balance between the probability of faults and their consequences, [Nordel, 1992]. A deterministic criterion is then followed; several contingencies have been defined to test the grid; FG1- Common single faults, which do not affect transmission lines or other series components, FG2- Common single faults that affect transmission

lines or other series components, FG3- Uncommon single faults and special combinations of two simultaneous faults, FG4- Other combination of two faults with a common cause, FG5- Other multiple faults, two independent simultaneous faults, and three or more simultaneous faults. Faults FG1 and FG2 are the most frequent ones. Fault group FG3 comprises less probable single faults and especial more common double faults. Fault groups FG4 and FG5 contain rare faults. Three-phase busbar faults in FG3 shall principally be taken into account for stations, which are of significance to join operations between countries. The operating conditions before any contingency occurs, and the consequences that are acceptable after they are applied on the system have been also defined: GC0- Grid intact, GC1- Grid not intact, scheduled work or scheduled maintenance, GC2- Grid not intact, unscheduled outage/spontaneous loss of a shunt component, GC3- Grid not intact, unscheduled outage/spontaneous loss of a series element. The system operating conditions after these contingencies can be; Stable operation with local consequences, controlled operation with regional consequences, or instability and breakdown.

4.3.3. Voltage Stability and Load Models

In order to calculate accurate transfer limits, it is important to include the load-voltage dependency in the voltage security analysis. The software includes the load representation by using a general static exponential voltage dependent load model. Four different load compositions have been chosen to define the load in the Nordic 32 test system, load-voltage dependency α equal to 0, 1, 1.5, and 2. The most critical value, α equal to 0, is chosen to represent the load in the winter season, when most of the electric heating is connected in the system, while the value α equal to 2 corresponds to summer time. The load-voltage dependency will result in a relief of load in the system, and therefore in larger transfer limits. However, and in order to obtain more accurate and reliable results from the Nordic 32 test system it would be necessary to have information about type of load and composition in each one of the regions of the system. The impact of the load representation in the size of security limits has been studied by making a comparison of results, when constant power load is used, and when a static exponential load model is used instead. Modal analysis computation is requested in the simulations.

The computation has been carried out both including and not the load models in the Jacobian matrix, as described in the first sections of this chapter. At the stability limit the powerflow solution does not converge. If modal analysis is requested, it will be computed at the last stable point before instability is reached. The eigenvalues of the Jacobian matrix (reduced Jacobian matrix) are calculated at that point.

4.3.4. Simulations and Results

One scenario has been proposed for studying the load effect on the determination of transfer limits for the Nordic 32 test system. A pre- and post-contingency analysis has been carried out in order to determine the pre- and post-contingency transfer limits for constant power, and for voltage dependent loads. Modal analysis at the stability limit for both pre- and post-contingency has been computed. The scenario proposes an increase of the export from the southwest region towards the central one. Therefore, the generation has been increased in the southwest region. In order to maintain the system in equilibrium, the generation has been then decreased in another area, the north region. A number of contingencies affecting the transmission system towards the central region have been defined, types FG1 and FG2. If a severe contingency affects the transmission system somewhere from the northern region towards the central one, the transfer limits will drastically be reduced and the system will be insecure. These conditions have been defined with the name of 'HALF' scenario. In order to maintain stable operating conditions, it will be necessary to either decrease the load consumption in the central region, or to increase the generation. These conditions are presented in the results as 'FULL' scenario. The necessary data files to define this scenario are included in [Romero, 2003]. Some data from the 'transfer file' is presented in Table 4.6.

For both pre- and post-contingency conditions, it has been found that there is a voltage violation at buses 1011, 1012, 1013 and 1014. The corresponding voltages at those buses are higher than the specified ones in the criterion file. The security assessment-monitoring tool specifies this violation as a warning. Table 4.7 and Table 4.8 show the transfer limits and the modal analysis at the stability limit for the pre-contingency conditions.

Scenario 'HALF'		Scenario 'FULL'	
Transfer File • Increase of export from the Southwest region (source) • Decrease of generation in the North region (sink) • Step size: 10 MW		**Transfer File** • Increase of export from the Southwest region (source) • Decrease of generation in the North region (sink) • Decrease of the power transfer towards the Central region by increasing generation in the Central region (source) • Step size: 10 MW	
Source X:	South Region	**Source X:**	South Region
Source D:	North Region	**Source D:**	North and Central Regions

Table 4.6: Transfer file for the proposed scenario

Voltage Stability Limit Base Case		
Scenario	**Sources**	**Pre-Contingency V Stability Limit [MW]**
HALF	Source X	2654
	Source D	2896
FULL	Source X	5875
	Source D	2525

Table 4.7: Pre-contingency analysis and transfer limits.

Modal Analysis Base Case				
Scenario	**Point**	**Pre-Contingency-Stability Limit**		**Pre-Contingency**
		X	**D**	**λ**
HALF	534	2650	2900	7.60
	535	2652	2897	0.16
FULL	147	5875	2525	-0.020

Table 4.8: Modal analysis computation at the stability limit.

Modal analysis shows that the system is very sensitive to power changes in the proximity of the stability limit. The system changes, from stable to unstable conditions, within a range of 2.5 MW, probably due to the fact that in the neighborhood of the stability limit some generators are working very close to their Var reactive limit reserves, and any small power increase will result in exceeding those limits.

The smallest obtained eigenvalue is associated to mode number 1 and to buses 4061, 4062, 4063, 61, 62 and 63, which are located in the southwest region. Figure 4.5 shows a PV curve representation for both scenarios 'HALF' and 'FULL' at bus 4061. The maximum power that the system could transfer to the load under the conditions described in scenario 'HALF', has been increased in around 3220 MW, by increasing the generation in the central region of the test system, scenario 'FULL'.

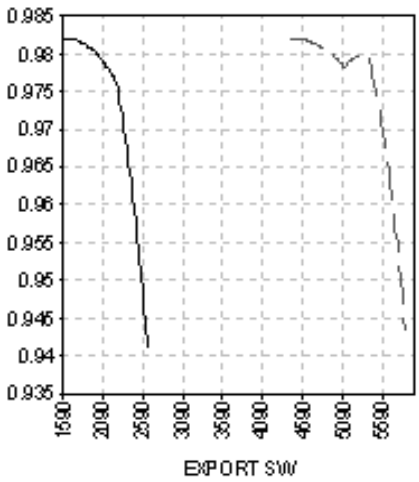

Figure 4.5: PV curve representation for both scenarios 'HALF' and 'FULL' at bus 4061 (solid line-'HALF', dash line-'FULL')

A contingency analysis has been carried out to determine transfer limits, but also to investigate which contingency affects more severely to the system. The load has been defined as constant power. Eleven different contingencies, type FG1 and FG2, (branch faults), which affect the transmission system from the northern region towards the central one have been defined. Table 4.9 presents transfer limits for each one.

Contingencies 8, 9, 10 and 11 will directly make the system insecure, and therefore they will not be included as 'acceptable contingencies'. Contingency 5, shadowed in gray color, has been found to be the most severe contingency.

Voltage Stability Limit Contingency Analysis			
Scenario	**Sources**	**Post-Contingency V Stability Limit** [MW]	**Pre-Contingency V Stability Limit [MW]**
Contingency 1: Open Branch 4012-4022			
HALF	**Source X**	2640	2652
	Source D	2910	2897
FULL	**Source X**	5860	5875
	Source D	2540	2525
Contingency 2: Open Branch 4011-4021			
HALF	**Source X**	2650	2652
	Source D	2900	2897
FULL	**Source X**	Insecure	Insecure
	Source D	Insecure	Insecure
Contingency 3: Open Branch 4012-4071			
HALF	**Source X**	No limit	2652
	Source D		2897
FULL	**Source X**	5872	5875
	Source D	2527	2525
Contingency 4: Open Branch 4011-4071			
HALF	**Source X**	No limit	2652
	Source D		2897
FULL	**Source X**	5870	5875
	Source D	2530	2525
Contingency 5: Open Branch 4032-4042			
HALF	**Source X**	2620	2652
	Source D	2930	2897
FULL	**Source X**	5760	5875
	Source D	2640	2525
Contingency 6: Open Branch 4021-4032			
HALF	**Source X**	2640	2652
	Source D	2910	2897
FULL	**Source X**	5790	5875
	Source D	2610	2525
Contingency 7: Open Branch 4011-4022			
HALF	**Source X**	2640	2652
	Source D	2910	2897
FULL	**Source X**	5850	5875
	Source D	2550	2525
Contingency 8: Open Branch 4021-4042			
HALF	**Source X/D**	Insecure	Insecure
FULL	**Source X/D**	Insecure	Insecure
Contingency 9: Open Branch 4022-4031			
HALF	**Source X/D**	Insecure	Insecure
FULL	**Source X/D**	Insecure	Insecure
Contingency 10: Open Branch 4032-4044			
HALF	**Source X/D**	Insecure	Insecure
FULL	**Source X/D**	Insecure	Insecure
Contingency 11: Open Branch 4031-4041			

HALF	**Source X/D**	Insecure	Insecure
FULL	**Source X/D**	Insecure	Insecure

Table 4.9: Contingency analysis

The system transfer limits for contingency 5 have been calculated for different load-voltage dependencies, i.e. different values for the parameter α. The results are presented in Table 4.10.

Voltage Stability Limit Contingency 5: Open Branch 4032-4042				
Scenario	**Sources**	**Post-Contingency V Stability Limit [MW]**	**Pre-Contingency V Stability Limit [MW]**	**Load Dependency α**
HALF	**Source X**	2626	2654	0
	Source D	2924	2896	
FULL	**Source X**	5760	5875	0
	Source D	2640	2525	
HALF	**Source X**	2626	2654	1
	Source D	2924	2896	
FULL	**Source X**	5780	5875	1
	Source D	2620	2525	
HALF	**Source X**	2626	2654	1.5
	Source D	2924	2896	
FULL	**Source X**	5790	5875	1.5
	Source D	2610	2525	
HALF	**Source X**	2626	2654	2
	Source D	2924	2896	
FULL	**Source X**	5800	5875	2
	Source D	2600	2525	

Table 4.10: Contingency analysis for contingency 5, open branch 4032-4042, for different load compositions.

The transfer limits for post-contingency conditions vary with the load-voltage dependency (the program does not take into consideration the load models for pre-contingency conditions). The larger the parameter α is, the larger transfer limits are obtained, i.e. the load-voltage dependency results in load relief. The relief is larger under summer conditions, where it has been assumed that the parameter α is closer to 2. The most critical conditions are when the load behaves as constant power, α equal to 0, or when it even takes negative values because of the use of tap changers for voltage regulation. Modal analysis for pre- and post-contingency cases at

the stability limit has been performed, with and without the load models included in the Jacobian matrix.

MODAL ANALYSIS FOR CONTINGENCY 5 (α = 0)				
Scenario	**Post-Ctgcy (no load in J) λ**	**Post-Ctgcy (load in J) λ**	**Pre-Ctgcy (no load in J) λ**	**Pre-Ctgcy (load in J) λ**
HALF	Point 519 0.16	'Same'	Point 534 0.074	'Same'
FULL	Point 133 -0.020	'Same'	Point 147 -0.020	'Same'
MODAL ANALYSIS FOR CONTINGENCY 5 (α = 1)				
Scenario	**Post-Ctgcy (no load in J) λ**	**Post-Ctgcy (load in J) λ**	**Pre-Ctgcy (no load in J) λ**	**Pre-Ctgcy (load in J) λ**
HALF	Point 519 0.16	'Same'	Point 534 0.074	'Same'
FULL	Point 135 0.12	Point 135 0.08	Point 147 -0.020	'Same'
MODAL ANALYSIS FOR CONTINGENCY. 5 (α = 1.5)				
Scenario	**Post-Ctgcy (no load in J) λ**	**Post-Ctgcy (load in J) λ**	**Pre-Ctgcy (no load in J) λ**	**Pre-Ctgcy (load in J) λ**
HALF	Point 519 0.10	'Same'	Point 534 0.074	'Same'
FULL	Point 136 -1.48	Point 136 -0.98	Point 147 -0.020	'Same'
MODAL ANALYSIS FOR CONTINGENCY. 5 (α = 2)				
Scenario	**Post-Ctgcy (no load in J) λ**	**Post-Ctgcy (load in J) λ**	**Pre-Ctgcy (no load in J) λ**	**Pre-Ctgcy (load in J) λ**
HALF	Point 519 0.33	Point 519 0.18	Point 534 0.074	'Same'
FULL	Point 137 -1.49	Point 137 -0.96	Point 147 -0.020	'Same'

Table 4.11: Modal analysis for contingency 5, open branch 4032-4042, for different load compositions, α, not including, (no load), and including the load models, (load), in the Jacobian matrix

4.4 Conclusions

The voltage stability limits for an ideal four-bus case has been studied for different load compositions. The load representation affects the location of the stability limits, i.e. a PV curve representation shows that a system reaches its stability limit at the nose of the curve for constant power load,

while this limit will be located below the nose for voltage dependent loads. Modal analysis has been used to determine the mentioned limits. QV curves for different load compositions reach their minimum at the mentioned limits, and below them, any injection of reactive power will be associated with lower voltage and instability.

A simplified security assessment on the Nordic 32 test system has been carried out. A scenario has been proposed and simulated for four different load compositions, and the corresponding transfer limits, voltage stability limits, and modal analysis computations have been carried out. The results show that the transfer limits vary with the load-voltage characteristic. The larger the parameter α (load-voltage sensitivity) is, the larger transfer limits are obtained, i.e. the load-voltage dependency results in load relief. The relief is larger under summer conditions, where it has been assumed that the parameter α is closer to 2. The most critical conditions are when the load behaves as constant power, α equal to 0.

This work has been carried out based on general information from the Nordic 32 test system and assuming that the load type is equally distributed in the whole system. The data and models used for the simulations are accurate enough to show the procedure for calculation of transfer limits and security margins. However, for more reliable results on voltage stability limits for the Nordic 32 test system, more accurate models and detailed data would be necessary.

Part II

Load-voltage Characteristic during Normal Operation

Summary: *Due to the large amount of electric heating loads in Sweden and its effect on voltage stability, Hill and Karlsson, [Karlsson and Hill, 1994], have proposed a load model with exponential recovery. The model is expressed as a set of nonlinear differential equations, where the real and reactive load powers have a nonlinear dependency with voltage. The standard dynamic active load model is characterized by three parameters, steady state load-voltage dependence, transient load-voltage dependence and a load-recovery time constant. The same applies to reactive load. As an extension of the mentioned work, the present author proposes an automatic method for the determination of parameters in standard dynamic load models.*

Field measurements from continuous normal operation have provided a large amount of data covering all seasons during the time period July 2001-June 2002. The determination of the load parameters based on this data has resulted in valuable information on the load characteristic and its dependency with weather and season of the year. The work has also contributed to a better approach for the normalization of traditional reactive load models.

.

Chapter 5

Field Measurements

The main contribution of this chapter is a continuous recording of field measurements from normal operation. The use of normal operating data is advantageous from a technical and economical point of view. The alternative of running a test involves alterations in the normal operation at the substation, and inconveniences for the customers due to repeated switching on/off capacitors. The need for manpower further results in very expensive tests. From a technical point of view, the data provides information on the load-voltage characteristics, but also on the normal operation of the system. By analyzing the load-voltage characteristics it is observed that the load response is influenced by the effect of voltage variations, but also by load variations from the consumer side, i.e. spontaneous load variations. Voltage step variations are of special interest due to their relation with daily normal operation at a substation, i.e. connection and disconnection of capacitors and tap changer operations. In conclusion, the extra information obtained from normal operation helps to understand the nature of the load dynamics, and therefore to decrease uncertainty margins.

5.1 Field Measurements

Field measurements from two different experiments are presented in this chapter, called test No.1 and test No.2. The recordings included in test No.1 are part of the results obtained from a previous field test [Le Dous, 1999], carried out during 1996 in the South East of Sweden, Blekinge. Test No.2

describes a continuous acquisition field measurement process from normal operation, including a description of the data acquisition process and the measuring equipment. The test was carried out during the period July 2001-June 2002, in the South of Sweden, in a branch of the distribution system at Tomelilla. The fact that both tests, No.1 and No.2 have been run under different periods of time and in different load areas, i.e. load composition is not the same, will make it possible to study the effect of different conditions in the results presented further in this thesis.

The information provided from the continuous recording process is large and of great interest due to its relation to normal operation. A post-processing of the data from test No.2 is presented in this chapter. Also, it includes the determination of daily, weekly, monthly and seasonal consumption load average profiles, the description of daily normal operations at the substation, and possible deviations from normal operation.

5.2 Test No.1

Test No.1 is a part of the recorded data during a field test in the South East of Sweden [Le Dous, 1999], Blekinge, in the distribution area of Sydkraft during June 1996.

5.2.1. Load area description

The total load of the measurements area was around 115 MW, which consisted mainly of countryside and private homes and farms of different sizes. Two larger industries were fed with approximately 20 MW. Part of the test grid is a village with a load of about 30 MW. The industrial load consisted mainly of induction motors, around 13% of the average total load.

Figure 5.1 shows the composition of the load in the area of measurements. The test was carried out during June 1996, a Saturday night and Sunday morning; hence a large part of the load consisted of street lighting. The outdoor temperature was about 10°-11°C and approximately 20% of the load in the area consisted of electrical heating.

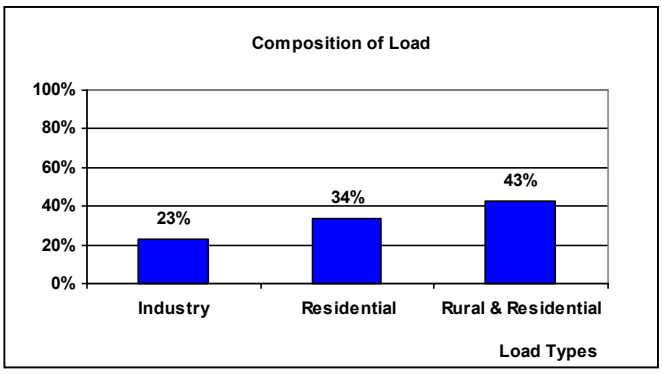

Figure 5.1: Composition of load in %, in the measurement area from test No.1.

5.2.2. Measurement description

The data originate from six different experiments in the 400-130 kV-transmission system. The voltage changes were made by simultaneous manual operation of the tap changers on the 400/130 kV transformers. By acting 1, 2 and 3 steps in both directions, the voltage changes are up to ±5%. An outline of the test system is presented in Figure 5.2. Measurements of voltage, active and reactive load on the 130 kV-side were selected for the analysis of the dynamic relation between voltage and load. The model aggregates all the loads up to the 130 kV-level. In the original experiment, an extra test consisting of switching off a 90 MVar shunt capacitor bank connected to the 130 kV-bus was realized. This operation resulted in an instantaneous voltage step. The data resulting from this last test has not been used in this thesis.

5.2.3. Voltage signals

During test No.1 voltage variations because of ideal voltage steps have been recorded. The test has been performed as shown in Figure 5.3. By the action of 1, 2 and 3 taps in both directions and taking into account that the tap size is equal to 1.67%, the resulting variations are in the orders of ± 1.7%, ± 3.4% and ± 5.0%. Notice that the steps that require the action of more than

1 tap in the same direction are not completely ideal, since there is a short time-delay between each tap changer action. Figure 5.4 shows the mentioned voltage variations, where a), b), c), d), e) and f) correspond to –1.7%, +1.7%, -3.4%, +3.4%, -5% and +5% respectively.

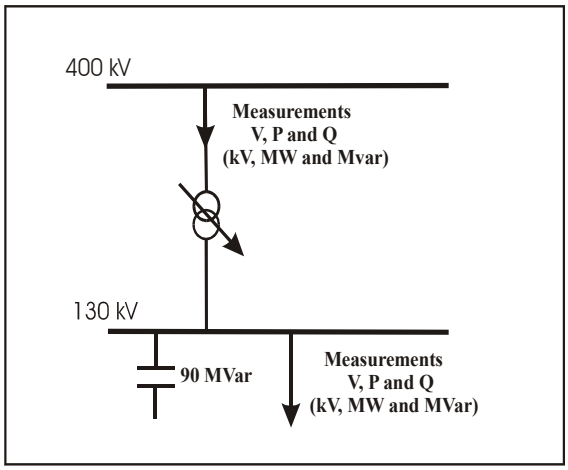

Figure 5.2: Simplified outline of the test system No.1.

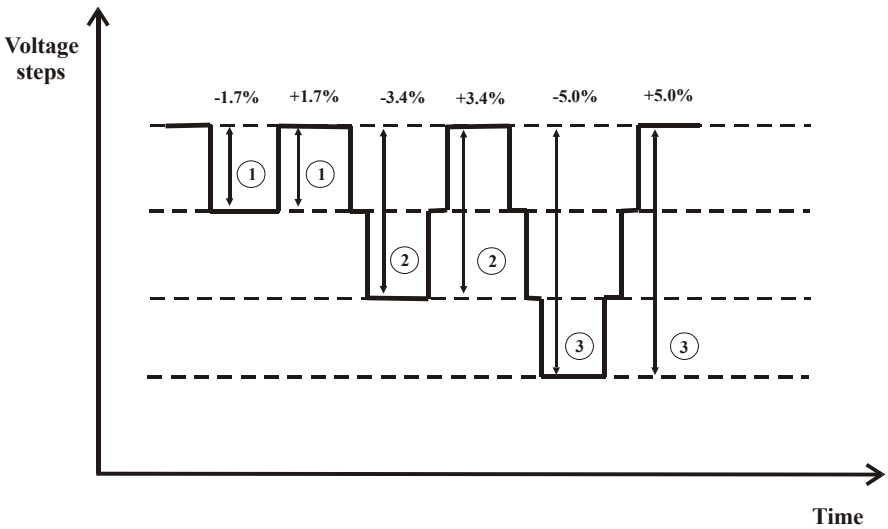

Figure 5.3: Implemented voltage steps.

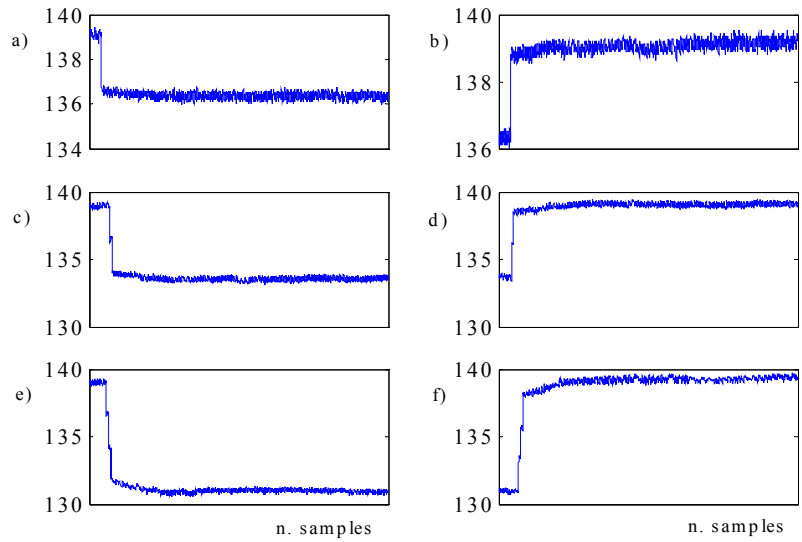

Figure 5.4: Measured voltage variations corresponding to a) –1.7%, b) +1.7%, c) -3.4%, d) +3.4%, e) -5% and f) +5%.

5.3 Test No.2

Test No.2 deals with field measurements resulting from a continuous acquisition of data from normal operation.

A continuous acquisition of data from normal operation, will not only track daily, weekly and seasonal variations in load, but also large deviations from normal operating ranges. The continuous recording process brings up large amounts of information related to daily operations, but also to the nature of the load dynamics affecting the system at every instant. The analysis of this data will make it possible to study daily normal operation activities, and it will also contribute to a better understanding of the load behavior, which is necessary for obtaining a more accurate load representation.

5.3.1. Load area description

The measurements have been carried out in a branch of the distribution system in the South of Sweden, at Tomelilla, during the time July 2001-June 2002. Since the weather conditions differ during the measurements, the outdoor temperature is varying and therefore updated information has been necessary. Based on data from the Danish Meteorological Institute [Meteorol, 2002] two places have been selected for reading weekly and monthly temperatures, Københavns Lufthavn, Copenhagen Airport, and Dueodde, which is situated on Bornholm, the Danish island southeast of Ystad. Figure 4.5 shows a map of the South of Sweden. Malmö is depicted on the West part, and Tomelilla is placed in the Southeast part of the country. In [RomeroLic, 2002] the temperatures recorded during the test are documented.

Figure 5.5: Map of the county Skåne (Scania) in the south part of Sweden.

A simplified scheme of the test area is shown in Figure 5.6. It includes the distribution system from the 130 kV-level and downward. At the 130 kV bus, two three-windings 100/100/40MVA, 130/50/20 kV tap changing transformers are connected in parallel. They are both operating during winter due to the increase in power demand, while only one of them is active during the summer. On the 130 kV bus bar, two manually controlled capacitor banks of 20 and 40 MVar respectively, are connected. They make reactive compensation from 20 to 60 MVar possible. The connection and disconnection of the capacitors is controlled from the operation center in Malmö twice a day, morning and evening. However, and based on the recorded data, it will be shown further in this thesis that this switching operation is quite irregular in typical daily operations. The tap changers, which are controlling the voltage at the 20 kV-level, are placed on the 130 kV windings. The minimum tap size of the tap changers at Tomelilla is equal to 1.67 % of the voltage level.

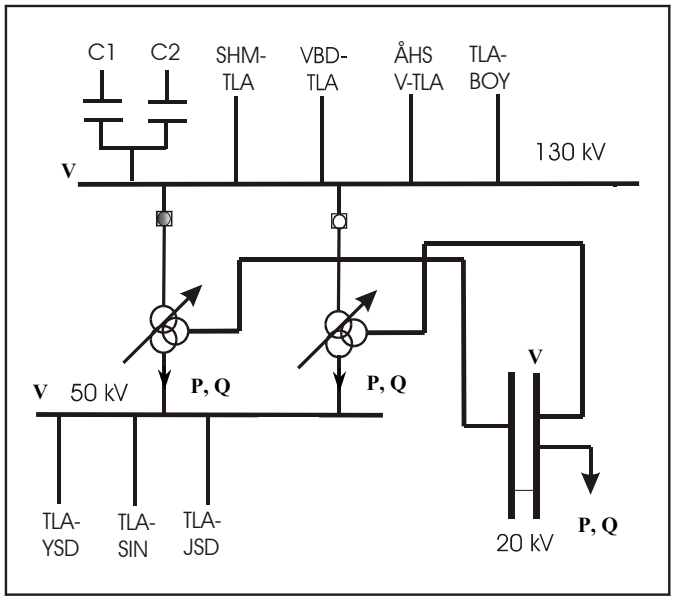

Figure 5.6: Simplified test system at Tomelilla. Measurements of voltage, active and reactive power, are expressed in kV, MW and MVar respectively.

A load of about 62 MW is connected to the 20 kV side of the transformers. A large percent of the load corresponds to residential and rural type, around 53%. This residential load includes mainly private houses, residential buildings, and public service buildings. On the other hand, the rural type aggregates the demand of the countryside, i.e. farms of different sizes with own production, such as corn, milk and meat production. The residential and rural load mainly corresponds to electric heating, radiators and boilers, as well as some heat pumps and electric/oil combined heating. A large industrial customer, around 15 MW, and other minor industries are directly fed from the 20 kV-level; their load is primarily constituted of induction motors and electric heating.

It has to be taken into account that the load composition will depend not only on the type, residential, rural, commercial and industrial, but also on weather conditions and variations in load demand during the measurements. As an example, the effect of electric heating will be larger during cold periods and therefore in wintertime. During the summer time, the heating demand will decrease, and consequently the effect of electric heating, but on the other hand, due to air conditioner actions, the percent of induction motors in the area may increase. Figure 5.7 shows the composition of the load at the 20 kV-level. It is classified in residential, rural, industrial and commercial types. More details about the composition of the load are shown in [Romero Lic, 2002].

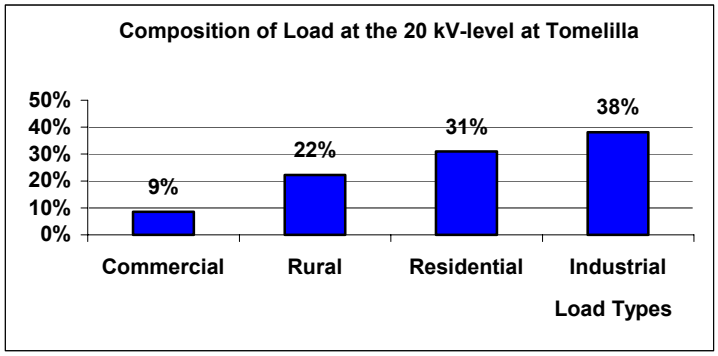

Figure 5.7: Composition of load at the 20 kV-level at Tomelilla.

The 50 kV side of the transformers is connected to a 50/20 kV substation at Järrestad. Besides, the 50 kV bus feeds mainly secondary distributors, i.e. companies supplying power to the cities Ystad and Simrishamn.

Part of the load on the 50 kV bus emanates from a converter station for the railway. Further analysis at this level is not included in this study.

5.3.2. Measurement description

The measurement equipment is a Macintosh computer with 4 GBytes hard disk capacity, which allocates an analog input card, National Instruments MIO16, and software for the configuration and activation of the functions of the card (LABVIEW). Thirteen different channels have been used for the acquisition, see Table 5.1.

TOMELILLA MEASUREMENTS					
CH	OBJECT	SIGNAL	MEASURE VALUE	TRANSDUCER PT RATIO	CONVERSION FACTORS
0	T1/T2 20 kV	V	0-22 kV	22/0.11	0.012695 kV/bit
1	T1/T2 50 kV	V	0-55 kV	55/0.11	0.03222 kV/bit
2	TLA-BOY	V	0-137.5 kV	132/0.11	0.080566 kV/bit
3	ÅHS V-TLA	V	0-137.5 kV	132/0.11	0.080566 kV/bit
4	VBD-TLA	V	0-137.5 kV	132/0.11	0.080566 kV/bit
5	T1 20 kV	P	0-60 MW	22/0.11	0.0292 MW/bit
6	T1 20 kV	Q	-30-0-30 MVar	22/0.11	0.0292MVar/bit-30 MVar
7	T2 20 kV	P	0-60 MW	22/0.11	0.0292 MW/bit
8	T2 20 kV	Q	-30-0-30 MVar	22/0.11	0.0292MVar/bit-30 MVar

9	T1 50 kV	P	0-130 MW	55/0.11	0.063476 MW/bit
10	T1 50 kV	Q	-70-0-70 MVar	55/0.11	0.068359MVar/bit-70 Mvar
11	T2 50 kV	P	0-130 MW	55/0.11	0.063476 MW/bit
12	T2 50 kV	Q	-70-0-70 MVar	55/0.11	0.068359MVar/bit-70 Mvar

Table 5.1: Characteristics of the signals chosen for the acquisition, and conversion factors between the substation and the analog input card.

Note that four different signals are necessary for measuring active and reactive load on the 50 kV and 20 kV sides of the three-winding transformers. During winter both transformers will be connected, and the active and reactive load consumption will be the sum of the recordings at T1 and T2. During the summer one of the transformers will be disconnected, so two of the signals will be zero. The data is sampled with a frequency of 3 Hz, and it is stored continuously in files of 12 hours duration, labeled with date and time. The program includes a real time monitoring of the size of the files and the recorded values in the substation expressed in binary code. Different transformation factors are necessary to convert directly, on real time, from binary code to real numbers (see Table 5.1). Since the aim is to analyze the load-voltage characteristic in a time frame of about 10 seconds to 10 minutes, the choice of the proper sampling frequency is crucial for the acquisition of significant information during the test. The chosen frequency of 3 Hz is sufficiently fast to capture the transient dynamics of the load. Spontaneous variations due to load switching operations from the customer side are also captured.

5.3.3 Measurement results

The measurements presented in this chapter correspond to recorded voltage, active and reactive load at 130 kV, 20 kV and 50 kV under the period July 2001 to June 2002. Due to the length of the test and to technical problems in the hardware, some periods of time are missing, however the acquired data fulfils the requirements of this project. The available data from the recording process is presented in Figure 5.8.

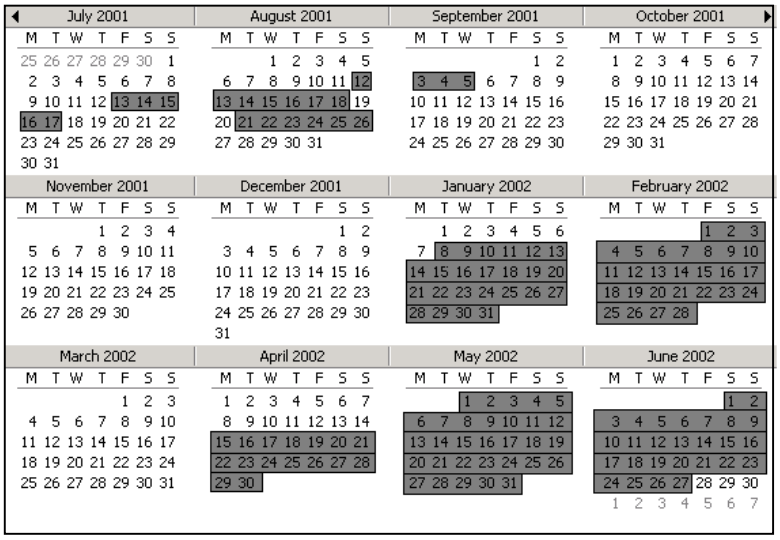

Figure 5.8: The available data from the recording process (marked in gray).

5.4 Analysis of Normal Operation Data

The measurements resulting from test No.2 provide a large amount of information, which is especially advantageous since it originates from continuous recording from normal operation. An off-line processing of the data will make the most of this information, and will evidence the importance of running these measurements instead of running shorter tests, which involve alterations in the normal operation at the substation. The data is relevant from the technical point of view, its analysis will make it possible to describe typical operations at the substation such as, switching on/off capacitors related to reactive compensation actions, voltage regulation due to tap changer operations, high and low voltage warning situations, but also to study the load-temperature characteristic, and to obtain monthly, weekly and daily load consumption profiles. Moreover, the data contains repeated voltage step variations, which, as mentioned earlier in this thesis result in an exponential recovery of the load, and consequently they are of great interest for analyzing the load-voltage characteristic in a

time frame of 10 seconds to 10 minutes. At last, a proper filtering of the data will eliminate possible effects of high frequency noise during the acquisition.

Due to the large amount of information and results, only a reduced part is presented in this chapter. Further information can be found in [Romero1, 2001], [Romero2, 2001]**.** Different aspects are presented in the following pages:

- Voltage, active and reactive load at 20 and 50 kV;
- Load consumption profiles;
- Typical daily operations;
- Analysis of the load-temperature characteristic;
- Voltage step variations.

5.4.1 Measured voltage and power

Figure 5.9 and Figure 5.10 show the recorded voltage, active and reactive load response at the 20 and 50 kV-level during the Thursday 23 August 2001. In Figure 5.9, it is observed that during the first hours in the morning until around 6:00 a.m, the active load demand remains constant and at a low level. During the night there is little consumption in residential areas, only a small percent corresponds to electric heating in winter, and to air conditioner in summer. A larger percent of the consumption during these hours corresponds to street lighting and to some industrial processes, which are active during the night.

Between 6:00 a.m and 8:00 a.m, the daily activities in residential areas start. Notice that the data correspond to a weekday, and therefore, it is expected not only an increase because of pure domestic use but also, because of offices and business activities, and in industrial areas, because of connection of some industrial processes. The load consumption increases around 50 % between those hours and it reaches its peak at around 12:00 p.m. The load consumption during the time frame between 8:00 a.m and 4:00 to 5:00 p.m is mainly related to commercial and industrial activities, and the load during those hours, remains at a high level. From around 5:00 p.m to 10:00 p.m

most of the consumption is due to pure domestic use and industrial processes, since the commercial schedule is finished. After 10:00 p.m, the demand changes again to a low value due to disconnection of industrial processes and the decrease of activities in residential areas.

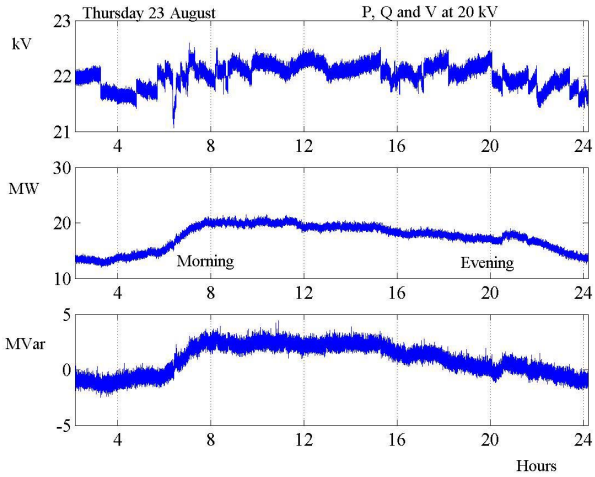

Figure 5.9: Voltage, active and reactive load at 20 kV at Tomelilla, on Thursday 23/08/01.

In relation to the reactive load consumption, when the network is heavily loaded during the morning or during peak loads, the reactive consumption of the lines increases proportionally with the square of the current, and therefore reactive compensation is necessary to improve the power transfer capability and the voltage stability. Operations of switching capacitors are scheduled to be done manually twice a day, morning and evening, at an operation center in Malmö. However, the scheduled time for the operations is altered often during the daily operations. By checking the reactive load profile in Figure 5.9, note that around 6:00 a.m, when the active load demand starts to increase, a capacitor connection is done in order to compensate the reactive consumption of the lines and transformers. In the evening, at around 6:00 p.m to 7:00 p.m, the capacitors are disconnected. Notice that in Figure 5.9, at around 8:00 p.m, there is an increase in the active demand, probably due to the connection of an industrial load. At the same time, and at a non-scheduled time, a new capacitor connection is

performed due to the requirements at the substation. The description above can be applied to the 50 kV-level. Figure 5.10 shows the recorded voltage, active and reactive load response at the 50 kV-level. After a general description of the active and reactive load behavior during 24 hours, it is interesting to compare if there is any difference, and in that case, which are the differences in load profile during a weekday and a weekend day, and which are the peak hours in load demand for both cases. Figure 5.11 shows the voltage, active and reactive load at 20 kV during the weekend 13-14-15 July, (starting on Friday 13 in the evening).

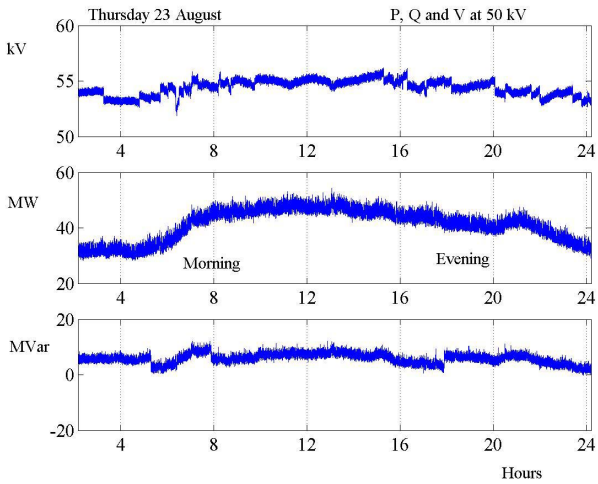

Figure 5.10: Voltage, active and reactive load at 50 kV at Tomelilla, on Thursday August 23, 2001.

The main difference between a weekday and a weekend day load consumption, is that the first one presents a more homogeneous load profile since a big percent of the consumption corresponds to industrial and commercial operations, i.e. the load demand increases when the working time starts, it reaches a maximum at around 12:00 p.m, and it starts to decrease when the working hours are over. On the other hand, the load profile during Saturdays and Sundays is more irregular, and the load consumption is mainly due to domestic use, and some commercial operations during the Saturday morning. The load profile follows domestic habits and the increasing slope during the morning, at around 8:00 a.m is softer than during a weekday. The load demand during a weekend day

remains at a high level until later hours at night probably due to different activities during holidays. However, and based on the recorded information the average load consumption seems to be higher during a weekday than during a weekend day, but the peak load values are higher on weekend time rather than during the rest of the week.

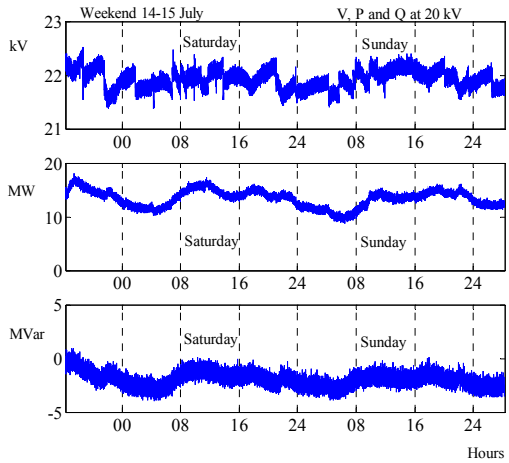

Figure 5.11: Voltage, active and reactive load at 20 kV during the weekend.

The same conclusions can be applied to 50 kV. Figure 5.12 shows the voltage, active power and reactive power responses at 50 kV during the weekend of 14-15 July. The results show that the active load consumption at 50 kV is slightly higher than at 20 kV. The active load profile during a weekday behaves in the same way as explained above for 20 kV, i.e. the load demand starts to increase at around 8:00 a.m, starting time for business and commercial activities, it reaches its maximum, peak load, at around 12:00 p.m, and remains constant until around 8:00 p.m, where it decreases to a low value. The load demand during a weekend day presents different peak load hours, and its load profile is more irregular, mainly due to its relation to domestic activities. The average load consumption seems to be higher during a weekday than during a weekend day, but on the other hand, the peak loads are higher during the weekend.

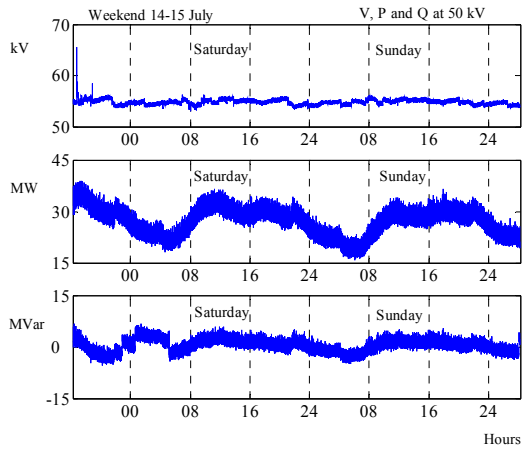

Figure 5.12: Voltage, active and reactive load at 50 kV during the 14-15 July.

It was mentioned in section 5.3.1 that the composition of the load would not only depend on the load type, residential, rural, commercial and industrial, but also on the weather conditions. The changes in temperature during a year affect the distribution in the load composition, and the average load demand. Figure 5.13 shows a comparison between the active and reactive load consumption at 20 kV during a summer and a winter day, Monday 13 August 2001 and Monday 18 February 2002. The outdoor temperature was about 9.5 to 27.5°C, and -5.7 to 3.8°C respectively.

In Sweden, in general, the average load demand is higher during wintertime. Checking Figure 5.13, the average load at 20 kV during Monday 18 February is approximately 70 % higher than during Monday 13 August. In the area of the measurements, South of Sweden, and during the winter the temperatures have moved in the range of -12.3 to 11.3°C. Due to those temperatures, electric heating in the houses is necessary. A large percent of the load during this period of time consists of electric heating, either radiators or boilers, and heat pumps. During the summer, the temperatures have varied in the range from 5.1 to 27.5°C. Due to the mild weather conditions, heating is not necessary, and air conditioners are not often used. Moreover, the consumption can be considerably lower during July and August since they are holiday months and some commercial and industrial activities are stopped until late August. At Tomelilla, the described two three windings 130/50/20 kV tap changer transformers connected in parallel

will be both operating during winter and during high demand conditions, while during the summer only one of them, T1, will be in service.

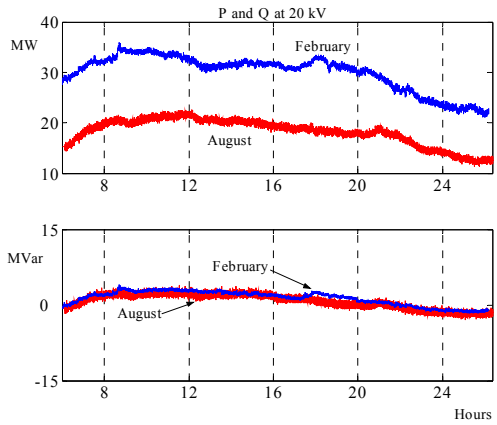

Figure 5.13: Active and reactive load consumption at 20 kV, during Monday 13.

Figure 5.14 shows a comparison between the active and reactive load consumption at 50 kV during a summer and a winter day, Monday 13 August 2001 and Monday 18 February 2002

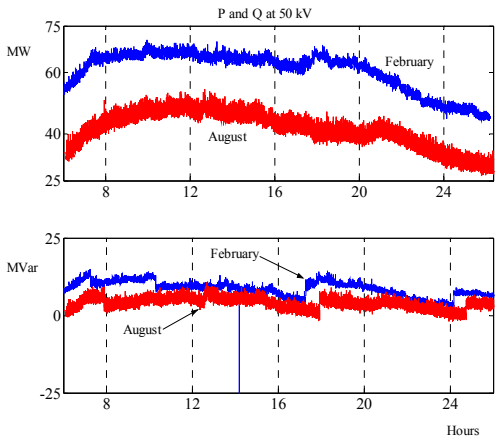

Figure 5.14: Active and reactive load consumption at 50 kV, during Monday 13 and February 18 February 2002.

5.4.2. Daily operations

Normal operating data are of great value for understanding typical daily operations at a substation, but also to detect unusual situations that deviate from normal operation and may drive the system to severe conditions. At the operation centers the information from normal operation is continuously updated. This information is normally stored in large databases. With help of the reported log-files at the Malmö operation center and by checking the recorded data it is possible to determine if there is any pattern in the schedule of the realization of the operations at Tomelilla, and to obtain detailed information of how the operations are performed. Figure 5.15 shows the measured voltage at 20 kV during Monday 13 August. As an example two voltage regulation operations are pointed at in the figure. The regulation is performed by the action of tap changers and, in this case, it has taken around one minute to perform it.

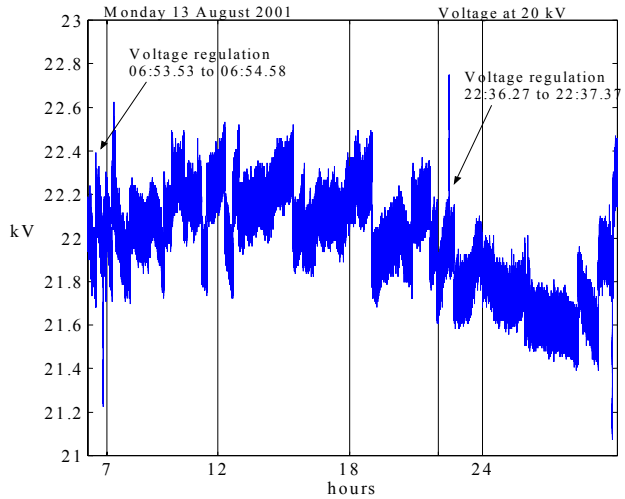

Figure 5.15: Voltage regulation due to action of tap changers during Monday 13 August.

In Figure 5.16 one of these operations is described. At 22.30.27 hours, the tap changers start regulating the voltage to a higher value. The action is done by two upward tap operations. Since the tap changers are working in a discrete-tap mode, each tap operation corresponds to a step variation in the

order of 1.67%. After the second tap connection, the reached voltage is too high and therefore it needs to be regulated again. A warning signal is detected at the operation center in Malmö, and a manual disconnection of capacitors is performed to finally stabilize the voltage.

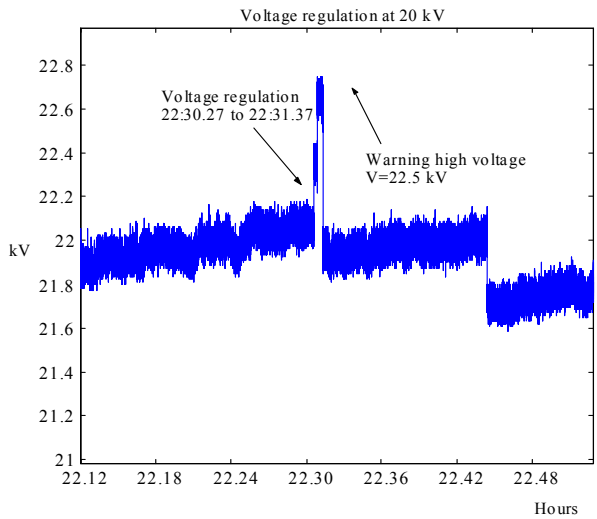

Figure 5.16: Voltage regulation and disconnection of capacitors due to high voltage conditions.

Figure 5.17 shows the measured voltage at two different places at the 130 kV-level during Friday 17 August. At 07.09.26 hours a capacitor connection is performed to compensate the increasing load demand in the first hours of the day. In the evening the opposite operation is performed. The voltage variation due to switching capacitor operations is in the order of ±3 %.

During the day different critical situations are detected at the operation center. The figure shows how at 10:00 a.m the voltage has reached a high value, a warning signal is received at the operation center, and voltage regulation by the action of tap changers is started until an acceptable value is reached again.

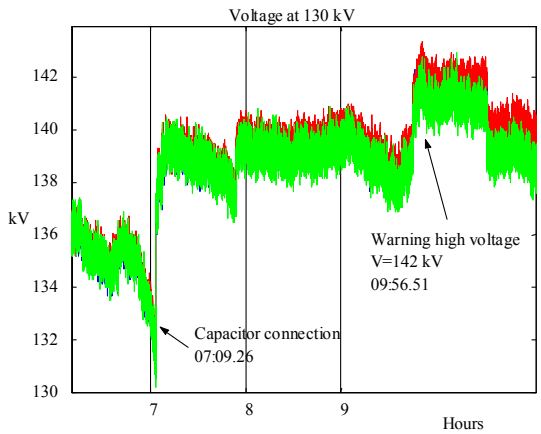

Figure 5.17: Capacitor connection and voltage regulation due to high voltage conditions at 130 kV.

In spite of the fact that the switching capacitor operation is usually ordered twice a day, morning and evening, and since it is an operation that requires manpower, there are often many irregularities in the scheduled hours for its realization. As an example Figure 5.18 shows voltage, active and reactive load at the 20 kV-level, during the first weekend of February (February 2 and 3). During these two days it is possible to check the differences in time for connecting and disconnecting capacitors. C1 and C2 correspond to two different connections in the morning, while D1 and D2 correspond to disconnections in the evening.

Weekend1 2/02/02 to 3/020/02

- C1 Connection of capacitor at 130 kV. Saturday 02/02/02, time 09.50.00
- D1 Disconnection of capacitor at 130 kV. Sunday 03/02/02, time 03.11.48
- C2 Connection of capacitor at 130 kV. Sunday 03/02/02, time 09.11.47

- D2 Disconnection of capacitor at 130 kV. Sunday 03/02/02, time 23.11.47

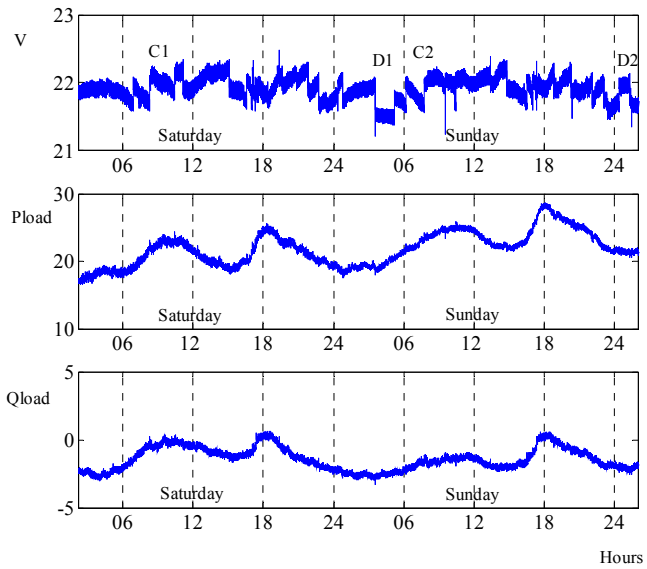

Figure 5.18: Voltage, active and reactive load at 20 kV during the first weekend of February 2002. The voltage is measured in kV, *Pload* in MW and *Qload* in MVar.

5.4.3. Voltage step variations

The data described throughout section 5.4 is valuable information for studying the load-voltage characteristic in a time frame of about 10 seconds to 10 minutes.

During the recording time repeated voltage step variations due to switching capacitor and tap changers operations have occurred. The minimum voltage variation experienced at Tomelilla, due to these operations, corresponds to the tap size in the tap changers and is equal to 1.67 %, while the variations due to switching capacitors are in the order of ±3% or larger. The effect of a voltage step variation will result, as mentioned in earlier chapters, in a pure exponential recovery of the load.

More aspects related to voltage variations and their detection, will be discussed in Chapter 7.

Chapter 6

Determination of Parameters in Dynamic Load Models

6.1 Introduction

This chapter introduces an improved method for the estimation of parameters in dynamic load models. Instead of curve fitting and manual inspection technique a more accurate procedure has been used. The method avoids possible errors by manual inspection, gives an accurate solution and reduces the time for the parameter determination.

The method will make it possible the study of the daily, weekly and seasonal active and reactive load parameters. Values from time constants, transient and steady state voltage dependencies, give an idea of how fast the recovery of load is after a change in voltage, the composition of the load, and how well the load fits the proposed model.

6.2 Linearization

The dynamic load model introduced in Chapter 2, is presented as a set of non-linear equations, equations (6.1) and (6.2), where real (active) and reactive power have a non-linear dependency on voltage. The nonlinearities are necessary to reproduce variations in power for large changes in voltage, even though the changes are very rare. Furthermore, the non-linear representation complicates the identification procedure since it is not

possible to apply the general identification methods because they are only valid for linear systems. Linearizing the system makes the model valid only for small variations, but simplifies parameter identification drastically.

$$T_p \frac{dP_r}{dt} + P_r = P_o \left(\frac{V}{V_o}\right)^{\alpha_s} - P_o \left(\frac{V}{V_o}\right)^{\alpha_t} \tag{6.1}$$

$$P_l = P_r + P_o \left(\frac{V}{V_o}\right)^{\alpha_t} \tag{6.2}$$

Considering the model described in (6.1) and (6.2), the first step is to linearize around an operating point (V^*). Small deviations around the nominal point are denoted by Δ, and by using Taylor series expansion and removing all the constant terms, the model is given by:

$$\begin{aligned} \Delta P_l &= \Delta P_r + \alpha_t \cdot P_o \cdot \left(\frac{V^*}{V_o}\right)^{\alpha_t - 1} \cdot \frac{\Delta V}{V_o} \\ T_p \frac{\Delta P_r}{dt} &= \alpha_s \cdot P_o \cdot \left(\frac{V^*}{V_o}\right)^{\alpha_s - 1} \cdot \frac{\Delta V}{V_o} - \alpha_t \cdot P_o \cdot \left(\frac{V^*}{V_o}\right)^{\alpha_t - 1} \cdot \frac{\Delta V}{V_o} - \Delta P_r \end{aligned} \tag{6.3}$$

By introducing new quantities, A, B and u, the identification process is simplified. The state space representation of the model is given by (6.4) and (6.5):

$$A = \alpha_t \cdot \left(\frac{V^*}{V_o}\right)^{\alpha_t - 1} \quad B = \alpha_s \cdot \left(\frac{V^*}{V_o}\right)^{\alpha_s - 1} \quad u = \frac{\Delta V}{V_o}$$

$$\Delta P_l = \Delta P_r + A \cdot P_o \cdot u \tag{6.4}$$

$$T_p \cdot \frac{\Delta P_r}{dt} = B \cdot P_o \cdot u - A \cdot P_o \cdot u - \Delta P_r \tag{6.5}$$

By applying Laplace- transformation and introducing $T_1 = T_p \cdot A$, the load variation ΔP_l is given by (6.7):

$$\Delta P_l = \frac{B-A}{1+s\cdot T_p}\cdot P_o\cdot u + A\cdot P_o\cdot u$$
$$\frac{\Delta P_l}{P_o} = \frac{B+s\cdot A\cdot T_p}{1+s\cdot T_p}\cdot\frac{\Delta V}{V_o} \tag{6.6}$$

$$\boxed{\frac{\Delta P_l}{P_o} = \frac{B+s\cdot T_1}{1+s\cdot T_p}\cdot\frac{\Delta V}{V_o}} \tag{6.7}$$

Equation (6.7) represents the load response when a voltage change occurs in the system. It is characterized by three parameters, steady state voltage dependency B, transient voltage dependency A, and time constant T_p. ΔP_l and ΔV represent deviations from the steady state values P_o and V_o. ΔP_l represents the difference between the initial value P_o, and the last value P after a voltage variation. ΔV is the difference between the initial V_o and the voltage V after a variation. By checking equation (6.7), when s goes to zero the value for the steady state parameter B is obtained. While when s goes to ∞ ($T1/Tp$) will be obtained, i.e. the transient parameter A.

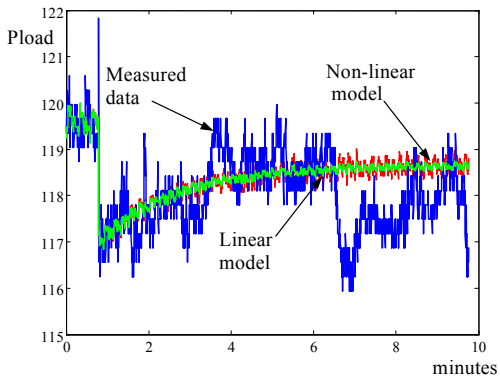

Figure 6.1: Measured and simulated load response (linear and non-linear models), for ΔV of -1.8% at the 130 kV-level.

Figure 6.1 shows a comparison between the non-linear and linear model, when a voltage step of -1.8% from the nominal point (130 kV) has been applied. Both models capture the dynamic response, and agree well with each other. The difference between the measured and simulated data corresponds to spontaneous load changes. They are thus not related to

voltage variations, and to the load exponential response, which is the matter of this study. It can be thus concluded that the linearized model is sufficiently accurate for our identification purposes.

6.3 Optimization

An automatic determination of parameters is meant to be used on continuously recorded data. The result of that determination will give information about the time variations of the parameters. The aim is then to use the described linearized model (6.7) and to identify its parameters with measured data.

The algorithm uses N samples of input signals (*voltage,* $V(t_k)$) and output signals (*power,* $P(t_k)$), $k=1...N$, and the objective is to obtain estimates of the parameter vector $\theta=(T_p, \alpha_s, \alpha_t)$ to minimize the difference between the measured and the simulated data (as a quadratic criterion). The measured data corresponds to the load response when a voltage variation has occurred in the system, while the model described by (6.7) represents the variation of the load from its steady state value (ΔP) due to the voltage variation; i.e. the total simulated load response will be equal to its initial value P_o, plus that variation (ΔP). The objective function to be minimized using a quadratic least square criterion is:

$$F\ (\theta) = \sum_{k=1}^{N} (P_{simulated}(t_k, \theta) - P_{measured}(t_k, \theta))^2 \tag{6.8}$$

$$F_N(\theta) = \sum_{k=1}^{N} ((P_o + \Delta Pl) - P_{measured}(t_k, \theta))^2 \tag{6.9}$$

Where,

$$\Delta P_l = P_o \cdot \frac{B + s \cdot T_1}{1 + s \cdot T_p} \cdot \frac{(\Delta V)}{V_o}$$

$$\Delta P_l = (P_o - P_{simulated}(t_k, \theta))$$

$$\Delta V = (V_o - V(t_k, \theta))$$

The least squares optimization algorithm is used to minimize the function (6.9) and to obtain the initial values of the parameter vector θ. By using iteration for the data sequence, the final values for the linear model are calculated, and the corresponding non-linear model parameters are straightforward to determine by using equations (6.10) and (6.11):

$$B = \alpha_s \cdot \left(\frac{V^*}{V_o}\right)^{\alpha_s - 1} \quad (6.10) \qquad A = \alpha_t \cdot \left(\frac{V^*}{V_o}\right)^{\alpha_t - 1} \quad (6.11)$$

By using equation $A=T_1/T_p$, it is possible to obtain the value of the time constant T_p. The equations above are solved by iteration. Assuming that $V^*=V_o$, the first estimates are given by:

$$\alpha_{s,0} = B \quad \alpha_{t,0} = A$$

The general expression for the following estimates is given by (6.12):

$$\alpha_{s,k+1} = \frac{B}{\left(\frac{V^*}{V_o}\right)^{\alpha_{s,k}-1}} \quad \alpha_{t,k+1} = \frac{A}{\left(\frac{V^*}{V_o}\right)^{\alpha_{t,k}-1}} \quad (6.12)$$

The procedure determines the value of the linear model parameters. By assuming that large disturbances are not affecting the system, the non-linear model parameters can be calculated from the linearized model parameters.

6.4 Robustness of the Model

Based on field measurements from Test No.1, which has been previously described in Chapter 5, the introduced method for estimation of parameters in dynamic load models has been tested. The simulations presented in this section represent an extension of previous studies [Le Dous, 1999], [Karlsson, 1992], and they prove the robustness of the method, i.e. possible errors by manual inspection are avoided, and accurate solutions are obtained.

The data originates from six different experiments in the 400-130 kV-transmission system. The voltage changes were made by simultaneous

manual operation of tap changers on the 400/130 kV transformer feeding one area with an aggregated load of 150 MW. By acting 1, 2 and 3 steps in both directions, the voltage changes are up to about ±5%. Measurements of voltage, active and reactive load on the 130 kV-side were used for analysis of the dynamic relation between voltage and load. The model aggregates all the loads up to the 130 kV-level. For six different sets of data, the identification process has been applied. Both the non-linear and the linear models have been fitted to the data. Table 6.1 and Table 6.2 show the results of the identification for both, the active and reactive response respectively.

No	$\Delta V/V_0$ [%]	T_p [s]	α_t	α_s
1	-1.8	135	1.36	0.25
2	+1.9	40	1.70	-0.10
3	-3.7	61	1.31	-0.16
4	+3.7	74	1.35	-0.54
5	-5.3	70	1.65	-0.32
6	+5.4	78	1.60	-0.08

Table 6.1: Identified parameters for active response under six different voltage steps.

No	$\Delta V/V_0$ [%]	T_q [s]	β_t	β_s	Qo [MVar]
1	-1.8	89	-181.18	7.90	-0.974
2	+1.9	256	-687.20	975.60	-0.046
3	-3.7	88	87.67	31.86	-2.850
4	+3.7	105	104.50	-148.56	0.867
5	-5.3	78	77.89	19.35	-2.840
6	+5.4	94	94.18	-49.75	1.254

Table 6.2: Identified parameters for reactive response under six different voltage steps. Normalizing factor of the reactive load Q_o.

From the results presented in the tables, and under voltages steps in the order of ±1.8% to approximately ±5.4% from the nominal value (130 kV-level) it can be concluded that:

- The active load (Table 6.1) behaves much like a resistance for fast voltage changes (transient). α_t is in the order of 1.35 to 1.7.

- The exponential recovery of the active load shows time constants of 40 to 135 seconds.
- The steady state voltage dependency parameter α_s, in some of the cases, presents a negative value. The stationary level reached by the load after the recovery is equal to (around 0) or higher than the expected one, probably due to the effect of the on load tap changer action, i.e over and undershooting.
- In general, both the active and reactive load time constants are in the same order, even though the reactive load recovery seems slightly slower.

The obtained values for the reactive transient (β_t) and steady state (β_s) parameters fit the proposed model, however, they deviate from the expected values probably due to the fact that the value Q_o used in the normalization in equation (6.2) may be equal to zero because of the effect of reactive compensation.

Table 6.3 shows the results obtained by normalizing the reactive dynamic load in equation (6.2) with S_o, sum of the active and reactive load just before the voltage variation, instead of by only using Q_o. This problem will be further discussed in Chapter 7.

Based on the new results presented in Table 6.3 it can be concluded that:

- The steady state voltage dependency parameter β_s presents negative values in some of the cases probably due to the effect of tap changer actions, in the same way as it has been described for the active load steady state parameter α_s.
- The transient voltage dependency parameter β_t is mainly related to the load composition and the percent of induction motor load in the area. Since the field measurements from test No.1 were carried out approximately during the same hours of the day and the same season of the year, the composition of the load was fairly stable, and the parameter β_t hardly varies, moving in the range of 2 to 2.6.

No	$\Delta V/V_0$ [%]	T_q [s]	β_t	β_s
1	-1.8	88	2.43	0.12
2	+1.9	165	2.02	-0.64
3	-3.7	88	2.08	-0.77
4	+3.7	89	2.42	-0.98
5	-5.3	78	2.22	-0.48
6	+5.4	92	2.62	-0.49

Table 6.3: Identified parameters for reactive response under six different voltage steps. Normalizing factor of the reactive load S_o.

Next figures, Figure 6.2 and Figure 6.3 show the voltage variation, and both, the active and reactive load response for two of the cases presented above.

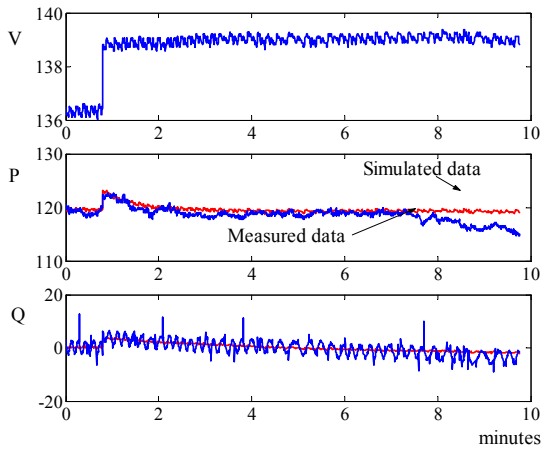

Figure 6.2: Measured and simulated load response (active and reactive), ΔV of +1.9% (case No.2) from the 130 kV-level, during 10 minutes.

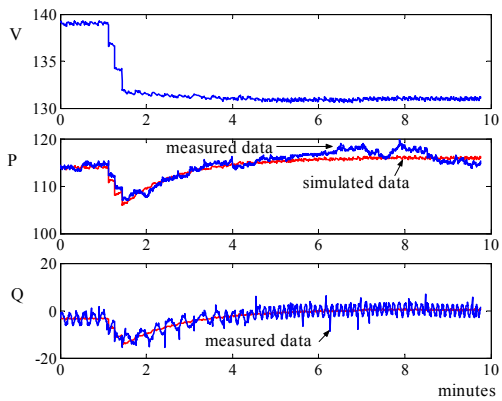

Figure 6.3: Measured and simulated load response (active and reactive), ΔV of –5.3% (case No.5) from the 130 kV-level, during 10 minutes.

6.5 Effect of Spontaneous Load Variations

The load demand is the amount of power needed by the customers in a specific area, under normal conditions of voltage and frequency. This quantity is predicted based on detailed information from the consumption side, such as characteristics of the single loads, but also histograms, average load profiles of the area, and taking into account the transfer limits of the network. On the other hand, the amount of power measured under particular conditions of voltage and frequency is called load, and this value usually differs from the forecasted demand.

Figure 6.4 shows a simplified scheme of a distribution network. The variations in the active and reactive power load, P and Q, are due to both changes on the generation side and on the consumer side. On the generation side, the action of tap changers and the switching capacitor operations result in voltage variations, voltage steps, and thus in a load variation with exponential recovery. On the consumer side, the spontaneous connection and disconnection of individual loads will alter the load. Since this phenomenon is unrelated to voltage changes, it will be uncorrelated with the exponential recovery of the load described by equations (6.1) and (6.2).

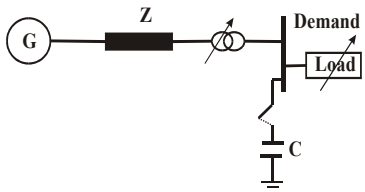

Figure 6.4: Simplified scheme of a distribution network for describing both actions, from generation and consuming side that produce load variations.

Throughout this chapter it has been shown that a voltage step gives enough information to determine the transient behavior α_t with good accuracy. On the other hand the steady state load-voltage dependency, and the time constant estimates are less accurate due to the effect of the spontaneous changes in the active load. The accuracy of those two parameters is depending on the measuring time used for the identification purpose. There is a trade-off between the minimum measuring time for the identification and the influence of spontaneous changes in the load response. If the load is strongly affected by spontaneous changes, the measuring time for capturing the effect of a voltage step should be short (trying to avoid other kind of information), but if this time is very small, there will not be enough information (sample points) for capturing the real dynamics of the system.

The active load recovery leads to a stable value approximately 10 minutes after the step has occurred. At this time the spontaneous changes still do not affect the response much. These variations hardly affect the reactive power response. The reactive load response follows the behavior of the voltage, and it is hardly affected by spontaneous changes in the load. Figure 6.5 shows a comparison between the simulated and the measured load response (P and Q), during 20 minutes. After 6.5 minutes the active load response is strongly affected by spontaneous changes. During the first 6.5 minutes, there is enough information to describe the transient but also the steady state behavior of the load.

To conclude, there is a great uncertainty in determining the proper analysis window for every case of data since spontaneous load variations may occur in the system. Therefore, the identification of load parameters on-line becomes more complicated. This problem will be discussed throughout the next chapter.

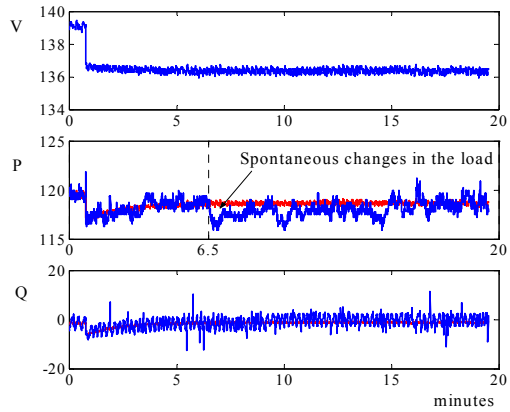

Figure 6.5: Influence of spontaneous changes in the load response. ΔV of -1.8 % (case No.1) from the 130 kV-level. Simulation time of 20 minutes.

Chapter 7

Automatic Determination of Parameters

An on-line determination of parameters requires a continuous acquisition of data, an automatic detection of voltage variations (excitation signal), and an automatic method to identify the parameters. Figure 7.1 shows a simplified scheme of the process.

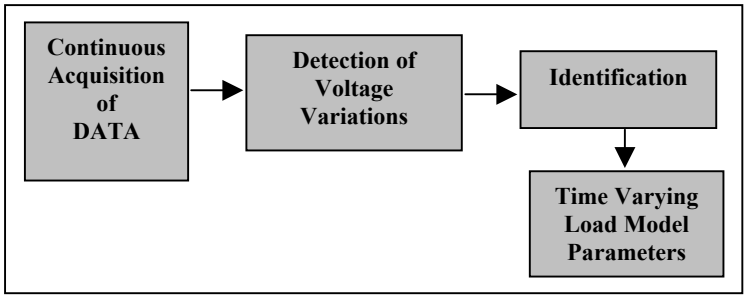

Figure 7.1: Simplified scheme of an automatic process for determination of parameter in dynamic load models.

The continuous acquisition of normal operation data will result in non-stationary load data sequences, i.e. every data case differs from the others, and different considerations will have to be taken into account for analyzing the information.

This chapter describes the difficulties that may appear during the identification, and the conditions that must be set up for carrying out the parameter estimation, i.e. the detection of significant voltage variations and the determination of the analysis window for every data set. In section 7.5,

the critical effect of the normalization factor in the reactive load representation has been studied. It has been found that an inappropriate value will affect the variability of the identified model parameters.

7.1 Conditions for Parameter Estimation

In order to get useful results from the identification it is important to determine which kind of input signal (voltage variation) is of interest and to ensure that the signal has significant excitation on the model under study [Bergh, 1996]. Afterwards, and since the recorded data provides long sequences of information, a procedure for detecting the voltage variations must be applied. The first challenge is thus to detect when the excitation starts. At that point, the detection is stopped, and the analysis for studying the physical process and to identify the load parameters is started. Right after this procedure is finished, the detection will continue.

As mentioned in Chapter 6, the determination of the window length for the identification is not easy since the data are strongly affected by the presence of spontaneous load variations. Moreover, the data must be filtered in order to reduce the noise introduced by the measuring devices or originated by the process itself during the acquisition.

7.2 Excitation

The interest of this thesis is focused on studying the load-voltage characteristic on a time scale of about 10 seconds to 10 minutes. Voltage step variations are basically the most important excitation signals in this test, since their effect will result in a pure exponential recovery of the load, as mentioned in Chapter 2. Furthermore, a step includes enough information to identify the transient behavior of the load variation, but also, and after the step, the voltage remains constant for a sufficiently long time to make it possible to describe the recovery of the load.

During normal operation at Tomelilla, step changes in voltage are caused by switching capacitors and by tap changer operations. The minimum voltage step related to these operations corresponds to one tap change, i.e. equal to ± 1.6%, and therefore it will be interesting to study variations in the order of ± 1.6% or larger.

7.3 Detection of Voltage Variations

Since the acquisition process provides long data sets, a procedure for detecting significant voltage excitation must be applied. The detection stops when a voltage variation occurs and the analysis of data is then started.

The procedure is applied to the 12 hour files acquired at Tomelilla, and it reacts when a significant voltage variation is detected. The variations are detected by comparing the mean value of the last old 20 samples with the mean value of the newest 20 acquired samples. In case there is a significant change, in the order of ± 1.6% or larger, a window of 650 samples is opened. For those 650 samples, the same procedure is applied (comparing the old samples with the newest ones) in order to detect if a new variation is occurring. If this happens a new window of 650 samples is opened at that point.

Before the detection starts, the data is low-pass filtered and resampled to 1 Hz, eliminating the effects of high frequency noise during the acquisition process. Figure 7.2 shows a flow chart describing the detection procedure.

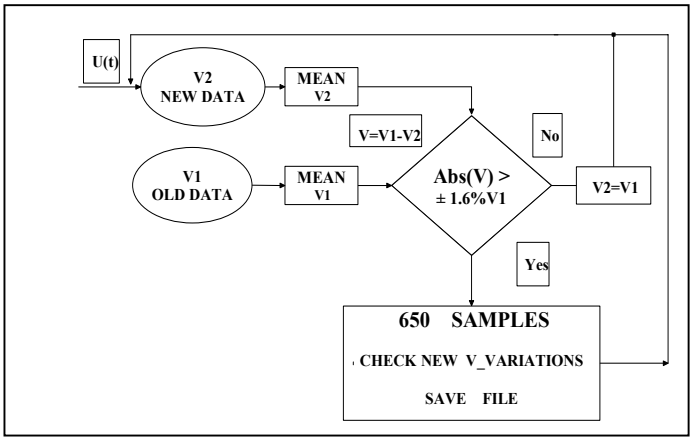

Figure 7.2: Flow chart for detection of voltage variations in the order of ± 1.6% or larger from normal operation.

The detection procedure has been tested with reported information from daily operations at Tomelilla, but also by comparing the results with those coming from another work on detection [Svantesson, 2002]. Figure 7.3 shows the data corresponding to voltage at the 20 kV-level during 2/02/02.

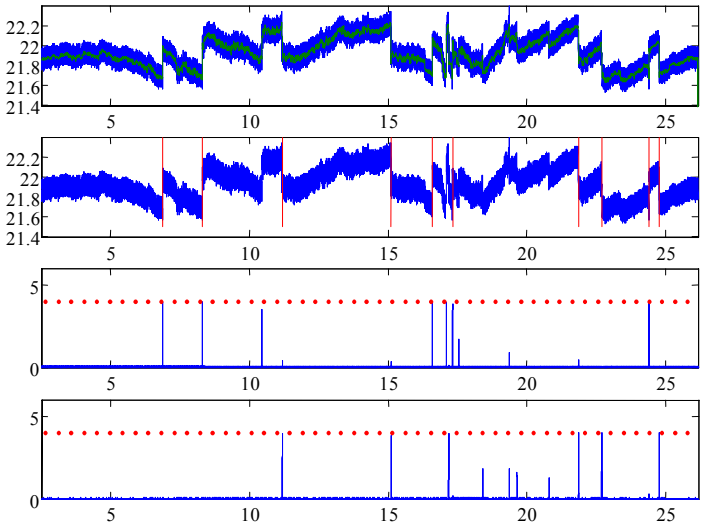

Figure 7.3: Detection of voltage steps at the 20 kV-level during Saturday 2/02/2002. The first part of the plot presents the recorded data, while the second one points at the detected steps. The third and fourth part of the figure shows the positive and negative detected steps.

7.4 Data Sequence Length

The number of samples used for the identification strongly affects the quality of the estimates, and therefore its selection is critical for the accuracy of the results. As described in Chapter 6, a large measuring time could lead to a situation very much affected by possible spontaneous load variations, i.e. connection or disconnection of loads, variations due to tap changer operations, and therefore to corrupted information. On the other hand, a very short identification time will result in a sufficiently accurate value for the transient characteristic, but inadequate for calculating time constant and steady state value, because the load response will not yet have

reached a stable level. Thus there is a trade-off between the minimum measuring time for the identification and the influence of spontaneous changes in the load response.

7.4.1. Data analysis

Measurements at the 20 kV-level during Saturday 14 July 2001 from test No.2 have been selected for studying the influence of the number of samples during the identification. Table 7.1 shows the results obtained by applying the voltage detection process described in section 7.2 and the identification procedure for 150, 200, 300 and 400 samples respectively.

The quality and robustness of the results for the different data sequence lengths have been checked by using curve fitting, and by calculating the residuals of the model [Ljung, 1995]. The values in bold represent the best estimates for every voltage variation, based on the mentioned tests.

Saturday 14 July 2001 at Tomelilla 20 kV-level							
No.	**L**	**PLOAD**			**QLOAD**		
		T_p	α_t	α_s	T_q	β_t	β_s
1	150	245	2.40	-0.30	34	-7.00	-9.00
	200	**110**	**2.30**	**1.30**	312	-8.60	-5.30
	300	110	2.30	0.50	**244**	**-8.0**	**-6.00**
	400	235	2.20	0.70	422	-9.30	-0.90
2	150	9	1.00	1.20	18	-7.60	-5.90
	200	**153**	**1.30**	**0.80**	**219**	**-7.00**	**-2.50**
	300	187	1.30	0.60	520	-7.00	2.90
	400	197	1.20	0.70	604	-7.20	5.40
3	150	**87**	**1.60**	**-0.80**	**181**	**-3.50**	**-4.50**
	200	19	1.80	0.60	270	-3.30	-6.00
	300	606	0.70	1.20	599	-2.40	-14.80
4	150	40	1.30	2.20	446	-5.70	-8.00
	200	**179**	**1.40**	**2.40**	**238**	**-5.70**	**-3.20**
	300	240	1.50	2.60	148	-6.60	-3.50
	400	811	1.40	6.41	172	-6.50	-3.50

Table 7.1: Results from the identification by using 150, 200 and 300 samples respectively.

Figure 7.4 shows the detected voltage variation and the corresponding active and reactive response for case No.2. Residuals and curve fitting tests have been applied, and the results are included in Table 7.2. Ok or Not Ok define if the result of a test is accepted and if the quality of the estimates is good enough.

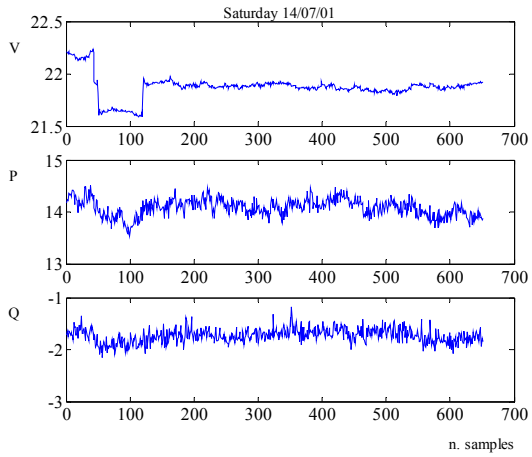

Figure 7.4: Detected voltage variation and its corresponding dynamic active and reactive response, for case No.2.

Saturday 14 July 2001 at Tomelilla				
L	RESIDUALS		FITTING	
	P	Q	P	Q
150	Ok	Ok	Not Ok	Not Ok
200	Ok	Ok	Ok	Ok
300	Not Ok	Ok	Ok	Ok
400	Not Ok	Ok	Not Ok	Ok

Table 7.2: Curve fitting and residuals.

Figure 7.5 shows a comparison between the simulated and the measured load during 10 minutes. The load response is strongly affected by spontaneous variations during the first samples, i.e. disconnection of a load. At around sample no 250 the load response reaches a stable value. After 300 samples some oscillations, overshooting and undershooting due to tap changer operations may affect the accuracy of the identification. The second

plot in Figure 7.5 presents the difference between the measured and simulated data. This difference describes the effect of the mentioned variations, which are not included in the exponential load model.

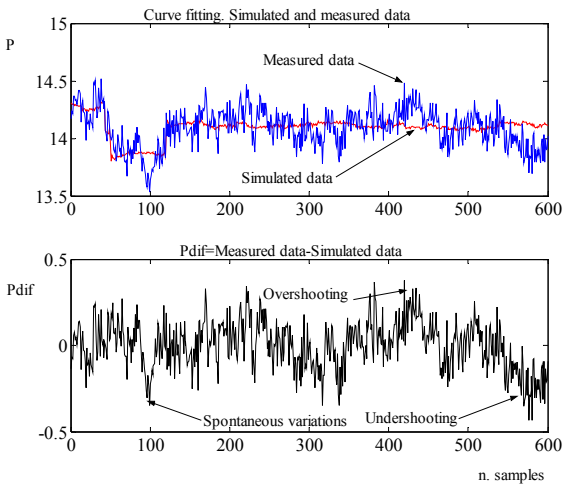

Figure 7.5: Influence of spontaneous variations in the load.

Figure 7.6 shows the correlation of the residuals of the system when 200 samples have been used for the identification. The result deviates from the expected white noise profile, which is related to those variations not included in the model.

The lower part of Figure 7.6 displays the autocorrelation function of *e*, residuals or prediction error, and the cross correlation between *e* and the inputs. A 99% confidence interval for those variables is also displayed, assuming that *e* is white noise and independent from the input *u*. If the correlation function goes significantly outside of that interval the model cannot be accepted because there is linear dependency in the residuals and consequently the model is not properly fitting the data. Correlation between *e* and *u* for negative lags means output feedback, and it is not a reason to reject the model. Only correlation on positive lags is of interest for validation, i.e. only when the data is shifted to later dates.

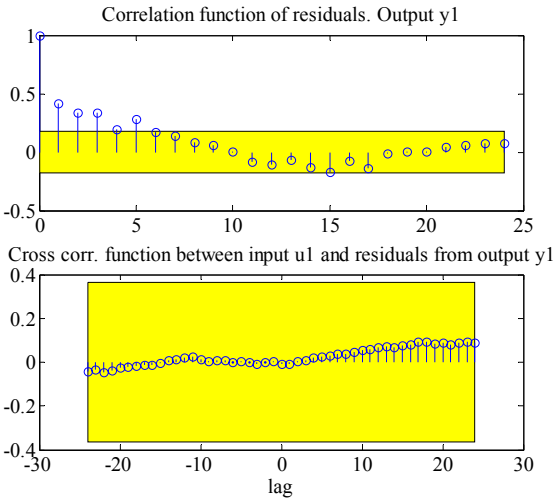

Figure 7.6: Calculated residuals for 200 samples.

The reactive response is hardly affected by spontaneous load variations. Figure 7.7 verifies that this influence is small. In Figure 7.8 the residuals of the system when 200 samples have been used for the identification are presented.

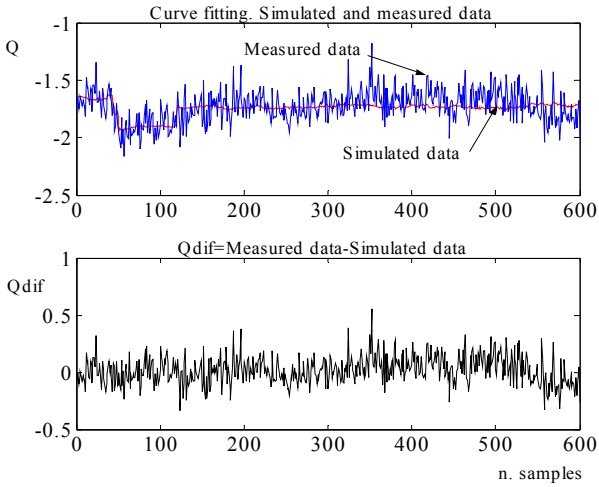

Figure 7.7: Influence of spontaneous variations in the load.

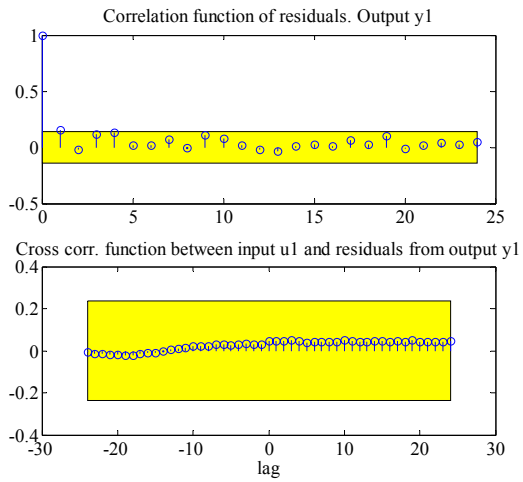

Figure 7.8: Calculated residuals for 200 samples.

If the number of samples used for the identification is increased, the quality of the estimates will be compromised and the residual plot will result in a less accurate profile. Figure 7.9 shows the result of the residuals when 400 samples have been used in the identification.

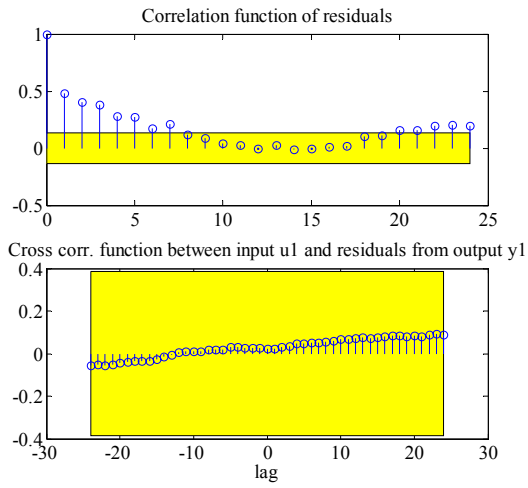

Figure 7.9: Calculated residuals for 400 samples.

In general, it can be concluded that a good estimation is obtained by choosing the measuring time to about 2.5-3 times the value of the load time constant, after the voltage variation has happened.

7.4.2. Resistive characteristic of the load

Whereas this window length achieves accurate estimates for the three parameters, the measuring time can be considerably reduced to a value close to the disturbance time if the identification purpose is limited to determining the transient behavior of the load. In the transient frame the active power demand of most loads, including heating and motors, behave like constant impedance. This is equivalent to an algebraic quadratic voltage dependence, which corresponds to the value 2 of the exponent α_t. Figure 7.10 shows the voltage in File No.1, a step change.

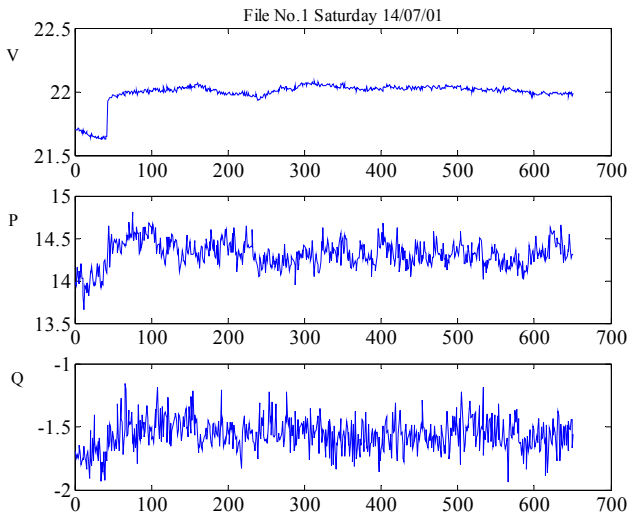

Figure 7.10: Voltage variation, active and reactive power.

Table 7.3 and Table 7.4 show the values for the transient estimates for active and reactive load, α_t and β_t respectively, using different number of samples just after the step has occurred (t=43 seconds). Assuming that α_t should be in the neighborhood of 2, the values in Table 7.3 can be

evaluated. According to these results and depending on the identification purpose, it is possible to study the dynamic load response in a shorter or longer time frame. Figure 7.11 shows the principal behavior of the exponential recovery of the load after a voltage step.

Active Transient Characteristic of the load		
Percent of T_p	**Window Length**	**α_t**
5%	49	1.69
10%	54	1.99
15%	60	2.32
20%	65	2.06
25%	71	1.99
30%	75	1.80

Table 7.3: Identification of the transient behavior for active load under a step change at t=43 seconds. T_p=110 seconds.

Reactive Transient Characteristic of the load		
Percent of T_q	**Window Length**	**β_t**
5%	55	-11.30
10%	67	-4.30
15%	80	-6.30
20%	92	-7.87
25%	104	-7.97
30%	116	-7.47

Table 7.4: Identification of the transient behavior for reactive load under a step change at t=43 seconds. T_q=244 seconds.

A window length of approximately 15% of the value of the load time constant is enough for identifying accurately the short-term characteristic of the load. During (15-30)% of the value of the load time constant, the load has a resistive characteristic. By increasing the window length to 2.5-3 times the load time constant, an accurate value for the steady state behavior and for the time constant will be also obtained.

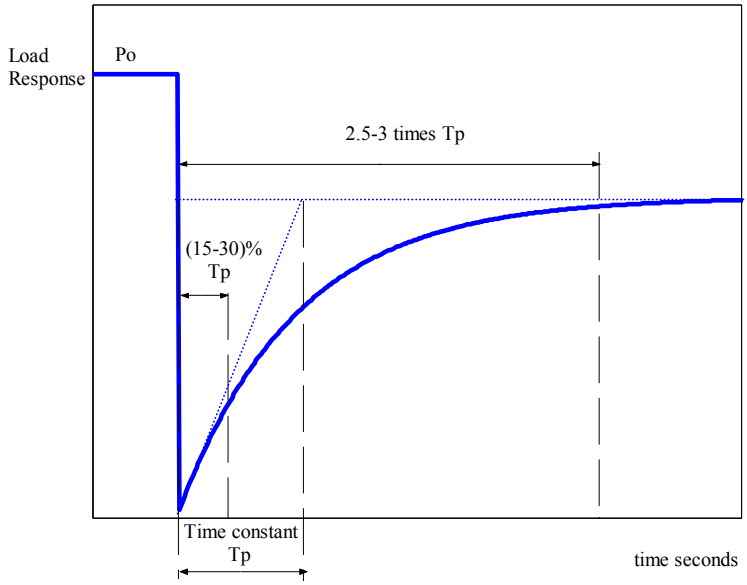

Figure 7.11: Exponential recovery of the load.

7.5 Normalization of Dynamic Reactive Load Models

The critical effect of the normalization factor in the variability of the reactive load parameters has been mentioned in Chapter 6, where the identified reactive steady state and transient parameters deviated to very large values, when the value Q_o used in the normalization in Equations (6.1) and (6.2), was close to zero. By using measured data from normal operation it is shown that the reactive power level, which has previously been used, as normalization factor is inappropriate. If instead apparent power level is used for normalization, the variability in the parameters that describe the reactive load response is drastically reduced. The common value Q_o used in the normalization of the reactive load models may be close to zero due to the effect of reactive compensation, and therefore the reactive load parameters that describe the load response will deviate to very large values. The measured data is collected with different amounts of reactive compensation. This makes it possible to describe how the reactive load parameters change with the value of Q_o.

7.5.1 Determination of parameters in reactive load models

Based on the described nonlinear model in Chapter 6, equations (6.1) and (6.2), the corresponding reactive load representation is given by (7.1) and (7.2), and characterized by three parameters, reactive steady state load-voltage dependence, reactive transient load-voltage dependence and a load-recovery time constant.

$$T_q \frac{dQ_r}{dt} + Q_r = Q_o \left(\frac{V}{V_o} \right)^{\beta_s} - Q_o \left(\frac{V}{V_o} \right)^{\beta_t} \tag{7.1}$$

$$Q_l = Q_r + Q_o \left(\frac{V}{V_o} \right)^{\beta_t} \tag{7.2}$$

V_o and Q_o are the voltage and power consumption before a voltage step change. Q_r is the reactive power recovery, Q_l is the total reactive power response, T_q is the reactive load recovery time constant, β_t is the transient reactive load-voltage dependence, and β_s is the steady state reactive load-voltage dependence. In analogy with Chapter 6 the non-linear model is simplified to a linear identification problem by linearizing around an operating point (V^*). New quantities have been introduced, and the state space representation is given by (7.3) and (7.4):

$$A_q = \beta_t \cdot \left(\frac{V^*}{V_o} \right)^{\beta_t - 1} \qquad B_q = \beta_s \cdot \left(\frac{V^*}{V_o} \right)^{\beta_s - 1} \qquad u = \frac{\Delta V}{V_o}$$

$$\Delta Q_l = \Delta Q_r + Aq \cdot Q_o \cdot u \tag{7.3}$$

$$T_q \cdot \frac{\Delta Q_r}{dt} = B_q \cdot Q_o \cdot u - A_q \cdot Q_o \cdot u - \Delta Q_r \tag{7.4}$$

By introducing $T_{q1} = T_q \cdot A_q$, the reactive load variation ΔQ_l is given by (7.5). A similar equation can be derived for the active load variation.

$$\frac{\Delta Q_l}{Q_o} = \frac{B_q + s \cdot Tq_1}{1 + s \cdot Tq} \cdot \frac{\Delta V}{V_o} \tag{7.5}$$

The transfer function (7.5) represents the load response when a voltage change is occurring in the system. It is characterized by three parameters, reactive steady state voltage dependency B_q, reactive transient voltage dependency A_q, and reactive time constant T_q. ΔQ_l and ΔV represent deviations from the steady state values Q_o and V_o. The reactive load equation has been normalized by using Q_o. The aim is then, to use the described linearized model (7.5) and to identify its parameters with measured data. The least squares optimization algorithm is used in the identification.

7.5.2 Normalization in dynamic load models

The identification process proposed above has been applied to different sets of data, as exemplified by test No.1 and No.2.

Test No.1

The test, check section 4.2, is based on previous measurements in the power system in the South of Sweden [Le Dous, 1999], [Karlsson, 1992]. The data originates from six different experiments in the 400-130 kV-transmission system during June 1996. The voltage changes were made by simultaneous manual operation of tap changers on the 400/130 kV transformer. Six different sets of data have been used in the simulation.

No	$\Delta V/V_0$ [%]	T_p [s]	α_t	α_s
1	-1.8	135	1.36	0.25
2	+1.9	40	1.70	-0.10
3	-3.7	61	1.31	-0.16
4	+3.7	74	1.35	-0.54
5	-5.3	70	1.65	-0.32
6	+5.4	78	1.60	-0.08

Table 7.5: Identified parameters for active load response under six different voltage steps.

No	$\Delta V/V_0$ [%]	T_q [s]	β_t	β_s	Qo [MVar]
1	-1.8	89	-181.80	7.90	-0.974
2	+1.9	256	-687.20	975.60	-0.046
3	-3.7	88	87.67	31.86	-2.850
4	+3.7	105	104.50	-148.56	0.867
5	-5.3	78	77.89	19.35	-2.840
6	+5.4	94	94.18	-49.75	1.254

Table 7.6: Identified parameters for reactive load response under six different voltage steps. Normalizing factor of the reactive load Q_o.

The identified parameters for the active load, Table 7.5, exhibit low variability and correspond to acceptable values. The reactive parameters, however, are less reliable. Even though the reactive transient *(β_t)* and steady state *(β_s)* parameters fit the proposed model in each case, they deviate from the expected values. An important factor contributing to this may be that the value Q_o used in the normalization in equations (7.1) and (7.2) may be close to zero because of the effect of reactive compensation. By checking the factor Q_o in Table 7.6 it is observed that for those values closer to zero, the deviation in the identified parameters is larger. Figure 7.12 shows a simple representation of the total load as the sum of the effect of the active and reactive power.

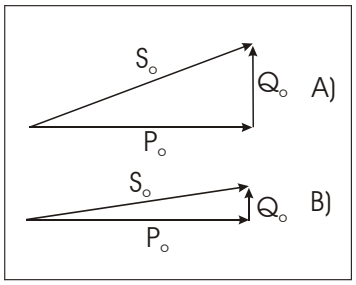

Figure 7.12: Total load S_o, as the sum of the active and reactive effect, P_o and Q_o, when reactive compensation is and is not needed, figure B) and A) respectively.

The load response in Figure 7.12.A is not affected by reactive compensation while it is in Figure 7.12.B. The value Q_o is reduced to a value closer to zero due to the effect of capacitors, but P_o remains constant. Since theoretically,

when Q_o tends to zero, the model parameters will go to infinity, it is necessary to normalize the reactive load model by some other factor that is not affected by this phenomenon. Suggested candidates are P_o or S_o. By normalizing by S_o the reactive load representation is then given by equations (7.6) and (7.7):

$$T_q \frac{dQ_r}{dt} + Q_r = S_o \left(\frac{V}{V_o} \right)^{\chi_s} - S_o \left(\frac{V}{V_o} \right)^{\chi_t} \tag{7.6}$$

$$Q_l = Q_r + S_o \left(\frac{V}{V_o} \right)^{\chi_t} \tag{7.7}$$

V_o and S_o are the voltage and apparent power levels before a voltage step change. Q_r is the reactive power recovery, Q_l is the total reactive power response, T_q is the reactive load recovery time constant, χ_t is the transient reactive load-voltage dependence, and χ_s is the steady state reactive load-voltage dependence. Table 7.7 shows the results obtained by normalizing the reactive dynamic load in equation (7.2) by S_o. The quality of the reactive power parameter estimates is now similar to those for the active power.

No	$\Delta V/V_0$ [%]	T_q [s]	χ_t	χ_s
1	-1.8	88	2.43	0.12
2	+1.9	165	2.02	-0.64
3	-3.7	88	2.08	-0.77
4	+3.7	89	2.42	-0.98
5	-5.3	78	2.22	-0.48
6	+5.4	92	2.62	-0.49

Table 7.7: Identified parameters for reactive load response under six different voltage steps. Normalizing factor of the reactive load S_o.

Test No.2

The data originates from a continuous acquisition from normal operation data in the 130-50-20 kV distribution system in the South of Sweden, see section 5.3. Due to the fact that the continuous acquisition of data provides

large amount of information that corresponds to non-stationary load data sequences, i.e. every data case differs from the others, it has been possible to study the impact of reactive compensation during daily operations on the representation of the reactive load. Measurements at the 20 kV-level during February 2002 have been selected for the analysis. The identification procedure described in this thesis has been applied to the mentioned data.

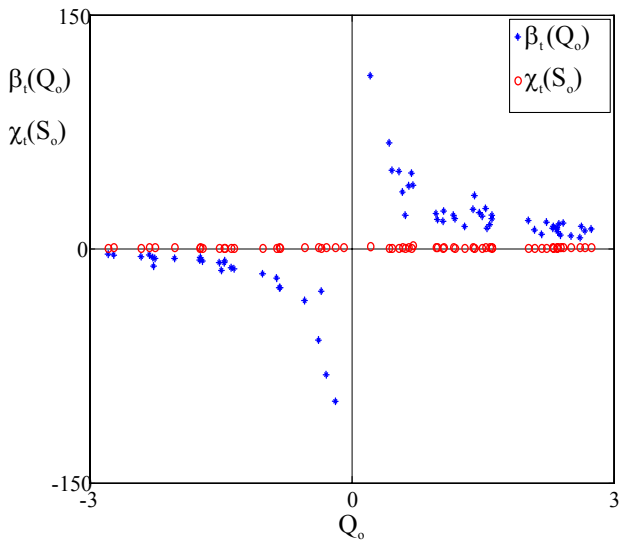

Figure 7.13: Effect of the reactive compensation in the identification of the parameter χ_t, using the normalization factor Q_o and S_o respectively.

Figure 7.13 shows the result of the identification for the reactive transient part of the load, plotted against the power level Q_o, when the reactive load equation has been normalized by Q_o, asterisk '*', and by S_o, circle 'o', respectively. By normalizing with Q_o, when the value Q_o goes to zero, the transient parameters, β_t, tend to plus or minus infinity, and they apparently deviate significantly from their normal values. On the other hand, by normalizing with S_o, the transient parameter χ_t, exhibits small variability. When the value Q_o is in the neighborhood of 0, the parameters do not deviate from the physically expected values, since S_o is hardly affected by the effect of reactive compensation.

Figure 7.14 presents the result of the identified parameter χ_t, when the normalization factor is S_o. The identified parameters remain in a limited interval.

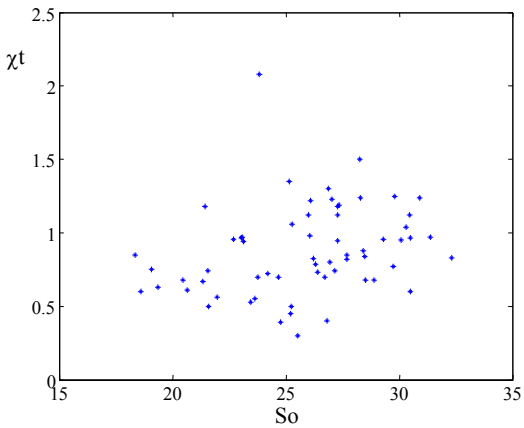

Figure 7.14: Effect of the reactive compensation in the identification of the parameter χ_t using the normalization factor S_o.

7.5.3 Conclusions

The availability of continuous normal operation data has provided long data sets. An automatic procedure to detect voltage variations has been implemented.

The influence of the data sequence length for the identification has been studied. A good estimation is achieved by choosing a window length of 2.5-3 times the load time constant, after a voltage change. If the identification is limited to determining the transient characteristic of the load, the measuring time can be considerably reduced to an approximate value of 15% of the time constant. Moreover, the measurements have verified that during the first 15-30% of the recovery the load behaves as a resistance, i.e. transient characteristic in the neighborhood of 2.

The effect of normalization on dynamic load models has been studied. The factor Q_o previously used to normalize the reactive load model is inappropriate since it may be equal to zero due to the effect of switching

capacitor operations. The identification of parameters for the reactive load model when normalizing by Q_o shows that these parameters tend to infinity when Q_o goes to zero. On the other hand, an accurate representation of the reactive load is achieved by normalizing with the factor S_o, since this factor is hardly affected by reactive compensation.

Chapter 8

Analysis of Experimental Results

The collected data have provided information to investigate the daily, weekly and seasonal variations of the load model parameters. The process described in Chapter 6 and Chapter 7 to determine load model parameters has been applied to data from normal operation during the periods indicated in Figure 8.1. The identified parameters and associated time of day are addressed in several tables in [RomeroLic, 2002].

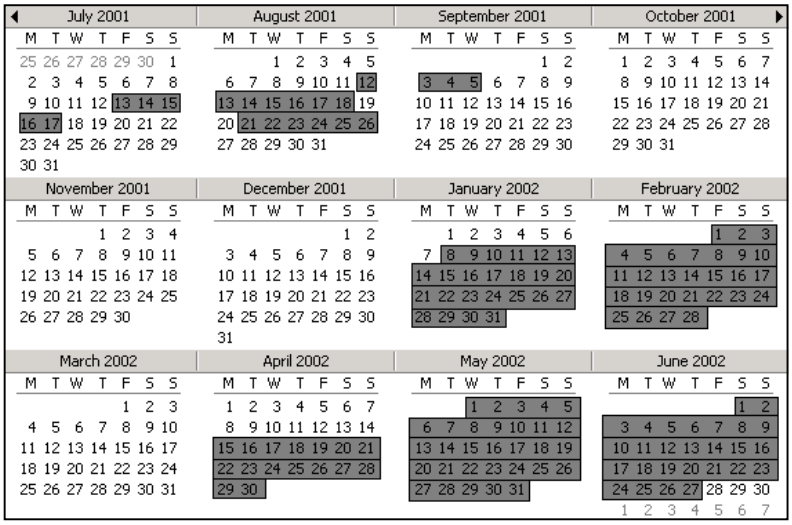

Figure 8.1: Periods of normal operation during July 2001-June 2002, when data has been acquired.

8.1 Analysis of Variability of the Parameters

The large amount of information presented in [RomeroLic, 2002] makes the study of the variability of the parameters difficult, because it corresponds to different seasons and times of the year, but also to large variety of load processes. Sections 8.1.1 and 8.1.2 present the annual and daily variability of the parameters respectively.

The availability of data is shorter during some periods of time due to initial problems in the acquisition process. This has resulted in deviations in some of the identified parameters.

8.1.1 Annual variability

The monthly mean value and standard deviation for each of the identified parameters have been calculated, and they are presented in Table 8.1.

DATE	PLOAD			QLOAD		
	T_p	α_t	α_s	T_q	β_t	β_s
July 01	145 (112)	1.58 (0.33)	1.20 (1.43)	196 (60)	0.87 (0.21)	0.61 (0.67)
Aug. 01	140 (79)	1.43 (0.37)	0.81 (1.21)	180 (76)	1.20 (0.35)	0.39 (0.94)
Sept. 01	168 (156)	1.52 (0.27)	0.65 (0.69)	155 (96)	1.31 (0.30)	0.51 (0.38)
Jan. 02	127 (52)	1.84 (0.50)	0.63 (1.00)	126 (48)	0.79 (0.22)	0.48 (0.59)
Feb. 02	161 (104)	2.08 (0.62)	0.60 (0.90)	151 (78)	0.87 (0.30)	0.30 (0.48)
Apr. 02	134 (55)	1.75 (0.51)	0.57 (1.23)	132 (55)	0.77 (0.22)	0.58 (0.66)
May 02	123 (51)	1.65 (0.63)	0.44 (1.24)	132 (52)	0.95 (0.32)	0.58 (0.78)
June 02	123 (56)	1.38 (0.67)	0.34 (1.16)	126 (51)	1.11 (0.37)	0.75 (0.79)

Table 8.1: Monthly mean values for the identified parameters in the proposed dynamic load model. Standard deviations are shown within parentheses.

Figure 8.2 shows the variability of each one of the above mentioned parameters, active power time constant T_p, active power transient voltage dependency α_t, active power steady state voltage dependency α_s, reactive power time constant T_q, reactive power transient dependency β_t, and reactive power steady state dependency β_s, during the period of time July 2001 to June 2002. It should be noted that the standard deviation is sometimes very large compared to the parameter value. This is further discussed in this chapter.

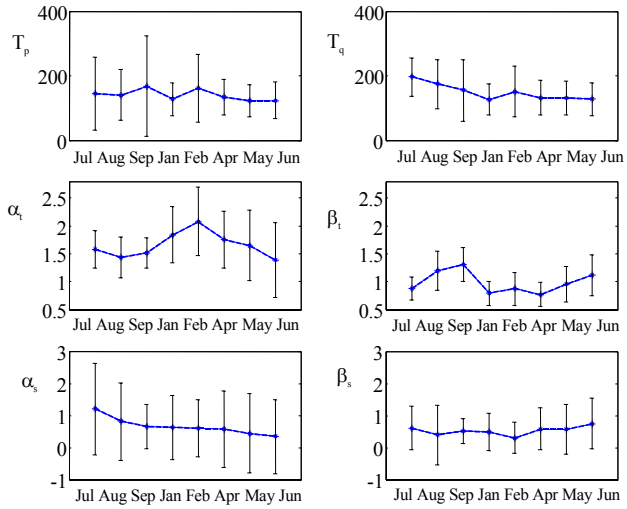

Figure 8.2: Annual variability of active and reactive power parameters in dynamic load models based on monthly averages.

Based on both Table 8.1 and Figure 8.2 it has been observed:

Time constants, T_p and T_q

- In general the active recovery of the load seems slightly faster in summer than in winter. The monthly active time constant for September (Figure 8.2) shows a different pattern. This value is not trustable since it has been calculated using few data points.

- The value of both the active and reactive time constants move in the same order in a range of about 80 to 200 seconds. Figure 8.3 shows the correlation between these two parameters for all the available data from July 2001 to June 2002. A correlation factor equal to 0.41 has been found. The figure shows a high concentration around the mentioned range, while the disparity in the results increases for values larger than 200 or smaller than 80 seconds.

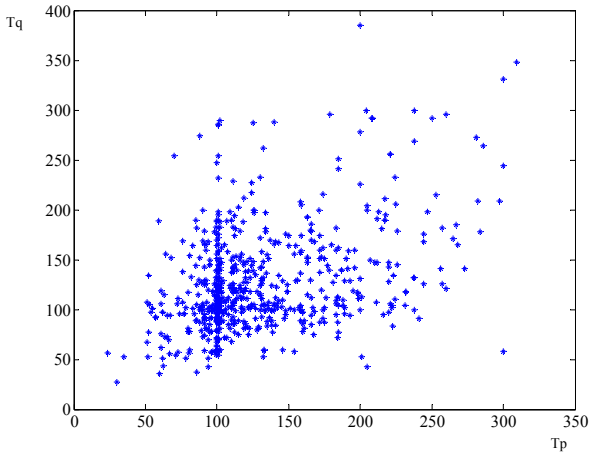

Figure 8.3: Correlation between active and reactive load time constants.

- Both time constants move in the same order, however, the reactive load recovery seems slightly slower. The main recovery of the reactive load is produced by the increase of the reactive losses due to the active recovery of the load at low voltages. This conclusion is justified further in this chapter.

- Figure 8.3 shows, especially between 80 to 200 seconds, how the variability of the correlation between both parameters is not constant. For example for a 100 seconds active time constant, different values for the reactive time constant have been obtained and therefore different correlation between both parameters. The real and reactive powers are coupled and both real and reactive power load models should be simultaneously identified, with coupling effects. The correlation is not constant all the time, since it is depending on how much other external stochastic disturbances affect the system, i.e. spontaneous load variations or other unmodeled dynamics. A more accurate dynamic model will be desired in order to decrease uncertainty in the determination of these two parameters. A good suggestion for future work is the implementation of a dynamic model as a combination of the studied physical model and a stochastic extension.

- Figure 8.4 shows the correlation between the active and reactive load time constants, when instead of using all the available data like in Figure 8.3, the monthly average active and reactive time constants are used. A correlation factor of 0.50 has been obtained. Later on it will be examined how the parameters can be better correlated during certain operating conditions.

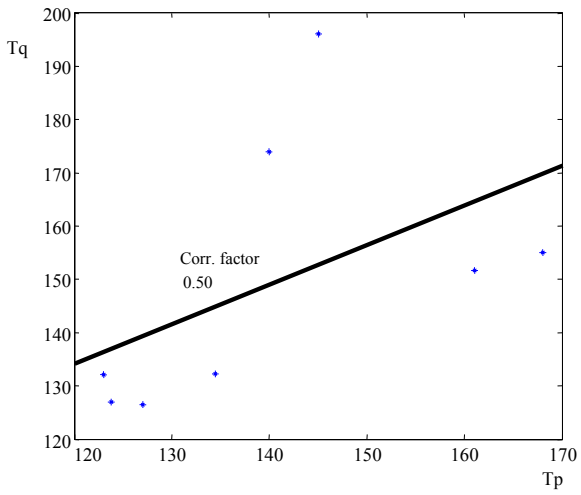

Figure 8.4: Correlation between the monthly average active and reactive load time constants during July 2001-June 2002.

There is an outlier in the data corresponding to July. July has few data points, and the weekend is a significant part of the data. This factor may have affected the value of the identified time constants.

During the weekends most of the load type is residential. However industrial processes, which are characterized by larger time constants, may be started during Saturday and Sunday nights. The standard deviation for the identified active and reactive time constants is large. The reason may be related to the daily diversity of load processes. The measured load aggregates different load classes, industrial, residential and commercial, but also different load compositions, induction motors, electric heating, street

lighting, which are described by different load characteristics. Table 8.2 shows the time constant values of some of the most common loads.

Type of Load	Load Recovery Time Constant
Induction Motors	Few seconds
Tap Changers & Voltage Regulators	10 seconds-several minutes
Constant energy resistive loads	Several minutes
Fluorescent Lamps	1-2 minutes

Table 8.2: Approximate time constant values for some of the most common loads.

Active transient load-voltage dependence α_t

- During the winter and due to the low temperatures, the heating demand increases, and therefore the use of heating with thermostat control. This kind of device presents a resistive characteristic. Table 8.1 shows α_t moving in a range of 1.30 to 2.10. The value 2.10 has been obtained for the coldest month, and it is associated to a pure resistive behavior of the load. The active transient part of the load is strongly correlated to the temperature, i.e. the colder it is the larger parameter α_t is obtained. Figure 8.5 shows this correlation. Correlation factor of –0.82.

Reactive transient load-voltage dependence β_t

- The obtained values of β_t are in the range of 0.70 to 1.30. The parameter β_t is depending on the temperature, (see Figure 8.2). The parameter is higher during warm months and lower during winter. Since the measurements have been carried out in the same area, and the load composition hardly has changed, the variability of the identified values for this parameter may be related to dis/connection of air conditioners and heat pumps, and other similar loads during winter/summer. Figure 8.6 shows the estimated correlation between this parameter and the temperature.

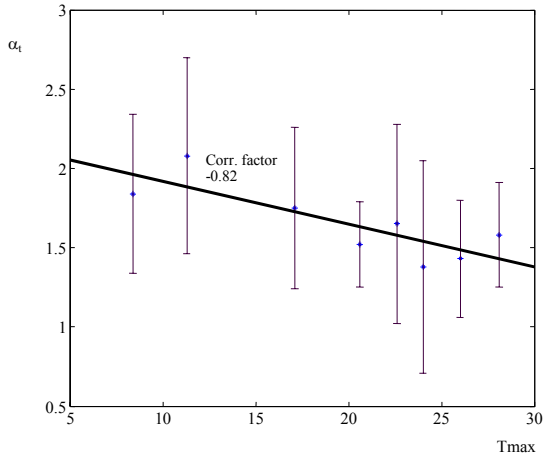

Figure 8.5: Correlation between the monthly average values for the active transient load-voltage dependence α_t and the corresponding maximum average temperature for every month.

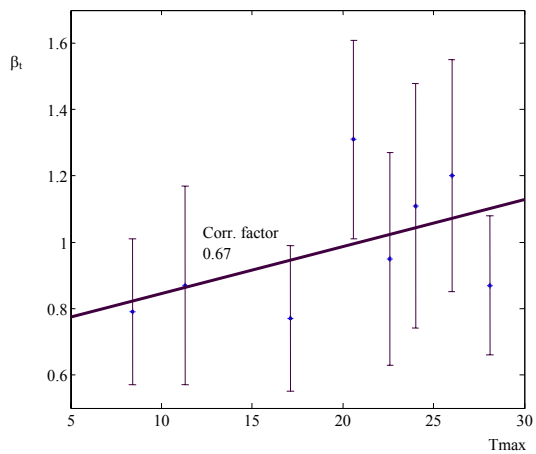

Figure 8.6: Correlation between the monthly values for the reactive transient load-voltage dependence β_t and the corresponding maximum average temperature for every month.

Active and reactive steady state load-voltage dependence α_s β_s

- Table 8.1 shows that the parameters α_s and β_s move in a range of about 0.30 to 1.20 and 0.30 to 0.75 respectively. Furthermore, the identified parameters present a large variability that can be associated to the large diversity of load processes mentioned before.

- In some cases the parameters present negative values. The stationary level reached by the load after the recovery is equal to or higher than the expected one, probably due to the effect of the tap changers, resulting in an over or undershooting of the load. An important contribution to voltage instability may be caused by unexpected values of these parameters, such as active or reactive load overshooting resulting from negative values of α_s or β_s.

8.1.2 Daily variability of the parameters

Since the variability of the values of the time constants and steady state characteristics is still large, a new distribution of the results has been done. The 24 hours of a day has been divided into three periods of time, as follows:

- Period I: Day, for the interval of hours from 6:30 to 17:30. This period of time includes the commercial and working hours.

- Period II: Evening, for the interval of hours from 17:30 to 22:00. The time corresponds mainly to residential activity and some street lighting.

- Period III: Night, for the interval of hours from 22:00 to 6:30. This period of time corresponds to some industrial activity during the night, but mainly to street lighting.

The monthly mean value and standard deviation for day, evening and night hours, have been calculated for each one of the identified parameters presented in [RomeroLic, 2002]. The results are presented in the next three tables, Table 8.3 for monthly variability during the day, Table 8.4 for monthly variability during the evening, and Table 8.5 for the variability during the night.

DAY	PLOAD			QLOAD		
	T_p	α_t	α_s	T_q	β_t	β_s
July	195 (98)	1.60 (0.46)	1.07 (1.53)	216 (51)	0.91 (0.20)	0.33 (0.56)
Aug	133 (92)	1.52 (0.19)	0.60 (1.70)	176 (80)	1.34 (0.36)	0.49 (0.26)
Sept	168 (156)	1.52 (0.27)	0.65 (0.69)	155 (96)	1.31 (0.30)	0.51 (0.38)
Jan	122 (45)	1.89 (0.43)	0.39 (1.00)	129 (53)	0.87 (0.21)	0.66 (0.63)
Feb	125 (68)	2.03 (0.55)	0.40 (0.85)	142 (71)	0.88 (0.32)	0.52 (0.63)
Apr	136 (61)	1.70 (0.56)	0.46 (0.41)	138 (58)	0.81 (0.23)	0.56 (0.64)
May	122 (49)	1.53 (0.56)	0.48 (1.21)	136 (54)	1.04 (0.32)	0.64 (0.74)
June	125 (53)	1.50 (0.80)	0.68 (1.17)	128 (44)	1.17 (0.37)	0.82 (1.03)

Table 8.3: Variability of load model parameters during day hours.

EVEN.	PLOAD			QLOAD		
	T_p	α_t	α_s	T_q	β_t	β_s
July	99 (11)	1.45 (0.07)	0.90 (0.80)	163 (109)	0.72 (0.14)	1.65 (0.26)
Aug	122 (64)	1.26 (0.74)	0.93 (0.97)	214 (73)	1.33 (0.15)	0.66 (0.59)
Sept	168 (156)	1.52 (0.27)	0.65 (0.69)	155 (96)	1.31 (0.30)	0.51 (0.38)
Jan	124 (51)	1.76 (0.55)	0.73 (0.88)	122 (45)	0.76 (0.17)	0.36 (0.55)
Feb	119 (53)	1.85 (0.47)	0.59 (0.72)	127 (65)	0.80 (0.25)	0.36 (0.52)
Apr	147 (55)	1.67 (0.43)	0.31 (0.85)	137 (54)	0.79 (0.16)	0.67 (0.60)
May	126 (55)	1.78 (0.59)	0.42 (1.28)	122 (45)	0.89 (0.27)	0.56 (0.70)
June	107 (38)	1.40 (0.73)	0.63 (1.12)	118 (35)	0.96 (0.23)	0.83 (0.96)

Table 8.4: Variability of load model parameters during evening hours.

NIGHT	PLOAD			QLOAD		
	T_p	α_t	α_s	T_q	β_t	β_s
July	133 (64)	1.61 (0.27)	0.86 (0.76)	205 (30)	0.90 (0.37)	0.41 (0.09)
Aug	141 (111)	1.45 (0.28)	0.60 (0.17)	189 (79)	1.00 (0.31)	0.05 (1.10)
Sept	168 (156)	1.52 (0.27)	0.65 (0.69)	155 (96)	1.31 (0.30)	0.51 (0.38)
Jan	134 (58)	1.82 (0.51)	0.68 (0.90)	126 (42)	0.73 (0.23)	0.39 (0.55)
Feb	126 (65)	2.23 (0.53)	0.43 (0.25)	140 (61)	0.67 (0.21)	0.33 (0.59)
Apr	134 (49)	1.71 (0.46)	0.45 (0.60)	116 (45)	0.72 (0.24)	0.51 (0.61)
May	119 (47)	1.65 (0.50)	0.60 (0.99)	138 (59)	0.75 (0.28)	0.40 (0.86)
June	118 (55)	1.37 (0.58)	0.58 (1.14)	133 (63)	0.96 (0.27)	0.55 (1.28)

Table 8.5: Variability of load model parameters during night hours.

In general, the standard deviation of the identified time constants has decreased probably because of the fact that the results have been grouped

into three different classes with different load characteristics, and therefore the diversity of load processes in each of these groups has decreased. On the other hand, even though the standard deviation has decreased considerably, it is still large for some of the parameters. To achieve more accurate results it would be necessary to apply more advanced data analysis techniques. By sorting the data differently the results may be improved further. A new classification could be by grouping the data in a weekend and week type, especially in July 2001 when the weekend is a significant part of the available data. Other suggestion is to group in relation to the type of process, industrial residential, commercial, rural, or even considering different patterns for a weekday (day, evening and night), a Saturday, and a Sunday.

Based on the information in Table 8.3, Table 8.4 and Table 8.5, a comparison of the variability during the day, evening and night hours for each one of the parameters has been done. The information from September is not included, since the few acquired samples during this period make the data unreliable. It has been observed:

Active and reactive time constants

- Figure 8.7 shows the variability of the active time constant. This parameters seems uncertain and difficult to track. On one hand it seems that the recovery of the load is slightly faster during the summer than the winter, check Figure 8.7 during June, July and August. This may be due to the fact that during summertime the demand of electric heating is considerably reduced, the effect of thermostats is reduced, most of the load is street and commercial lighting, and therefore the recovery of the load is lower i.e. shorter time to reach the steady state. The lowest values of the time constants are obtained during the evening hours, and during summer time. The load processes are related to residential activity. On the other hand unexpected fast recoveries during February, and small differences with summertime values during January have been obtained.

- The only conclusion the author could draw with certainty is that the variability of the time constants may be dependent on temperature but mainly on the composition of the load. The fact that aggregated

load has been used for this work makes it difficult to study how the different load processes affect the variability of the parameter.

- Both active and reactive time constant values move approximately in the same order.

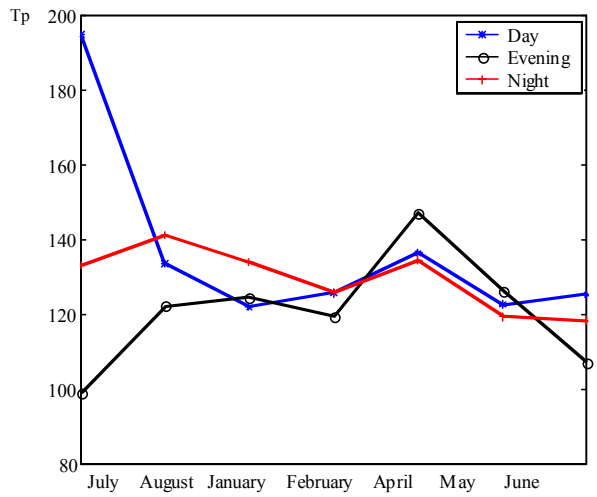

Figure 8.7: Annual variability of the active time constant for day, evening and night hours.

Active transient load-voltage dependence α_t

- Figure 8.8 shows the dependency of this parameter on the temperature for the three times of the day. The larger values have been obtained for the colder months and the lower for the warmer ones because of the variation in heating demand.

- During the summer the parameter exhibits the lowest values; values during evening and night hours are 1.4 and 1.3 respectively. Higher values correspond to day hours. The reason is probably due to the mild weather and the increase of light hours, which will change the residential habits, and therefore decrease the heating demand.

- During the winter, the higher values are associated to the night hours, which is justified by the large percent of electric heating connected due to the cold temperatures.

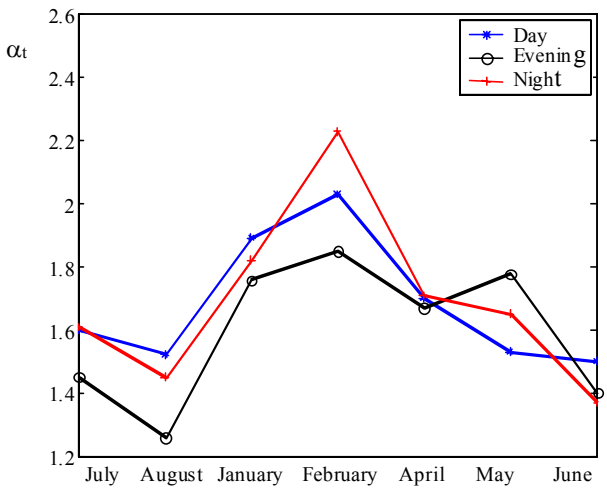

Figure 8.8: Annual variability of the active transient load-voltage dependence α_t for day, evening and night hours.

Reactive transient load-voltage dependence β_t

- Figure 8.9 shows the dependency of this parameter on temperature; the values are larger during the summer and lower during the winter. Since the summers in the South of Sweden are characterized by mild temperatures the connection of air conditioner units is hardly necessary, and – if it occurs - only during the day hours. The lowest parameter values have been obtained during night hours, while the highest ones during day hours.

- During the winter the parameters exhibit low values for the three times of the day. The highest values correspond to day hours, mainly associated to industrial processes.

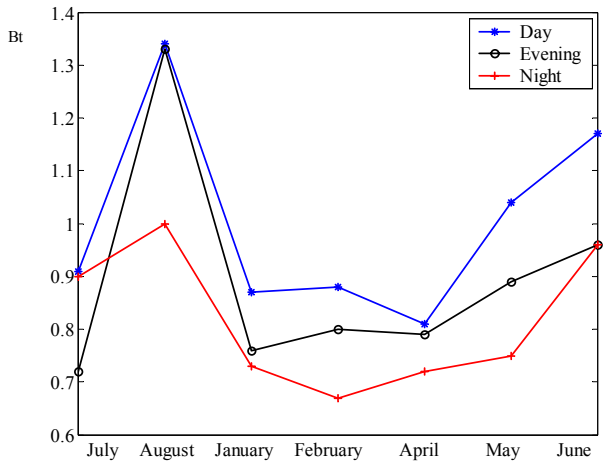

Figure 8.9: Annual variability of the reactive transient load-voltage dependence β_t, during day, evening and night hours.

Active and reactive steady state load-voltage dependence α_s β_s

- Figure 8.10 shows the variability of the active steady state load-voltage dependence of the load. The values of this parameter are associated to the values obtained for the respective active time constant.

- For wintertime the values of α_s are closer to 0 and therefore to a full restoration of the load. During wintertime most of the load is electric heating and the energy demand is high. The thermostats in the heating are active almost all the time, and the load fully recovers, α_s is zero, or even reaches values larger than in the pre-disturbance situation, values smaller than zero. Larger values of the parameter have been found for summer time when electric heating is not a big percent of the load.

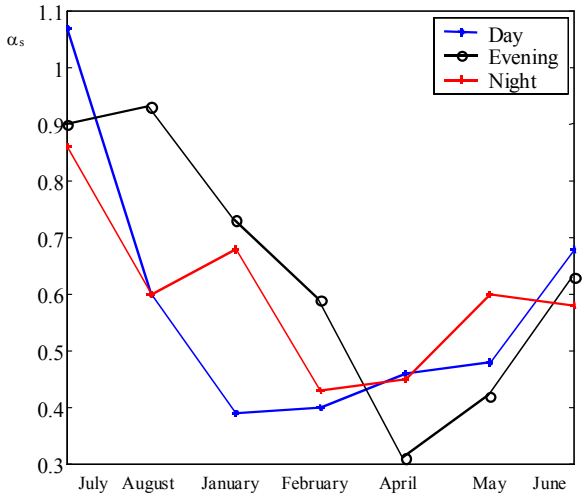

Figure 8.10: Annual variability of the active steady state load-voltage dependence α_s for day, evening and night hours.

- Figure 8.11 shows that there is correlation between the parameter α_s and the load recovery time constant. The correlation function corresponds to day hours, with a correlation coefficient of 0.88. Smaller correlation coefficients have been found for evening and night hours, -0.70 and 0.30 respectively.

- The value corresponding to July strongly affects the correlation sign between both parameters. This may be related, as mentioned before in this chapter, to the reduced number of data points available during that month, and the significant percent of weekend days in the data.

The conclusions described above for the active steady state parameter, and its relation with the active recovery time of the load can be applied in the same way for the reactive steady state parameter and the reactive recovery time constant. The correlation coefficients obtained for day, evening and night hours are then, -0.86, 0.31 and –0.56 respectively.

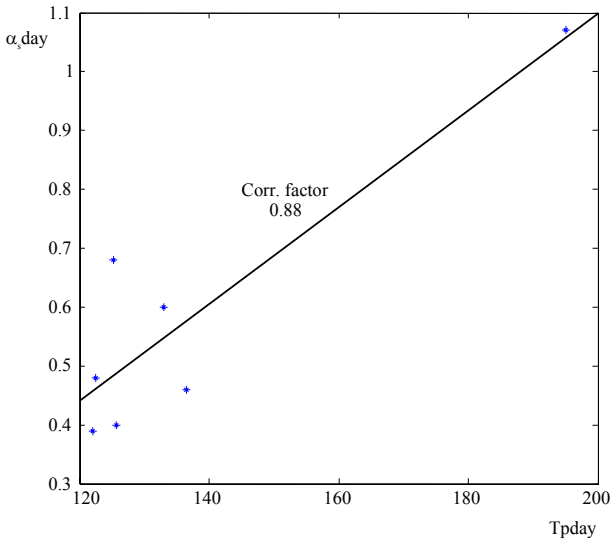

Figure 8.11: Correlation between the monthly values for the active steady state load-voltage dependence α_s for day hours, and the corresponding monthly values for the active time constant.

8.2 Active and Reactive Load Correlation

Regarding the time constant values presented in the previous section in Table 8.1, it has been shown that both the active and reactive time constants move in the same range of about 80 to 200 seconds, and are correlated to each other with a correlation factor equal to 0.50. See Figure 8.4. The reason for this correlation is studied throughout this section.

The small differences in the order of both active and reactive time constants may be related to spontaneous load variations, and therefore unrelated to voltage variations, but the main recovery of the reactive load is produced by the increase of the reactive losses due to the active recovery of the load at low voltage.

In order to check whether the reactive recovery really originates from the mentioned increased reactive losses, the simplified distribution system model shown in Figure 8.12 has been used to estimate those losses. The distribution system under the recording point at the 130 kV-level has been modeled with a series reactance equal to the sum of both reactances at 130 and 20 kV according to Appendix II. The measured values at the 20 kV-level have been used to determine the value of the losses (*Qlosses*).

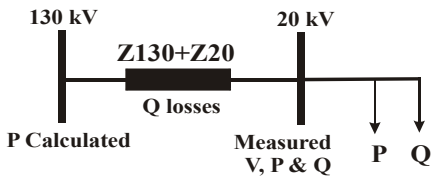

Figure 8.12: Simplified distribution system from the 130 kV-level to the 20 kV-level for determining the reactive load losses.

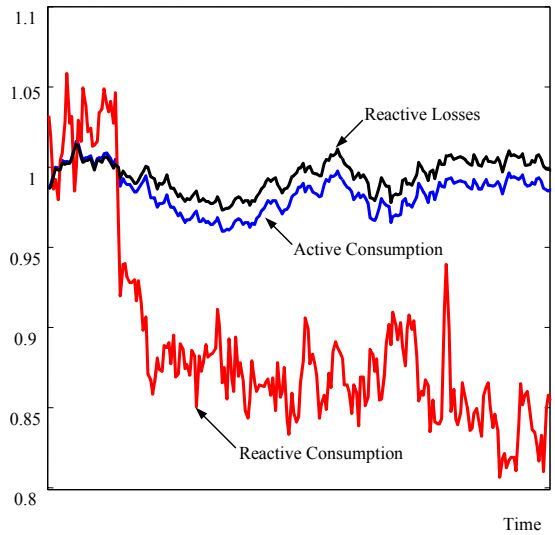

Figure 8.13: Comparison of the reactive losses and the active consumption curves. Time is given in minutes.

Figure 8.13 shows the calculated *Qlosses* curve together with the curves for the active and reactive consumption at the 20 kV. All the quantities are

presented in per unit. The value before the voltage change for each one of the quantities has been chosen as the base value.

8.3 Conclusions

An identification process for determining the active and reactive parameters in dynamic load models from normal operation data has been applied. The monthly and daily standard deviations of the resulting identified parameters show a large variability in the distribution of the results, probably due to the high diversity of load processes, even during the day. The values of both time constants move in the same order and they are correlated to each other. The active and reactive transient load-voltage dependence α_t and β_t exhibit a dependency with the outdoor temperature, and therefore with the season and time of the day. The active and reactive steady state load-voltage dependence α_s *and* β_s, are correlated to their respective active and reactive time recovery. It has been found that during wintertime the parameter α_s is closer to 0, which indicates a full restoration of the load.

The distribution of the identified seasonal active and reactive load parameters, the calculated correlation factors, and in general the material presented throughout this chapter offers unique and pioneering information for the study of the load characteristic and the analysis of the load dynamics. Other previous studies in dynamic load models do not include the mentioned results.

Part III

Load Models For Large Voltage Variations

Summary: *Extensive work has previously been done for studying the load-voltage characteristic under small voltage variations and to find a more accurate load model representation for voltage stability studies. However, additional efforts must be devoted to the analysis of the load-voltage characteristic also during large voltage variations, to be able to determine the risk of instability. The majority of current load models are valid for small voltage variations around an operating point. Research and studies have indicated that the transient load characteristic might be represented by impedance for those conditions. The load may then recover towards constant power, or another load characteristic, after a while. There are very few examples of models that have been verified for large voltage variations.*

This section provides analysis of the load-voltage characteristic during voltage dips based on field measurements in a non-effectively earthed system. Moreover, the validity of existing traditional load models has been investigated during these conditions.

Chapter 9

Field Measurements

Measurements of phase currents and voltages from three-phase, phase to phase and phase to ground faults from a non effectively earthed system at the 50 kV-level have been carried out for studying the load-voltage dependency during voltage dips. The data has been collected using recording units (RET 521) from ABB, with a sampling rate of 1000 Hz. The measurements were carried out in the Swedish island of Öland, Figure 9.1, whis is located in the South East of Sweden. The recordings correspond to system faults that occurred during the summer 2003, within the months June to September.

This chapter includes a description of the measurements, the area they belong to, and the equipment and software that has been used for the recording process. Further information from the test system can be found in [Randrup, 2003].

9.1 The System Description

A scheme of the test area is shown in Figure 9.2. A submarine AC cable connects a substation in Stävlö (SLÖ) to a substation in Linsänkan (LIN), i.e. the mainland distribution system at the 130 kV-level to the distribution system in the island of Öland. The mainland distribution system at the 130 kV-level and downwards is aggregated at Stävlö, while the full distribution system at Öland (LIN) is included. Moreover, note that the island of Öland is connected to mainland at the 130 kV-level (SLÖ), but also at the 50 kV (SLÖ_FKTV). During normal operation the 130 kV cable is in use, while

the 50 kV cable is only in operation if needed. The 50 kV cable is however usually connected to the 50 kV system in Öland and therefore injecting reactive power into the Öland system. The reactive power produced by these cables is 1.8 MVar at 53.6 kV in LIN. This value varies during high and light load conditions. One transformer of 100 MVA connects the 130 kV-level to the 50 kV-level in Linsänkan. The transformer regulates the voltage on the 50 kV side within 53.2 and 53.8 kV. Two capacitor banks of 2.25 MVar and 2.0 MVar are connected at the 3.3kV-level at Degerhamns Cement (DHN_CEM) and at the 10 kV-level in Borgholm (BHM) respectively, for voltage regulation. At DHN_CEM there is a large industry, Cementa AB, whose production can be relatively large. The capacitor bank connected at this point compensates the high reactive consumption of motors. At lower voltage system levels, there are 12 tap changing transformers connecting the 50 kV- to the 10 kV-level. The transformers regulate the voltage on the 10 kV side between 10.4-11.0 kV, and their capacity varies between 4.0 and 16 MVA. In Degerhamn there is also a 50/20 kV transformer, which is the connecting point of 10 MW wind power generation at Utgrunden (Figure 9.2), [Randrup, 2003].

9.2 Load Area Description

The load consumption in Öland fluctuates during a year. The tourism and the weather conditions make it very variable and uncertain, and therefore difficult to quantify. During the summer the number of tourists visiting the island increases and therefore the energy consumption. Residential and rural consumption increases, and air conditioner units are connected due to the increase in temperatures. During the winter, the weather conditions become significantly different as the outdoor temperatures drop below zero. The electric heating consumption increases due to these low temperatures. The lightest load conditions occur during spring and autumn, while the heaviest ones occur during summer and winter. For example during December 2001 it was registered a peak load of about 84.5 MW and 11.0 MVar in the 50 kV system and downward. These losses were separately calculated and were of about 3 MW and 5.8 MVar.

The load consists mainly of electric heating and lighting, small and medium-sized motors, and the aggregated load from the countryside. The average load demand during light conditions is about 14 MW and 10 MVar.

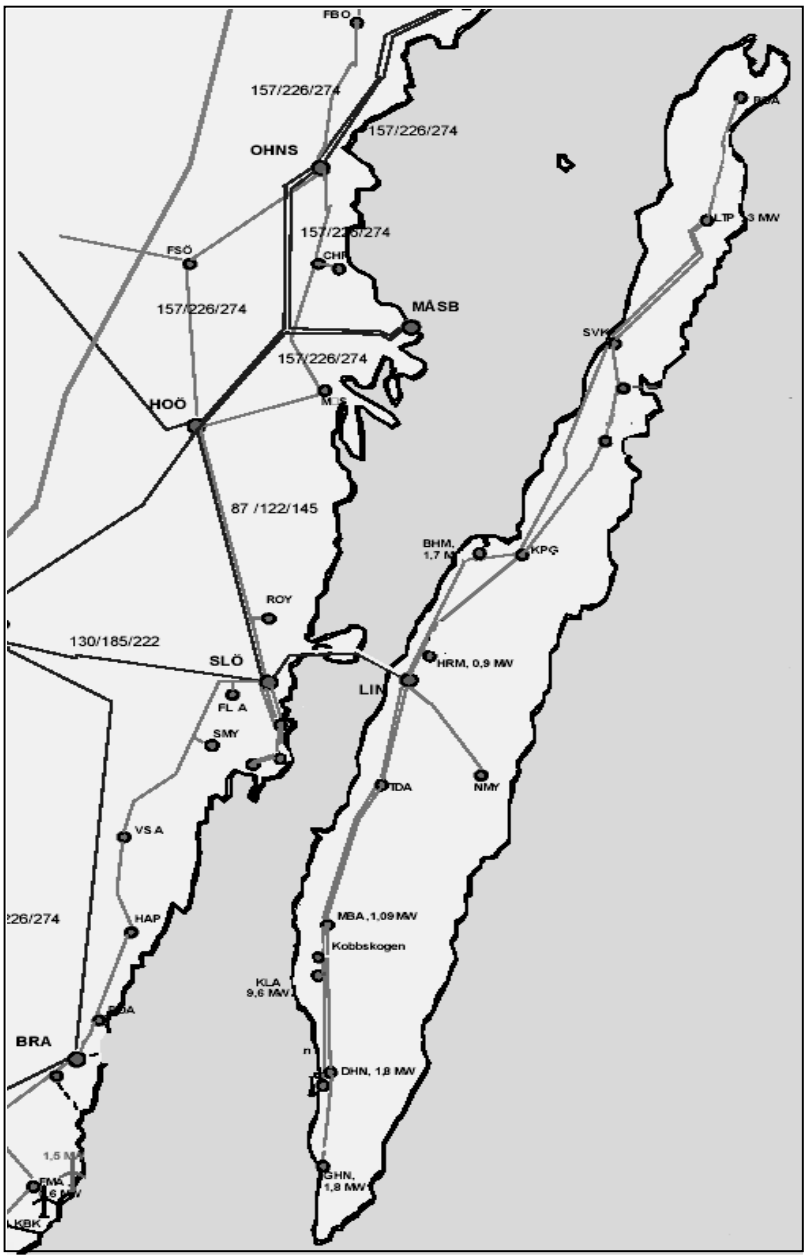

Figure 9.1: Island of Öland in Sweden (about 120 km from north to south).

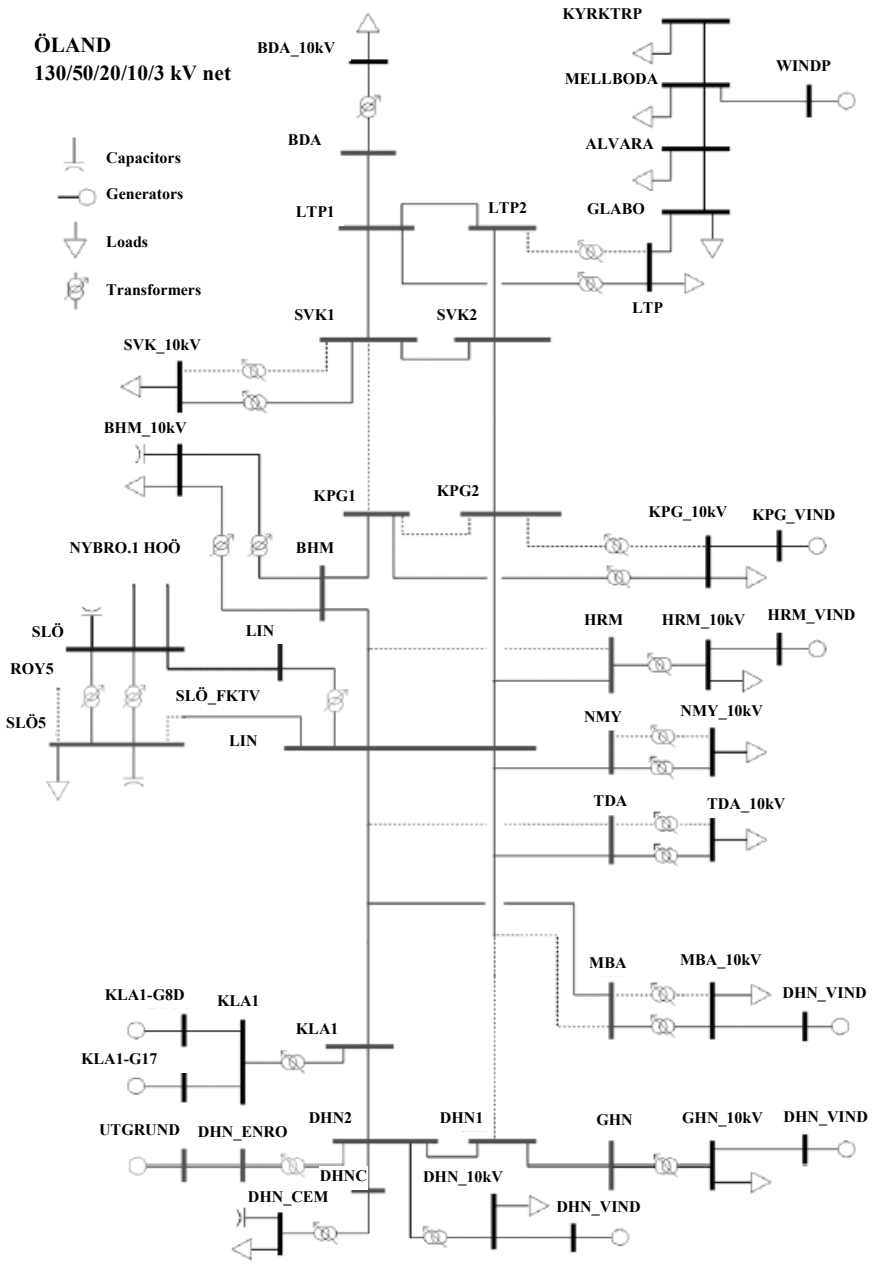

Figure 9.2: Simplified outline of the 130/50/20/10/3 kV system in Öland.

9.3 Field Measurements

Four large feeders are connected to the 50 kV-level in Linsänkan (LIN). Two of them, feeders 54 and 56, head toward Löttorp and feed the Northen part of the system, while the other two, feeders 59 and 60, feed the Southern part of the system, (Figure 9.2). Measurements from phase currents and voltages during fault conditions have been recorded at these four feeders. However, only the measurements from feeders 54 and 59 have been analyzed in this section.

Feeder 54 is connected to two substations in Borgholm (BHM) and Köpingsvik (KPG1) in the North of the island, which feed the small cities of Borgholm and Köpingsvik through two parallel and one single tap changing transformers respectively. The tap changing transformers regulate the voltage on the secondary side of the transformer. A capacitor bank of 2 MVar is constantly connected at BHM for load compensation. Moreover, at the 10 kV-level in Köpingsvik (KPG_Wind), 15 MW wind power generation is connected. Feeder 59 is connected to two substations, Norra Möckleby (NMY) and Torslunda (TDA). They feed the small residential areas of Nörra Mörckleby and Torslunda through two tap changing transformers respectively. The tap changing transformers regulate the voltage on the secondary side of the transformer.

The measurements have been carried out during faulted conditions, recordings from phase-to-phase faults and three-phase faults on two radial feeders on Öland, feeder 54 and 59. Phase to ground faults are not relevant for this study since the system is a non-effectively earthed system. A phase to ground fault in the transmission system will not alter the voltage triangle seen by the load. Figure 9.3 shows the three-phase equivalent voltage triangle for a phase to phase and phase to ground fault. The recorded disturbances exhibited voltage variations at the load bus in the range of 4% up to 30%. The variations depend on the severity of the fault, and its proximity to the load bus.

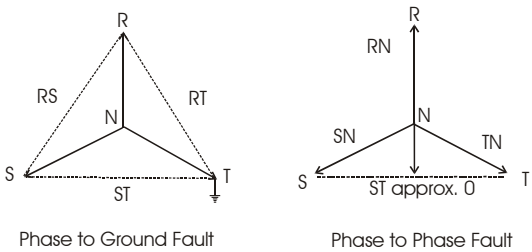

Figure 9.3: Voltage triangles for a phase to phase and a phase to ground fault.

9.4 Measurement Equipment

ABB and Sydkraft (Swedish utility) have provided the measurements and additional information on the load area described in the previous sections. Disturbance recorder facilities have been used to carry out the measurements. These facilities capture, store and retrieve the instantaneous values of currents and voltages. The waveforms are sampled with a sampling rate of 1000 Hz, which makes it possible to get additional information on load behavior by analyzing disturbance recordings from power system faults. Two RET 521 2p1 terminals (transformer protection terminals) have been used as disturbance recording terminals in Linsänkan. Each RET 521 has 1 x AIM module with 7 current and 3 voltage inputs and 1 x IOM module with 8 binary inputs and 12 binary outputs. Therefore one RET has been used for monitoring two lines (6 currents and 3 voltages). Software from ABB has been used to display the recorded measurements.

9.5 Wind Power Presence

Approximately 30 MW wind power capacity is today installed in the distribution system of Öland. This capacity is generated by 51 wind power plants with asynchronous (induction) generators, which are distributed along the whole island, see Figure 9.2. Some of these units are located at LTP (3 MW), KPG (15 MW), BHM (1.7 MW), HRM (0.9 MW), DHN (1.8 MW), GHN (1.8 MW), Utgrunden (10 MW), etc. The total generation is able to satisfy the total demand in Öland during light conditions, 13.7 MW and 9.7 MVar; 13.7 MW are consumed by the load, 15 MW are exported to mainland, and the rest is consumed by system losses. Feeder 60 consumes

half of them. The maximum reactive losses in lines and transformers are around 3.0 MVar. During high load conditions, 84.6 MW and 11 MVar, the wind power production is the same as described above (30.2 MW), but a total of 56.8 MW and 21.8 MVar need to be imported from mainland. Due to the heavy loaded conditions, the system losses are higher, about 2.4 MW. The feeder 54, which connects Linsänkan to Borgholm is the most loaded branch in the system with a loading of 80% of its rated capacity. The losses at this single feeder are about 0.5 MW. The rest of the losses are distributed along the system. The reactive losses in lines and transformers may go up to 11.9 MVar.

Plans to increase the installed wind power capacity up to 40-60 MW have been discussed, in order to decrease the amount of power that must be imported from the mainland during heavy loaded conditions. This would optimize the transport of power through the feeders in the island and decrease system losses. Moreover, the design of new distribution networks aims at ensuring an acceptable quality of supply to customers under normal operation, and protecting the system during faulted conditions.

Chapter 10

Determination of Load Estimates

A method for determining the active and reactive load estimates per phase from recordings of phase currents and voltages during unsymmetrical conditions is described throughout this chapter. From instantaneous values of voltage and current and by using symmetrical components, the sequence phasors for the voltage and the current, and the corresponding three-phase voltages and currents are determined. Assuming that the load is aggregated at one point in the distribution system and that the aggregated load is represented as an impedance, the time-varying load parameters resistance *R(t)* and reactance *X(t)* in each phase have been calculated. The active and reactive power is then straightforward to obtain.

The method has been validated by determining the phase time-varying parameters *R(t)* and reactance *X(t)* for a simplified distribution system simulated with the software package PSCAD [PSCAD, 2001].

10.1 Determination of Symmetrical Components

Figure 10.1 shows a simplified power system, which is disturbed at a certain instant by a three-phase to ground fault. The effect of this fault is studied at the load bus 2, where the voltage experiences a large variation, which size mainly depends on the distance from the load to the fault, and the severity of the fault. Assuming that the aggregated load is represented by an equivalent three-phase impedance, (the representation of the aggregated load is further discussed at the end of this chapter), it is proposed the determination of the load parameters resistance *R(t)* and reactance *X(t)*,

from instantaneous values of voltage *v(t)* and current *i(t)*. In order to make the method valid for both balanced and unbalanced system conditions, symmetrical components have been used. The first step is thus the estimation of the (1) positive-, (2) negative, and (0) zero-sequence components of sets of three-phase currents and voltages [Lindahl, 2003]. The estimation of the sequence components for a general three-phase signal is described below, where equation (10.1) defines the available data per phase $(_p)$, w_o in rad/s is the fundamental angular frequency, and f_o is the fundamental frequency in Hz. Further description of this method is included in Appendix III.

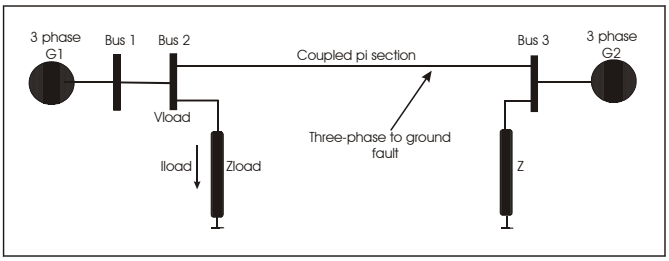

Figure 10.1: Equivalent system, disturbed by a 3-phase to ground fault.

$$S_p(k) = S_p \cdot \sin\left(kw_o\Delta t + \varphi_p\right) \quad for\ k = 1,2,...total\ samples \tag{10.1}$$

$$w_o = 2\pi f_o \tag{10.2}$$

Equation (10.3) gives the three-phase signal as a sum of the positive-, negative- and zero-sequence components.

$$S_p(k) = S_{1p}(k) + S_{2p}(k) + S_{0p}(k) \tag{10.3}$$

Equations (10.4), (10.5) and (10.6) define the positive-, negative- and zero-sequence components for phases *a, b* and *c*.

The aim is to find the magnitude and phase of the sequence components, S_1, S_2, S_0, ϕ_1, ϕ_2 and ϕ_0, from the sampled values of the phase signals. There are *M* samples per fundamental frequency cycle $Mw_0\Delta t=2\pi$ and *M* has been set to 20. The determination of the parameters S_1 and ϕ_1 for the positive-sequence is described below. Rectangular coordinates are used instead of

polar coordinates to simplify the parameter estimation. Two new parameters have been introduced, A_1 and B_1.

$$\begin{aligned} S_{1a}(k) &= S_1 \cdot \sin(kw_o\Delta t + \phi_1) \\ S_{1b}(k) &= S_1 \cdot \sin\left(kw_o\Delta t + \phi_1 - \frac{2\pi}{3}\right) \\ S_{1c}(k) &= S_1 \cdot \sin\left(kw_o\Delta t + \phi_1 - \frac{4\pi}{3}\right) \end{aligned} \tag{10.4}$$

$$\begin{aligned} S_{2a}(k) &= S_2 \cdot \sin(kw_o\Delta t + \phi_2) \\ S_{2b}(k) &= S_2 \cdot \sin\left(kw_o\Delta t + \phi_2 - \frac{4\pi}{3}\right) \\ S_{2c}(k) &= S_2 \cdot \sin\left(kw_o\Delta t + \phi_2 - \frac{2\pi}{3}\right) \end{aligned} \tag{10.5}$$

$$\begin{aligned} S_{0a}(k) &= S_0 \cdot \sin(kw_o\Delta t + \phi_0) \\ S_{0a}(k) &= S_0 \cdot \sin(kw_o\Delta t + \phi_0) \\ S_{0a}(k) &= S_0 \cdot \sin(kw_o\Delta t + \phi_0) \end{aligned} \tag{10.6}$$

Equation (10.8) gives the relation between them and S_1 and ϕ_1 in the polar representation.

$$\begin{aligned} S_{1a}(k) &= A_1 \cdot \cos(kw_o\Delta t) + B_1 \cdot \sin(kw_o\Delta t) \\ S_{1b}(k) &= A_1 \cdot \cos\left(kw_o\Delta t - \frac{2\pi}{3}\right) + B_1 \cdot \sin\left(kw_o\Delta t - \frac{2\pi}{3}\right) \\ S_{1c}(k) &= A_1 \cdot \sin\left(kw_o\Delta t - \frac{4\pi}{3}\right) + B_1 \cdot \sin\left(kw_o\Delta t - \frac{4\pi}{3}\right) \end{aligned} \tag{10.7}$$

$$S_1 = \sqrt{A_1^2 + B_1^2} \qquad \tan(\phi_1) = \frac{A_1}{B_1} \tag{10.8}$$

The least-square method is used to find the parameters A_1 and B_1, i.e. the function given by equation (10.9) is minimized to obtained A_1 and B_1. Equation (10.9) is the sum of the squared deviation over one complete fundamental period.

$$V(A_1, B_1) = \sum_{k=1}^{M} \left[A_1 \cdot \cos(\theta_k) + B_1 \cdot \sin(\theta_k) - S_a(k)\right]^2 +$$
$$\sum_{k=1}^{M} \left[A_1 \cdot \cos(\theta_k - \frac{2\pi}{2}) + B_1 \cdot \sin(\theta_k - \frac{2\pi}{2}) - S_b(k)\right]^2 + \tag{10.9}$$
$$\sum_{k=1}^{M} \left[A_1 \cdot \cos(\theta_k - \frac{4\pi}{2}) + B_1 \cdot \sin(\theta_k - \frac{4\pi}{2}) - S_c(k)\right]^2$$

$$\theta_k = kw_o \Delta t$$

The function is differentiated with respect to the parameters A_1 and B_1, to find a minimum. The final result is given by the following equations:

$$A_1 = \frac{2}{3M} \sum_{k=1}^{M} \left[S_a(k) \cdot \cos(\theta_k) + S_b(k) \cdot \cos(\theta_k - \frac{2\pi}{3}) + S_c(k) \cdot \cos(\theta_k - \frac{4\pi}{3})\right]$$

$$B_1 = \frac{2}{3M} \sum_{k=1}^{M} \left[S_a(k) \cdot \sin(\theta_k) + S_b(k) \cdot \sin(\theta_k - \frac{2\pi}{3}) + S_c(k) \cdot \sin(\theta_k - \frac{4\pi}{3})\right]$$

A similar procedure can be followed to determine the parameters A_2, B_2, S_2, ϕ_2 and A_0, B_0, S_0, ϕ_0 for the negative- and zero-sequence components of the signal. This procedure is applied to determine the positive-, negative- and zero-sequence components for a given set of three-phase voltages and currents.

10.2 Load Estimates

If V_s and I_s denote the vectors of sequence phasor voltages $[V_1\ V_2\ V_0]^T$ and currents $[I_1\ I_2\ I_0]^T$ respectively, the sequence impedance Z_s, $[Z_1\ Z_2\ Z_0]^T$ is calculated from equation (10.10). The corresponding three-phase voltages $V_p=[V_R\ V_S\ V_T]^T$, and currents $I_p=[I_R\ I_S\ I_T]^T$, are given by equations (10.11) and (10.12), where $a = \exp(j2\pi/3)$.

$$\hat{Z}_s(k) = \frac{V_s(k)}{I_s(k)} \tag{10.10}$$

$$\begin{bmatrix} V_R \\ V_S \\ V_T \end{bmatrix} = \begin{bmatrix} 1 & 1 & 1 \\ 1 & a^2 & a \\ 1 & a & a^2 \end{bmatrix} \cdot \begin{bmatrix} V_0 \\ V_1 \\ V_2 \end{bmatrix} \tag{10.11}$$

$$\begin{bmatrix} I_R \\ I_S \\ I_T \end{bmatrix} = \begin{bmatrix} 1 & 1 & 1 \\ 1 & a^2 & a \\ 1 & a & a^2 \end{bmatrix} \cdot \begin{bmatrix} I_0 \\ I_1 \\ I_2 \end{bmatrix} \tag{10.12}$$

The time-varying three-phase impedance Z_p, $[Z_R\ Z_S\ Z_T]^T$, is obtained from equation (10.13), being R_p, $[R_R\ R_S\ R_T]^T$, and X_p, $[X_R\ X_S\ X_T]^T$, the corresponding three-phase time-varying resistance and reactance.

$$\hat{Z}_p(k) = \frac{V_p(k)}{I_p(k)} \tag{10.13}$$

$$\hat{Z}_p(k) = \hat{R}_p(k) + j\hat{X}_p(k) \tag{10.14}$$

$$\hat{X}_p(k) = w \cdot \hat{L}(k)$$

$$w \approx 2 \cdot \pi \cdot f_o$$

10.3 Estimates of the Active and Reactive Power

The three-phase apparent power S_p, $[S_R\ S_S\ S_T]$, and the corresponding active and reactive power consumed by the load are given by equation (10.15)-(10.18).

$$S_p(k) = V_p(k) \cdot I_p^*(k) = V_p(k) \cdot \frac{V_p^*(k)}{(\hat{Z}_p(k))^*} \tag{10.15}$$

$$S_p(k) = P_p(k) + jQ_p(k) \tag{10.16}$$

$$P_p(k) = \mathrm{Re}(S_p(k)) \tag{10.17}$$

$$Q_p(k) = \mathrm{Im}(S_p(k)) \tag{10.18}$$

10.4 Load Representation

The load consists of an aggregate number of components of different nature and characterized by different dynamics. It is therefore complex to define a unique load representation. Field validation is the best way to prove the adequacy of the models. Field validation has been used for long time based on availability of data. Loads may influence harmonics and electromagnetic transients, but these effects are often neglected. Several studies have been carried out to study this phenomenon [IEEETransient, 2001].

A series or a parallel RL load model provides correct values for initial conditions but they may be inaccurate for higher frequencies. An improved method is to consider the load representation as a combination of a series and a parallel circuit. The series RL circuit represents the losses in lines and distribution transformers, while the parallel circuit represents the load at the customer side. Note that to this model, it should be added the effect of reactive compensation as well as the contribution of distributed generation if it is present in the area. Figure 10.2 shows a possible load representation, where P_d and Q_d is the dissipated power in distribution transformers and lines, Q_c represents the effect of reactive compensation along the distribution feeders and line capacitive generation, and P_l and Q_l are the active and reactive customer consumption.

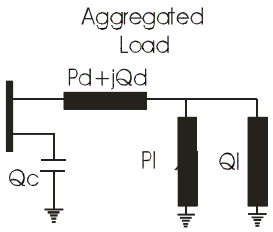

Figure 10.2: Aggregated Load Representation.

10.5 Load Estimates from Field Measurements

The method described throughout this chapter is now applied to the measurements introduced in Chapter 9. The recorded disturbances exhibited voltage dips at the load bus in the range of 4% up to 30%. These variations depend on the severity of the fault, and its proximity to the load bus. The following analysis focuses on a significant disturbance recorded at feeder 54. This is a phase-to-phase fault from July 17 2003. Further results from other disturbances are included in Chapter 11 and Chapter 12.

Figure 10.3, Figure 10.4 and Figure 10.5 show the three-phase, and the corresponding positive-, negative- and zero-sequence components of the voltage, current and impedance, for the mentioned disturbance. At about 220 ms a phase-to-phase fault between phases S and T results in a voltage variation of 30% at the load bus. The duration of the fault is about 100 ms. The negative- and zero-sequence components of the voltage and the current were expected to be zero before and after the disturbance. The deviation from zero indicates initial unbalanced conditions.

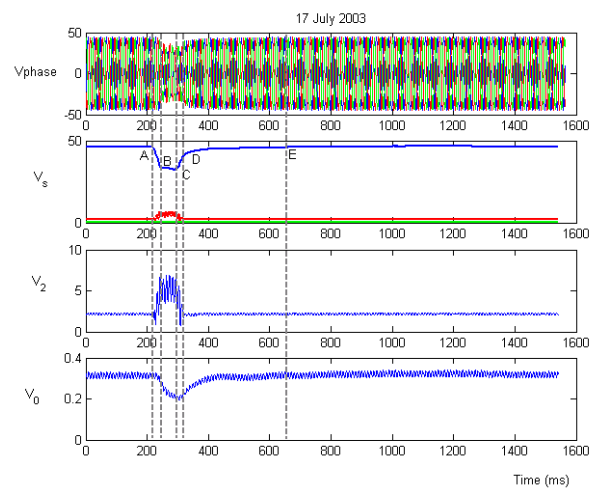

Figure 10.3: Phase voltages (Vphase), Sequence voltage V_s $[V_1\ V_2\ V_0]$ shown in kV, (2) negative- and (0) zero-sequence components of the voltage during a phase-to-phase fault.

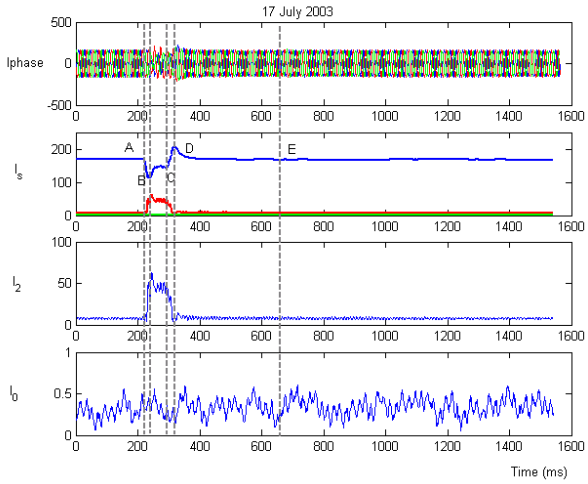

Figure 10.4: Phase currents (Iphase), Sequence current I_s $[I_1\ I_2\ I_0]$ shown in kA, (2) negative- and (0) zero-sequence components of the current during a phase-to-phase fault.

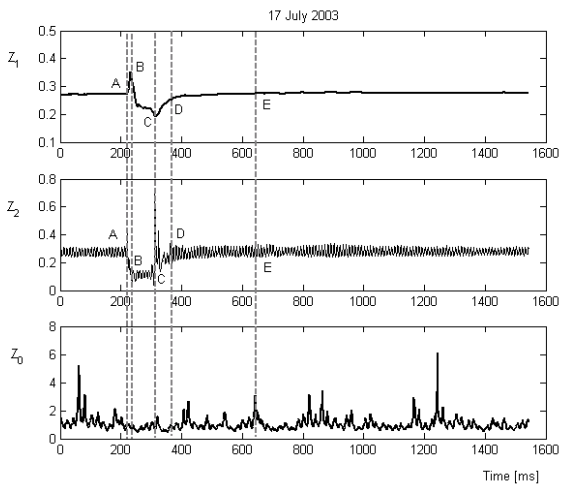

Figure 10.5: (1) Positive-, (2) negative- and (0) zero-sequence of the impedance.

The load estimates in each phase, active and reactive power per phase consumed by the load, Figure 10.6 and Figure 10.7, have been calculated

following the description in Section 10.3. The time interval has been divided into different segments, which are marked with letters A to E. The switching operations, A-B and C-D, occur in short periods of time and are not relevant for this study. However, the behavior of the load during and after the fault, B-C and D-E is critical for transient stability.

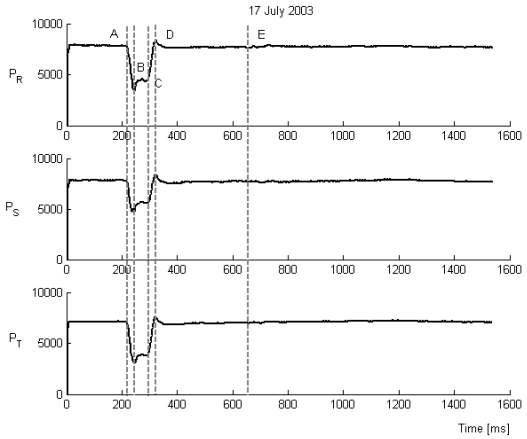

Figure 10.6: Estimated phase active power consumed by the load before, during and after the fault. Power measured in kW.

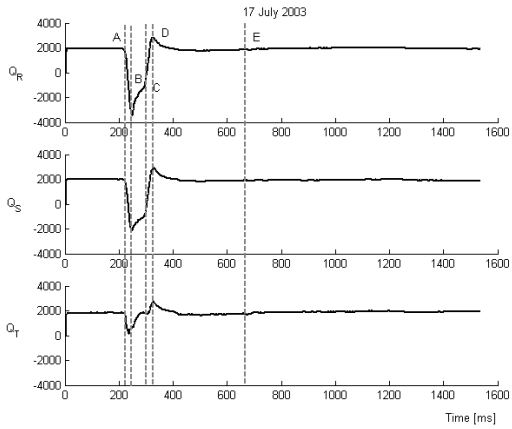

Figure 10.7: Estimated phase reactive power consumed by the load before, during and after the fault. Reactive power measured in KVar.

In general both the active and reactive load changes are in phase with the change in voltage. Once the fault is cleared, point D, the voltage rapidly recovers to about 90% of its pre-disturbance value. The full recovery, segment D-E, takes about another 200 ms. During this time some load may be reconnected after automatic protective disconnection, and motors accelerate to reach (close to) synchronous speed. The load response experiences a significant increase of the active power right after the fault is cleared, and a higher consumption of current, i.e. increase of reactive power consumption, since motors re-accelerate and draw higher currents.

The presence of induction motors in the load area increases the severity of the system conditions during and after the fault. During a phase-to-phase fault, the motors keep feeding through one phase. They will slow down more than for other single disturbances, and draw higher currents during and after the fault clearance. Due to this, the voltage drop during the fault and the post-disturbance conditions will be more severe than for a single-phase-to-ground fault.

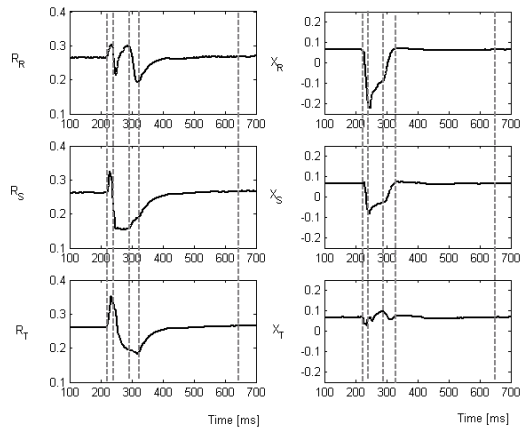

Figure 10.8: Time-varying load estimates *R* and *X* for each one of the three phases during and after the fault conditions. Period of time [100-700] ms. *R* and *X* are measured in ohms.

Figure 10.8 shows the time-varying load estimates *R* and *X* for each one of the three phases respectively. The segments from A-E used to describe the previous figures are also used in this case.

10.6 Conclusions

A method for determining the phase active and reactive load estimates from measurements of instantaneous values of currents and voltages has been proposed and tested with field measurements.

In general both the active and reactive load changes are in phase with the change in voltage. After the fault is cleared, the voltage rapidly recovers to about 90% of its pre-disturbance value, while the full recovery takes some more time, which varies depending on the load composition. Both the active and reactive power increase significantly, i.e. the reactive power consumption increases since motors re-accelerate and draw higher currents.

The analysis of the load estimates during faulted conditions has shown the impact that motor load has on the load characteristic. The presence of induction motors in the load area increases the severity of the system conditions during and after the fault.

Chapter 11

Dynamic Load Models

Extensive work has been done to investigate the load characteristic, and to validate existing load models during small voltage variations. This has provided interesting results on the load-voltage and frequency characteristic. However, few studies investigate the validity of these models during large voltage excursions, [Ihara, *et al.*, 1981], [Sabir and Lee, 1982], [Concordia and Ihara, 1982], [Vaahedi, *et al.*, 1988], [Price, *et al.*, 1988], and [Choi, 1990].

During large voltage variations, the nonlinear behavior of the power system and the loads increase, and most of the existing load models may no longer be accurate. This chapter investigates the load characteristic during these conditions, and the adequacy and limitations of existing traditional models for its representation based on field measurements.

11.1 Load Response during Large Voltage Variations

Few studies have been carried out to investigate the load characteristic during large disturbances. During these variations a power system operates under more stressed conditions; its nonlinear behavior is accentuated and the motor load dynamics become critical. The load composition and the size of the voltage dips are therefore important factors to take into consideration for determining the validity of existing traditional load models. Figure 11.1-Figure 11.3, show the measured load-voltage dependence at three different locations in the South of Sweden; Tomelilla, Trelleborg and Stävlö respectively. Three tests were carried out to obtain the different sized

voltage changes. Tomelilla is mainly a residential and rural area with a large concentration of electric heating, Stävlö load consists mainly of residential and commercial load highly dominated by induction motors, and street and commercial lighting, and the Trelleborg data is from an industrial area. The figures show the transition from a linear to a nonlinear load-voltage sensitivity depending on the load area composition and the size of the experienced voltage variations. The measured voltage variations ΔV are plotted against the active and reactive variations, ΔP and ΔQ respectively. The implementation of the tests is described in [Sydkraft1, 1958]-[Sydkraft3, 1958].

The different load-voltage dependencies are related to the load area composition. In Figure 11.3, note that both the active and reactive load-voltage sensitivity deviate from the linear characteristic due to the fact that larger variations have been recorded as compared with the ones in Figure 11.1 and Figure 11.2. The nonlinear behavior of the load is more apparent for the reactive load characteristic.

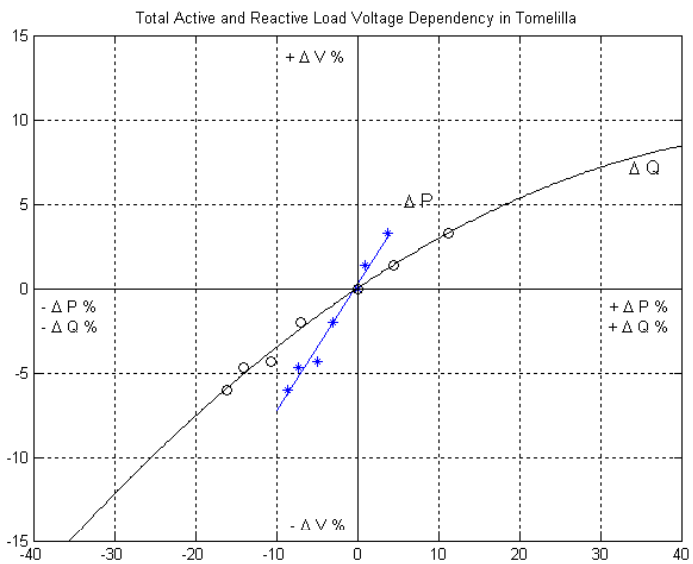

Figure 11.1: Measured voltage variations ΔV plotted against the active and reactive variations, ΔP and ΔQ, in Tomelilla (large percent of electric heating).

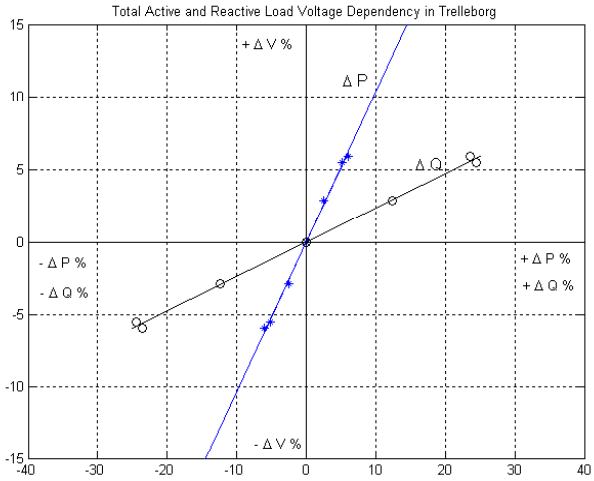

Figure 11.2: Measured voltage variations *ΔV* plotted against the active and reactive variations, *ΔP* and *ΔQ*, in Trelleborg (mostly an industrial area).

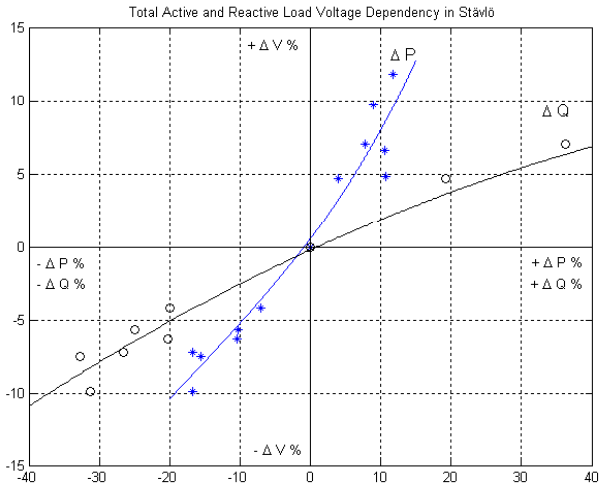

Figure 11.3: Measured voltage variations *ΔV* plotted against the active and reactive variations, *ΔP* and *ΔQ*, in Stävlö (significant presence of induction motors)

Figure 11.4 and Figure 11.5 show a comparison of the active and reactive load-voltage sensitivity at the three different locations. The active load characteristic is similar for the measurements from the three substations, while the reactive load shows a more nonlinear behavior in Stävlö, where the presence of induction motors is relatively high.

Based on this description, it is obvious that during large voltage variations the nonlinear behavior of the power system and the loads increase. The aim is then to verify if the existing load models are appropriate for the load representation during stressed conditions and if not, to find a suitable load representation for these conditions. The modeling work is focused on the dynamics occurring in a time range of about 100 ms to several seconds, i.e. mainly on asynchronous machines. Dynamics from electric heating load and tap changers are too slow to be considered in this time interval. They are represented as static load in these kind of studies.

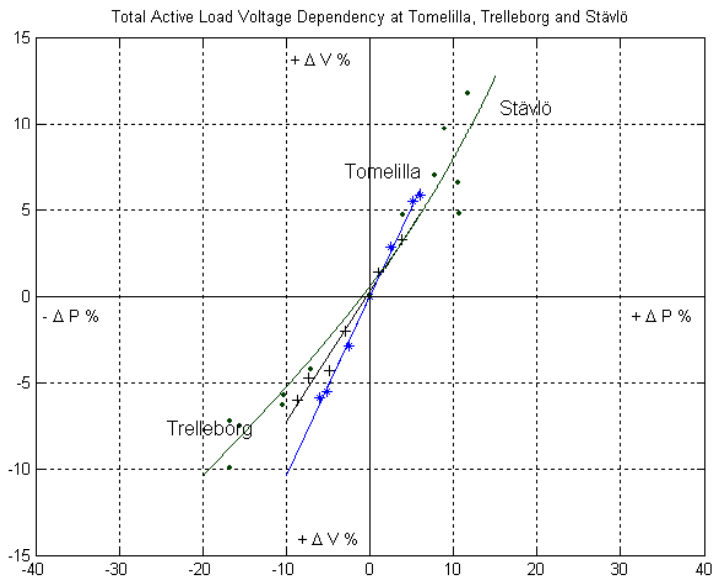

Figure 11.4: Measured voltage variations ΔV plotted against the active variations ΔP at three different locations. Tomelilla (+), Trelleborg (*) and Stävlö (.).

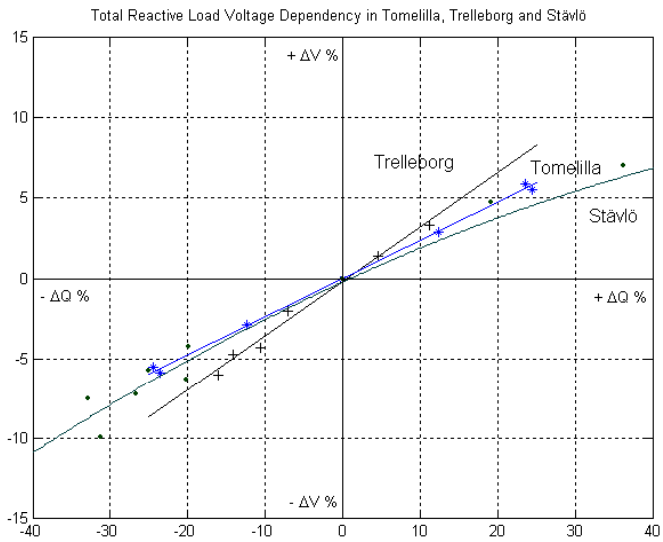

Figure 11.5: Measured voltage variations ΔV plotted against the reactive variations ΔQ at three different locations. Tomelilla (+), Trelleborg (*) and Stävlö (.).

11.2 Induction Motors

The motor load and its representation for voltage stability studies have briefly been introduced in Part I, Chapter 2. However a more detailed description of this component is necessary in order to understand its impact on the stability of power systems.

11.2.1 Generalities

Load areas with large concentration of induction motors are critical in stability studies, even more if little generation is available in the neighborhood of the load. In such a load area motors consume typically 60 to 70 % of the total electrical energy, and their dynamics are important in stability studies.

Induction motors are present in residential, commercial and industrial areas. Residential and commercial areas consist mainly of small and medium sized motors, which are characterized by a low inertia (0.1-0.3), [Taylor, 1994]. Common applications of this type of load are compressors for air conditioning and refrigeration. Residential and commercial motors are seldom under-voltage protected. They include an over-current protection. However, during extreme conditions the over-current protections will allow currents that are 3-4 times the normal operation ones, i.e. motors draw high currents, and the system may go unstable if the appropriate corrective actions are not taken in time. Capacitor banks are often installed in the neighborhood of heavily loaded areas to compensate the high reactive consumption of motors.

Industrial load mainly consists of diverse processes that are driven by motors of different sizes. They are mainly large motors with a large inertia. They often include under-voltage protection equipment and reactive bank capacitors for reactive compensation, and to protect the equipment from start and stalling conditions, [Cutsem and Vournas, 1998] and [Taylor, 1994].

11.2.2 Modeling

Extensive work has been carried out for the analysis of induction motors, [Iliceto and Carpasso, 1973], [Shackshaft, *et al.*, 1977] and throughout the time different models have been proposed for their representation [Martins, *et al.*, 2003], [Kundur, 1994]. Different transients are present in an induction machine; the stator transients (often neglected), the rotor electric transients and the rotor mechanical transients. It is often assumed that the rotor electric transients are faster than the mechanical ones and therefore the motor is only represented by its mechanical dynamics, which are given by the acceleration equation, equation (11.1). A traditional simplified induction motor model has been already presented in Chapter 2, in Figure 2.1.

Equation (11.1) represents the rotor motion dynamics, and gives the relation between the rotor speed, and the motor electrical and mechanical torque at each instant. J is the moment of inertia of the rotor and the connected load, T_m the mechanical torque including the effect of mechanical losses and T_e is the electrical torque.

$$J \cdot \frac{dw}{dt} = T_e - T_m \tag{11.1}$$

$$s = \frac{w_s - w}{w_s} \tag{11.2}$$

The slip of the motor s is defined by equation (11.2), where w_s is the electrical angular frequency and w is the rotor speed in radians per second. Both the mechanical and electrical torque depend on the speed of rotation and therefore on the value of the slip. Figure 11.6 shows the speed-torque characteristic, which describes the behavior of induction motors. The torque is considered positive or negative depending on the mode of operation of the machine, as a motor or as a generator. A third mode corresponds to braking, where the direction of rotation is opposite to that of the rotation field ($s>1$) and the motor absorbs both electrical and mechanical power.

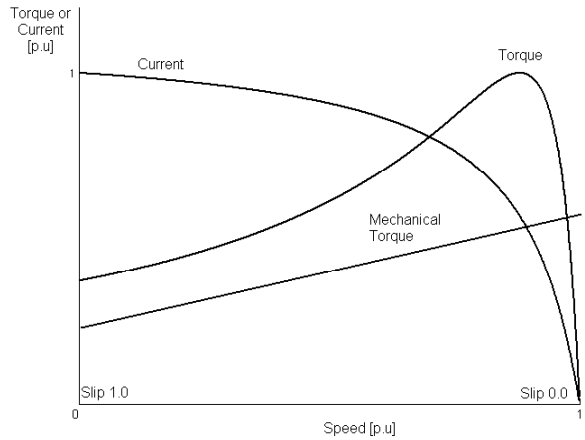

Figure 11.6. Torque-speed and current-speed characteristics for induction motors. The electrical torque varies with voltage square.

At starting, the motor is originally at standstill ($s=1$). At these conditions and if the electromagnetic torque T_e exceeds the mechanical torque T_m, the motor will start to accelerate. The starting impedance for $s=1$ is significantly smaller than that of normal operation, where s is very small,

and therefore the starting currents are several times larger than at normal operation. During stalling conditions the stator current is high, but smaller than the starting current. If the motor stalls, it will eventually come to a complete stop and its current will become equal to the starting one. Stalling of motors may cause cascade stalling of other motors as the result of active protective control devices for low voltages, over-currents or because of reaching thermal limits, and the final result may be a loss of load in the system, instability and collapse.

Large disturbances, such as short circuits in the neighborhood of the load area, may result in severe conditions. After a short circuit, a motor will respond by reducing its electrical torque by the square of the voltage, and therefore by decreasing its speed. When the fault is cleared only a part of the voltage is recovered, while the full recovery will take some extra time depending on the duration, type of the fault and the area load composition.

11.3 Traditional Dynamic Load Model

The adequacy of the dynamic load model with exponential recovery given by (11.3) to represent the load in voltage stability studies in Sweden, has been motivated several times in this thesis. The model is defined by two nonlinear functions P_s and P_t, the static and transient load functions respectively, and the time constant T_p. For the nonlinear functions in (11.4), the model is given by (11.5), where real power has a non-linear dependency on voltage. The same is applied to the reactive power.

$$\begin{aligned} &T_p \frac{dP_r}{dt} + P_r = P_s(V) - P_t(V) \\ &P_l = P_r + P_t(V) \end{aligned} \tag{11.3}$$

$$P_s(V) = P_o\left(\frac{V}{V_o}\right)^{\alpha_s} \qquad P_t(V) = P_o\left(\frac{V}{V_o}\right)^{\alpha_t} \tag{11.4}$$

$$\begin{cases} T_p \dfrac{dP_r}{dt} + P_r = P_o\left(\dfrac{V}{V_o}\right)^{\alpha_s} - P_o\left(\dfrac{V}{V_o}\right)^{\alpha_t} \\ P_l = P_r + P_o\left(\dfrac{V}{V_o}\right)^{\alpha_t} \end{cases} \tag{11.5}$$

Finding a dynamic load model that is able to describe the short and the long-term, and is accurate for small and large voltage variations, has been a goal in the last years. A broad study, Part II, has been carried out to validate the linearized form of the model given by (11.5) during small voltage variations on a time-scale of minutes, where the effects of tap-changers and other control devices are included. The model has also been validated on a time-scale of a few seconds, a time scale that captures the behavior of induction motors [Karlsson and Pehrsson, 1985]. During a voltage step the induction motor slip cannot change, so the aggregate load appears static. Thus a step of voltage produces a step of demand power. [Karlsson and Pehrsson, 1985] proposed a model from laboratory measurements on a combined *PQ* and induction motor load. However, the accuracy of the model is compromised for large voltage variations.

The aim is now to investigate the validity of this model in the time scale of ms, when large disturbances affect the system.

11.4 Identification of Nonlinear Systems

Finding an accurate model to describe the load behavior, whose mathematical structure is based on physical laws is important. A physical approach makes it possible to gain insight into and knowledge of the behavior of the phenomenon itself; each parameter is associated to a part, dynamic or not, of the real system. Moreover, a physical representation makes it possible to add or eliminate individual dynamics that may be or not aggregated to the load. However, real systems are complex entities to model; many input/output variables are involved, the systems are often time-varying, disturbances from other external processes may appear simultaneously with the main phenomenon, it may be difficult or even impossible to measure some variables that are relevant for the model, and the system may present nonlinearities.

System identification methods are applied to estimate unknown parameters of a chosen mathematical structure. If a load model is based on physical insight it will contain a number of parameters derived from physical laws, and the analysis under different operating conditions, will result in a valuable contribution for system planning and operation. The identification

is more complicated when the model is a nonlinear model. However, if the model is linear in the parameters the problem can be made more tractable.

11.4.1 Conditions for Parameter Estimation

In order to get useful results from the identification, it is important to ensure the identifiability of the model parameters, i.e. to ensure that the input signal has enough excitation on the model, and that the model parameters can be uniquely identified [Bergh, 1996].

The input signal determines the operating conditions of the system. Faulted conditions have been chosen for this analysis. The input signal is the voltage measured at the load bus before, during and after a fault. The signal consists of a double step, which is enough information to identify the transient behavior of the load. Moreover, after the step, the voltage remains constant for enough time to describe the dynamics of the load after a fault is cleared. The window length for the identification has been chosen within the interval of ms to approximately 1 second, since the focus of Part III in this thesis is the analysis of the load-voltage characteristic in the short-term.

11.4.2 Identification of Model Parameters

Consider the model given by equation (11.5). The relationship between the measured signals, active power P and voltage V at the load bus, and the parameters α_s, α_t and T_d is nonlinear. The model is nonlinear in state variables but also in the parameters, which makes the identification task very complex. A discrete approximation of the model is given by (11.6), where a forward difference has been used to approximate the derivative on the left side of the equation. The parameter h is the length of the sampling interval, and k is the sampling instance.

$$\begin{cases} T_p\left(\dfrac{P_r(k+1)-P_r(k)}{h}\right)+P_r(k)=P_o\left(\dfrac{V(k)}{V_o}\right)^{\alpha_s}-P_o\left(\dfrac{V(k)}{V_o}\right)^{\alpha_t} \\ P_l(k)=P_r(k)+P_o\left(\dfrac{V(k)}{V_o}\right)^{\alpha_t} \end{cases} \tag{11.6}$$

Which is rewritten on the form given by (11.7),

$$\begin{cases} P_r(k+1) = P_r(k) + \dfrac{h}{T_p}\left(-P_r(k) + P_o\left(\dfrac{V(k)}{V_o}\right)^{\alpha_s} - P_o\left(\dfrac{V(k)}{V_o}\right)^{\alpha_t} \right) \\ P_l(k) = P_r(k) + P_o\left(\dfrac{V(k)}{V_o}\right)^{\alpha_t} \end{cases} \tag{11.7}$$

There is a large variety of identification methods. The selection depends on the specific application and is crucial for guaranteeing the accuracy of the results. The description and comparison of these methods is not the objective of this thesis, and therefore this material is not included but referenced.

The LSQ method, Least Squares, applied to nonlinear systems has been chosen to identify the parameters in (11.7). The method uses the nonlinear LSQ formulation [MATLABOptm, 1992] to fit the nonlinear model to a set of data. The objective is then to obtain the best estimates for the parameter vector θ (α_s, α_t,T_p), which minimizes the difference between the estimated active power and the simulated one. The objective function to be minimized is given by equation (11.8). The same procedure is applied for the reactive power.

$$F\ (\theta_p) = \sum_{k=1}^{N} (P_{simulated}(t_k, \theta) - P_{measured}(t_k, \theta))^2 \tag{11.8}$$

The solution from the identification is the determination of the global minimum of the objective function, i.e. the best estimates for the model. However, the identification of nonlinear systems is more complex due to the nonlinearities, and it may lead to wrong solutions if the function has a local minimum or if there are several solutions. The nonlinear model parameters cannot be estimated using simple matrix techniques, and instead an iterative approach is required. The algorithm procedure follows:

1. An initial estimate X_o for the parameters is selected;
2. The best fit is then determined by using the initial estimate X_o;

3. The best estimates are compared with the initial estimates, and it is determined whether the fit improves or not. The direction and magnitude of the adjustment depend on the fitting algorithm (*trust region, Levenberg-Marquardt, Gauss-Newton*), [MATLABOptm, 1992];

4. The iteration process finishes at this step if the fit fulfills the specified convergence criteria. If not the process returns to step 2.

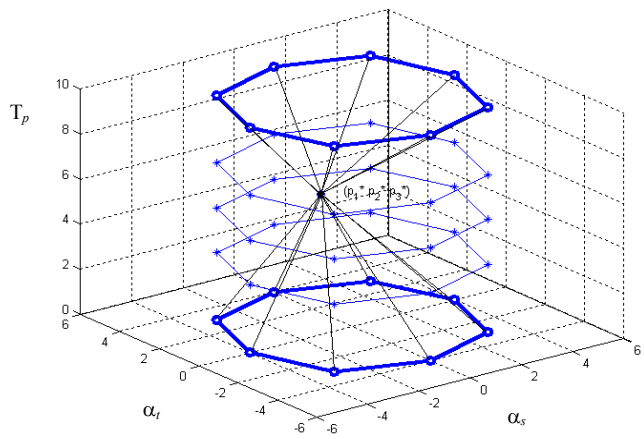

Figure 11.7: Convergence area.

The adequacy of the nonlinear LSQ method has been tested. Figure 11.7 shows the region of convergence studied for this problem. For different initial conditions $\theta_0\,(p_1,p_2,p_3)$ where p_1, p_2 *and* p_3 *are equal to* α_s, α_t, and T_p respectively, the method converges always to the same solution (p_1^*, p_2^*, p_3^*). From this, it can be concluded that the method is adequate here. The values represent a wide spectrum of possible values for θ_0.

11.5 Load Model Validation

The adequacy of the exponential nonlinear model given by (11.5) to represent the active and reactive load during large voltage variations is studied in this section. Field measurements from a non-effectively earthed

system from phase to phase faults on the 50 kV-level at a substation in Sweden have been used for the study (Chapter 9). The recorded disturbances exhibited voltage variations at the load bus in the range of 4% up to 30%. The same data as in Chapter 10 has been used for the analysis; the proposed model has been fitted to that data. Figure 11.8-Figure 11.10 show the measured and simulated phase active and reactive power at feeder 54 for the phase-to-phase fault under study.

For the active power, the simulated and measured data agree well with each other. The fit is very accurate for the non-faulted phase R, while for the faulted phases the accuracy decreases. However, the model is not appropriate to represent the reactive load response during and after the disturbance, since it fits neither the amplitude of the reactive change nor the dynamics occurring during and after the fault.

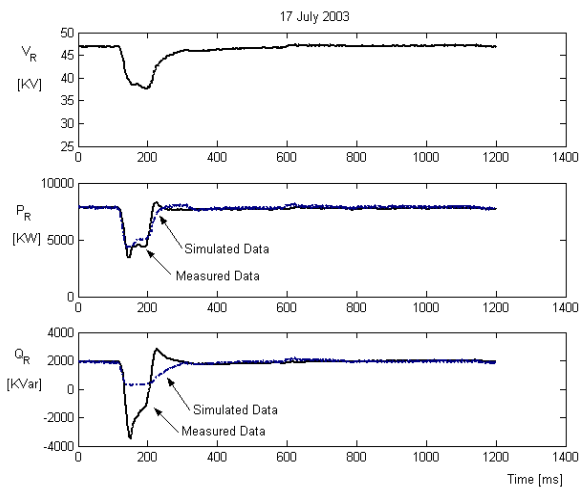

Figure 11.8: Phase voltage, and estimated and simulated phase active and reactive power during and after the fault conditions. Phase R, feeder 54.

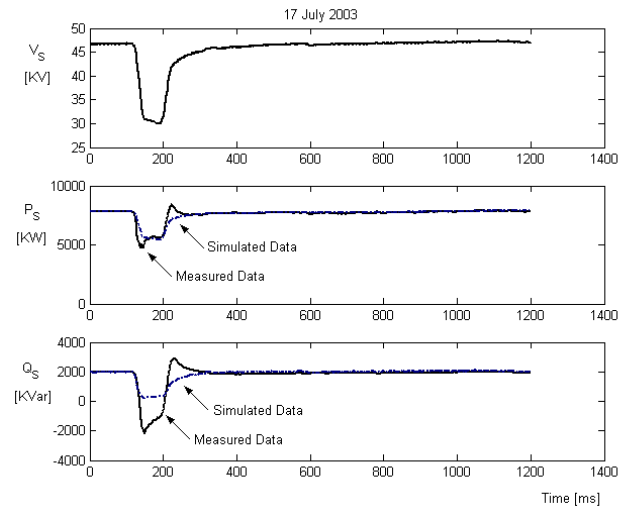

Figure 11.9: Phase voltage, and estimated and simulated phase active and reactive power during and after the fault conditions. Phase S, feeder 54.

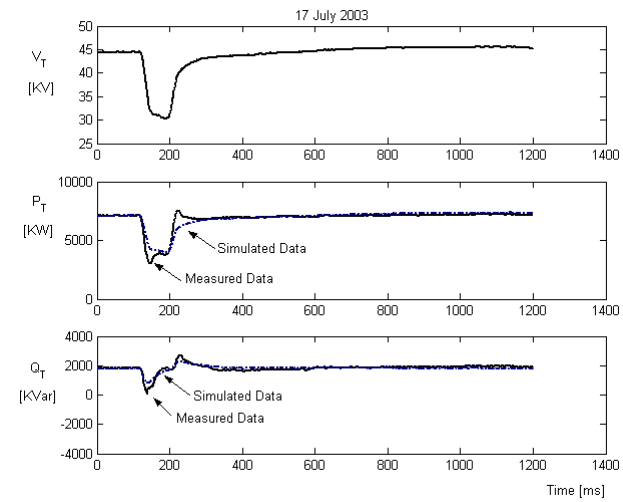

Figure 11.10: Phase voltage, and estimated and simulated phase active and reactive power during and after the fault conditions. Phase T, feeder 54.

Figure 11.11 shows the active and reactive power at feeder 54 during and after the fault, plotted versus the voltage for each one of the phases. Both the active and reactive load responses show the necessity of a dynamic model for the load representation.

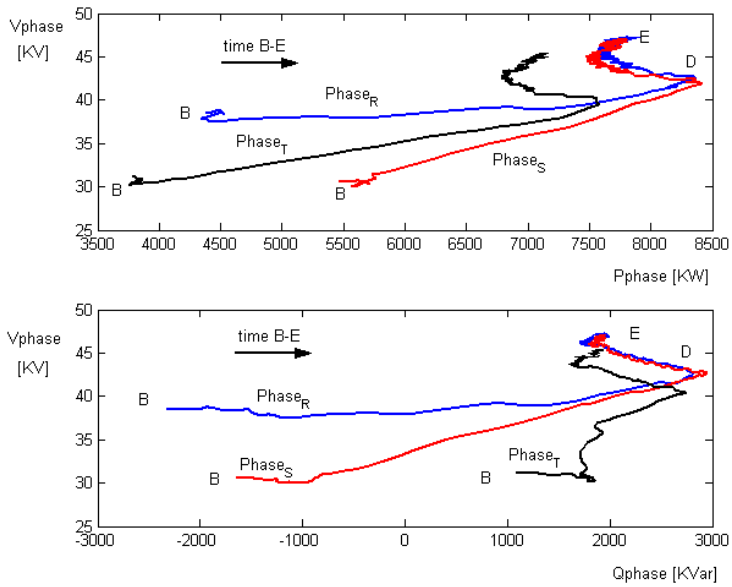

Figure 11.11: Phase active and reactive power plotted versus phase voltage during and after the fault conditions. Segment B-E.

The adequacy of the model given by (11.5) has been studied for different recordings in the same area. The model agrees well with the measured active load for voltage variations up to even 30%. Based on the analysis, the suitability of the model for the reactive load seems limited to voltage dips of about 12%.

For larger values, the nonlinear behavior of the reactive power increases, and the nonlinear model deviates from measurements. It can be concluded that the proposed model needs to be improved to capture the dynamics involved during and after severe disturbances that result in voltage variations larger than 12%.

Figure 11.12 and Figure 11.13 show some of the results from the model validation. The model has been tested for voltage dips in the order of 7.6 %, 8.7%, 8.8%, 10.9%, 11.3%, 13.2%, 13.4%, 14.3%, 30.4% and 34.8 %, during 6 July, 6 July (2), 20 July, 18 August, 20 July (2), 17 July, 20 July (3), 17 July (2), 17 July (3) and 24 June respectively. The thin curves represent the model, and the thick curves the measured data. The results show good agreement for the active power for voltage dips up to 30 %. However, the model is compromised for the reactive power.

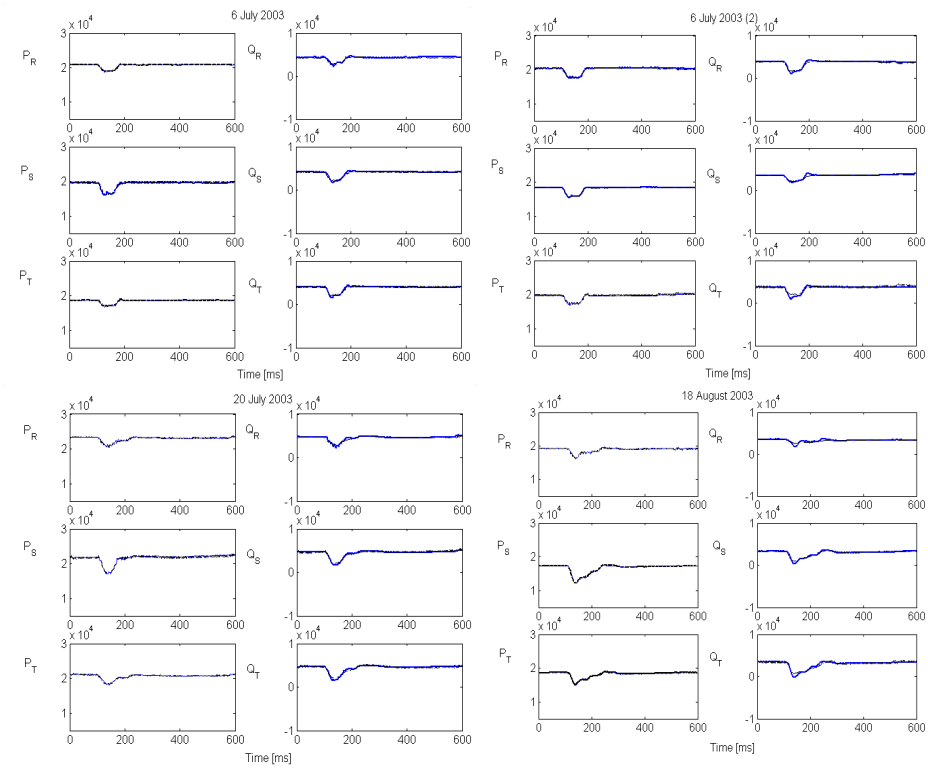

Figure 11.12: Model validation for voltage dips in the order of 7.6 %, 8.7%, 8.8% and 10.9%, during the 6 July, 6 July (2), 20 July, 18 August, respectively, (model-thin curves, measured-thick curves).

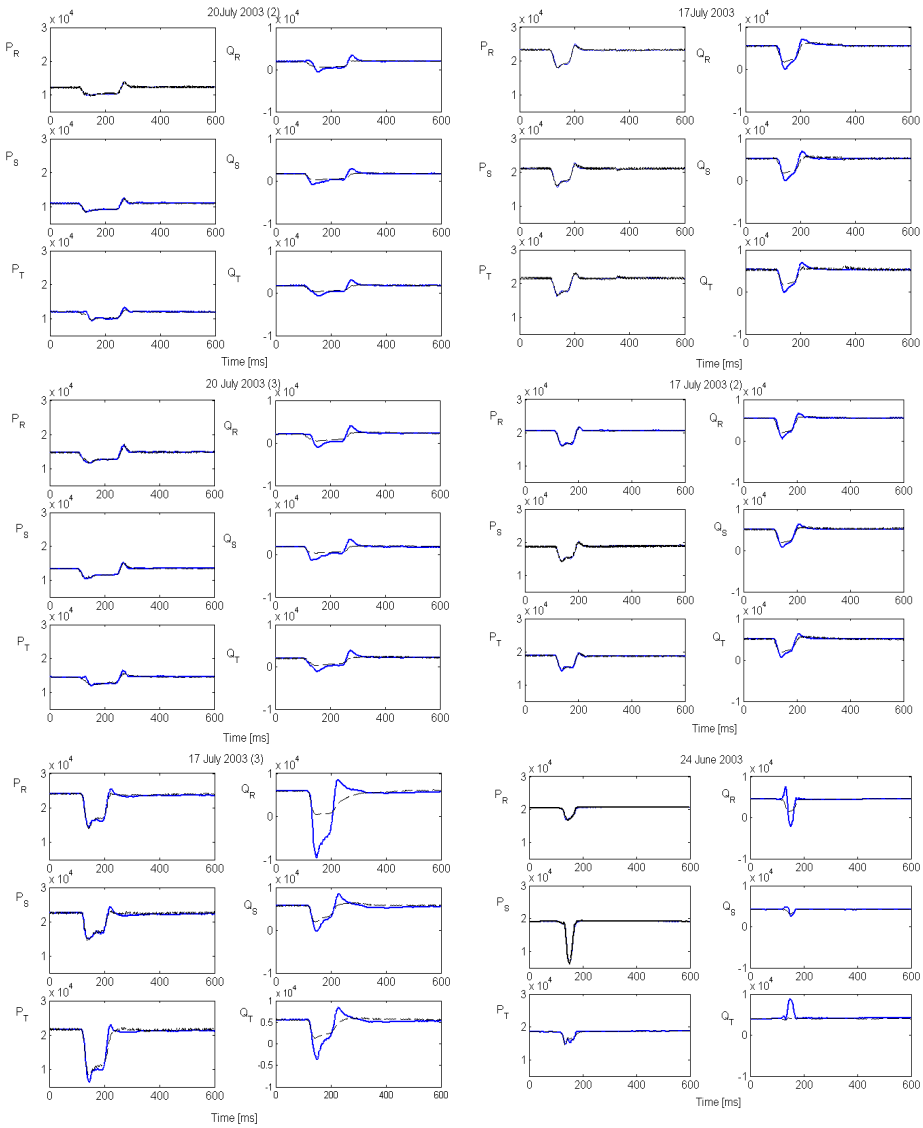

Figure 11.13: Model validation for voltage dips in the order of 11.3%, 13.2%, 13.4%, 14.3%, 30.4% and 34.8 %, during the 20 July (2), 17 July, 20 July (3), 17 July (2), 17 July (3) and 24 June respectively, (model-thin curves, measured-thick curves).

11.6 Load-voltage characteristic

During large voltage and/or frequency excursions, it is necessary to represent the system with dynamic models, which fully represent the nonlinearities of the power system. The load characteristic at low voltages deviates from the traditional load-voltage relationship, and exhibits a nonlinear behavior, which accentuates with the severity of the disturbances. Figure 11.14 shows the filtered rms voltage, active and reactive power for phases R, S and T for the phase-to-phase disturbance during 17 July described previously in Chapter 9.

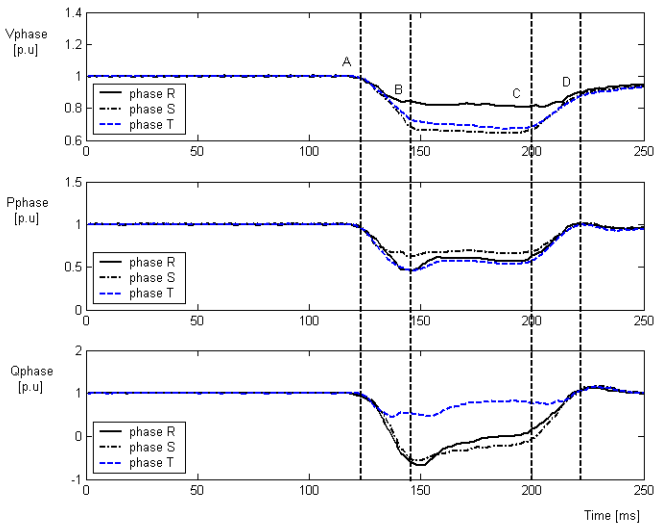

Figure 11.14: Filtered rms voltage, active and reactive power for phases R, S and T for the phase-to-phase disturbance during 17 July.

Figure 11.5 shows the active and reactive load-voltage characteristic for the phases R, S and T during and after the disturbance presented in Figure 11.4. The characteristic is divided into three different segments A-B, B-C and C-D. The segment A-B represents the corresponding drop in the active and reactive power when the disturbance occurs. The load behaves as constant impedance since the slip of motors cannot change rapidly due to mechanical inertia. The point B corresponds to the lowest reached value for the active and reactive power. Observe that this point does not correspond to the

lowest voltage. After the short circuit and due to the low voltage conditions, segment B-C, the motor reduces its electrical torque and decelerates, which results in an increase of reactive consumption. The active and reactive load will then increase, making the system voltages even more depressed. Observe that the lowest voltage is reached at point C. A partial recovery of the voltage occurs then from point C to D, right after the fault has been cleared. Then, the active and reactive power consumption increase even over the pre-disturbance conditions, i.e. the motors draw high currents in order to accelerate and to reduce their slip.

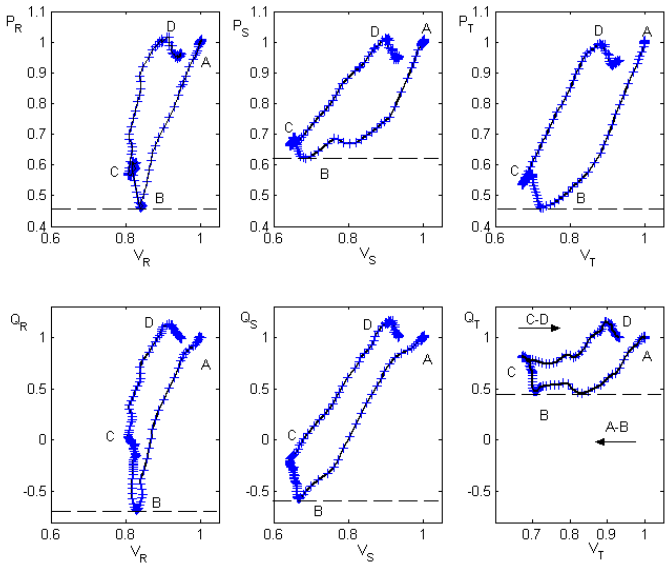

Figure 11.15: Active and reactive load-voltage characteristic for phases R, S and T, for the phase-to-phase disturbance during 17 July.

The full restoration of the load will take some extra time depending on the loading conditions and the severity of the disturbance. For example, [Agneholm, 1999], mercury and sodium lamps will shut down for voltages lower than 0.85 p.u. The full re-connection will take between 2-5 minutes after the fault is cleared, and during the re-connection their consumption is just 50 % of their stationary value. For fluorescent lamps the re-connection

is much faster, and some seconds after the clearance of the fault the power reaches 90 % of its steady state value.

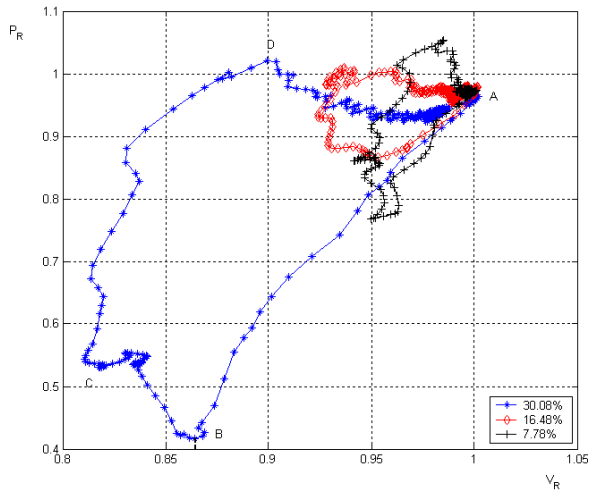

Figure 11.16: Active load characteristic for phase R for three voltage dips.

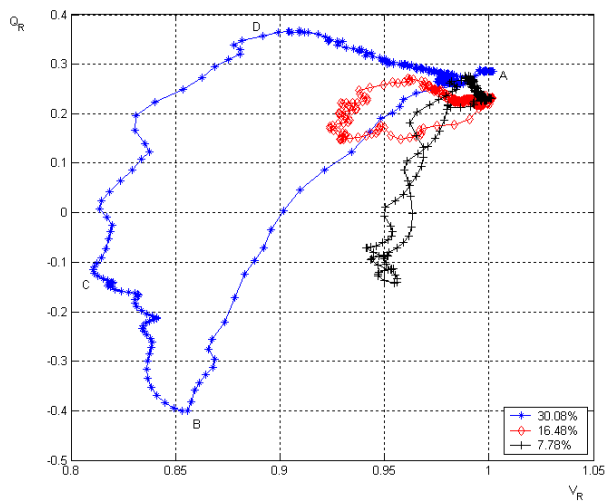

Figure 11.17: Reactive load characteristic for phase R for three voltage dips.

The load-voltage characteristic has been studied for different recordings, which exhibit different sized voltage dips. Figure 11.16 and Figure 11.17, active and reactive load characteristic against voltage for phase R, show the result from this investigation during three voltage dips. It is clearly observed that the nonlinear behavior of the load increases with the size of the disturbance. The load behavior is less predictable with the increasing size of the voltage changes since its nonlinear behavior accentuates for more system stressing conditions. This fact is more noticeable for the reactive load characteristic.

11.7 Conclusions

This chapter investigates the load-voltage characteristic during large voltage variations, and provides an analysis of adequacy for existing traditional models to represent the load during these conditions. It can be concluded that the model given by (11.5) is no longer valid during severe voltage reductions. The load behavior uncertainty critically increases with the size of the voltage changes since its nonlinear behavior accentuates for more system stressing conditions. This fact is more noticeable for the reactive load characteristic.

The adequacy of the model given by (11.5) has been studied for different recordings in the same area. The model agrees well with the measured active load for voltage variations up to even 30%. Based on the analysis, the suitability of the model for the reactive load seems limited to voltage dips of about 12%. For larger values, the nonlinear behavior of the reactive power increases, and the nonlinear model deviates from measurements.

Furthermore, an appropriate representation for induction motors is necessary in order to investigate the characteristic of the load during severe conditions. The short-term dynamics of the motors has a significant influence on the stability of the power system.

Chapter 12

Alternative Dynamic Load Models

The induction motor load must be appropriately modeled, in order to investigate the load characteristic during severe conditions. The influence of the short-term dynamics of motors must be considered for stability calculations. The modeling task is complex since the load contains a large number of other components other than motors, which also need to be represented. The network effects, losses in the distribution system from lines and transformers, the reactive compensation placed along the feeders, and the effect of other control devices, are also aggregated to the load, and must be accurately identified and separated from the load model representation on the customer side.

The adequacy of a dynamic load model, which represents both the static load and the dynamic characteristic of motors, is investigated in this chapter. The model has been validated with field measurements, and the model parameters have been identified. Moreover, the network effects and the influence of reactive compensation in the measurement area have been calculated.

12.1 Introduction

Chapter 11 has shown that the adequacy of the traditional exponential model given by (11.5) to represent the load is compromised during large voltage variations. Measurements have shown that for voltage reductions larger than some 12% the adequacy of the model decreases, this effect being more critical for the reactive load.

Large voltage variations are the result of abnormal operation of the power system. During these conditions the power system is highly stressed and the nonlinearities dominate the operation. They are for example produced by short circuits. The duration of short circuits with a successful fault clearing are about 100-200 ms. During the time frame of about hundreds of ms to a second, the long-term dynamics from OLTCs and thermostatic load are too slow and therefore they are not critical. However, the effects of asynchronous motors and discharge lighting, highly concentrated in residential and commercial areas, become critical for transient stability specially for increasing large voltage variations.

12.2 Dynamic Load Model for Short-Term Stability

The model given by equations (12.1) and (12.2) has been addressed in [Tomiyana, *et al.*, 2003] and [Ihara, *et al.*, 1994], to represent the active and reactive load during large voltage excursions. However, few tests have been carried out to verify its adequacy to represent the load, and to investigate its model parameters.

$$P = \left[1 + K_p \cdot (V - 1)\right] \cdot \left(1 - P_{drop}\right) + P_{dyn} \cdot \left(G \cdot V^2 - 1\right) \tag{12.1}$$

$$Q = \left[1 + K_q \cdot (V - 1)\right] \cdot \left(1 - Q_{drop}\right) + Q_{dyn} \cdot \left(B \cdot V^2 - 1\right) \tag{12.2}$$

The model describes the effect of both the static and dynamic load in the area. The first term in (12.1) represents the behavior of the static load, which remains connected in the load area during and after a disturbance. Some types of load may disconnect during low voltage conditions in order to be protected from damage by undervoltage protection; the percent of this load is represented by the parameter P_{drop}. The static active load is characterized by the parameters K_p, the active load-voltage sensitivity. The second term in (12.1) describes the dynamic characteristic. The parameter P_{dyn} accounts for the percent of dynamic load in the area. The same is applied to the reactive power given by (12.2). The voltages V and the corresponding active and reactive estimates P and Q have been normalized by the pre-disturbance values V_o, P_o and Q_o. The model is characterized by a time constant T. After a fault is cleared the recovery of the voltage to its pre-disturbance value is delayed. The full restoration of the voltage will take longer, depending on the duration and type of the fault, distance to faulted

point, and the load area composition. The more severe the disturbance is, the longer time it will take for the system to return to steady state conditions. Since most of the dynamics appearing after the fault clearance are related to the motor load, the value of the time constant is obtained from the load characteristic of an induction motor. Equation (12.3) describes the motor inertia dynamics.

$$\frac{dG}{dt} = -\frac{1}{T} \cdot \left(G \cdot V^2 - 1\right) \tag{12.3}$$

From the calculated time-varying estimates of the aggregated load resistance R and reactance X, (Chapter 10), the conductance G and susceptance B can be determined. After a fault is cleared the conductance of the motors becomes significantly large, since the motors will re-accelerate and their slip will decrease. Motors will then draw more reactive power, bus voltages will be even more depressed, the electrical torque will be reduced, and the recovery of the voltage will be slower. The measurements presented at the end of this chapter show that right after a fault is cleared both the active and reactive power increase over the pre-disturbance values, and show exponential dynamics until they reach steady state.

12.3 Validation of the Model

The model introduced in the previous section is now validated with field measurements. The estimated phase active and reactive power calculated in Chapter 10 during faulted conditions, have been used for the validation. The disturbance July 17 2003 is analyzed again in order to compare with previous results.

12.3.1. Identification

Consider the model given by equation (12.1). The nonlinear relationship between the measured signals, active power P, voltage V at the load bus and the estimated conductance G, and the parameters K_p, P_{drop} and P_{dyn} can be simplified by re-parametrization, and the model can be written as a linear regression, equation (12.8).

$$P = \left[1 + K_p \cdot (V - 1)\right] \cdot x(1) + P_{dyn} \cdot \left(G \cdot V^2 - 1\right) \tag{12.4}$$

$$P = \left[x(1) + x(2) \cdot (V - 1)\right] + P_{dyn} \cdot \left(G \cdot V^2 - 1\right) \tag{12.5}$$

$$x(1) = (1 - P_{drop}) \tag{12.6}$$

$$x(2) = x(1) \cdot K_p \tag{12.7}$$

$$y(t) = \varphi^T(t) \cdot \theta_p \tag{12.8}$$

$$\theta_p = (x(1), x(2), P_{dyn})$$

The Least Squares method has then been used for the identification. The objective is to obtain the best estimates for the parameter vector θ_p, which minimizes the difference between the estimated active power and the simulated one (as a quadratic criterion). The simulated data is given by equation (12.1). The same procedure is applied for the parameter identification for the reactive load, equation (12.2). The objective function to be minimized using a least square criterion is given by equation (12.9). The final parameters are determined directly from the expressions in (12.6) and (12.7).

$$F(\theta_p) = \sum_{k=1}^{N} (P_{simulated}(t_k, \theta_p) - P_{measured}(t_k, \theta_p))^2 \tag{12.9}$$

The least squares method is used to minimize the function (12.9) and to obtain the best estimates for the parameter vector θ_p.

12.3.2. Validation of the Model

Based on the field measurements described in Chapter 9, the model given by (12.1) and (12.2) has been validated. The results show the adequacy and robustness of the proposed model to represent the load characteristic during large voltage variations. The nonlinear dynamic behavior of the load during and after large disturbances is mainly accounted to the asynchronous motors. Figure 12.1, Figure 12.2 and Figure 12.3, show the measured and simulated phase active and reactive power at the load bus for the phase-to-

phase fault occurring during 17 July 2003. Further results are presented in Section 12.5.

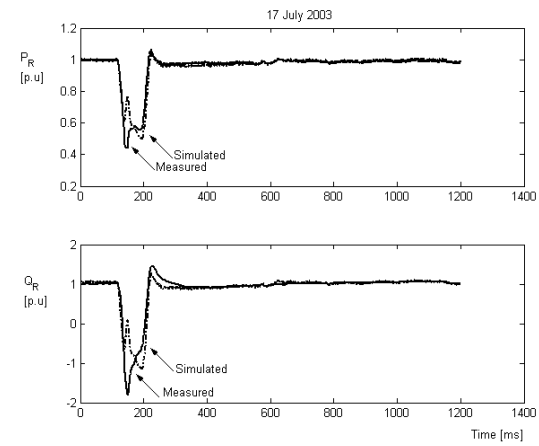

Figure 12.1: Estimated and simulated phase active and reactive power during and after the fault conditions. Phase R.

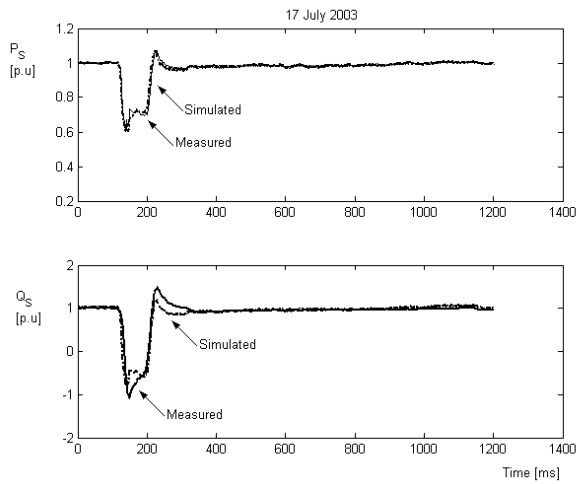

Figure 12.2: Estimated and simulated phase active and reactive power during and after the fault conditions. Phase S.

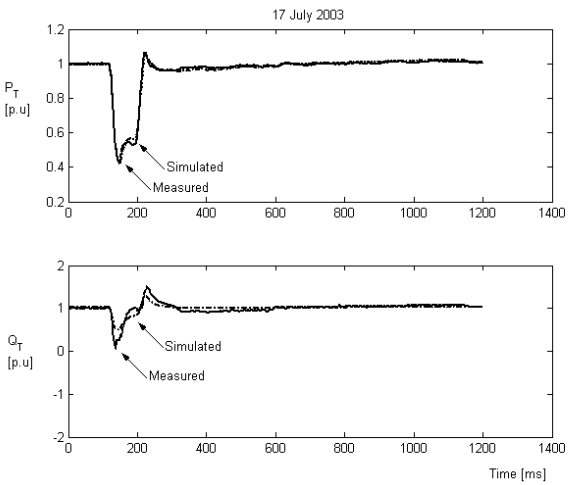

Figure 12.3: Estimated and simulated phase active and reactive power during and after the fault conditions. Phase T.

The model fits the active power for the three phases. Note that some transients have been found in both the active and reactive load response during the faulted time. Those transients can be neglected since the time interval where they are acting is very short. A good agreement is also found for the reactive load representation. Therefore, it can be concluded that the model can accurately represent both the active and reactive load. The model fits both the amplitude of the load, but also the dynamics involved during and after the disturbance.

The time constant T is estimated from equation (12.3). A discrete time approximation, equation (12.10), has been determined by using a forward approximation for the derivative of the conductance, and by taking into consideration the relations between two different sampling times, k and k+1, as described in Figure 12.4. T is determined directly from equation (12.10).

$$\frac{G(k+1)-G(k)}{h} = -\frac{1}{T}\cdot\left(G(k)\cdot V(k)^2 - 1\right) \tag{12.10}$$

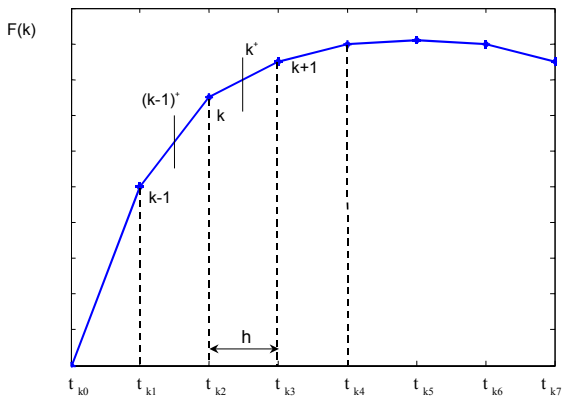

Figure 12.4: Relation between two different sampling times, *k* and k+1, in a forward approximation.

The obtained values for the time constant move within the interval 140-240 ms; these values could have been directly obtained from Figure 12.1-Figure 12.3. Note that these figures represent the active and reactive aggregated load per phase, including the losses from lines and transformers, and the effect of reactive compensation in the distribution system. The network effects and the reactive compensation are investigated in the next section.

12.4 Network Effects and Reactive Compensation

12.4.1. Introduction

The per phase load estimates P and Q represent the per phase aggregate consumption of a large number of individual loads, but also the power consumed by the downstream 50 kV and lower distribution systems, i.e. losses in lines and power transformers, the effects of reactive compensation, fixed and switched shunt capacitors placed along the feeder, as well as the effects of other control devices. Long feeders and distribution transformers represent a large share of the distribution system impedance; delivery

transformers reactances are 8-11 % on the transformer base and impedances of distribution transformers are 2-4% [Taylor, 1994].

The total phase estimated P and Q at the 50 kV-level can be modeled as in Figure 12.5, where P and Q are the sum of the power consumed by the equivalent impedance that represents the losses in distribution lines and transformers P_d and Q_d, the effects of reactive compensation Q_c, and the power consumed by the load P_l and Q_l. It is therefore necessary to separate the effects of the network and the reactive compensation, from the total consumption at the 50 kV-level. The effect of saturation in transformers is not taken into account since the magnitude of the magnetizing currents during voltage disturbances in the order of 30% is not significant [CIGRE, 1998].

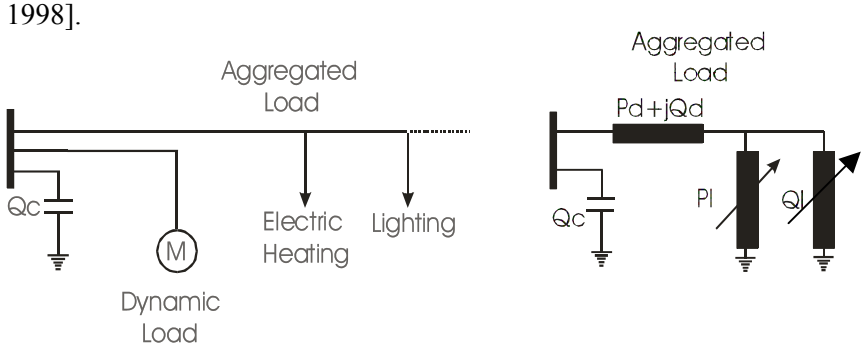

Figure 12.5: Simplified representation of the load.

12.4.2. Distribution System Active and Reactive Losses

The distribution system losses for feeders 54 and 59 have been calculated and removed from the total estimated load at the 50 kV-level. The losses have been calculated by determining the equivalent Thevenin impedance seen from the 50kV-level and downwards for each feeder. Appendix IV includes the transmission and distribution network parameters for the Öland system. Phase resistance and reactance values for lines and transformers are available. The active and reactive losses have been calculated by using equations (12.11) and (12.12). The load on the customer side is then calculated as the difference between the estimated load at the 50 kV-level and the load consumed by losses, equations (12.13) and (12.14) respectively.

$$P_d = R_{thevenin} \cdot I^2_{measured_50kV} \tag{12.11}$$

$$Q_d = X_{thevenin} \cdot I^2_{measured_50kV} \tag{12.12}$$

$$P = P_{estimated_50kV} - P_d \tag{12.13}$$

$$Q = Q_{estimated_50kV} - Q_d \tag{12.14}$$

Table 12.1 includes the average total active and reactive consumption at feeders 54 and 59, and the active and reactive power consumed by losses.

Feeder	Active Power [kW]	Active Losses [kW]	[%]	Reactive Power [kVar]	Reactive Losses [kVar]	[%]
Feeder 54						
Phase R	7848	19	0.23	1913	238	12.40
Phase S	7836	19	0.24	1986	241	12.13
Phase T	7102	18	0.24	1815	220	12.09
Feeder 59						
Phase R	6911	39	0.56	1788	329	18.41
Phase S	6998	39	0.56	1738	334	19.21
Phase T	6390	37	0.56	1718	303	17.65

Table 12.1: Total phase estimated active and reactive power for feeders 54 and 59, and value of the corresponding losses in the distribution system.

The table shows that the reactive losses are substantially high and therefore must be taken into consideration when modeling the load.

12.4.3. Effects of Reactive Compensation

The aggregated reactive load represents the individual load components but also the effects of reactive compensation. Reactive compensation affects system voltages and therefore the load-voltage characteristic. Part of this compensation is fixed and switched capacitors placed by utilities for voltage control during heavy load conditions, but also shunt capacitors placed close to large industrial loads where the percent of motor load is high, or in the neighborhood of independent generation units. In order to quantify the effects of the reactive compensation and to separate them from the reactive consumption at the customer side, the load P and Q in the model given by

(12.1) and (12.2) has been normalized by the quantity S_o, instead of by the pre-disturbance values P_o and Q_o. This approach has already been introduced and motivated in Part II of this thesis. The common value Q_o used in the normalization of the reactive load models may be close to zero due to the effect of reactive compensation, and therefore the identified parameters that represent the reactive load may deviate from the expected values. The pre-disturbance apparent power S_o is used instead.

The effect of the reactive compensation can also be calculated from the pre-disturbance data. However, this approach is limited by the availability of pre-disturbance data, and it does not account for spontaneous switching compensation on the customer side. The total phase active and reactive power from feeders 54 and 59 is plotted in Figure 12.6. Most of the operating points can be fitted by a line model, which represents the phase load characteristic seen from the 50 kV bus, including the effects of shunt reactors and capacitors located in the distribution system.

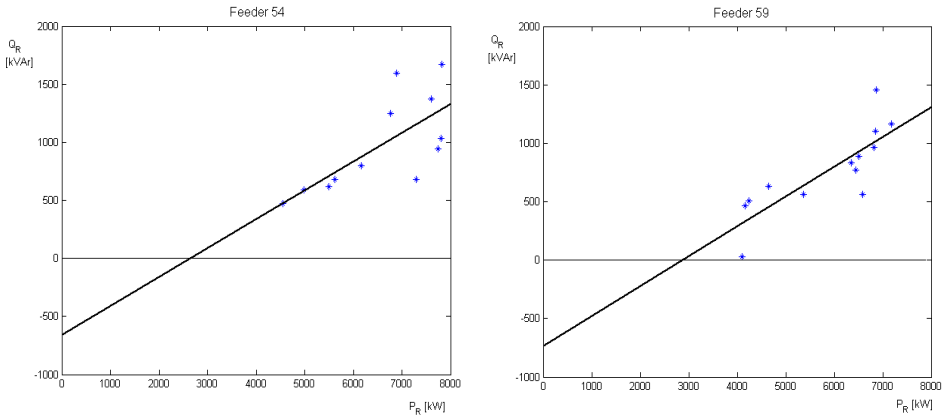

Figure 12.6: Line model that represents the phase load characteristic seen from the 50 kV bus including the effects of shunt reactors and capacitors located in the distribution system.

The line model for feeder 54 intersects the vertical axis at –656 kVar and the horizontal one at 2625 kW. For feeder 59 the model intersects at –731 kVar and 2813 kW. Both line models are given by equations (12.15) and (12.16). The same procedure can be applied for phases S and T.

$$y = 0.25 \cdot x - 656 \tag{12.15}$$

$$y = 0.26 \cdot x - 731 \tag{12.16}$$

The measured phase reactive power at the 50 kV-level is the sum of the reactive consumption of the load and the reactive power generated from shunt capacitors. The expressions for the total reactive load at the customer side without the effects of reactive compensation for feeders 54 and 59 are given by equations (12.17) and (12.18) respectively.

$$Ql = Q + 656 \cdot V^2 \tag{12.17}$$

$$Ql = Q + 731 \cdot V^2 \tag{12.18}$$

An analysis of the distribution system in Öland shows that at feeder 54 there is a 2 MVar bank capacitor, which is constantly connected to the 10 kV-level. Moreover, the two parallel cables connected to the 50 kV-level in Linsänkan (Figure 9.2), are constantly injecting reactive power in the distribution system; 1.8 MVar measured at 53.6 kV in Linsänkan, is injected to the main four feeders 54, 55, 59 and 60. No other significant information is available from utilities about other reactive sources, but it may be considered the presence of other shunt reactors and capacitors from independent small customers, and the effects of the wind power generation units.

12.5 Analysis of the Results

This section presents further results. Field measurements from a non-effectively earthed system from phase to phase faults on the 50 kV-level at a substation in Sweden have been used for the study. The recorded disturbances exhibited voltage dips at the load bus up to 30%. The same procedure, described throughout Chapters 10-12, has been applied to each one of these sets. Figure 12.7 and Figure 12.8 show the positive sequence voltage, and the estimated active and reactive power per phase for the recordings from feeders 54 and 59 respectively. The network effects, losses and reactive compensation, have been considered in the results. When a fault occurs the voltage drops and so does the active and reactive power. The active and reactive power will however start increasing right after this

first drop due to the motor load response. The drop in voltage will result in a decrease in the electrical torque, and in deceleration of the motors in the load area (increasing slip). At low speeds motors draw very high reactive currents. When the fault is cleared the power increases even above the pre-disturbance conditions, which is related to the motors re-acceleration.

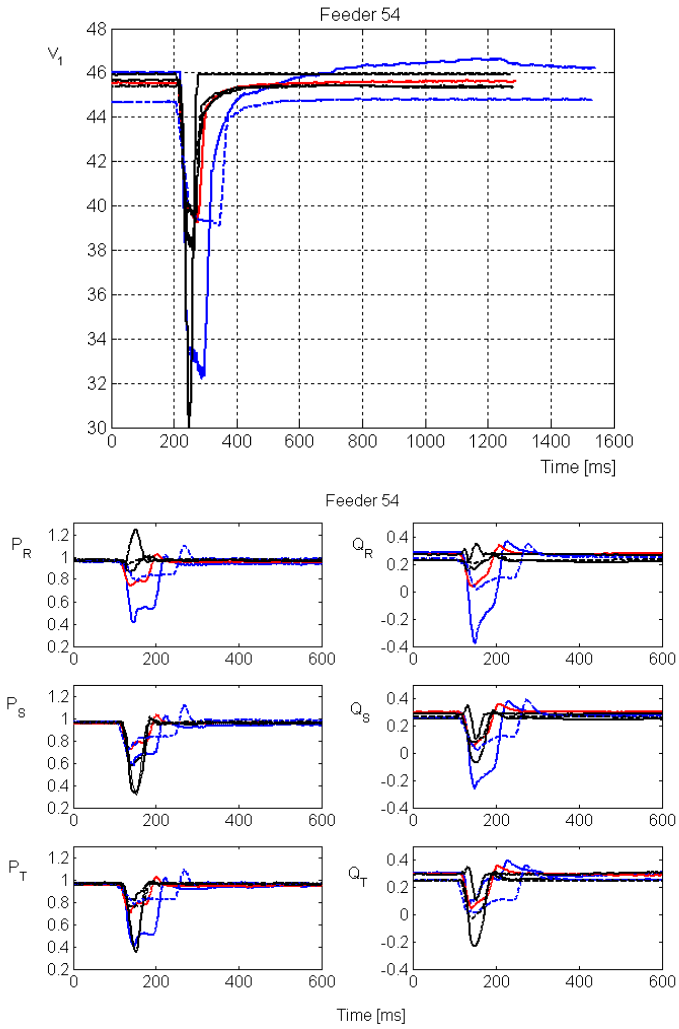

Figure 12.7: Positive sequence of the voltage at the 50 kV-level, and active and reactive power per phase for different voltage dips at feeder 54.

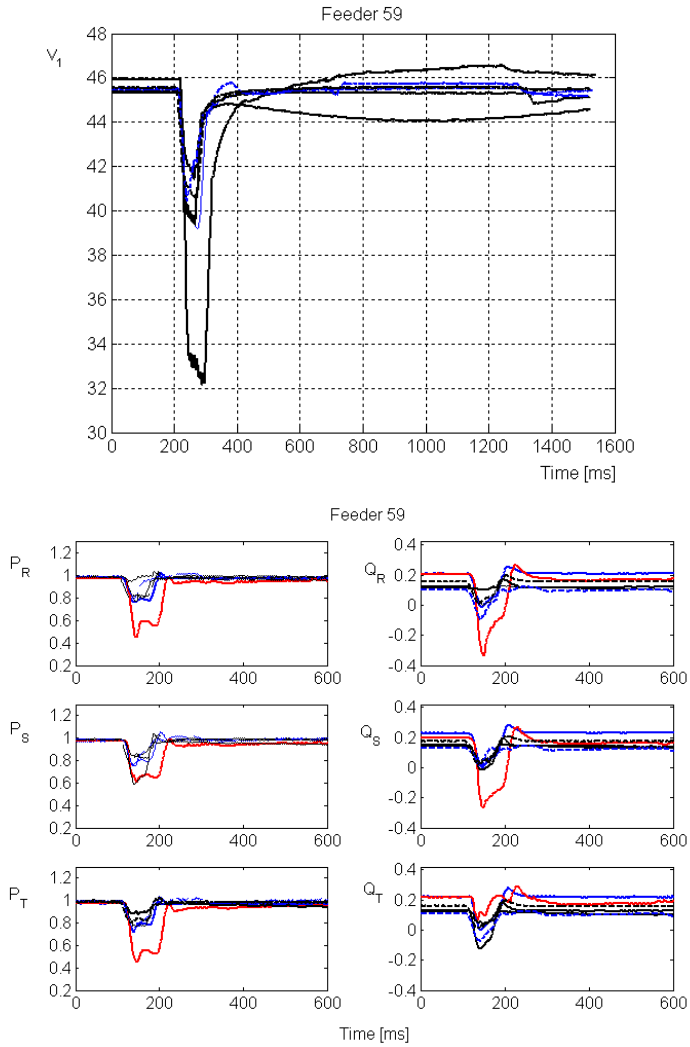

Figure 12.8: Positive sequence of the voltage at the 50 kV-level, and active and reactive power per phase for different voltage dips at feeder 59.

Both the active and reactive load exhibit exponential dynamics in response to the voltage drop. The model given by (12.1) and (12.2) has been validated for all the cases presented. The results are shown in the following figures:

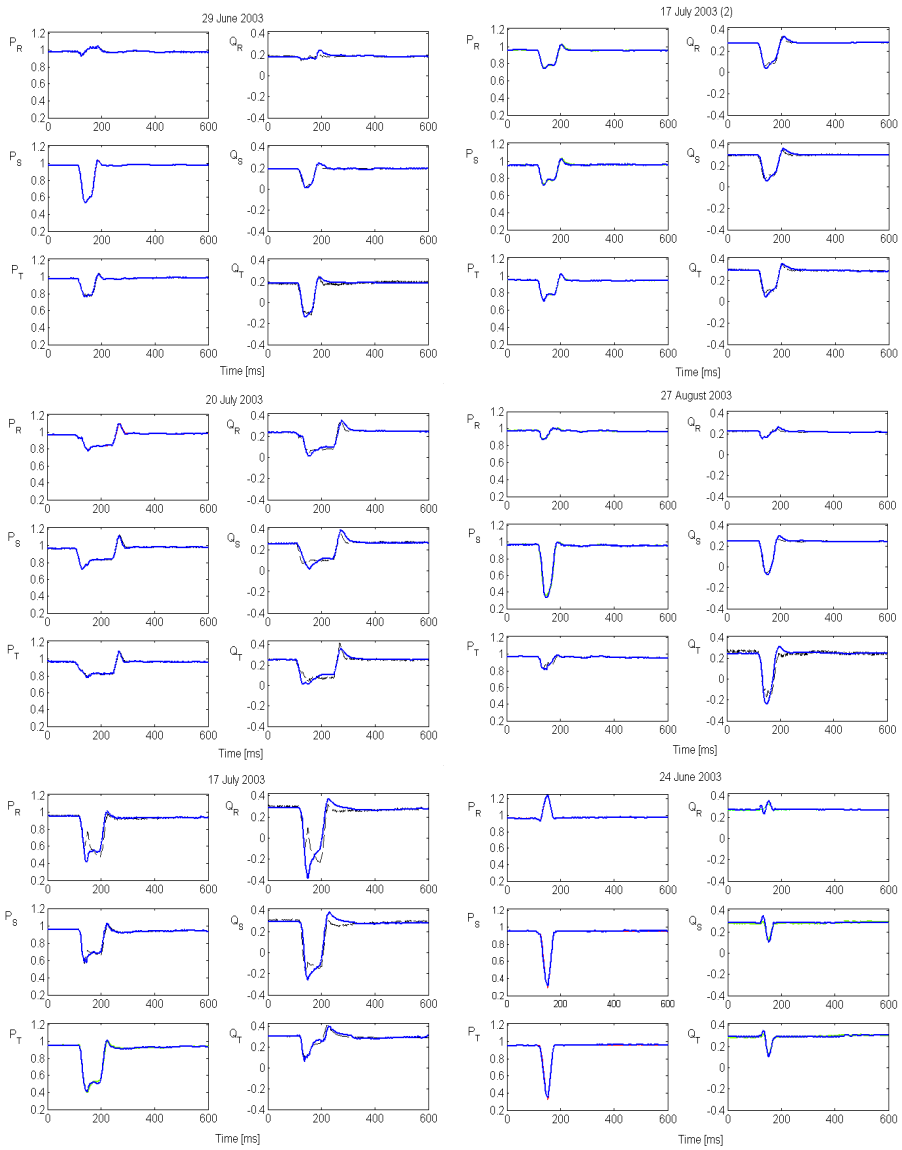

Figure 12.9: Model validation. Measured and simulated active and reactive power per phase at feeder 54 for different voltage dips; 13.2 %, 13.2 %, 13.3 %, 17.4 %, 30.4 % and 34.8%, during the 29 June, 17 July (2), 20 July, 27 August, 17 July and 24 June respectively, (model-thin curves, measured-thick curves).

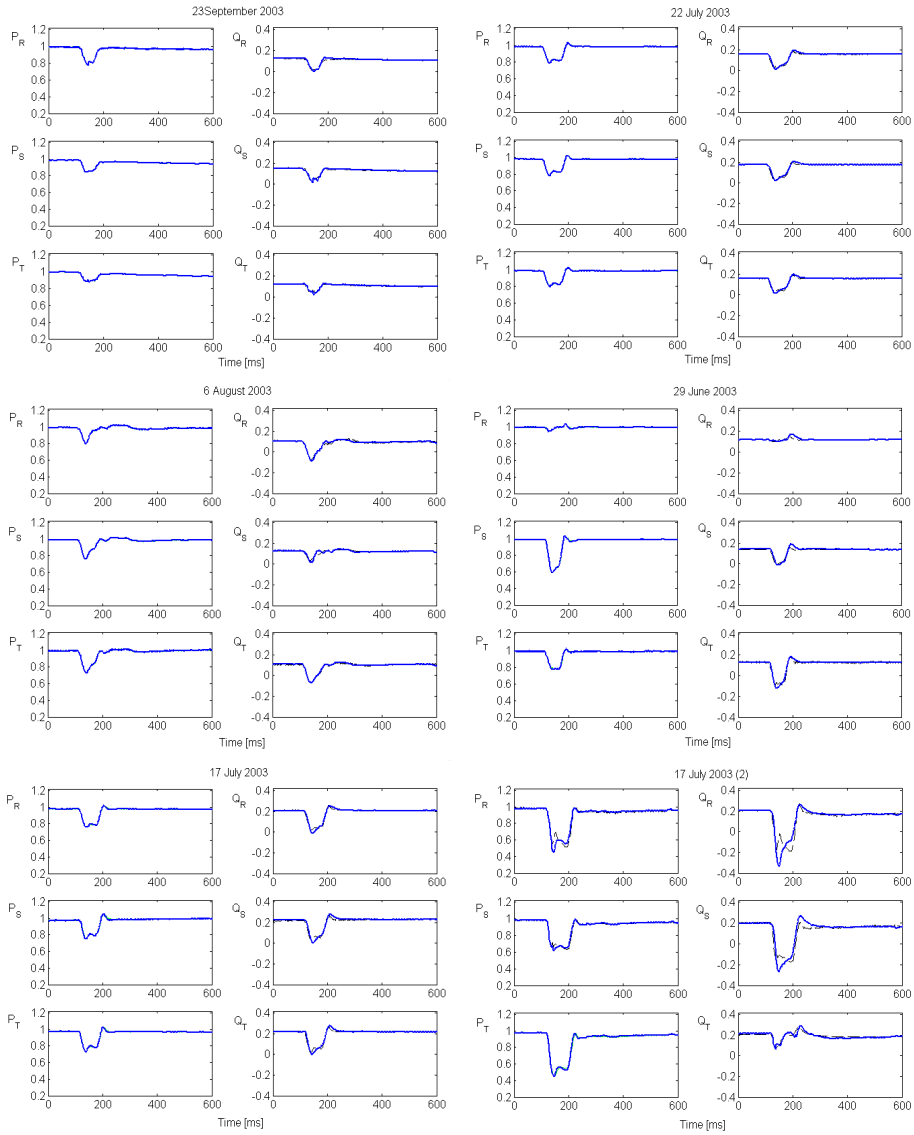

Figure 12.10: Model validation. Measured and simulated active and reactive power per phase at feeder 59 for different voltage dips; 9.8 %, 10.9 %, 10.9 %, 13.3 %, 13.3 %, and 30.4 %, during the 23 September, 22 July, 6 August, 29 June, 17 July and 17 July (2) respectively, (model-thin curves, measured-thick curves).

The model fits the drop in active and reactive power at the initiation of the fault, but also the recovery of the active and reactive power during and after the recovery of the voltage for all the cases. Note that the disturbance during the 17 July at feeder 54, which has been described throughout Part III of this thesis, shows the worst fit for the model. However, the differences between the measured and simulated data are very small, and the model is acceptable for this case as well.

The parameters for both the active and reactive load given by (12.1) and (12.2) have been investigated for each one of the disturbances. Significant loss of load has not been observed. All the disturbances were recorded during the same season of the year (from June to September), which means that the effect of the outdoor temperature and humidity conditions are not relevant in this investigation. Note that the study has been carried out in Sweden, where the summer outdoor temperatures are mild, and the presence of air conditioner units is low. Figure 12.11 shows the results obtained for both the active and reactive load static characteristic K_p and K_q.

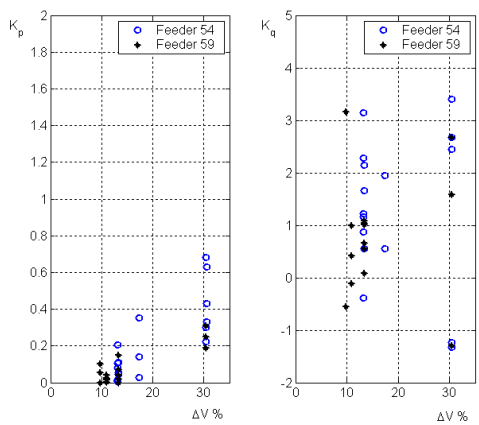

Figure 12.11: Active and reactive static characteristic of the load K_p and K_q for both feeders 54 and 59.

In general both the active and reactive load characteristics do not exhibit big differences from one to another event. The static characteristic of the load seems independent on the size of the disturbance. Therefore the identified parameters move within the same interval for different voltage variations. The static load characteristic K_p moves from constant power to constant

current (values from 0 to 1). K_q, the static reactive characteristic, exhibits larger values (values between –2 to 5). Both the active and reactive load, present a large percent of dynamic load given by the parameters P_{dyn} and Q_{dyn} respectively, which is mainly related to the motor dynamics (see Figure 12.12).

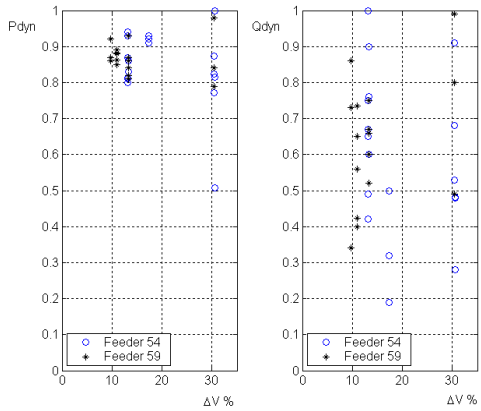

Figure 12.12: Percent of active and dynamic load *Pdyn* and *Qdyn* present in the area for both feeders 54 and 59.

In general, it is observed that the reactive load model parameters present larger variability than the active ones. Three main reasons may have affected the results; firstly, only 12 sets of data, six sets from each feeder, have been used to carry out this investigation. In order to obtain significant results more data for the identification is recommended. Secondly, this investigation has not accounted for the influence of distribution generation in the area. Thirdly, the identification of the parameters has been done per phase. Those phases affected by the disturbance exhibit the same parameter values, however the non-affected phases present different values. The differences in the values are much larger for the reactive power.

At three of the recorded events, which exhibit voltage dips in the order of 30.4 %, 17.4 % and 13.2 %, the reactive power presents an unexpected behavior. It dramatically drops at the faulted time to a negative value, which tends to zero in about 100 ms. From a voltage stability point of view it is

difficult to understand that during faulted conditions the load may produce a capacitive current. An investigation has been carried out to study this phenomenon. The load aggregates among other components induction motors and generators. During faulted conditions a third order model (chapter 2) is often used to study the behavior of these machines. At the faulted time the voltage drops and so does the active and reactive power. During some ms the motors behave as constant impedance since the slip has not had enough time to change due to the inertia of the machines. Afterwards, the slip of the motors will increase, the motor will decelerate and the consumption of reactive power will increase. This model accounts for the mechanical transients in the rotor, however, the electrical transients, which are much faster, are often neglected. Figure 12.3 shows a simplified scheme of the test area where the measurements have been carried out. Firstly, it is assumed that the load at the load bus, bus 3, is mainly induction motor load. If a fault occurs at point A, a capacitive current will flow from the load to A.

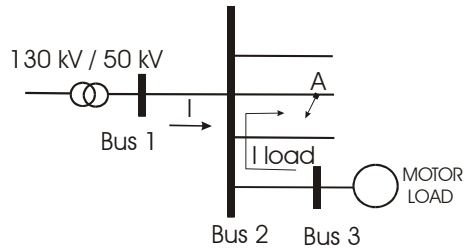

Figure 12.13: Simplified test system from the measurements area. Flow of the load current during a fault at A.

When the fault occurs, the rotor currents still continue rotating at the same speed until the slip of the motor changes, and therefore inducing voltages in the stator. The polarity of these induced emfs is however changed and a capacitive current will flow towards the fault location. This capacitive current will decrease towards zero.

A simplified test system, Figure 12.14, has been used to verify these conclusions. A generator is connected through a long transmission line and a transformer to the load area. At the load bus, induction motor load is connected. A single-phase to ground, a phase-to-phase, and a three-phase fault have been applied to the transmission system during 200 ms. The behavior of the reactive power at the load bus has been then observed, see

Figure 12.15-Figure 12.17. PSCAD has been used for the simulations [PSCAD, 2001].

For the three cases the reactive power becomes negative when the fault occurs. Then the reactive power increases towards zero. The amount of capacitive reactive power produce during asymmetrical conditions is much higher than for a balanced fault. During asymmetrical faults the motor can still be fed by the healthy phases.

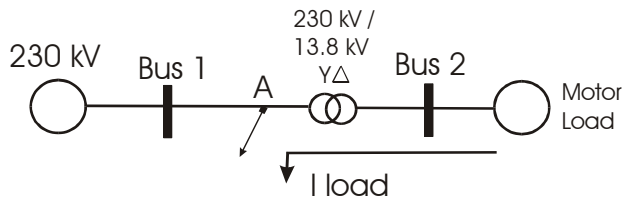

Figure 12.14: Test system to study the reactive consumption of induction motors during faulted conditions.

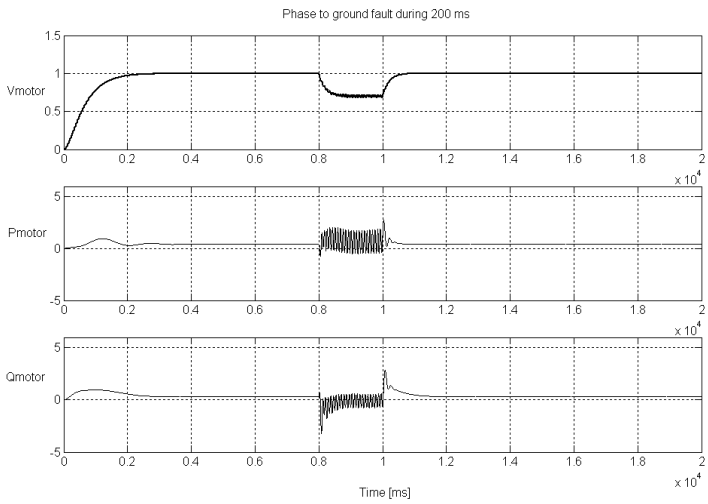

Figure 12.15: Three-phase voltage, active and reactive power measured at the load bus, during a phase to ground fault at the transmission system.

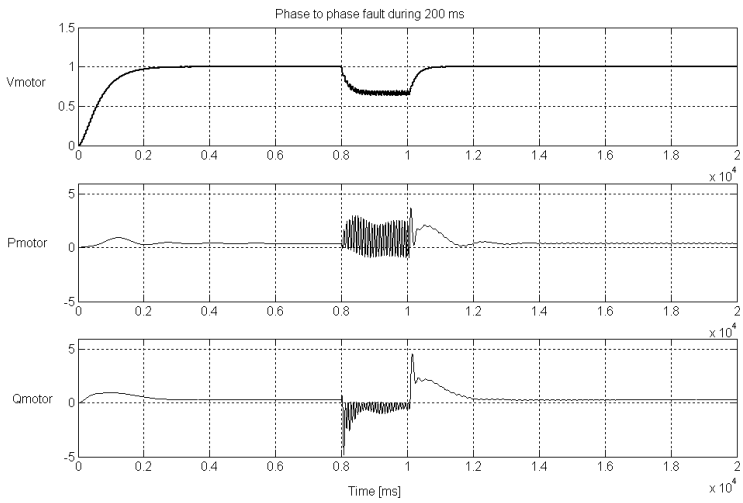

Figure 12.16: Three-phase voltage, active and reactive power measured at the load bus, during a phase to phase fault at the transmission system.

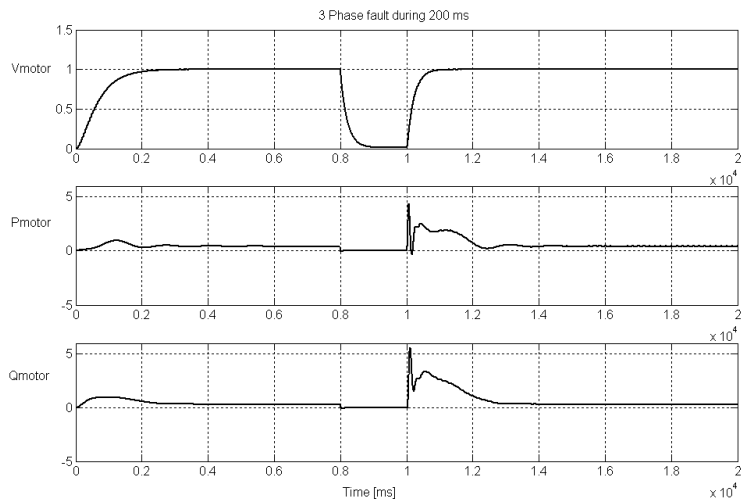

Figure 12.17: Three-phase voltage, active and reactive power measured at the load bus, during a three-phase fault at the transmission system.

In the measurements area the load aggregates a large number of components. For large concentration of induction motors it is possible to observe this capacitive current. This may be the reason of why this phenomenon has not been observed for all the cases.

Similar recordings have been observed in previous investigations [Ihara, *et al.,* 1994], [Tomiyana, *et al.,* 1998], [Kermendey, *et al*., 1999], [Shaffer, 1997]. However, this phenomenon has not been comented.

12.6 Conclusions

An appropriate representation of induction motors is necessary in stability studies, in order to investigate the characteristic of the load during severe conditions. A nonlinear model for the load that accounts for both the static and dynamic characteristic of the load has been introduced in this Chapter. The model has been positively validated for different sets of data. The model fits both the active and reactive load response. The network effects, losses in distribution transformers and lines have been calculated. The model has been normalized by the pre-disturbance apparent power S_o instead of by the quantities P_o and Q_o to account for the effects of the reactive compensation at the load bus.

The model parameters have been identified from field measurements. Significant loss of load has not been observed. In general both the active and reactive load characteristics do not exhibit big differences from one to another event. Both the active and reactive load, present a large percent of dynamic load given by the parameters P_{dyn} and Q_{dyn} respectively, which is mainly related to the motor dynamics.

Last, the reactive power response at the load bus during symmetrical and asymmetrical faults, when a large amount of induction motors is present in the area, has been investigated. Induction motors produce a capacitive current, which tends to zero at the initiation of the fault due to the induced voltages in the stator by the rotor currents. Higher order models that represent the electrical transients in the rotor are necessary to model this response. This effect is more noticeable in asymmetrical faults.

Part IV

Conclusions

Summary: *The topic of this thesis has been focused on the investigation of the load characteristic in several time-scales and for different sized voltage variations, and its effect in stability studies. This investigation has provided deep insight into the nature of load dynamics and their dependency with voltage, and has made it possible to carry out an adequacy study of traditional models for load representation.*

The last part of this thesis provides some guidelines for industry and academia to better account for the load in stability studies. It also describes a number of steps to develop a load modeling procedure for an arbitrary location from operational data. This procedure makes it possible to determine the diurnal and seasonal load parameters for the area under study from a chosen load model structure. Moreover, the main conclusions of the thesis and potential sources for future research are also included.

Chapter 13

Load Modeling Recommendations

The first objective of this chapter is to give some guidelines to better account for the load in stability studies, in order to get a more accurate calculation of transfer limits and determination of corresponding security margins. Moreover, a number of steps to investigate the load at a general location from operational data are included in this section. These steps cover the planning, implementation and the determination of the diurnal and seasonal load parameters for the area under study from a chosen load model structure.

13.1 Loads and Critical Scenarios

Throughout this thesis a number of references have been addressed, which show that the significance of load modeling for stability studies has been noticed for a long time. Several large disturbances, which have ended in voltage instability and collapse at different locations in the world, have indicated that the load dynamics in combination with other dynamics are among the main contributors to this instability. Moreover, the disturbances have shown that the load responds in different ways depending on the time frame of actuation, short- or long-term, and the type of disturbances affecting the system, small or large.

These practical experiences are a huge source of information to get a better insight into the load behavior. They are continuously showing novelties, which trigger new investigations. As a brief description, this author has decided to point at the following major disturbances, Sweden 1983, Sweden

2003, and some disturbances in the North American system. Different load dynamics have been involved in these disturbances. They are good examples to indicate that work still needs to be done.

Sweden 1983

On December 27 1983, a busbar section at the 400 kV in eastern Sweden was affected by an earthfault. A breakdown of a disconnector in Hamra transformer station (one of the stations feeding Stockholm) caused tripping of all line connecting to the station, and affected two of the 400 kV lines that transfer power from the middle to the southern Sweden [SINTEF, 2004]. Before the disturbance, the transmission system was highly loaded, i.e. the transfer from North to South of Sweden was close to the maximum recommended.

A number of events followed the disturbance; due to the overloaded conditions, the eastern transmission route from the North was interrupted, reducing the robustness of the southern system. However, the system remained stable and the frequency constant. 50 seconds after the initial fault, one more 400 kV line tripped, other lines became overloaded, and cascade tripping took place. Then, the southern Sweden became isolated. The power unbalance in the area resulted in a rapid decrease in voltage and frequency, tripping of the generating units, and in a blackout.

The initial fault was the event that triggered the blackout, resulting in a weaker system and more overloaded conditions. Low voltages and an increased transfer from the central part dominated the situation. The load characteristic (recovery of the load after the initial voltage drops) was one main contributor to these low voltage levels; low temperatures due to winter conditions forced the system to be working close to its transfer limits. The combination of the long-term dynamics from tap changers and the load resulted in an increase of load and therefore in lower voltages. Moreover, studies have shown, [Walve, 1986], that for voltages under 0.8 p.u, the load did not behaved as traditionally is represented in stability studies.

Figure 13.1 shows a recording from western Sweden just before and during the cascade tripping.

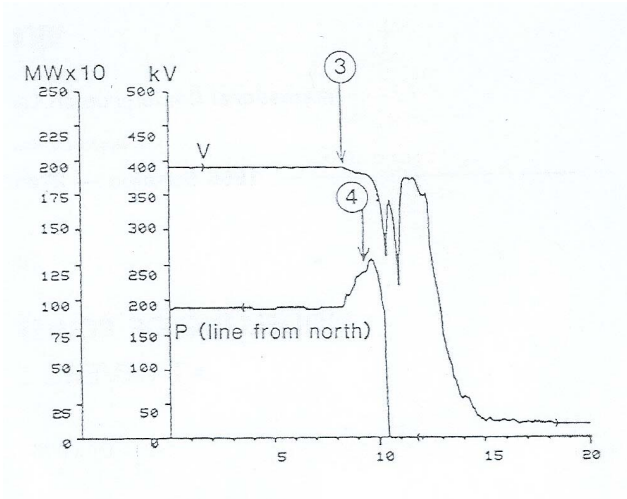

Figure 13.1: Recordings at a western busbar station in Sweden. Picture taken from [Walve, 1986].

Sweden 2003

On September 23 2003, the Nordic power system experienced the most severe disturbance after 1983; The Southern part of Sweden and the eastern part of Denmark had a blackout, [Svk, 2003]. The operating conditions before the disturbance were stable and within the recommendations from the operational planning and grid security assessment. However, several components of the system were out of operation due to maintenance work; the nuclear generation in the affected area was limited (only one of the three generators was in operation in Oskarshamn, in the southeast of Sweden). There was no generation in Barsebäck (a nuclear plant in the southernmost province of Sweden) due to the permanent closure of one of its units and maintenance of the other. Minor hydro and local CHP generation was in service in southern Sweden, two 400 kV lines in the area were out of service, and the HVDC links to Poland and Germany were taken out of operation. At 12.30 hours the only unit in operation at the nuclear power plant at Oskarshamn shutdown due to internal problems. The system managed the disturbance and remained stable. At 12.35 pm, a double busbar fault occurred in a 400 kV substation on the western coast of Sweden. The

fault affected two busbar sections that should have been independent of eachother, due to a damage of a disconnector device located between both busbars. As a result two major nuclear units tripped and the transmission capacity along the west coast was significantly reduced. A number of events followed; power oscillations in the system, a drop in frequency to a level around 49.00 Hz, and low voltages due to heavily loaded conditions in the southeast and south-central parts. Some tens of seconds after the busbar fault the system remained stable, but the load started to recover by action of the numerous tap-changers. This resulted in even lower voltages on the 400 kV grid, and led the system to collapse in the south-west of Stockholm. The system then split up into two parts, and the entire southern system collapsed. Figure 13.2 shows the voltage at the 50 kV-level in a substation in the South East Sweden.

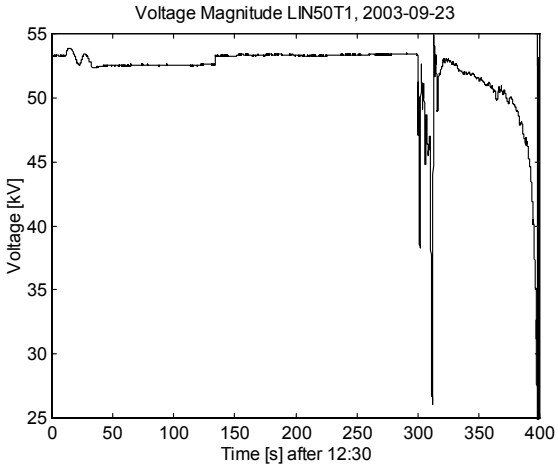

Figure 13.2: Voltage measured at a 50 kV substation in the South East of Sweden.

The tap positions for a tap changer at the 400/130 kV in the South of Sweden are shown in Figure 13.3. Note that the position of the tap changer increases from position 17 to 26 in only 80 seconds, in order to restore the voltage to its pre-disturbance value.

During the final stage of the collapse the system frequency increased considerably while the load dropped due to the very low voltages in the southern Sweden. The cause-effect relation is the following: The low voltage makes the load decrease and the associated real/reactive power

unbalance leads to a frequency increase. Figure 13.4 shows the recordings of the voltage and system frequency during the blackout.

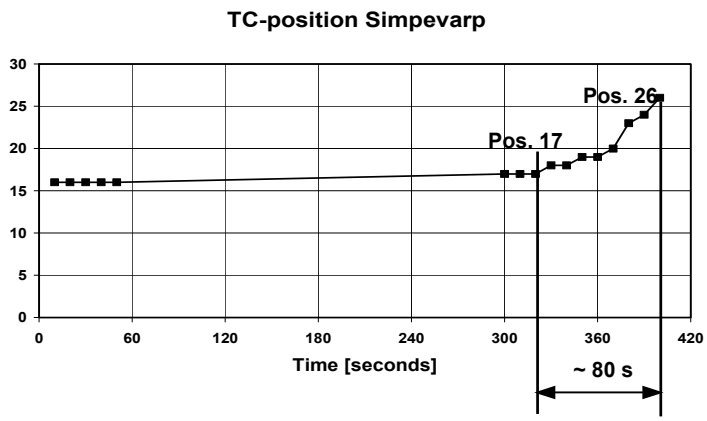

Figure 13.3: Tap changer positions at the 400/130 kV during the disturbances. Measured time is in seconds after 12.30. Picture taken from [Karlsson and Lindahl, 2004].

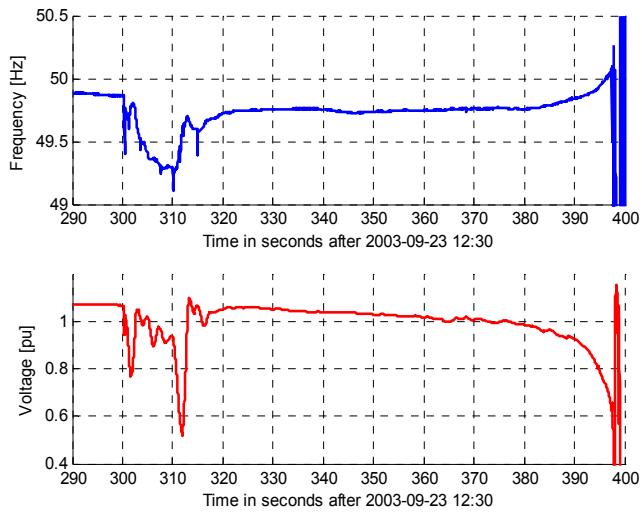

Figure 13.4: Frequency and voltage during the Swedish blackout in September 2003. Figure taken from [Svk, 2003].

North America

Several severe scenarios, which have resulted in either blackout or low-voltage conditions, have hit the North American system during high load and very hot temperature conditions; Western Tennessee (August 1987), Mississippi (July 1987), Washington (August 1981), The Western North American system (July 1996), etc. The starting point for each one of these scenarios was different, but the causes that led the systems into voltage collapse or prolonged low-voltage conditions were similar; summer weather conditions, with abnormally high temperatures, low available generation, and peak load conditions due to a high percent of air conditioner units. The result from these conditions is a higher reactive demand, an increased power transfer, and lower voltage levels. Moreover, the motor-load reactive requirements during extreme conditions prolong the low-voltage depression, which increases the risk for collapse. Figure 13.5 shows the voltage collapse scenario during the 2 July 1996 in the Western interconnection.

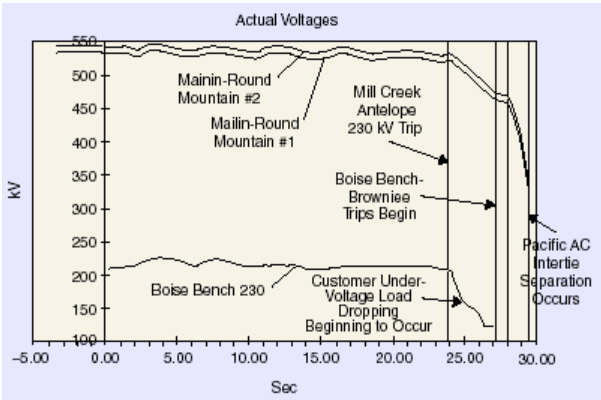

Figure 13.5: Voltage collapse during the 2 July 1996. Event in the Western interconnection in North America. Picture taken from [Pereira, 2004].

These three examples have pointed at the fact that the load dynamics very much influence the scenario during voltage instability conditions. However, the load dynamics associated to each one of the examples have been different; combination of tap-changer operation and long-term electric heating dynamics during heavily loaded conditions, nonlinear characteristic of the load for voltages under 0.8 p.u, load-frequency characteristic, and load characteristic of air conditioner units during high temperatures.

13.2 Load Modeling Guidelines for Stability Studies

This section includes some guidelines to better account for the load in stability studies, in order to get a more accurate calculation of transfer limits and determination of the corresponding security margins.

13.2.1. Physical vs. Black-box models

The importance of finding a physical model to describe the load behavior, has been already motivated; each parameter of the model is associated to a part, dynamic or not, of the real system. A physical load representation makes it possible to add or eliminate individual dynamics that may be or not aggregated to the load. A basic model will provide accurate simulations.

A practical representation for the distribution system is presented in Figure 13.6. The distribution system has been divided into small units. During long-term voltage stability studies, it is necessary to represent the response of tap changers by a dynamic model, while during transient voltage studies this component can be represented as static load. The capacitor X_c accounts for the net effect of reactive compensation in the area. The network effects, losses in lines and transformers, are represented by Z_{losses}.

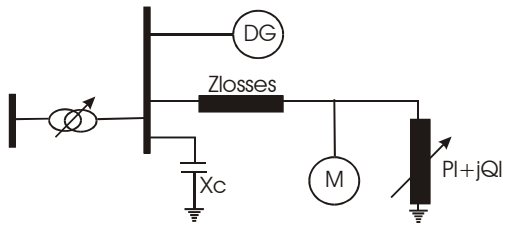

Figure 13.6: Modeling of the distribution system.

The load at the customer side is represented as a combination of a motor, which aggregates the motor load in the area, and an aggregated load, which represents the rest of the load in the area, both static and dynamic. The presence of Distribution Generation (DG) is becoming more and more common in the distribution system, and therefore its effect must be properly

modeled. The model DG accounts for the aggregated power generation in the load area.

13.2.2. Measurement-based vs. Component-based models

Constructing load models based on the estimated composition of loads by components and the characteristics of those components is a complex task due to the lack of relevant data sources. The author suggests instead a *measurement-based approach,* which involves direct measurements at representative substations and feeders to determine the voltage and frequency sensitivity of the load, Part II of this thesis. The main advantage of this approach is the large availability of actual data from the system under study, and the possibility to track diurnal and seasonal variations but also deviations from normal operation.

Part III of this thesis has shown that digital fault recorders (DFR) can be of great advantage for the investigation of the load characteristic during voltage dips. DFR are often located in many modern relays and they register faulted conditions and in general other disturbances that deviate from normal operation. Therefore they can provide significant data for the analysis of the load during faulted conditions. Sampling rates cover hundreds of Hz to KHz.

13.2.3. Static vs. Dynamic load models

Dynamic load models are needed for accurate stability analysis and therefore for an optimized dimensioning of transfer limits and security margins. See Chapter 3.

13.2.4. Linear vs. non-linear models

Chapter 11 has shown that in general the load characteristic increases its nonlinear behavior with more stressing conditions of the system (heavily loaded conditions, lack or reactive power support in the load area, and in general during large disturbances). The nonlinearities are more accentuated in the reactive load behavior. Moreover, some load components such as thermostatically controlled load and induction motors present a non-linear

characteristic during large voltage variations, however the nonlinearities can be linearized if the variations are not very large. During small voltage variations, tap changer operation, switching on/off capacitors and variations around 12 %, loads can be represented with linear or linearized models. During large disturbances it is necessary to fully represent both the dynamics and the nonlinearities of the load.

13.2.5. Short-term vs. Long-term

Long-term dynamics are associated to tap-changer operation, and thermoelectrically controlled loads. The nonlinearities during the long-term are associated to the mechanical functioning of these components. The short-term dynamics are mainly associated to motors and electric lighting, and the nonlinearities represent the characteristic of motors, the equipment that trips the motors, and the restoration characteristic of some types of lighting.

13.2.6. Load Model Parameter Ranges

An accurate representation of the load is necessary for a more optimized determination of transfer limits and dimensioning of security margins, and therefore for a more economical planning and operation of the power system. Transfer limits vary with the load-voltage characteristic. The larger the parameter α (load-voltage sensitivity) is, the larger transfer limits are obtained, i.e. the load-voltage dependency results in load relief.

The seasonal load parameters from a nonlinear model with exponential recovery from normal operation data, has been investigated in Part II of this thesis. The area under study is characterized by a large percent of electric heating and relatively low outdoor temperatures during the winter, and which experience mild temperatures during the summer (low percent of air conditioner units). Estimated load parameters to calculate transfer limits based on field measurements from summer and winter conditions, are presented in Table 13.1.

LOAD MODEL PARAMETERS FOR TRANSFER LIMTS CALCULATIONS						
Season	**Active Power**			**Reactive Power**		
Summer	T_p	α_t	α_s	T_q	β_t	β_s
	[110-140]	[1.4-1.6]	[0.3-1.2]	[120-190]	[0.9-1.1]	[0.4-0.7]
Winter	T_p	α_t	α_s	T_q	β_t	β_s
	[120-160]	[1.8-2.1]	[0.3-0.6]	[126-150]	[0.8-0.9]	[0.3-0.5]

Table 13.1: Estimated load model parameters to calculate transfer limits for a residential load area with high presence of electric heating units.

13.3 Load Model Overview

The models presented in the following tables have been classified according to the size of the voltage excitation, small or large voltage variations, and the time of actuation of the load dynamics, long- and short-term dynamics. For all the cases presented in these tables (13.2.a and 13.2.b), the frequency remains constant. The load-frequency sensitivity has not been investigated in this work.

LOAD MODEL FOR STABILITY STUDIES		
Voltage Variation	**Short-term**	**Long-term**
Small voltage variations	**CASE I** $T_p \frac{dP_r}{dt} + P_r = P_s(V) - P_t(V)$ $P_l = P_r + P_t(V)$ [Karlsson and Hill, 1994]	**CASE II** $T_p \frac{dP_r}{dt} + P_r = P_s(V) - P_t(V)$ $P_l = P_r + P_t(V)$ [Karlsson and Hill, 1994]
Large voltage variations	**CASE III** $P = \left[1 + K_p \cdot (V-1)\right] \cdot \left(1 - P_{drop}\right) + P_{dyn} \cdot \left(G \cdot V^2 - 1\right)$ $\frac{dG}{dt} = -\frac{1}{T} \cdot \left(G \cdot V^2 - 1\right)$ [Ihara, *et al.*, 1994]	**CASE IV** $T_p \frac{dP_r}{dt} + P_r = P_s(V) - P_t(V)$ $P_l = P_r + P_t(V)$ [Karlsson and Hill, 1994]

Table 13.2.a: Recommended load models for short- and long-term, during small and large voltage changes.

LOAD MODEL FOR STABILITY STUDIES
CASE I- Small voltage variations, short-term
- *Validity: several seconds* - Linearized form of [Karlsson and Hill, 1994] - References: [Karlsson and Pehrsson, 1998], [Mansour, 1990], [Dobson and Chiang, 1989] - *Validity: ms-s* - [Karlsson and Hill, 1994] model for up to around 12 % voltage dips - References: Part III of this dissertation
CASE II- Small voltage variations, long-term
- *Validity: min-hours* - A linearized form of [Karlsson and Hill, 1994] is valid for small voltage variations (normal operation) - References: Part II of this dissertation, [RomeroLic, 2002]
CASE III- Large voltage variations, short-term
- *Validity: ms-s* - Nonlinear representation [Ihara, *et al.*, 1994] - References: Part III of this dissertation
CASE IV- Large voltage variations, long-term
- *Validity: min-hours* - [Karlsson and Hill, 1994] model. The validity of a linearized form is depending on the size of the voltage steps - References: [Karlsson and Hill, 1994]

Table 13.2.b: Validity and characteristics of the models presented in Table 13.2.a.

Figure 13.7 presents the characteristic response for the models in Table 13.2.a for different time scales (ms and s) and for small and large voltage steps and dips.

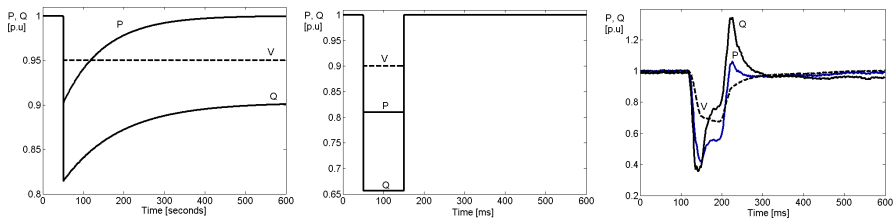

Figure 13.7: Model response to different input signals (steps and dips) and for different time-scales. The figure on the left shows the step response of slow dynamics, from s-min-hours (CASE I, II and IV); the figure in the middle corresponds to the response of [Hill and Karlsson, 1992] to short-term disturbances (ms-s) for small sized voltage dips (CASE I); the figure on the right represents the load response to large voltage dips during faulted conditions (CASE III).

13.4 Load Modeling Procedure

A number of steps to develop a load modeling procedure in an arbitrary location from operational data follow. The procedure describes the planning, implementation and the determination of the model structure and seasonal parameters for the area under study.

13.4.1. Planning

- Measurements area and purpose of the measurements.
- Analysis of the power system in the area under study, locating the biggest areas of generation and load, limiting factors such as stability limits, and other possible weak points of the system.
- Survey of the load to determine the main activity of the area; industrial, residential, commercial load, or a combination of any of them.
- Survey of the main components present in the load area; motors, electric heating, boilers, pumps, air conditioner units, lighting, tap-changers, etc.
- Accounting for heavy industry (load); large industrial drives or large resistance heating systems.
- Weather conditions such as outdoor temperature and humidity.
- High and low peak demand; determination of daily, weekly and seasonal load patterns based on weather conditions and people habits in the area.
- Accounting for the reactive compensation in the area.
- Accounting for the location of the distributed generation units if there are any in the system under study.

13.4.2. Implementation

Based on the previous information it can be determined which type of dynamics are critical in the area under study and therefore which model structure is the most appropriate for the investigation, see Table 13.2. The next step is the determination of the type of measurements and their characteristics.

- If the interest is focused on the study of the seasonal dependency of the load, a complete study will require the setting of a recording device, able to capture normal operation information for up to a year to cover all the possible variations.
- Determination of the type of measurements; active and reactive power, voltage and frequency, or phase voltages and currents, depending on the application.
- The frequency of sampling for the measurements will depend on the time of the actuation of the dynamics under investigation; for example for the analysis of tap-changer operation and electric heating a sampling frequency of 1 Hz is enough to capture all the relevant information. However, if the interest is focused in looking at the dynamics of induction motors higher frequency will be necessary.

13.5 Conclusions

Three different events have shown that the load characteristic contributes to prolonged low voltage conditions or even voltage collapse. The three disturbances have also shown that the load may response in different ways depending on the severity of the disturbance, the time scale under study, and the composition of the load area. An accurate load representation for the different responses is necessary for accurate stability studies.

This thesis recommends a number of load models to represent the load-voltage characteristic, which validity has been tested with field measurements. The load frequency characteristic has not been investigated in this work, but it is an interesting topic for further investigation.

Chapter 14

Conclusions and Further Work

As an extension of previous studies on modeling and identification of non-linear dynamic load models, and motivated by finding more accurate ones, the work presented here has investigated the load-voltage characteristic during normal operation but also faulted conditions.

This chapter includes two main sections. Section 14.1 summarizes the main results obtained in Part I, Part II and Part III of this thesis. Section 14.2 proposes some topics as an interesting continuation to this work.

14.1 Summary of the Main Results

The main conclusions of this thesis have been organized in three sections according to the first three parts of the thesis, Part I Load and Voltage Stability, Part II Load-voltage Characteristic during Normal Operation and Part III Load Models For Large Voltage Variations.

14.1.1 Part I: Load and Voltage Stability

Influence of the load characteristic on voltage stability

The effect of the load characteristic on voltage stability studies has been investigated. The use of the traditional static load models should change in favor of the dynamic ones in order to get a better representation of the load, and therefore to optimize the system operation.

The fact that loads are generally voltage dependent is a critical aspect for the design of security margins. A very pessimistic design may over-emphasize this security and this may result in a poor utilization of the system. On the other hand, a very optimistic design may lead the system to voltage collapse. Simulations have shown that the voltage sensitivity of the load may help the stability of the system by providing some system load relief.

Moreover, some types of load such as electric heating are especially critical for stability because of their thermostatic characteristic. After a disturbance in the system, (voltage and power drop), and due to the effect of the thermostats, the aggregated load tends to increase the nominal load to a level close or equal to the pre-disturbance one, at the low voltage. This situation may result in severe conditions for the system operation. However, during the recovery time it may be possible to take some corrective actions such as local reactive compensation, load shedding, starting small-scale gas turbines, which may lead the system to stable operating points instead.

Limits for Voltage Dependent Loads

PV curves show that a system reaches its stability limit at the nose of the curves when load is defined as constant power, but this point is located further below the nose for voltage dependent loads. The maximum power that can be transferred from the system to the load for different load characteristics has been investigated. Also, it has been studied if those operating conditions coincide or not with the stability limit of the system. Modal analysis has been used to determine the mentioned limits. The evaluation of the reduced Jacobian matrix of a system, when it includes the load-voltage characteristic, shows that at the stability limit there is at least one eigenvalue equal to zero or in its neighborhood. The main observations from the simulations are summarized as follows.

- For a *pure constant PQ load*, the stability limit of the system coincides with the maximum power that can be delivered from the system to the load.
- For a *pure impedance/current load*, the voltage instability cannot occur. The maximum power delivered to the load at a given power factor is independent of the load type. The system is stable for all the points in the lower part of the PV curves.

- For a *mixed load composition*, the stability limit has been found to be below the nose of the PV curve, where the load characteristic becomes a tangent to the system PV curve, i.e. saddle-node bifurcation. Below this point the system is unstable.

QV curves for different load compositions reach their minimum at the mentioned limits, and below them, any injection of reactive power will be associated with lower voltage and instability.

Voltage Security Assessment

A simplified security assessment on the Nordic 32 Test system has been carried out. A scenario has been proposed and simulated for four different load compositions, and the corresponding transfer limits and voltage stability limits have been calculated. The results show that the transfer limits vary with the load-voltage characteristic. The larger the parameter α (load-voltage dependence) is, the larger transfer limits are obtained, i.e. the load-voltage dependency results in load relief. The relief is larger in summer conditions, where the load parameter α is closer to 2. The most critical conditions are when the load behaves as constant power, α equal to 0.

14.1.2 Part II: Load-voltage Characteristic during Normal Operation

An automatic method for the determination of the load parameters from normal operation data is proposed. A nonlinear model has been chosen for this purpose. The non-linear model is reduced to a linear identification problem by linearization, and the identification of the load parameters is achieved straightforward by using the Least Squares criterion. The method is robust with respect to the data, provided that data has been properly screened. The availability of continuous normal operation data has provided large amount of information that has been critical for the accomplishment of this work. The realization of expensive tests has been avoided, and information of high value related to the load dynamics has been provided. This information has helped to track seasonal variations in load and to analyze typical daily operations at a substation. The main conclusions obtained follow:

Window length

The influence of the data sequence length has been studied. A good estimation is achieved by choosing a window length of 2.5-3 times the load time constant, after a voltage change. If the identification is limited to determining the transient characteristic of the load, the measuring time can be considerably reduced to an approximate value of 15% of the time constant. Typical window lengths used in the identification are [200-500] and [15-30] seconds respectively. Moreover, the measurements have verified that during the first 15-30% of the recovery the load behaves as an impedance, i.e. transient characteristic in the neighborhood of 2.

Normalization on reactive dynamic load models

The influence of the normalization in dynamic reactive load models has been studied throughout Section 7.5. By using measured data from normal operation it is illustrated that the reactive power level Q_o traditionally used to normalize reactive load models is inappropriate, since it may be equal to zero due to the effect of reactive compensation. The identification of parameters for the reactive load model when normalizing by Q_o provides values that tend to infinity when Q_o goes to zero. If instead active power level P_o, or apparent power level S_o is used as a base, the variability in the parameters that describe the reactive load response is drastically reduced.

Dynamic load parameters

According to the identified results from the determination of the active and reactive load parameters in Chapter 8 the following has been achieved:

Active and reactive time constants

In general, the values of both time constants move in the same order and direction in a range of about 80 to 200 seconds, and they are correlated to each other with a correlation factor of 0.50. The main recovery of the reactive load is produced by the increase of the reactive losses due to the active recovery of the load at low voltage. The average seasonal and daily time constant values indicate, faster recovery of the load during warmer months. The lowest values correspond to evening hours during summertime when the load demand reaches its minimum due to holidays season and to

low consumption of electric heating. However, the monthly and daily standard deviation of the parameters shows large variability in the distribution of the results due to the high diversity of load processes, even during the day. In order to group the results more accurately, it would be useful to apply alternative analysis techniques as well as other ways of grouping the data.

Active transient load-voltage dependence α_t

The obtained correlation factor (-0.82) between this parameter α_t and the outdoor temperature during the measurements shows the strong dependency of the active transient characteristic of the load with the season, time of the day and weather conditions. The larger values of this parameter, close to 2, correspond to the colder months of the year, especially during the night, and they show a pure resistive characteristic of the load, which is related to the increase in using electric heating load. On the other hand, the lower values of the parameter correspond to summertime where the heating load consumption is very low.

Reactive transient load-voltage dependence β_t

The parameter β_t is associated to the load composition and the presence of induction motors in the area. A high dependency of this parameter on the temperature has been found, where the higher values correspond to summertime and day hours, and the lower to wintertime and night hours. Since the measurements correspond to the same area, the main varying condition is the temperature, and the low variability in the parameter is probably related to connection/disconnection of air conditioners, heat pumps, and other similar loads during winter and summer.

Active and reactive steady state load-voltage dependence α_s β_s

The active and reactive steady state characteristics of the load, α_s and β_s, describe the respective active and reactive time recovery. It has been found that during wintertime the values of α_s are closer to 0, and therefore to a full restoration of the load, while larger values are obtained during summertime. Moreover, some of the results exhibit negative values, corresponding to overshooting in the recovery of the load, probably related to the action of

discrete tap changers under low voltage conditions, that may contribute critically to the voltage stability of the system.

14.1.3 Part III: Load Models for Large Voltage Variations

Extensive work has been done to investigate the load characteristic, and to validate existing load models during small voltage variations. However, few studies investigate the validity of these models during large voltage variations. The load characteristic during large voltage variations, and the adequacy and limitations of existing traditional models for its representation, have been investigated. The main findings are summarized below:

Determination of Load Estimates

A method for determining the phase active and reactive load estimates from measurements of instantaneous values of currents and voltages has been proposed and tested. By using symmetrical components, the sequence phasors for the voltage and the current, and the corresponding three-phase voltages and currents are determined. Assuming that the entire load is aggregated at the load bus and represented as an impedance, the phase time-varying load parameters resistance $R(t)$ and reactance $X(t)$ have been calculated. The phase active and reactive power is then straightforward obtained. Field measurements have been used to validate the method and to analyze the load estimates.

- In general both the active and reactive load change in phase with the change in voltage.
- After a disturbance is cleared, the voltage rapidly recovers to about 90% of its pre-disturbance value, while the full recovery takes some more time, which varies depending on the load composition. Both the active and reactive power, dramatically increase due to the re-acceleration of motors after the fault.

Study of Adequacy for Traditional Load Models

Few studies investigate the validity of traditional models during large voltage reductions. During large voltage variations, the nonlinear behavior

of the power system and the loads increase, and most of the existing load models may no longer be accurate.

The adequacy and limitations of existing traditional models to represent the load during faulted conditions has been investigated. The proposed traditional model agrees well with the measured active load for voltage variations up to even 30%. However, the suitability of the model to represent the reactive load seems limited to voltage dips of about 12%. For larger values, the nonlinear behavior of the reactive power increases, and the nonlinear model deviates from measurements.

Alternative Dynamic Load Models

Existing traditional models need to be improved to capture the dynamics involved during and after severe disturbances that result on voltage dips larger than 12%. An appropriate representation for induction motors is necessary in order to investigate the characteristic of the load during severe conditions and the influence of the short-term dynamics of motors in the stability of the system.

A dynamic nonlinear model, which properly describes the static and dynamic load has been adapted and validated with field measurements. Network effects, losses in the lines and transformers, have been calculated, and the model has been normalized. The results from model validation have shown that the model fits the drop in active and reactive power at the initiation of the fault, but also the nonlinear recovery of the active and reactive power during and after the recovery of the voltage for all the cases. Moreover, the identification of the model parameters has resulted in the following:

- The identified parameters for both feeders move in the same range since the load composition is similar for both feeders. The static load characteristic K_p moves from constant power to constant current (values from 0 to 1). K_q, the static reactive characteristic, exhibits larger values (values between –2 to 5).

- Both the active and reactive load, present a large percent of dynamic load given by the parameters P_{dyn} and Q_{dyn} respectively, which is mainly related to the motor dynamics.
- The active and reactive time constants present similar values and move within the interval 140-240 ms.

14.2 Future Research

The load-voltage characteristic during large disturbances has been investigated, however the availability of data has been limited. A larger study, which would include the analysis of different sized voltage dips for different load composition areas and operating conditions, would make it possible to generalize results on the seasonal variations of the model parameters during severe disturbances, as well as to get better insight into the nonlinear behavior of the load.

This thesis has investigated the validity of traditional load models for voltage dips up to 30 %. However, larger dips have not been studied. When the voltage drops to about 0.6 p.u, the risk of stalling from induction motor increases, and large percent of load may be disconnected due to under-voltage protection. The nonlinear behavior of the reactive power is then accentuated due to tripping and motor stalling. Moreover, the restoration of the load after severe voltage dips is a complex process (cold load pick-up) since it involves different individual loads, whose characteristics are active in different time scales. An interesting continuation to this work would be the study and validation of load models during these conditions.

The presence of Distribution Generation (DG) is becoming more and more common in the distribution system, and therefore as a part of the aggregated load. DG must be properly accounted for and further research is needed to investigate its impact on load modeling.

This thesis investigates the load-voltage characteristic during two different time scales. However, the load frequency sensitivity has not been analyzed. Few investigations have been carried out in this field, and few models are available to represent this dependency. Further research will contribute to a better understanding of the load response and therefore to decrease operational uncertainty.

References

[Agneholm, 1999] E. Agneholm, 'Cold load pick-up', Doctoral Thesis No. 354, Department of Electric Power Engineering, Chalmers University of Technology, Göteborg, Sweden 1999.

[Ajjarapu and Lee, 1992] V. Ajjarapu and B. Lee, 'Bifurcation Theory and its Application to Nonlinear Dynamical Phenomena in an Electrical Power System', IEEE Transactions on Power Systems, Vol. 7, No. 2, pp. 424-431, February 1992.

[ARISTO, 1993] 'ARISTO. Model Reference Manual', Version 1.0, Copyright 1993-1998, Svenska Kraftnät.

[Arnborg, 1997] S. Arnborg, 'Emergency Control of Power Systems in Voltage Unstable Conditions', Doctoral Thesis TRITA-EES-9701 ISSN 1100-1607, Department of Electrical Power Engineering, Royal Institute of Technology, Stockholm, Sweden 1997.

[Arnborg, et al., 1998] S. Arnborg, G. Andersson, D.J. Hill and Ian A. Hiskens, 'On influence of load modeling for undervoltage load shedding studies', IEEE Transactions on Power Systems, Vol.13, No.2, pag. 395-400, May 1998.

[Åström and Wittenmark, 1997] K.J. Åström, B. Wittenmark, 'Computer Controlled Systems. Theory and Design', Prentice-Hall, Inc., Englewood Cliffs, N.J. 07632, USA, 3rd edition 1997.

[Bearden, 2000] T.E. Bearden, 'The Unnecessary Energy Crisis: How to Solve It Quickly', Association of Distinguished American Scientists (ADAS), Final Draft, June 24, 2000.

[Begovic and Phadke, 1990] M. M. Begovic, A.G. Phadke, 'Dynamic Simulation of Voltage Collapse', IEEE Transactions on Power Systems, Vol. 5, No. 1, pp. 198-203, February 1990.

[Bergh, 1996] S.G. Bergh, 'Diagnosis problems in wastewater settling', Technical Licentiate Thesis ISBN 91-88934-01-2, Department of Industrial Electrical Engineering and Automation, Lund Institute of Technology, Lund, Sweden 1996.

[Cañizares, *et al.*, 1992] C. A. Cañizares, F. L. Alvarado, C. L. DeMarco, I. Dobson, W. F. Long, 'Point of Collapse Methods Applied to AC/DC Power Systems', IEEE Transactions on Power Systems, Vol. 7, No. 2, pp. 673-683, May 1992.

[Choi, 1990] S. S. Choi, 'Field Testing of a Long Radial Transmission System and Verification of Computer Simulation Results', IEE Proceedings, Vol. 137, Pt. C, No. 3, May 1990.

[CIGRE, 1993] CIGRE TF 38-02-10, 'Modeling of Voltage Collapse Including Dynamic Phenomena', 1993.

[CIGRE, 1995] 'Long Term Dynamics Phase II', Final Report, CIGRE TF 38-02-08, Belgium, March 1995.

[CIGRE, 1998] 'Temporary Overvoltage Withstand Characteristics of Extra High Voltage Equipment', CIGRE WG 33.10 Electra No. 179, pp. 39-49, August 1998.

[Concordia and Ihara, 1982] C. Concordia, S. Ihara, 'Load Representation in Power System Stability Studies', IEEE Transactions on Power Apparatus and Systems, Vol. PAS-101, No.4, pp. 969-967, April 1982.

[Cutsem and Vournas, 1998] T. Van Cutsem, C. Vournas, 'Voltage Stability of Electric Power Systems', Kluwer Academic Publishers, Boston /London /Dordrecht, 1998.

[DeLeon and Taylor, 2002] J.A. Diaz de León II, C.W. Taylor, 'Understanding and Solving Short-term Voltage Stability Problems', Proceedings of the IEEE/PES 2002 Summer Meeting, Volume 2, pp. 745–752, 21-25 July 2002.

[Dobson and Chiang, 1989] I. Dobson, H.D. Chiang, 'Towards a Theory of Voltage Collapse in Electric Power Systems', Systems & Control Letters, Vol. 13, pp. 253-262, 1989.

[Dovan, *et al.*, 1987] T. Dovan, T.S. Dillon, C.S. Berger, K.E. Forward, 'A Microcomputer Based On-line Identification Approach to Power System Dynamic Load Modeling', IEEE Transactions on Power System, Vol. PWRS-2, No. 3, August 1987, pp 539-533, 1987.

[Gao, *et al.*, 1992] B. Gao, G.K. Morrison, P. Kundur, 'Voltage Stability Evaluation Using Modal Analysis', IEEE Transactions on Power Systems, Vol. 7, No. 4, pp. 1529-1542, November 1992.

[Hill, 1993] D.J. Hill, 'Nonlinear dynamic load models with recovery for voltage stability studies', IEEE Transactions on Power Systems, Vol.8, No.1, pp. 166-176, February 1993.

[Hill and Hiskens, 1994] D.J. Hill, Ian A. Hiskens, 'Modeling, stability and control of voltage behavior in power supply systems', IV Symposium of Specialists in Electrical Operational and Expansion Planning, Foz do Iguacu, Brazil, May 1994.

[IEEE, 1990] IEEE Committee Report, 'Voltage Stability of Power Systems: Cocepts, Analytical Tools, and Industry Experience', IEEE/PES 90^{TH}0358-2-PWR, 1990.

[IEEELoad, 1993] IEEE Task Force on Load Representation for Dynamic Performance, 'Load representation for dynamic performance analysis', IEEE Transactions on Power Systems, Vol.8, No.2, pp. 472-482, May 1993.

[IEEELoad, 1995] IEEE Task Force on Load Representation for Dynamic Performance, 'Standard load models for power flow and dynamic performance simulation', IEEE Transactions on Power Systems, Vol.10, No.3, pp. 1302-1313, August 1995.

[IEEEStability, 1990] IEEE Stability Special: 'Voltage Stability of Power Systems: Concepts, Analytical Tools and Industry Experience' IEEE Special Publication, 90^{TH}0358-2-PWR, 1990.

[IEEEStability, 2002] IEEE Stability 'Voltage Stability Assessment: Concepts, Practices and Tools', IEEE/PES Special Publication, Power System Stability Subcommittee. August 2002.

[IEEEStability, 2004] IEEE/CIGRE Joint Task Force on Stability Terms and Definitions, 'Definition and Classification of Power System Stability', IEEE Transactions on Power Systems, Vol. 19, No. 2, pp. 1387-1401, May 2004.

[IEEETransient, 2001] 'Tutorial on Electromagnetic Transient. Program Applications to Power System Protection', IEEE Power Engineering Education Committee and System Relaying Committee, 2001.

[Ihara, *et al.*, 1981] S. Ihara, G.L. Paulsen, N.W. Simons, 'Bismarck Load Behavior during Field Tests', IEEE Transactions on Power Apparatus and Systems, Vol. PAS-100, No.11, pp. 4540-4545, November 1981.

[Ihara, *et al.*, 1994] S. Ihara, M. Tani, K. Tomiyana, 'Residential Load Characteristics Observed at KEPCO Power System', IEEE Transaction on Power Systems, Vol. 9, No. 2, pp. 1092-1101, May 1994.

[Iliceto and Capasso, 1973] F. Iliceto, A. Capasso, 'Dynamic Equivalents of Asynchronous Motor Loads in System Stability Studies', IEEE Power Engineering Society Winter Meeting, New York 1974.

[Johansson, 1993] R. Johansson, 'System Modeling and Identification', Prentice-Hall, Englewood Cliffs, NJ 1993.

[Johansson and Sjögren, 1995] S. Johansson, F. Sjögren, 'Voltage Collapse in Power Systems. 'The influence of generator current limiters, on-load tap changers and load dynamics', Technical Report No. 192L, Department of Electrical Power Engineering, Chalmers University of Technology, Göteborg, Sweden 1995.

[Ju, *et al.*, 1996] P. Ju, E. Handschin, D. Karlsson, 'Nonlinear dynamic load modeling: model and parameter estimation', IEEE Transactions on Power Systems, Vol.11, No.4, pp. 1689-1697, November 1996.

[Karlsson and Pehrsson, 1985] D. Karlsson, T. Pehrsson, 'A dynamic power system load model and methods for load model parameter estimation', Technical Report 22L, Department of Electrical Power Systems, Chalmers University of Technology, Göteborg, Sweden 1985.

[Karlsson, 1992] D. Karlsson, 'Voltage stability simulations using detailed models based on field measurement', Doctoral Thesis No. 230, Department of Electrical Power Systems, School of Electrical and Computer Engineering, Chalmers University of Technology, Göteborg, Sweden 1992.

[Karlsson and Hill, 1994] D. Karlsson, D.J. Hill, 'Modeling and identification of nonlinear dynamic loads in power systems', IEEE Transactions on Power Systems, Vol.9, No.1, pp. 157-166, February 1994.

[Karlsson and Lindahl, 2004] D. Karlsson, S. Lindahl, 'System Protection Schemes Reviseted- Experiences from Recent Power System Blackouts', Bulk Power Systems Dynamics and Control VI, Cortina d'Ampezzo, Italy 2004.

[Kermendey, et al., 1999] E. Kermendey, N. Villalobos, M. Schmieg, 'The Impact of Load Behavior on Voltage Stability. An Application Case in ENELVEN/VENEZUELA', Conference paper IEEE-ANDESCON99, Margarita Island, Porlamar, Venezuela, 1999.

[Kundur, 1994] P. Kundur, 'Power System Stability and Control', pp 17-40, 271-312, 959-1000, Electric Power Research Institute, McGraw-Hill, USA, 1994.

[Kundur, *et al.*, 1993] P. Kundur, G.K. Morison, B. Gao, H. Hamadanizadeh, B. Danai, D. Maratukulam, 'Voltage Stability Analysis Program', Application Guide, Ontario Hydro, Canada and Electric Power Research Institute, California, November 1993.

[Kwatny, *et al.*, 1986] H.G. Kwatny, A.K. Pasrija, L.Y. Bahar, 'Static Bifurcations in Electric Power Networks: Loss of Steady state Stability and Voltage Collapse', IEEE Transactions on Circuits and Systems, Vol. 33, No. 10, pp. 981-991, October 1986.

[Larsson, 2000] M. Larsson, 'Coordinated voltage control in electrical power systems', Doctoral thesis No. ISBN 91-88934-17-9, Department of Industrial Electrical Engineering and Automation, Lund University, Lund, Sweden 2000.

[Le Dous, 1999] G. Le Dous, 'Voltage stability in power systems. Load modeling based on 130 kV field measurements', Technical Report No. 324L, Department of Electrical Power Engineering, Chalmers University of Technology, Göteborg, Sweden 1999.

[Lin, *et al.*, 1993] C. Lin, Y. Chen, C. Chiou, C. Huang, H. Chiang, J. Wang, L. Fekih-Ahmed, 'Dynamic Load Models in Power Systems Using the Measurement Approach', IEEE Transactions on Power Systems, Vol. 8, No. 1, pp 309-315, February 1993

[Liang *et al.*, 1998] Y. Liang, R. Fischl, A. DeVito, S.C. Readinger, 'Dynamic reactive load model', IEEE Transactions on Power Systems, Vol.13, No.4, pp. 1365-1372, November 1998.

[Lindahl, 2003] S. Lindahl, 'Symmetrical Components', Technical report, Department of Industrial, Electrical Engineering and Automation, Lund University, Sweden 2003.

[Ljung, 1995] L. Ljung, 'System Identification TOOLBOX', User's Guide. The Math Works Inc. August 1995.

[Machowski, et al., 1997] J. Machowski, J.W. Bialek, J.R. Bumby, 'Power System Dynamics and Stability', pp. 74-83, 235-253, Jonh Wiley & Sons, England 1997.

[Mansour, 1990] Y. Mansour, (ed.), 'Voltage Stability of Power Systems: Concepts, Analytical Tools, and Industry Experiences', IEEE Task Force Report, Publication 90TH0358-2-PWR.

[Martins, *et al.*, 2003] N. Martins, R.M. Henriques, A.A. Barbosa, S.G. Júnior, C.B. Gomes and A.C.B. Martins, 'Impact of Induction Motor Loads in System Loadability Margins and Damping of Inter-area Modes', IEEE Power Engineering Society Summer Meeting, Vol. 3, pp. 1384-1387, Toronto, July 2003.

[MATLABOptm, 1992] A. Grace, 'Optimization Toolbox for Use with MATLAB', The Math Works Inc. November 1992.

[Meteorol, 2002] Danish Meteorological Institute, Average monthly and weekly temperatures during July 2001-June 2002, www.dmi.dk/vejr/index.html

[Nordel, 1992] 'Nordel Grid Planning Rules for the Nordic Transmission System', Revised rules at the Nordel Annual Meeting in August 1992.

[Nordel, 2001] Nordel Annual Report. http://www.nordel.org/

[Olsson and Piani, 1992] G. Olsson and G. Piani, 'Computer systems for automation and control', ISBN 0-13-457581-4, Prentice Hall International (UK) Ltd., 1992.

[Padiyar, 1996] K.R. Padiyar, 'Power System Dynamics. Stability and Control', pp. 3-9, 567-570, Indian Institute of Science, Bangalore, John Wiley & Sons (Asia) Pte Ltd and Interline Publishing Pvt. Ltd (India) 1996.

[Pereira, 2004] L. Pereira, 'Cascade to Blackout. Similarities between the 14 August Blackout and the Western System Collapses of 1996', IEEE Power & Energy Magazine, pp. 54-57, May/ June 2004.

[Price, *et al.*, 1988] W.W. Price, K.A. Wirgau, A. Murdoch, J.V. Mitsche, E. Vaahedi, M.A. El-Kady, ' Load Modeling for Power Flow and Transient Stability Computer Studies', IEEE Transactions on Power Systems, Vol. 3, No. 1, pp. 180-187, February 1988.

[PSCAD, 2001] PSCAD Electromagnetic Transients. User's Manual, version 3.0, 2001.

[Randrup, 2003] M. Randrup, ‘Studie av elnätet på Öland och påverkan från befintlig samt planerad vinkraftproduktion’, Technical Report from the Danish Technical University and Sydkraft Nät AB, June 2003.

[Repo, 2001] S. Repo, 'On-line voltage stability assessment of power system-An approach of black-box modeling', Doctoral Thesis, Publications 344, Tampere University of Technology, Finland 2001.

[Romero1, 2001] I. Romero Navarro, 'Recording of Voltage, Active and Reactive Power at Tomelilla. TOMELILLA I', Technical Report CODEN: LUTEDX/(TEIE-7150), IEA, Lund, Sweden 2001.

[Romero2, 2001] I. Romero Navarro, 'Recording of Voltage, Active and Reactive Power at Tomelilla. TOMELILLA II', Technical Report CODEN: LUTEDX/(TEIE-7151), IEA, Lund, Sweden 2001.

[Romero, 2003] I. Romero Navarro, 'A Voltage Security Assessment of the Nordic 32 Test System using VSAT’, Technical Report CODEN: LUTEDX/(TEIE-7204), IEA, Lund University, Sweden 2003.

[RomeroLic, 2002] I. Romero Navarro, ‘Dynamic Load Models for Power Systems. Estimation of Time-varying Parameters during Normal Operation’, Technical Licentiate Thesis ISBN 91-88934-26-8, Lund University, Sweden 2002.

[Roos, 2002] F. Roos, ’Coordinated Voltage Control’, Technical Report LUTEDX/(TEIE-5158)/1-35/(2002), Department of Industrial Electrical Engineering and Automation, Lund University, Sweden 2002.

[Rudin, 1976] W. Rudin, ‘Principles of Mathematical Analysis’, Third Edition McGraw-Hill, USA 1976.

[Sabir and Lee, 1982] S.A.Y. Sabir, D.C. Lee, ‘Dynamic Load Models Derived from Data Acquired During System Transient’, IEEE Transactions on Power Apparatus and Systems, Vol. PAS-101, No. 9, September 1982.

[Sekine and Ohtsuki, 1990] Y. Sekine, H. Ohtsuki, 'Cascaded voltage collapse', IEEE Transactions on Power Systems, Vol.5, No.1, pp. 250-255, February 1990.

[Seydel, 1988] R. Seydel, ‘From Equilibrium to Chaos. Practical Bifurcation and Stability Analysis’, Elsevier Science Publishers, North-Holland (1988)

[Shaffer, 1997] J.W. Shaffer, ‘Air Conditioner Response to Transmission Faults’, IEEE Transaction on Power Systems, Vol. 12, No. 2, pp.614-621, May 1997.

[SINTEF, 2004] G. Doorman, G. Kjølle, K. Uhlen, E.S. Huse, N. Flatabø, ’Vulnerability of the Nordic Power System. Main’, Main Report, Report to the Nordic Council of Ministers, Technical Report TR A5962, SINTEF, May 2004.

[Svantesson, 2002] T. Svantesson, 'Automated Manufacture of Fertilizing Agglomerates from Burnt Wood Ash', Doctoral Thesis ISBN 91-88934-24-1, Department of Industrial Electrical Engineering and Automation, Lund University, Sweden 2000.

[Svk, 2003] ‘The Black-out in the Southern Sweden and Eastern Denmark, September 23, 2003’, Report from Svenska Kraftnät, the Swedish Transmission System Operator (TSO), 2003.

[Sydkraft1, 1958] ‘Undersökning av belastningens spänningsberoende. Tomelillasystemet’, Internal report Sydkraft Driftbyrån, Malmö, Sweden 1958.

[Sydkraft2, 1958] ‘Undersökning av belastningens spänningsberoende. Trelleborgsystemet’, Internal report Sydkraft Driftbyrån, Malmö, Sweden 1958.

[Sydkraft3, 1958] ‘Undersökning av belastningens spänningsberoende. Stävlösystemet’, Internal report Sydkraft Driftbyrån, Malmö, Sweden 1958.

[Taylor, 1994] C.W. Taylor, ‘Power System Voltage Stability’, pp 17-135. Electric Power Research Institute, McGraw-Hill, USA 1994.

[Tomiyama, *et al.*, 1998] K. Tomiyama, J.P. Daniel, S. Ihara, ’Modeling Air Conditioner Load for Power System Studies’, IEEE Transactions on Power Systems, Vol. 13, No. 2, pp. 414-421, May 1998.

[Tomiyama, *et al.*, 2003] K. Tomiyama, S. Ueoka, T. Takano, I. Iyoda, K. Matsuno, K. Temma, J. J. Paserba, ’Modeling of Load During and After System Faults Based on Actual Field Data’, IEEE Power Engineering Society Summer Meeting, Vol. 3, pp. 1391-1394, Toronto, July 2003.

[Uhlen, *et al.*, 2002] K. Uhlen, M. Pálsson, T.R. Time, Ø. Kirkeluten, J.O. Gjerde, ‘Raising Stability Limits in the Nordic Power Transmission System’, 14th PSCC Power System Computation, Spain, June 2002.

[Vaahedi, *et al.*, 1988] E. Vaahedi, H.M. Zein El-Din, W.W. Price, ’Dynamic Load Modeling in Large Scale Stability Studies’, IEEE Transactions on Power Systems, Vol. 3, No. 3, pp. 1039-1045, August 1988.

[VSAT, 2000] ‘VSAT. Voltage Security Assessment Tool’, Version 3.0, Installation Guide and User’s Manual, Powertech Labs Surrey 2000, British Colombia, Canada.

[Walve, 1986] K. Walve, ‘Modeling of Power System Components at Severe Disturbances’, CIGRE report 38-18, 1986.

[Willis, *et al.*, 1995] H. Lee Willis, Linda A. Finley, M. Buri, ’Forecasting Electric Demand of Distribution Planning in Rural and Sparsely Populated Regions', IEEE Transactions on Power Systems, Vol. 10, No.4, pp 2008-2013, November 1995.

[Xu and Mansour, 1994] W. Xu, Y. Mansour, 'Voltage stability analysis using generic dynamic load models', IEEE Transactions on Power Systems, Vol.9, No.1, pp. 479-486, February 1994.

Additional Reading

M. H. J. Bollen, ’The Influence of Motor Re-acceleration on Voltage Sags’, IEEE Industry Applications Society Annual Meeting, Vol. 3, pp.2235-2242, 1994.

F.T. Dai, J.V. Milanovic, N. Jenkins, V. Roberts, ‘Development of a Dynamic Power System Load Model’, Conference Publication No. 485, IEEE 2001 AC-DC Power Transmission, pp. 344-349, November 2001.

F. Mc.Dyer, F. Byrne, R.W. McGee, G. Rodgers, M. Hayashi, G. Testud, N. Roelofs, 'Load Modeling and Dynamics', Electra pp.122-141, May 1990.

M. Gustafsson, N. Krantz, 'Voltage Collapse in Power Systems. Analysis of Component Related Phenomena using a Power System Model', Technical Report No. 215L, Department of Electrical Power Engineering, Chalmers University of Technology, Sweden 1995.

IEEE Working Group, 'System Load Dynamics. Simulation Effects and Determination of Load Constants', Computer Analysis of Power Systems Working Group of the Computer and Analytical Methods, Power System Engineering Committee IEEE/ PES Summer Meeting, San Francisco, July 1972.

S. Johansson, 'Long-term Voltage Stability in Power Systems. Alleviating the Impact of Generator Current Limiters', Doctoral Thesis No.335, Department of Electric Power Engineering, Chalmers University of Technology, Göteborg, Sweden 1998.

M.H. Kent, W.R. Schmus, F.A. Mc. Crackin, L.M. Wheeler, ' Dynamic Modeling of Loads in Stability Studies', IEEE Transactions on Power Apparatus and Systems, Vol. PAS-88, No. 5, pp.756-763, May 1969.

G. Le Dous, A. Holmer, 'Frequency Dependence of the Load in the Nordic Power System', Technical Report No. 95/96:02, Department of Electric Power Engineering, Chalmers University of Technology, Göteborg, Sweden 1995.

R. Lind, 'Distribution Network Modeling. Method for distribution network reduction for voltage stability studies', Technical Report, Department of Electrical Power Engineering, Royal Institute of Technology, Stockholm, Sweden 1995.

K. Morison, H. Hamadani, L. Wang, 'Practical Issues in Load Modeling for Voltage Stability Studies', IEEE Power Engineering Society Summer Meeting, Vol. 3, pp. 1392-1397, Toronto, July 2003.

T. Segui, P. Bertrand, M. Guillot, P. Hanchin, P. Bastard, 'Fundamental Basis for Distance Relaying with Parametrical Estimation', IEEE Transactions on Power Delivery, Vol. 15, No. 2, pp. 659-664, April 2000.

G. Shackshaft, O.C. Symons, J.G. Hadwick, 'General-purpose model of power-system loads', IEE Proceedings- Generation, transmission and distribution, Vol. 124, pp. 715-723, August 1977.

W. Xu, E. Vaahedi, Y. Mansour, J. Tamby, 'Voltage Stability Load Parameter Determination from Field Test on B.C. Hydro's System', IEEE Transactions on Power Systems, Vol. 12, No. 3, pp. 1290-1297, August 1997.

B.R. Williams, W.R. Schmutz, D.C. Dawson, 'Transmission Voltage Recovery Delayed by Stalled Air Conditioner Compressors', IEEE Transactions on Power Systems, Vol. 7, No. 3, pp. 1173-1181, August 1992.

Appendix I

Load Models and Jacobian Matrix

Simplified 4 Bus-case

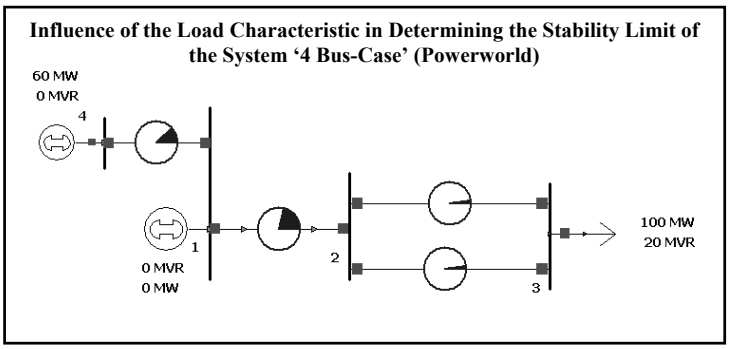

Figure I.1: Four Bus-case

Buses of the system: Bus 1- Slack Bus (V = 1 p.u, θ = 0°); Bus 3- PQ Load Bus (P = 100 MW, Q = 20 MVar); Bus 4- PV Bus (P = 60 MW, V= 1 p.u).

The Jacobian matrix has been built based on the following three equations:

$$[P + jQ] = [V] \cdot [Y]^T \cdot [V]^* \tag{I.1}$$

$$[Pbus + Plbus - Pgbus] = 0 \tag{I.2}$$

$$[Qbus + Qlbus - Qgbus] = 0 \tag{I.3}$$

P_{bus}, Q_{bus}; Active and reactive total power at each bus; P_{lbus}, Q_{lbus}; Active and reactive load at each bus; P_{gbus}, Q_{gbus}; Active and reactive generation at each bus. The system steady state full Jacobian matrix is given by equation (I.4). This matrix examines the relationship between the incremental change in bus voltage magnitude and the incremental change in bus virtual reactive power injection, equation (I.5).

$$J = \begin{bmatrix} J_{P\theta} & J_{PV} \\ J_{Q\theta} & J_{QV} \end{bmatrix} \quad \text{(I.4)}$$

$$\begin{bmatrix} \Delta P \\ \Delta Q \end{bmatrix} = J \cdot \begin{bmatrix} \Delta\theta \\ \Delta V \end{bmatrix} \quad \text{(I.5)}$$

By combining all the above equations it is possible to build the full Jacobian matrix for the 4-bus case system. The reduced steady state system Jacobian matrix is obtained by letting ΔP = 0 in equation (I.5). The resulting expression is given by equation (I.6):

$$J_R = J_{QV} - J_{Q\theta} \cdot J_{P\theta}^{-1} \cdot J_{PV} \quad \text{(I.6)}$$

Load Models in the Jacobian Matrix

This section describes the mathematical equations for representing the load for five different load compositions. The expressions must be included in the Jacobian matrix, when modal analysis including load models is requested. The load representation must be included at the load bus (bus 3) in equations (I.2) and (I.3).

Load Composition	Jacobian
	$J_{lbus} = \begin{bmatrix} J_{P\theta lbus} & J_{PV_{lbus}} \\ J_{Q\theta lbus} & J_{QV_{lbus}} \end{bmatrix}$
100 % Constant Power	$Pload = P_o \qquad \frac{\partial Pload}{\partial V_{lbus}} = 0$ $J_{PV_{lbus}}(new) = J_{PV_{lbus}} + \frac{\partial Pload}{\partial V_{lbus}} = J_{PV_{lbus}} + 0$ (I.7)

100 % Constant Current	$Pload = P_o \cdot V_{lbus} \qquad \frac{\partial Pload}{\partial V_{lbus}} = P_o$ $J_{PV_{lbus}}(new) = J_{PV_{lbus}} + \frac{\partial Pload}{\partial V_{lbus}} = J_{PV_{lbus}} + P_o$ (I.8)
25 % Constant Power **75 % Constant Current**	$Pload = 0.75 \cdot P_o \cdot V_{lbus} + 0.25 \cdot P_o \qquad \frac{\partial Pload}{\partial V_{lbus}} = 0.75 \cdot P_o$ $J_{PV_{lbus}}(new) = J_{PV_{lbus}} + \frac{\partial Pload}{\partial V_{lbus}} = J_{PV_{lbus}} + 0.75 \cdot P_o$ (I.9)
25 % Constant Power **75 % Const. Impedance**	$Pload = 0.75 \cdot P_o \cdot V_{lbus}^2 + 0.25 \cdot P_o$ $\frac{\partial Pload}{\partial V_{lbus}} = 1.5 \cdot P_o \cdot V_{lbus}$ $J_{PV_{lbus}}(new) = J_{PV_{lbus}} + \frac{\partial Pload}{\partial V_{lbus}} = J_{PV_{lbus}} + 1.5 \cdot P_o \cdot V_{lbus}$ (I.10)
25 % Constant Power **25 % Constant Current** **50 % Const. Impedance**	$Pload = 0.25 \cdot P_o + 0.25 \cdot P_o \cdot V_{lbus} + 0.50 \cdot P_o \cdot V_{lbus}^2$ $\frac{\partial Pload}{\partial V_{lbus}} = 0.25 \cdot P_o + P_o \cdot V_{lbus}$ $J_{PV_{lbus}}(new) = J_{PV_{lbus}} + \frac{\partial Pload}{\partial V_{lbus}} = J_{PV_{lbus}} + (0.25 \cdot P_o + P_o \cdot V_{lbus})$ (I.11)

Appendix II

Equivalent Distribution System

A simplified scheme of the area of measurements in Tomelilla is shown in Figure II.1. It includes the distribution system from the 130 kV-level and downward. At the 130 kV bus, two three windings 100/100/40MVA, 130/50/20 kV tap changing transformers are connected in parallel. The tap changers, which are controlling the voltage at the 20 kV-level, are placed on the 130 kV windings.

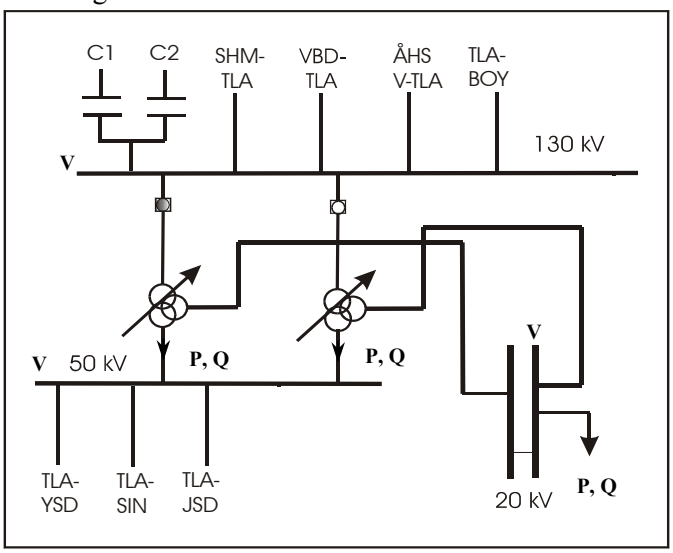

Figure II.1: Simplified test system at Tomelilla. Measurements of voltage, active and reactive power, are expressed in kV, MW and MVar respectively.

The equivalent circuit for each of the three-winding transformers is shown in Figure II.2.

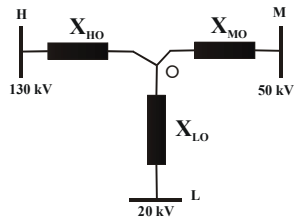

Figure II.2: Equivalent circuit of the three-winding transformer in Tomelilla. H, M and L name the high, medium and low voltage-side, respectively. X_{HO}, X_{MO} and X_{LO} are the equivalent transformer reactances for the high, medium and low voltage level.

As mentioned in Chapter 7, in order to check whether the reactive recovery really originates from the increase of reactive losses, the simplified distribution system shown in Figure II.3 has been used to determine those losses. The complete distribution system under the recording point at the 130 kV-level has been modeled with a series reactance equal to the sum of both reactances at 130 and 20 kV. The measured values corresponding to 20 kV have been used to determine the value of the losses (Qlosses). Values in per-unit have been used for the voltages and respective reactances [Roos, 2002].

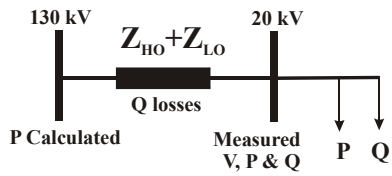

Figure II.3: Simplified distribution system from the 130 kV- level to the 20 kV-level for determining the reactive load losses.

Appendix III

Symmetrical Components

The determination of symmetrical components, the (1) positive-, (2) negative- and (3) zero-sequence components of a set of three-phase voltages or currents, is described throughout this section. The procedure is identical for currents and voltages and therefore the term *three-phase signal* will be used to refer to a set of three-phase currents or a set of three-phase voltages. Equation (III.1) defines the available data for each one of the phases, a, b and c respectively, being w_o in rad/s the fundamental angular frequency, and f_o in Hz the fundamental frequency.

$$\left.\begin{aligned} s_a(k) &= S_a \sin(k\omega_0 \Delta t + \varphi_a) \\ s_b(k) &= S_b \sin(k\omega_0 \Delta t + \varphi_b) \\ s_c(k) &= S_c \sin(k\omega_0 \Delta t + \varphi_c) \end{aligned}\right\} \quad for\ k = 0, 1, 2, \ldots \tag{III.1}$$

$$w_o = 2\pi f_o$$

Equation (III.2) gives the set of three-phase signal as a sum of the positive-, negative-, and zero-sequence components.

$$\begin{aligned} s_a(k) &= s_{1a}(k) + s_{2a}(k) + s_{0a}(k) \\ s_b(k) &= s_{1b}(k) + s_{2b}(k) + s_{0b}(k) \\ s_c(k) &= s_{1c}(k) + s_{2c}(k) + s_{0c}(k) \end{aligned} \tag{III.2}$$

Equations (III.3), (III.4) and (III.5) define the positive-, negative- and zero-sequence components for phases *a, b* and *c*.

$$\begin{aligned} s_{1a}(k) &= S_1 \cdot \sin(k\omega_0 \Delta t + \phi_1) \\ s_{1b}(k) &= S_1 \cdot \sin\left(k\omega_0 \Delta t + \phi_1 - \frac{2\pi}{3}\right) \\ s_{1c}(k) &= S_1 \cdot \sin\left(k\omega_0 \Delta t + \phi_1 - \frac{4\pi}{3}\right) \end{aligned} \tag{III.3}$$

$$\begin{aligned} s_{2a}(k) &= S_2 \cdot \sin(k\omega_0 \Delta t + \phi_2) \\ s_{2b}(k) &= S_2 \cdot \sin\left(k\omega_0 \Delta t + \phi_2 - \frac{4\pi}{3}\right) \\ s_{2c}(k) &= S_2 \cdot \sin\left(k\omega_0 \Delta t + \phi_2 - \frac{2\pi}{3}\right) \end{aligned} \tag{III.4}$$

$$\begin{aligned} s_{0a}(k) &= S_0 \cdot \sin(k\omega_0 \Delta t + \phi_0) \\ s_{0b}(k) &= S_0 \cdot \sin(k\omega_0 \Delta t + \phi_0) \\ s_{0c}(k) &= S_0 \cdot \sin(k\omega_0 \Delta t + \phi_0) \end{aligned} \tag{III.5}$$

The aim is to find the six parameters S_1, S_2, S_0, ϕ_1, ϕ_2 and ϕ_0 from the sampled values of the phase signals. There are M sampling intervals per fundamental frequency cycle $Mw_0\Delta t=2\pi$ and M has been selected equal 20. The determination of the parameters S_1 and ϕ_1 for the positive-sequence is described below. Rectangular coordinates are used instead of polar coordinates to simplify the parameter estimation. Two new parameters have been introduced, A_1 and B_1. Equation (III.7) gives the relation between them and S_1 and ϕ_1 in the polar representation.

$$\begin{aligned} s_{1a}(k) &= A_1 \cdot \cos(k\omega_0 \Delta t) + B_1 \cdot \sin(k\omega_0 \Delta t) \\ s_{1b}(k) &= A_1 \cdot \cos\left(k\omega_0 \Delta t - \frac{2\pi}{3}\right) + B_1 \cdot \sin\left(k\omega_0 \Delta t - \frac{2\pi}{3}\right) \\ s_{1c}(k) &= A_1 \cdot \cos\left(k\omega_0 \Delta t - \frac{4\pi}{3}\right) + B_1 \cdot \sin\left(k\omega_0 \Delta t - \frac{4\pi}{3}\right) \end{aligned} \tag{III.6}$$

$$\begin{aligned} S_1 &= \sqrt{A_1^2 + B_1^2} \\ \tan(\phi_1) &= \frac{A_1}{B_1} \end{aligned} \tag{III.7}$$

The least-square method is used to find the parameters A_1 and B_1, i.e. the function given by equation (III.8) is minimized to obtained A_1 and B_1.

$$V(A_1,B_1)=\sum_{k=1}^{M}\left[A_1\cdot\cos(\theta_k)+B_1\cdot\sin(\theta_k)-s_a(k)\right]^2+$$
$$+\sum_{k=1}^{M}\left[A_1\cdot\cos(\theta_k-2\pi/2)+B_1\cdot\sin(\theta_k-2\pi/2)-s_b(k)\right]^2+$$
$$+\sum_{k=1}^{M}\left[A_1\cdot\cos(\theta_k-4\pi/2)+B_1\cdot\sin(\theta_k-4\pi/2)-s_c(k)\right]^2 \tag{III.8}$$

$$\theta_k=kw_o\Delta t$$

The function $V(A_1,B_1)$ is the sum of the squared deviation over one complete fundamental period. It is then differentiated with respect to the parameter A_1 to find the minimum of the function $V(A_1,B_1)$.

$$\frac{dV(A_1,B_1)}{dA_1}=\sum_{k=1}^{M}2\cdot\left[A_1\cdot\cos(\theta_k)+B_1\cdot\sin(\theta_k)-s_a(k)\right]\cdot\cos(\theta_k)+$$
$$+\sum_{k=1}^{M}2\cdot\left[A_1\cdot\cos(\theta_k-2\pi/3)+B_1\cdot\sin(\theta_k-2\pi/3)-s_b(k)\right]\cdot\cos(\theta_k-2\pi/3)+$$
$$+\sum_{k=1}^{M}2\cdot\left[A_1\cdot\cos(\theta_k-4\pi/3)+B_1\cdot\sin(\theta_k-4\pi/3)-s_c(k)\right]\cdot\cos(\theta_k-4\pi/3) \tag{III.9}$$

The expressions is also differentiated with respect to the parameter B_1 to find the minimum.

$$\frac{dV(A_1,B_1)}{dB_1}=\sum_{k=1}^{M}2\cdot\left[A_1\cdot\cos(\theta_k)+B_1\cdot\sin(\theta_k)-s_a(k)\right]\cdot\sin(\theta_k)+$$
$$+\sum_{k=1}^{M}2\cdot\left[A_1\cdot\cos(\theta_k-2\pi/3)+B_1\cdot\sin(\theta_k-2\pi/3)-s_b(k)\right]\cdot\sin(\theta_k-2\pi/3)+$$
$$+\sum_{k=1}^{M}2\cdot\left[A_1\cdot\cos(\theta_k-4\pi/3)+B_1\cdot\sin(\theta_k-4\pi/3)-s_c(k)\right]\cdot\sin(\theta_k-4\pi/3) \tag{III.10}$$

Equation (III.11) gives the necessary conditions for a minimum:

$$\frac{dV(A_1,B_1)}{dA_1}=0 \quad and \quad \frac{dV(A_1,B_1)}{dB_1}=0 \tag{III.11}$$

By combining equations (III.9) and (III.11), equation (III.12) is obtained:

$$\begin{aligned}
&\sum_{k=1}^{M}\left[A_1\cdot\cos(\theta_k)+B_1\cdot\sin(\theta_k)\right]\cdot\cos(\theta_k)+\\
&+\sum_{k=1}^{M}\left[A_1\cdot\cos(\theta_k-2\pi/3)+B_1\cdot\sin(\theta_k-2\pi/3)\right]\cdot\cos(\theta_k-2\pi/3)+\\
&+\sum_{k=1}^{M}\left[A_1\cdot\cos(\theta_k-4\pi/3)+B_1\cdot\sin(\theta_k-4\pi/3)\right]\cdot\cos(\theta_k-4\pi/3)=\\
&=\sum_{k=1}^{M}s_a(k)\cdot\cos(\theta_k)+\sum_{k=1}^{M}s_b(k)\cdot\cos(\theta_k-2\pi/3)+\sum_{k=1}^{M}s_c(k)\cdot\cos(\theta_k-4\pi/3)
\end{aligned} \tag{III.12}$$

By combining equations (III.10) and (III.11), (III.13) is obtained:

$$\begin{aligned}
&\sum_{k=1}^{M}\left[A_1\cdot\cos(\theta_k)+B_1\cdot\sin(\theta_k)\right]\cdot\sin(\theta_k)+\\
&+\sum_{k=1}^{M}\left[A_1\cdot\cos(\theta_k-2\pi/3)+B_1\cdot\sin(\theta_k-2\pi/3)\right]\cdot\sin(\theta_k-2\pi/3)+\\
&+\sum_{k=1}^{M}\left[A_1\cdot\cos(\theta_k-4\pi/3)+B_1\cdot\sin(\theta_k-4\pi/3)\right]\cdot\sin(\theta_k-4\pi/3)=\\
&=\sum_{k=1}^{M}s_a(k)\cdot\sin(\theta_k)+\sum_{k=1}^{M}s_b(k)\cdot\sin(\theta_k-2\pi/3)+\sum_{k=1}^{M}s_c(k)\cdot\sin(\theta_k-4\pi/3)
\end{aligned} \tag{III.13}$$

Taking into consideration that $\cos(\theta)$ and $\sin(\theta)$ are orthogonal and that the norm of $\cos(\theta)$ and the norm of $\sin(\theta)$ are both equal to $M/2$, it is obtained:

$$\frac{3M}{2}A_1=\sum_{k=1}^{M}s_a(k)\cdot\cos(\theta_k)+s_b(k)\cdot\cos(\theta_k-2\pi/3)+s_c(k)\cdot\cos(\theta_k-4\pi/3) \tag{III.14}$$

$$\frac{3M}{2}B_1=\sum_{k=1}^{M}s_a(k)\cdot\sin(\theta_k)+s_b(k)\cdot\sin(\theta_k-2\pi/3)+s_c(k)\cdot\sin(\theta_k-4\pi/3) \tag{III.15}$$

The final result is then

$$A_1 = \frac{2}{3M}\sum_{k=1}^{M} s_a(k)\cdot\cos(\theta_k) + s_b(k)\cdot\cos(\theta_k - 2\pi/3) + s_c(k)\cdot\cos(\theta_k - 4\pi/3) \tag{III.16}$$

$$B_1 = \frac{2}{3M}\sum_{k=1}^{M} s_a(k)\cdot\sin(\theta_k) + s_b(k)\cdot\sin(\theta_k - 2\pi/3) + s_c(k)\cdot\sin(\theta_k - 4\pi/3) \tag{III.17}$$

A similar procedure can be followed to determine the parameters A_2, B_2, S_2, ϕ_2 and A_0, B_0, S_0, ϕ_0 for the negative- and zero-sequence components of the signal. This procedure is applied to determine the positive-, negative- and zero-sequence components for a given set of three-phase voltages and currents.

Appendix IV

Network Effects

A simplified scheme of the area of measurements in Öland is shown in Figure 9.2. It includes the distribution system from the 50 kV-level and downward in Öland, and the connection of the island at the 130 kV to mainland. Measurements at the 50 kV-level from feeders 54 and 59, have been used to investigate the aggregated load characteristic during large voltage variations. Equivalent circuits for each one of these two feeders have been calculated in order to separate the power consumed by customers, from the power consumed by system losses. Figures IV.1 and IV.2 show the different components at each one of the feeders.

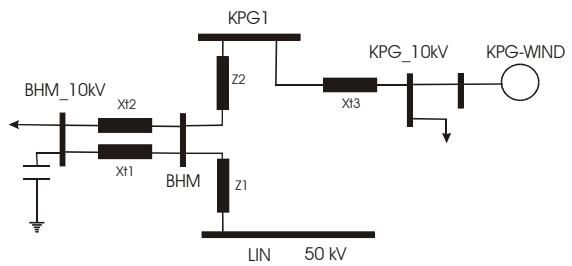

Figure IV.1: Equivalent circuit of feeder 54 from the distribution system of Öland. Xt1, Xt2 and Xt3, are the equivalent 50/10 kV transformer reactances, Z1 and Z2 are the equivalent line impedances of the system. KPG_WIND stands for 15 MW wind generation.

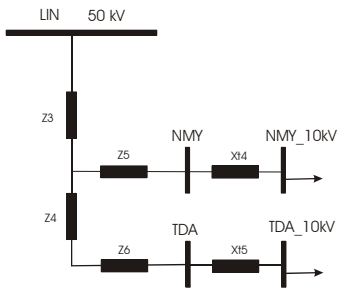

Figure IV.2: Equivalent circuit of feeder 59 from the distribution system of Öland. Xt4 and Xt5 are the equivalent 50/10 kV transformer reactances, and Z3, Z4, Z5 and Z6 are the equivalent line impedances of the system.

R1	X1	R2	X2	R3	X3	R4	X4	R5	X5	R6	X6
1.861	2.043	0.476	0.529	0.000	0.001	0.000	0.001	1.428	1.567	0.519	1.312

Rt1	Xt1	Rt2	Xt2	Rt3	Xt3	Rt4	Xt4	Rt5	Xt5
0.603	7.940	0.603	7.940	1.050	16.63	2.200	22.89	0.318	6.430

Table IV.1: Feeders' reactances, resistances and equivalent reactances for transformers given in p.u., (1000 MVA)

The parameters given in p.u have been transformed to ohms by using the expressions (IV.1)-(IV.3). The simplified schemes in Figures V.3 have been used to determine the losses of the system.

$$S_B = \frac{V_B^2}{Z_B} = 1000\ MVA \quad \text{(IV.1)}$$

$$Z_B = \frac{V_B^2}{S_B} = \frac{50\ kV^2}{1000\ MVA} = 2.5\ \Omega \quad \text{(IV.2)}$$

$$Z_{p.u} = \frac{Z_{ohms}}{Z_B} \quad \text{(IV.3)}$$

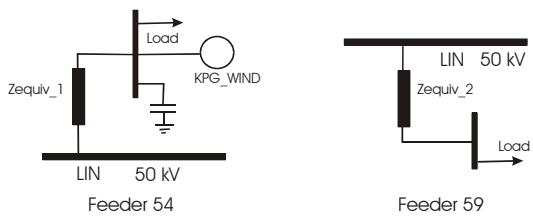

Figure IV.3: Simplified distribution system for the 50 kV-level and downwards for feeders 54 and 59 for determining active and reactive losses in the feeders